Determining the Action Spectrum of UVR-Induced Mitochondrial DNA Damage, and the Related UVR-Induced Cellular Effects in Human Skin.

Jennifer Anne Latimer

Submitted in fulfilment of the requirements for the degree of Doctor of Philosophy in the institute of Cellular Medicine, Newcastle University

2013

Abstract

Biological responses of human skin to ultraviolet radiation (UVR) are largely wavelength-dependent as shown by the action spectrum of UVR-induced erythema and nuclear DNA (nDNA) damage. As mitochondrial DNA (mtDNA) damage has been shown to be a reliable and sensitive biomarker of UVR exposure in human skin, the aim of this study was to determine the action spectrum for UVR-induced mtDNA damage in human skin cells. This involved the irradiation of both HaCaT (immortalised keratinocytes) and HDFn (human fibroblasts) cell lines and primary human keratinocyte cells with increasing doses of UVR. A wide variety of UVR sources were chosen for their unique overlapping UVR profiles, covering the entire UVA and UVB spectrum. Overall UVR induced mtDNA damage was assessed using a quantitative long real time PCR to amplify an 11 kb segment of the mitochondrial genome. Specific UVR-induced mtDNA deletions (3895 bp and 4977 bp) were investigated, as was the effect on cellular respiration using the novel Seahorse extracellular flux analyzer. Furthermore investigations sought to determine UVR-induced nDNA damage: This included the induction of p53 mutations, generation of the oxidative stress marker 8-OHdG, photoproduct production as well as differential gene expression. For investigations of general UVR-induced mtDNA damage, dose curves were produced for each of the UVR sources and cell types. From this an action spectrum was determined by a method known as de-convolution. A higher sensitivity was seen in the fibroblast cell type. The overall trend of the action spectrum of the UVR-induced mtDNA damage followed that of various previously determined action spectra with the most detrimental effects occurring over the shorter wavelengths of UVR. This was also shown for the production of photoproducts and with the differential gene expression analysis. UVA and UVB both also affected cellular respiration and gene expression. The UVR exposures used in the study were not effective in inducing detectable levels of either of the mtDNA specific deletions, mutations within the p53 gene or levels of 8-OHdG and this may have been affected by limitations of the analytical techniques. Further experiments saw that the addition of antioxidant type entities provided protection and the possible reversal of some of the UVR damaging effects.

Declaration

This thesis is submitted to the degree of Doctor of Philosophy at Newcastle University. The research was performed in the Department of Dermatology under the supervision of Prof Mark Birch-Machin (primary supervisor), Dr Jim Lloyd (secondary supervisor) and Dr Paul Matts (industrial supervisor; P&G) and is my own work unless otherwise stated within the text. I certify that none of the material offered in this thesis has been previously submitted by me for a degree or any other qualification at this or any other university.

Acknowledgements

This project was jointly funded by the engineering and physical sciences research council (EPSRC) and Procter and Gamble (P&G).

I would like to thank my primary supervisor Professor Mark Birch-Machin for his continuing support and guidance throughout my PhD. I would also like to thank my secondary supervisor Dr Jim Lloyd and industrial supervisor Dr Paul Matts for their interesting viewpoint, expertise and helpful discussions. Additionally I would like to express my gratitude to Dr John Oblong for all his help during my time at P&G Cincinnati.

Numerous individuals are mentioned throughout this thesis and I would therefore like to acknowledge their contributions. Further to this, without the much appreciated advice and assistance from both past and present members of dermatology the completion of this project would not have been possible. Namely: Dr Asif Tulah for his help with proof reading, Dr Trevor Booth for his microscope expertise, and Carol Todd for her patience and technical assistance. Specifically I would like to thank Dr Anne Oyewole for showing me the ropes, for her positive outlook, her endless supply of Polo's and for being a great friend.

I would additionally like to acknowledge the support of my friends and family throughout my PhD, in particular I am grateful to my parents for letting me return home during the week and stay with them for the last three and a half years. I would finally like to say a huge thank you to my husband Chris for always believing in me.

Contents

List of Figures

List of Tables

List of Abbreviations

ACN	Acetonitrile
ADP	Adenosine diphosphate
ALB	Albumin
ANOVA	Analysis of variance
ATP	Adenosine triphosphate
cDNA	Complementary deoxyribonucleic acid
CoQ_{10}	Coenzyme Q_{10}; Ubiquinone
CO_2	Carbon dioxide
CPD	Cyclobutane pyrimidine dimers
Ct	Cycle threshold
DHPLC	Denaturing high performance liquid chromatography
DMEM	Dulbecco's modified eagles medium
DMSO	Dimethylsulphoxide
DNA	Deoxyribonucleic acid
dNTP	Deoxyribonucleotide
DSB	Double strand DNA breaks
DUOX2	Dual oxidase 2
ECAR	Extracellular acidification
ECM	Extracellular matrix
EC_{50}	The dose of UVR needed to create 50 % cell death

EMEM	Eagle's minimum essential medium
ETC	Electron transport chain
e^-	Electron
FCCP	Carbonyl cyanide-ptrifluoromethoxyphenylhydrazone
FCS	Fetal calf serum
GPX5	Glutathione peroxidase 5
GSR	Glutathione reductase
HaCaT	High calcium and temperature immortalized keratinocyte cell line
HDFn	Human neonatal dermal fibroblast cell line
HEKn	Human neonatal epidermal keratinocytes
HKGS	Human keratinocyte growth supplement
H&E	Hematoxylin and eosin
H_2O	Water
H_2O_2	Hydrogen peroxide
H^+	Proton
IRA	Infrared A
IRB	Infrared B
IRC	Infrared c
IRR	Infrared radiation
J	Joule
KRT1	Keratin 1

MC1R	Melanocortin MC_1 receptor
MED	Minimal erythema dose
MLPA	Multiplex ligation probe-dependent amplification
MMP	Matrix metalloproteinase
MMP-1	Matrix metalloproteinase-1
MPTP	Mitochondrial permeability transition pore
MSRA	Methionine sulfoxide reductase A
mtDNA	Mitochondrial DNA
MTS	[3-(4,5-dimethylthiazol-2-yl)-5-(3-carboxymethoxyphenyl)-2-(4-sulfophenyl)-2H-tetrazolium, inner salt]
NADH	Nicotinamide adenine dinucleotide
NADPH	Nicotinamide adenine dinucleotide phosphate
NCF1	Neutrophil cytosolic factor 1
nDNA	Nuclear DNA
NER	Nucleotide excision repair
NFAT	Nuclear factor of activated T-cells
nm	Nanometer
NMSC	Non-melanoma skin cancers
NO	Nitric oxide
NOS2	Nitric oxidase synthase 2, inducible
OCR	Oxygen consumption
O_H	Origin of heavy strand replication

O_L	Origin of light strand replication
ONOO-	Peroxinitrite
OXPHOS	Oxidative phosphorylation
O_2	Oxygen
O_2^-	Superoxide radical
O2K	Oroboros Oxygraph-2k
PBS	Phosphate buffered saline
PCR	Polymerase chain reaction
P_i	Inorganic phosphate
P_H	Promoter of heavy strand transcription
P_L	Promoter of light strand transcription
PUVA	Psoralen + UVA
P&G	Procter and Gamble
QPCR	Quantitative real-time polymerase chain reaction
RANKL	Receptor activator of nuclear factor kappa-B ligand
RNA	Ribonucleic acid
RNS	Reactive nitrogen species
ROS	Reactive oxygen species
rRNA	Ribosomal ribonucleic acid
SED	Standard erythemal dose
SIS	Skin immune system

SPF	Sun protection factor
SSB	Single strand DNA breaks
TEAA	Triethyammonium acetate
TEA^+	Triethylammonium ion
TNF-α	Tumour necrosis factor-α
TPO	Thyroid peroxidase
tRNA	Transfer ribonucleic acid
UCA	Urocanic acid
UVA	Ultraviolet A
UVA1	Ultraviolet A 1
UVB	Ultraviolet B
UVC	Ultraviolet C
UVR	Ultraviolet radiation
VL	Visible light
W	Watt
XF	Extracellular flux
6-4 PP	Pyrimidine pyrimidone (6-4) photoproducts
8-OHdG	8-hydroxydeoxyguanosine
$^{\bullet}HO$	Hydroxyl radical

Chapter 1

Chapter 1 Introduction

Chapter 1 Introduction

1.1 Overview

The mechanisms of ageing are complex and still not completely understood but it can generally be defined as a reduced capacity of an organ to maintain a baseline tissue homeostasis and a decline in ability to adequately respond to physiological needs under stress (Sahin and DePinho, 2010). The physiological integrity of a cell relies on the integrity of its genome and therefore, due to the high turnover of DNA, there is a tendency for a progressive accumulation of damage over a lifetime. This has led to various studies focusing on DNA as a mechanism of ageing (Alexeyev *et al.*, 2004). As well as the nucleus, mitochondria also possess their own DNA (mtDNA) and have been indirectly linked with longevity. Both mtDNA mutations and deletions have been implicated in a number of human pathologies, and a cause and effect relationship between mutated and deleted mtDNA and ageing has been reported in various cell types (Birch-Machin *et al.*, 1998; Schroeder *et al.*, 2008). Specific examples include a higher prevalence of somatic mtDNA deletions in nervous and muscle tissue of aged individuals (Cortopassi *et al.*, 1992), in the associated tissues of age related degenerative diseases (Wallace, 1992) and in the skin cells of persons over the age of 60 (J. H. Yang *et al.*, 1994). Ageing has also been linked to inflammation, a reduced immune response as well as specific longevity genes (Tosato *et al.*, 2007). A further major link with ageing is the shortening of telomeres, which are repeats of the short-base sequence, TTAGGG, at the end of each chromosome. Telomeres prevent chromosome ends from being recognised as double strand breaks (DSB) and with every cell division a necessity of replications causes a loss of bases at the tip of the telomeres. This increasing telomere shortening means there is a limited number of cell divisions before a cell will become senescent (Gilchrest *et al.*, 2009). Furthermore, although the ageing of an organ tends to increase rapidly later in life, ageing can also be further aggravated by external factors. The theories of ageing are varied and therefore this thesis aims to focus on the association with DNA damage of specific external influences.

The exposed nature of the skin means that it is at more risk of environmental insults than most tissues, and the characteristics of aged skin such as wrinkles, laxity, uneven pigmentation, brown spots, and a leathery appearance are most prominent in areas of the body which are most exposed to ultraviolet radiation (UVR) such as the face and the hands (Figure 1.1). This suggests that these characteristics of ageing can be accelerated by UVR, an occurrence known as photo-ageing (Berneburg *et al.*, 2004; Schroeder *et al.*, 2008). It is therefore conceivable that exposure to UVR results in accumulation of mtDNA damage leading to an acceleration in the ageing process, a notion which has led to the development of mtDNA as a biomarker of UVR-induced damage by several research groups (Birch-Machin, 2000; Sligh *et al.*, 2002; Berneburg *et al.*, 2004). In relation to this, several studies have found an increase in incidence of specific deletions in mtDNA in sun-exposed skin as opposed to sun-protected skin (Birch-Machin *et al.*, 1998; Koch *et al.*, 2001; Krishnan *et al.*, 2004). In addition to this, damage to mtDNA can be induced *in vitro* by UVR-irradiation of cultured human skin cells and skin equivalents (Birch-Machin *et al.*, 1998; Birket and Birch-Machin, 2007).

A recent increase in exposure to both ambient and artificial UVR is related to changes in lifestyle, particularly those in industrialised nations (Berneburg *et al.*, 2004), and due to the increasing depletion of the ozone layer, irradiation of the skin by UVR is becoming more problematic. It can result in conditions such as erythema and hyperpigmentation and delayed changes such as cellular DNA mutations leading to carcinogenesis (Paz *et al.*, 2008), the latter of which are problems due to the long term exposure to UVR rather than chronological ageing (Birch-Machin *et al.*, 1998).

Although the action spectra of UVR-induced erythema and UVR-induced nuclear DNA (nDNA) damage have previously been investigated, UVR-induced mtDNA damage has not been studied. mtDNA has been established as a marker of UVR exposure in skin and has a strong association with ageing as well as skin cancer. Studying the action spectrum of UVR-induced mtDNA damage will provide important information about the mechanism of this damage, for its use as an aid tool for UVR exposure and UVR photo-therapy dosage and its potential use as a cancer biomarker. It will also aid in the evaluation of the efficacy of actives in cosmetics that serve to modulate sun damage.

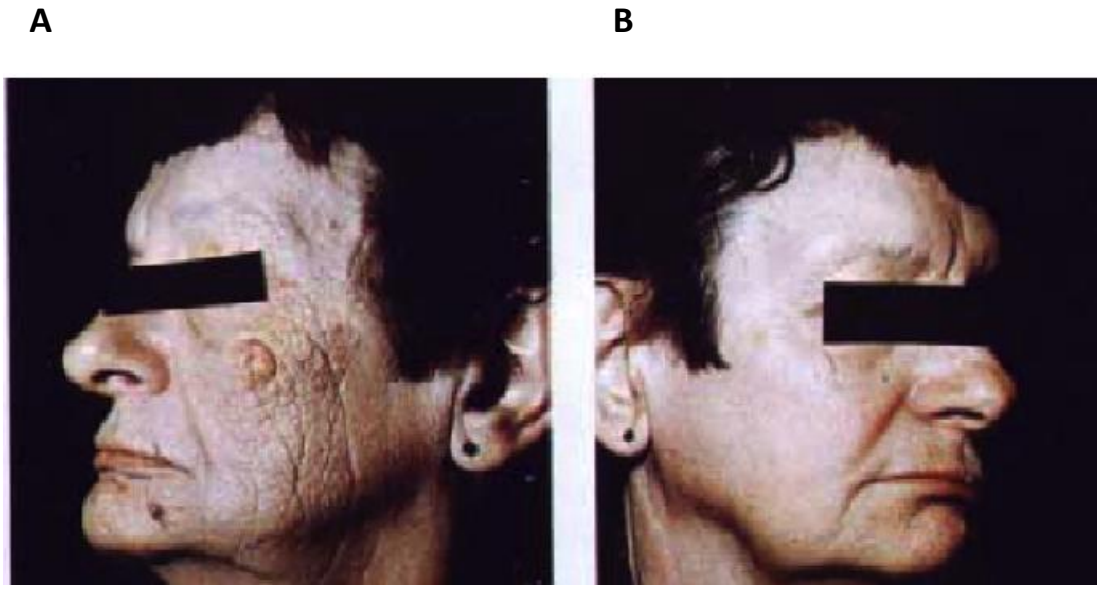

Figure 1.1: Photo-ageing versus Chronological Ageing. This image shows two sides of the same persons face whose occupation was as a taxi driver. (A) shows the effect of sunlight through an open window as opposed to (B) where there was not such an insult.

1.2 The Skin

The skin is the largest organ of the body, which forms a continuous external surface. It has a myriad of roles, these range from protecting the body from environmental insults to maintenance of water homeostasis (vital for normal physiology) and temperature regulation (Forslind and Lindberg, 2004). The skin is complex and multi-layered, consisting of numerous cell types and extracellular components and it also produces specific skin structures called appendages (hair follicles, sweat glands, sebaceous glands and apocrine glands) (Haake *et al.*, 2001). Two major components make up the skin; the upper layer known as the epidermis, and the lower layer dermis. These two defining layers are separated by the basal membrane which is a thin, extracellular matrix (ECM) structure mainly consisting of laminin, type IV collagen and heparin sulfate proteoglycan (Varani, 1998). There is also a third layer recognised which is known as the hypodermis; located beneath the dermis, this layer exists mainly as a fat store (Haake *et al.*, 2001) (Figure 1.2).

Skin is a useful tissue for research and is regularly used in scientific studies. Examples include wound repair, mechanisms of inflammatory and immunological tissue injury, the basis for benign and malignant hyper-proliferative diseases, as well as the natural ageing process (including the effect environmental insults (UVR) have on this process (Varani, 1998)).

1.2.1 The Epidermis

The epidermis is the layer of the skin that provides a barrier between the outside world and ourselves. This barrier prevents the penetration of chemicals and microbes and is also capable of withstanding mechanical force (Proksch *et al.*, 2008).

The epidermis is a stratified epithelium that is continually renewing itself. Keratinocytes (squamous epithelial cells) make up approximately 90-95 % of epidermal cells, and undergo a constant balance between proliferation and differentiation, or apoptosis. There are five typical divisions to the epidermis; the basal layer (stratum germinativum) is a single cellular layer closest to the dermis, the spinous cell layer (stratum spinosum) which is several layers thick, the granular cell layer (stratum granulosum) which also has several cells, the transition cell layer containing one cell and the cornified cell layer (stratum corneum) which contains 10 to 30 cell layers. The position in the epidermis and the state of differentiation of a keratinocyte is what determines the cells shape. The basal cell layer is where the epidermal stem cells are located and here the keratinocytes are cuboidal in form. As these cells migrate and differentiate to the stratum corneum they show a great change in structure. The resulting corneocytes of the stratum corneum become flat and anucleated, and these dead cells provide the skin with a protective layer (Gawkrodger, 1997; Haake *et al.*, 2001; Forslind and Lindberg, 2004).

Keratinocytes contain keratin intermediate filaments, which is a major structural protein. During the final stages of normal differentiation, the keratin filaments are aggregated into tight bundles aided by a matrix protein known as filaggrin. This is what causes the cell to collapse and flatten, and indeed the corneocytes are rich in keratin filaments and are surrounded by a cornified cell envelope which consists of both a protein and a lipid envelope (Proksch *et al.*, 2008).

As well as the keratinocytes, Langerhans cells, melanocytes and Merkel cells are the cell populations which make up the epidermis (Haake *et al.*, 2001). A more detailed overview of melanocytes can be found in section 1.5.1 . A detailed electron microscope image (A) and illustration (B) of the epidermis can be found in Figure 1.2.

1.2.2 The Dermis

The dermis is composed primarily of connective tissue, which provides the skin with its flexibility, elasticity and strength and it therefore contains fewer cells than the epidermis. Fibroblasts are the main cell type in the dermis and these cells synthesise collagen and elastin and other connective tissue. In addition to fibroblasts, dermal dendrocytes, mast cells, macrophages and lymphocytes can also be found in small numbers within the dermis. The dermis contains an unstructured fibrous extracellular matrix that surrounds the epidermal appendages, neurovascular networks, sensory receptors and the dermal cells. Interaction between the dermis and the epidermis occurs during development and enables the maintenance of the properties of both tissues (e.g. wound healing). The composition of the dermis can be predicted dependent on depth, but it does not undergo a series of differentiation matching that of the epidermis (Haake *et al.*, 2001).

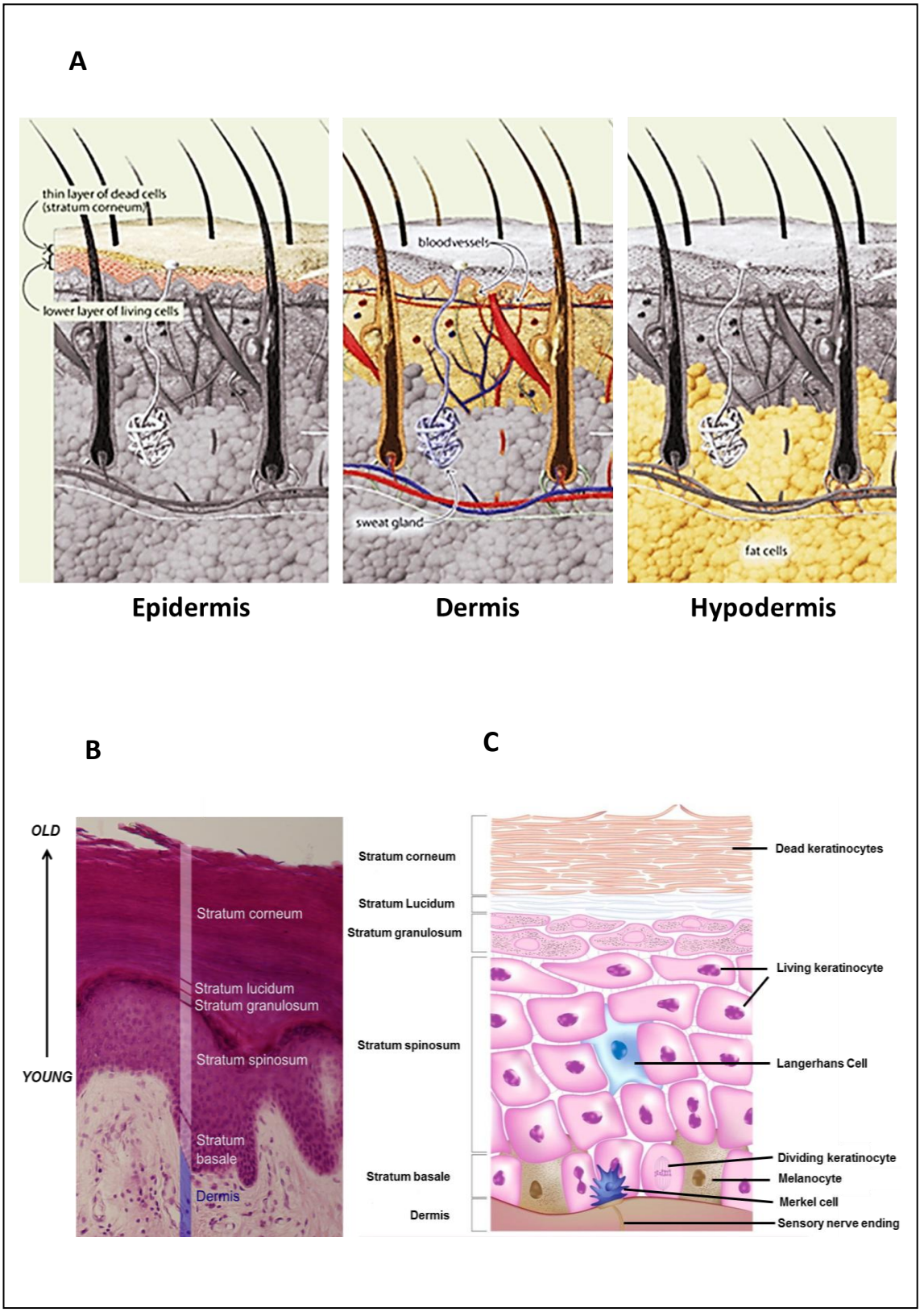

Figure 1.2: Cross Sections of the Skin. The principle layers of the skin, the epidermis, dermis and hypodermis are illustrated in (A) adapted from (Menton, 2009). A representational cellular H&E stain of the epidermis is shown in (B) and the different layers and associated cells of the epidermis are illustrated in a schematic (C) adapted from (Häggström, 2010; 4Below1, 2013) respectively. The age of a keratinocyte increases as they migrate to the surface of the epidermis.

1.3 Solar Radiation

The electromagnetic spectrum is what defines the division of various sources of radiation and is depicted in Figure 1.3 (A). The orderings are identified by the different wavelength or frequency of the radiation. Furthermore, the classifications of the electromagnetic spectrum can be determined by the energy its photons carry, and this decreases with an increase in wavelength (Anon, 1997). Within this study the different radiations will be referred to by their wavelength.

Relevant emissions from the sun include UVR, visible light (VL) and infrared radiation (IRR) and although only approximately 6 % of this is made up of UVR it is the main factor responsible for changes in the skins appearance. UVR lies between the VL and X-ray divisions of the electromagnetic spectrum, with wavelengths spanning 100 to 400 nm, which elicit varying biological effects. UVR is therefore further divided by wavelength into UVA (400-315nm), UVB (315-280 nm) and UVC (280-100 nm) (B. L. Diffey, 2002). Of the UVR emitted by the sun and which reaches the earth's surface, approximate measures of 6 % UVB and 94 % UVA can be made, although this is dependent upon various factors, including atmospheric and environmental conditions, time of day, season, altitude and latitude (Polefka *et al.*, 2012). The wavelengths of UVC are short and do not reach the earth's surface because they are completely absorbed by the stratospheric ozone layer and therefore this division of UVR has little biological importance (Lloyd, 2006; Birch-Machin and Wilkinson, 2008; Flockhart *et al.*, 2008; Paz *et al.*, 2008). Approximately 90 % of UVB is also absorbed, however ozone layer depletion has led to a rise in global UVR irradiance, meaning that the harmful effects of UVR are becoming more of a concern (Degruijl *et al.*, 1993; Paz *et al.*, 2008; Polefka *et al.*, 2012). The most abundant division of UVR which affects the skin is UVA, although it is thought to be less detrimental (Swalwell *et al.*, 2012).

In general, it is considered that shorter wavelengths of UVR (and therefore higher in energy) have a greater effect biologically and are more harmful to skin (Birch-Machin and Wilkinson, 2008). This is supported by the action spectrum of UVR-induced erythema where UVB radiation is more effective at causing erythema (reddening of the skin) than UVA. UVB radiation, however, cannot penetrate too deeply into the skin and mainly effects the upper epidermis of the skin and the cells which reside there (Paz *et*

al., 2008). UVA has the ability to penetrate deeper into the dermis, effecting epidermal cells as well as dermal fibroblasts and melanocytes (Berneburg *et al.*, 1999; Swalwell *et al.*, 2012) (Figure 1.3; B).

As well as UVR, the solar emissions of both VL and IRR penetrate deep into the dermal layers of the skin (Polefka *et al.*, 2012). An extensive review (Mahmoud *et al.*, 2008) found many studies had identified VL to cause various effects in the skin including erythema, pigmentation and reactive oxygen species (ROS) production. IRR has also been suggested to have an effect on the skin, even though it has a lower energy than UVR. IRA (a division of IRR), in particular, penetrates deeper into the skin than UVR where it is thought to elicit its effects (Maddodi *et al.*, 2012). Schroeder *et al.,* 2007 have reported IRA to cause an increase in intracellular ROS as well as an increase in the expression of matrix metalloproteinase-1 (MMP-1; involved in the breakdown of extracellular matrix, specifically collagens (Gebbers *et al.*, 2007)) in human dermal fibroblasts (Schroeder *et al.*, 2007). However the experimental practice of this study was criticised by Piazena and Kelleher, 2008 who suggested flawed irradiations of un-biologically high doses (Piazena and Kelleher, 2008). Furthermore, a similar study was unable to replicate the MMP-1 induction (Gebbers *et al.*, 2007).

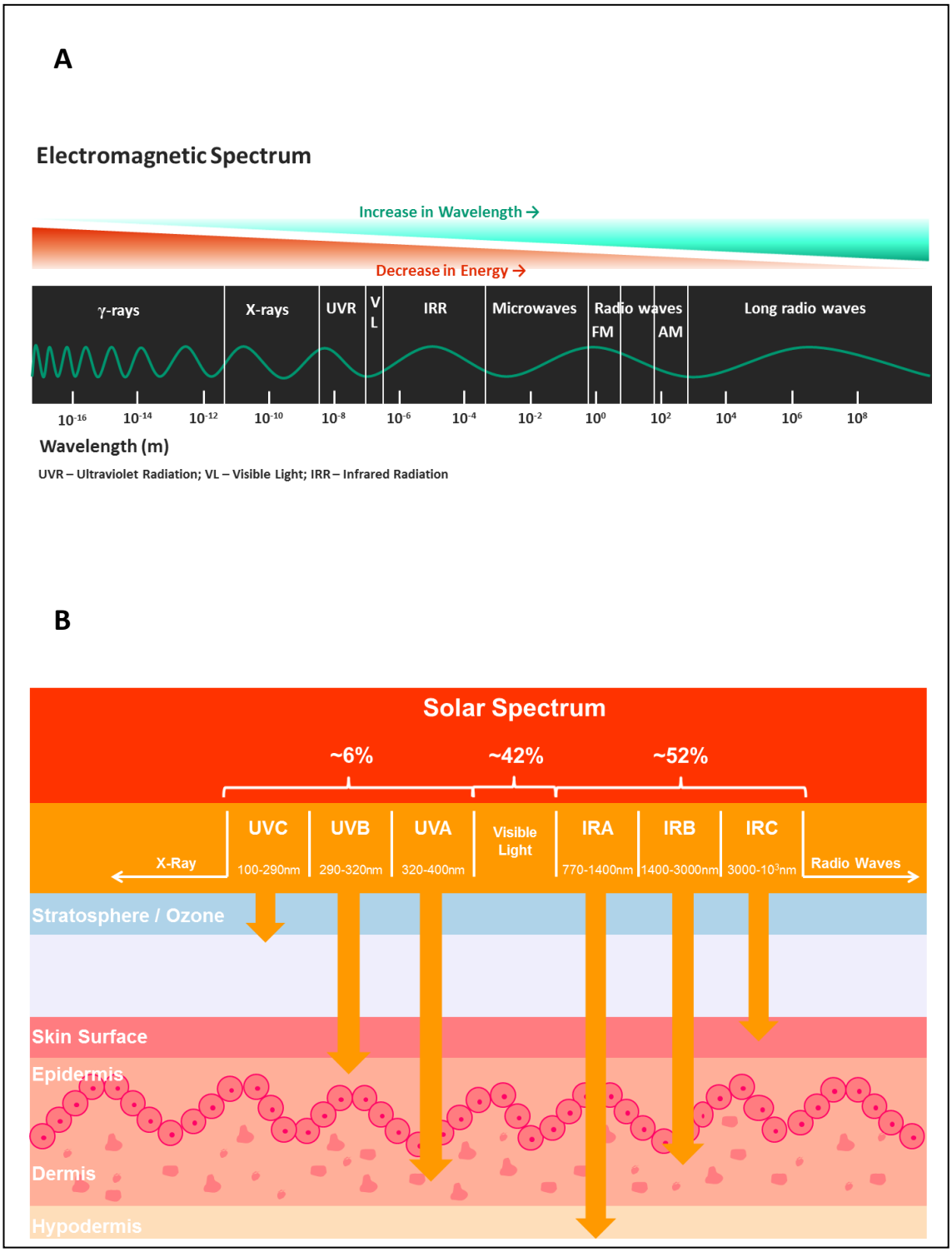

Figure 1.3: Images of the Electromagnetic Spectrum and Solar Spectrum Skin Penetration. Image (A) illustrates the divisions of the electromagnetic spectrum and (B) shows the solar spectrum and the penetration of UVR and IRR into the different layers of human skin.

1.4 Sources of UVR

UVR is generated naturally by the sun and occurs when a molecular electron is transferred from an excited state of high energy to a less active state. For this to occur artificially, the excitation is normally generated by passing an electrical discharge through a gas (Lloyd, 2006). Practically, the sun itself is not a valid tool in the use of photo-biological experiments. This is due to the previously mentioned varying factors (section 1.3), which mean that the UVR output of the sun is ever-changing. The varying wavelengths emitted by the sun can be mimicked using a solar simulator and more selective regions of the suns spectrum can be investigated with the aid of various UVR lamps. These UVR lamps can be described generally as UVA or UVB emitting. In reality, most of these lamps will emit UVA and UVB, as well as UVC, visible light and infrared radiation (B. L. Diffey, 2002). For a more specified wavelength of light, monochromators, which emit a very narrow selection of wavelengths, can be used.

Various UVR emitting lamps have historically been used, and continue to be used, in photo-therapy (Hoenigsmann, 2013), which is discussed further in section 1.5.5 . Artificial UVR is also used cosmetically, from common artificial tanning to utilisation within nail salons (Markova and Weinstock, 2013).

1.4.1 Measurement of UVR

Spectroradiometry is the fundamental way to characterise the emissions (spectral irradiance) of a particular light source (B. L. Diffey, 2002). A comprehensive description of this process can be found in the introduction to Chapter 3.

Confusion of usual radiometric and photometric measurements is quite common, however they are distinctly different. Photometry is solely the measure of VL, which is the radiation seen by the eye, and a quantification of illumination. Radiometry, on the other hand, measures the total power of a source (Anon, 1997). UVR can be quantified using radiometric terminology (Table 1-1). Addition of the prefix, “spectral”, enables these quantities to be expressed as a function of wavelength. The radiant flux is the total power emitted by the source and the irradiance is the radiant flux per unit area. The term radiant exposure can be loosely referred to as dose, and is the time integral

of irradiance (Anon, 1997; B. L. Diffey, 2002; Lloyd, 2006). Irradiance and radiant exposure can be used in a simple calculation in order to quantify the time of exposure to a particular source to gain a specific dose:

Exposure time (minutes) = Dose [1000 x J cm^{-2}] / Irradiance [60 x mW cm^{-2}]

Table 1-1: Radiometric Terms, Units and Symbols.

Term	Unit	Symbol
Wavelength	Nanometer (nm)	λ
Radiant Energy	Joule (J)	*Q*
Radiant Flux	Watt (W)	*W*
Radiant Intensity	Watt per steradian (W sr^{-1})	*I*
Radiance	Watt per square meter per sterdian (W m^{-2} sr^{-1})	*L*
Irradiance	Watt per square meter (W m^{-2})	*E*
Radiant Exposure (dose)	Joule per square meter (J m^{-2})	*H*

Adapted from (B. L. Diffey, 2002; Lloyd, 2006)

MED is the minimal erythema dose and can be measured for particular wavelengths (Parrish and Jaenicke, 1981). MED was commonly used as a measure of erythemal radiation, however it only measures an individual's erythemal response and does not give a standard value (B. L. Diffey, 2002). SED is the standard erythemal dose and measures a particular dose; this unit is progressively being introduced as it gives a standard number rather than MED. One measure of SED is equal to an erythemally effective dose of 100 J/m^2 (McKinlay and Diffey, 1987; Lloyd, 2006).

1.5 Effects of UVR on the Skin

Due to the exposed nature of skin and the inability of UVR to easily penetrate bodily tissues, it is the effect of UVR on the skin that is our primary concern. (Lloyd, 2006; Paz *et al.*, 2008). The most visual effect of UVR on the skin is the production of erythema, caused by the dilation of blood vessels (Mahmoud *et al.*, 2008), and the induction of pigmentation or "tanning". Another acute effect is temporary hyperplasia, of the stratum corneum, epidermis and dermis (Matsumura and Ananthaswamy, 2004).

Chronic exposure of the skin to UVR results in an acceleration in skin ageing and the development of tumours (Dayagrosjean *et al.*, 1995).

For UVR to initiate a biological effect it is absorbed by a biological molecule known as the chromophore (Lloyd, 2006). UVR is well known to have genotoxic effects most commonly associated with its damaging capabilities of DNA. In addition to its reactions with nucleic acids, UVR is also absorbed at specific wavelengths by other chromophores in the skin; known examples of which include urocainic acids, cofactors NADPH (nicotinamide adenine dinucleotide phosphate) and NADH (nicotinamide adenine dinucleotide), aromatic amino acids, tryptophan and tyrosine, riboflavins, porphyrins and melanins and their precursors (Maddodi *et al.*, 2012). On contact with the skin the energy of UVR is absorbed and transferred to the associated chromphore, which are wavelength specific. Following the absorption of the photons of energy, these entities will suffer a series of structural and chemical changes. The result is the UVR energy effect being dissipated; this means that the depth of penetration of UVR is dependent upon the absorption of different chromphores, and upon their position in the skin. The scattering of radiation can also effect the penetration of UVR into the skin (Mahmoud *et al.*, 2008). The shorter wavelengths of UVR, and therefore more energetic, tend to have a greater effect biologically, and are more harmful to skin. In terms of erythema production, the effect of UVB is 1000 times that of UVA (Birch-Machin and Wilkinson, 2008).

1.5.1 Pigmentation

Pigmentation in skin is determined by melanocytes, a secondary cell type found amongst keratinocytes in the basal layer of the epidermis. These cells synthesise melanin, which plays a crucial role in protecting the skin from UVR. Upon production, melanosomes are transferred by the melanocytes to the epidermis predominant keratinocytes. Within the keratinocyte, the melanin localises to the nucleus forming a protective cap by absorbing UVR and shielding the cellular DNA (Maddodi *et al.*, 2012).

The difference in skin pigmentation across the population is thought to be evolutionary by means of UVR protection balanced with a need for vitamin D synthesis (which is reduced by melanin absorption). Consequently high pigmentation occurred in

areas of annual sunshine whereas a lower pigmentation was associated with more seasonal parts. Indeed the influx of emigrants into Australia, for example, is associated with a high occurrence of skin cancers (Holman *et al.*, 1984). Furthermore, individuals whose melanin production is compromised, or redundant (i.e. in vitiligo, or albinism), have a higher rate of skin cancers. The pigmentation of an individual's skin is determined by over 100 genes; this coupled with determining effect of melanin in eye and hair colour as well as one's UVR responses has been characterised by the Fitzpatrick scale of skin photo-type classification. This scale identifies six distinct divisions: Type I-VI, the details of which can be found in Figure 1.4. A specific determinant of pigmentation is the melanocortin MC_1 receptor (MC1R); a G-protein coupled receptor, which is expressed in the melanocytes of the skin and hair. Polymorphisms of MC1R are common within the Caucasian population and are most generally linked with red hair colour, fair skin, poor tanning and increased risk of skin cancer (Beaumont *et al.*, 2011).

As well as genetically predisposed, pigmentation in the skin can be acquired upon induction by UVR. One immediate effect of UVR on the skin (5-10 min following exposure) is immediate pigment darkening which recedes shortly after. This is mainly UVA-dependent and occurs due to the oxidation and redistribution of pre-existing melanin and melanosomes, rather than increased melanin synthesis. A more delayed induction of pigmentation appears a few days after exposure and is longer lasting (up to weeks). This pigmentation is associated with both UVA and UVB and the delay is owed to the time taken to synthesise new melanin. The production of this melanin is the way our bodies act in an aim to protect against the harmful rays of UVR (Maddodi *et al.*, 2012; Videira *et al.*, 2013).

A

B

Fitzpatrick scale for skin-type classification

Skin type	Skin colour	Hair colour (darkest)	Eye colour (most common)	Description
I	White or very pale	Blonde	Blue, grey, green	Always burns, never tans
II	Pale white with beige tint	Chestnut or dark blonde	Blue	Always burns, sometimes tans
III	Beige to light brown	Dark brown	Brown	Sometimes burns, always tans
IV	Light to moderate brown - olive	Black	Brown	Rarely burns, always tans
V	Medium to dark brown	Black	Brownish black	Rarely burns, tans with ease
VI	Dark brown to black	Black	Black	Never burns

Figure 1.4: The Fitzpatrick Scale for Skin Type Classification. This figure shows a photographic representation of the Fitzpatrick scale (A), which is defined in the table below (B).

There are two distinct types of melanin; eumelanin (insoluble, black-brown in colour) and pheomelanin (soluble, red-yellow in colour). Eumelanin has the major photo-protecting capabilities, because, together with its precursors, it is able to act as an antioxidant, thereby reducing ROS. The levels of pheomelanin have been found to be consistently higher in lighter skin (Maddodi *et al.*, 2012; Videira *et al.*, 2013). There is evidence that melanin plays a dual role, not only as a photo-protector but also, conversely, as a photo-sensitizer. As well as it's UVR-filtering and ROS scavenging effect, melanin may increase the incidence of melanoma by an UVA-dependent mechanism (Swalwell *et al.*, 2012). Our group has provided evidence of this by showing an increase in damage of UVA-irradiated isolated mtDNA in the presence of melanin (Swalwell *et al.*, 2012).

1.5.2 Immune Suppression

The skin immune system has been labelled SIS and describes the participants in the skins immune function. There are numerous cell types involved in SIS and these include keratinocytes, monocytes, the epidermal homing T cells, the skin free nervous fibers, the dermal macrophage and the Langherhans cells (Amerio *et al.*, 2009). The Langerhans cells are the main antigen presenting cell in the skin and the keratinocytes produce various relevant cytokines. A complex interaction between these cells and numerous mediators, such as prostaglandins and the cytokines, completes the SIS and on exposure to UVR the function of this system is altered (T. Schwarz, 2005; Sreevidya *et al.*, 2010). The main immunosuppressive effects are the release of immune mediators such as platelet activating factor, tumour necrosis factor-α (TNF-α), interleukin-1β, prostaglandin E_2, RANKL (receptor activator of nuclear factor kappa-B ligand), histamine and neuropeptides (Gibbs and Norval, 2013). This is coupled with a reduction of Langerhans cells in the epidermis due to the emigration to the draining lymph nodes; this has been supported by detection of UVR damage in Langerhans cells in the draining lymph nodes (A. Schwarz *et al.*, 2005; T. Schwarz, 2005). Monocytes, macrophages and neutrophils have also been found to move into the skin at this stage (Gibbs and Norval, 2013). This is an effect which may be secondary to UVR-induced DNA damage (Matsumura and Ananthaswamy, 2004).

A major UVR chromophore in the skin is urocanic acid (UCA), which is a small molecule component of human skin (Laihia *et al.*, 2012). In the stratum corneum, trans-UCA is produced by the action $_{L}$-histidine ammonia lyase (histidase; HAL) has on histidine. Due to its UVR absorbing properties, UCA was used historically in sunscreens until an immunosuppressive effect was reported. Upon UVR irradiation, trans-UCA is isomerised to cis-UCA in the epidermis, and it is the cis isomer which causes the immunosuppressive effect of UCA, seemingly an effect due to ROS production (Gibbs and Norval, 2011).

Lindelof *et al*., 2000 found that following organ transplantation of various types there was an increase in the risk of developing skin cancer (Lindelof *et al.*, 2000). This has been shown numerous times and is due to the immunosuppressive treatment required with organ transplantation. This shows a clear link with the involvement of the immune system and carcinogenesis of the skin. This means that the damaging effect that UVR has on DNA may not be the only reason for skin cancer generation; its immunosuppressive effect also plays an important role (Dayagrosjean *et al.*, 1995; Matsumura and Ananthaswamy, 2004).

1.5.3 Skin Cancer

Exposure to UVR is the main cause of skin cancer, which can be divided into melanoma and non-melanoma. Non-melanoma skin cancers (keratinocyte carcinomas; NMSC) groups' basal cell and squamous cell carcinomas. These are the most common type of human cancers and the incidence of new diagnoses continues to rise year on year. These cancers fortunately are associated with a low metastatic potential and are, incidentally, readily treatable which means mortality rates are low (Madan *et al.*, 2010; Maddodi *et al.*, 2012).

The most severe of the skin cancers is malignant melanoma; as with NMSC the incidence of this cancer has increased substantially. Conversely, with this cancer, the mortality rates have also rapidly risen most notably in Europe and the USA (Swalwell *et al.*, 2012). Malignant melanoma is the 5th most common cancer in the UK and Cancer Research UK reported 12,818 new cases in 2010 (Cancer Research, 2011).

DNA acts as a chromophore primarily for UVB, absorbing four-fold more UVB than UVA (Maddodi *et al.*, 2012). The direct absorption of UVR photons produces dimeric photoproducts and wide DNA damage including protein-DNA crosslinks, thymine glycol and single strand DNA breaks (SSB). The most prevalent photoproducts are the cyclobutane pyrimidine dimers (CPDs) followed by the pyrimidine pyrimidone (6-4) photoproducts (6-4 PPs) (Ichihashi *et al.*, 2003). This leads to the induction of characteristic UVR-induced mutations commonly found within the p53 gene of UVR-induced cancer cells (Dayagrosjean *et al.*, 1995; Melnikova and Ananthaswamy, 2005; Paz *et al.*, 2008). Absorption of both UVA and UVB by other chromophores in the skin can lead to reactions with oxygen, which causes the generation of ROS and consequently oxidative stress. High levels of ROS have the ability to cause various forms of damage by the oxidation of DNA, proteins and lipids. One particular target is the DNA base guanine, which gives rise to 8-hydroxydeoxyguanosine (8-OHdG), a miscoding lesion leading to G to T transversion (Ichihashi *et al.*, 2003; Paz *et al.*, 2008; Birch-Machin and Swalwell, 2010). For more information about the induction of photoproducts and 8-OHdG please see the introduction to Chapter 6.

An inverse correlation between the amount of melanin and the induction of skin cancer including melanoma has been found. This has recently been further supported by Del Bino *et al.*, 2013 who found that the level of solar simulator UVR-induced photoproducts (specifically CPDs) were higher in lightly-pigmented skin as opposed to highly-pigmented skin types (Del Bino *et al.*, 2013). This possibly explains the susceptibility of certain skin types to melanoma. These melanoma-inducing effects are heavily associated with UVB irradiation; however our group has also provided evidence for UVA-induced damage in melanoma cells (Swalwell *et al.*, 2012).

1.5.4 Photo-ageing

The occurrence of ageing is well known to be a consequence of genetic factors as well as environmental influences. Genetic influences are well documented as the rate of ageing across different species varies substantially. Specific studies have also reported the identification of longevity genes which affect the lifespan in fruit flies, worms, and mice (Butler *et al.*, 2002).

Skin ageing is related to genetic (intrinsic) and environmental (extrinsic) factors, with UVR having a major effect. The differences between intrinsic and extrinsically aged skin can be distinguished at a clinical, histological and molecular level. The most visually (or clinically) apparent signs of extrinsic ageing are coarse wrinkles and pigment (age/liver) spots. This accelerating effect that UVR has on the skin is termed photo-ageing (Maddodi *et al.*, 2012). This effect is not owed solely to UVR, but also includes the exposure to tobacco smoke, airborne particulate matter, ozone, malnutrition and other solar wavelengths (Kohl *et al.*, 2011). The main contributions of the other solar wavelengths are owed to IRR (specifically IRA) which has been linked to extrinsic ageing in human skin (Kligman, 1982).

Interestingly, photo-ageing develops differentially across different ethnic groups. Caucasians see an initial severe wrinkling whereas the Japanese primarily acquire small pigments spots known as lentigines (Maddodi *et al.*, 2012).

Both UVA and UVB contribute to photo-ageing, however alterations within the dermis seem to be the fundamental cause. This means UVA has been identified to play a major role in photo-aged skin due to its ability to penetrate to the dermis (Kohl *et al.*, 2011; Maddodi *et al.*, 2012). Collagen and elastin are what provide the dermis with its firm structure (Fisher *et al.*, 1996), however UVA and UVB can induce the expression of matrix metalloproteinases (MMPs), which can degrade these proteins in the skin. Due to the structural nature of these proteins, the degradation of them is associated with the formation of wrinkles (Fisher *et al.*, 1996; Schroeder *et al.*, 2008). Furthermore, Sherratt *et al*., 2010 have found that UVB can directly alter the structure of, and mass distribution within, isolated fibrillin microfibrils, which are fundamental in mediating tissue elasticity (Sherratt *et al.*, 2010).

1.5.5 Beneficial Effects of UVR Exposure

Although the damaging effects of UVR are key to this investigation, it must be recognised that UVR can also provide a benefit. This includes the synthesis of vitamin D, the stimulation of hormones that regulate circadian rhythm and mood, as well as its usefulness in phototherapy (Polefka *et al.*, 2012).

Vitamin D is an essential precursor of the steroid hormone 1,25-dihydroxyvitamin D; essential for calcium absorption for bone development, growth and preservation. UVR stimulates the production of vitamin D by initial conversion of 7-dehydrocholesterol to pre-vitamin D, followed by a spontaneous conversion to vitamin D. Although vitamin D is available from our diet, foods such as eggs and fish only contain small amounts; this means our main source of vitamin D is from the sun. A reduced vitamin D intake can lead to detrimental bone conditions such as rickets (Utiger, 1998). In fact, rickets has actually been historically treated by phototherapy (Honigsmann, 2013).

There is an enjoyment found from spending time relaxing in the sun. A variation in sunlight exposure is thought to affect a person's mood and can be related to episodes of depression, a condition termed seasonal affective disorder (Ness *et al.*, 1999).

Phototherapy is widely used for the treatment of a variety of skin disorders, including: psoriasis, mycosis fungoides, vitiligo (a re-pigmentation of the skin) eczema, acne and atopic dermatitis (Matsumura and Ananthaswamy, 2004). Treatment can include the use of various UVR sources; initially the use of UVA as well as PUVA (the use of psoralen, with UVA) sources was common for treatments. UVB therapy was also found to be useful, particularly for clearing psoriasis, a common skin disorder (2 % prevalence worldwide) associated with phototherapy. UVR is thought to be so effective in clearing psoriatic plaques by reducing the excessive cell growth and by inducing apoptosis in the effected cells (Weatherhead *et al.*, 2013). Early treatment saw the use of broadband UVB lamp, with the more recent introduction of narrowband (311-312 nm) treatment solely delivering the most efficient psoriasis clearing wavelengths. UVA1 (340-400 nm) is a more recent introduction of UVR lamps used in phototherapy (C. Green *et al.*, 1992; Matsumura and Ananthaswamy, 2004).

1.6 Personal UVR Exposure Behaviours

As previously discussed, UVR is well known to be the leading cause of skin cancer. Reasoning behind the increase in the incidences, year on year, of skin cancer, is perhaps to be found within changes in sun exposure behaviours. A notable factor is regular travel to areas with a higher intensity of solar irradiation, or somewhere more "sunny". This has only been possible since the 1970s when flying became more

affordable. Furthermore, weekend trips outdoors and or spent in the garden on bright days has become more common and eating and drinking outside is largely in vogue. Our fashions have also changed, with more exposed skin now considered normal, but which was previously not acceptable (Roelandts, 2013). There have therefore been various sun exposure education campaigns released in an aim to decrease the risk of skin cancer. They tend to advise avoiding the sun at peak hours around midday as well as encouraging photo-protection by the use of sunscreens and clothing. As a result, most people are well aware of the damaging effects of UVR, however there is still a high sun-seeking population whom will seek sun exposure with the aim to sunbathe and tan (B. Petersen *et al.*, 2013; Roelandts, 2013).

Petersen *et al*., 2013 aimed to determine the effectiveness of such campaigns by monitoring the sun exposure behaviour of Danes over a one week winter holiday in a sunny location (B. Petersen *et al.*, 2013). For this the researchers utilised a personal electronic UVR dosimeter (worn on the wrist) combined with a data diary. They found that the majority spent most of the day outdoors and that the peak UVR exposure was between 11:00-13:00 h, meaning that the average total UVR dose accumulated to a high 57 SED. This was quite astonishing as the annual UVR exposure of a Danish indoor worker is only an average of 134 SED, showing a short sun holiday has a major influence. The study noted that the volunteers did show some compensatory behaviour by the addition of sunscreen on 85 % of the days; however the recommendations were largely ignored. They concluded that it may be necessary to employ a different method to change the activities of people who have a pro-tanning attitude (B. Petersen *et al.*, 2013).

Another type of UVR exposure is occupational, in which an individual's exposure is amplified by working outdoors. This type of exposure is linked with a higher incidence of NMSC when compared with indoor workers. A recent systematic literature review (Reinau *et al.*, 2013) found that occupational exposure was linked with low sun-protection and high sunburn rates, however sun exposure education campaigns have proven effective with these individuals.

The most worrying development within sun exposure behaviour is the use of artificial UVR to tan. The use of artificial UVR or indoor tanning was introduced in the 1970s,

and has increased in popularity. In the USA they are currently used by a reported ~1 million people per day (Balk *et al.*, 2013). Although these individuals know about the detrimental effect of UVR they continue to tan, believing that it makes their appearance more attractive and healthy (Balk *et al.*, 2013). Harrington *et al*., 2011 have suggested addictive-like behaviour for tanning as individuals continue to tan despite full knowledge of the harmful effects (Harrington *et al.*, 2011). The damaging effects of this type of UVR exposure are well known and various studies link the use of sun-beds with skin cancer induction (Bajdik *et al.*, 1996; Karagas *et al.*, 2002; A. Green *et al.*, 2007). In light of this, the UK government altered the legislation for sun-bed use in 2010, increasing the minimum age restriction to 18 (Tullo, 2010).

1.7 Sun Protection

Sunscreen is known to prevent the acute effects of UVR exposure such as the induction of erythema, the associated DNA damage and immunosuppression. It has also been shown to be useful in the avoidance of chronic effects including photo-ageing and some skin cancers (Lautenschlager *et al.*, 2007). Two main types of sunscreen are used, and they provide either organic (PABA derivatives, salicylates, cinnamates, camphor derivatives) or inorganic protection (titanium dioxide, Zinc oxide). Organic forms will absorb UVR and are mainly associated with UVB protection. Inorganic sunscreens provide a broader UVA and UVB protection by reflecting, scattering or absorbing UVR - the effect of which is dependent on wavelength (Serpone *et al.*, 2007; Kohl *et al.*, 2011).

The amount of protection a sunscreen can provide is measured by an entity known as its sun protection factor (SPF). This generally shows protection from UVB; it is defined as the sun UVR dose which produces 1 MED following an 2 mg/cm^2 application of sunscreen divided by the sun UVR dose required to produce 1 MED on unprotected skin. This means and SPF of 10 can filter out 90 % of UVB (Marks, 1995).

Sunscreens however, possibly have a negative effect on sun exposure. The use of a sunscreen could encourage individuals to stay in the sun for longer periods of time, as they believe that they are well protected. Sunscreen application is also associated with inadequate use, i.e. not enough or body areas missed. Interestingly, some case-control

studies have suggested an increased risk of melanoma with sunscreen use (B. Diffey, 2004).

1.7.1 Antioxidants

Mitochondria are a major source for the formation of free radicals and ROS, and this production can be exacerbated by UVR irradiation. Our skin has naturally occurring antioxidants including β-carotene, vitamin E, coenzyme Q_{10} (CoQ_{10}), ascorbic acid and nicotinamide to reduce the naturally forming ROS. However these endogenous antioxidants are insufficient when the skin is exposed to UVR, and therefore one way of restoring the antioxidant defence is by the use of exogenous antioxidants, either by topical application or orally (Kohl *et al.*, 2011). Due to the predominant production of ROS from the mitochondria, some individuals have sought investigations into selective mitochondria targeted molecules. These molecules are therefore designed to migrate to the mitochondria, where they accumulate, delivering their antioxidant capabilities; such examples include Mito Q (Murphy, 2004) and plastoquinone derivatives (Skulachev *et al.*, 2011).

A large proportion of an individual's cumulative UVR exposure is received in everyday life without sunscreen application, therefore oral antioxidant administration could prove an important protective factor (Kohl *et al.*, 2011). Recent evidence supports this notion and dietary antioxidants have been shown to provide further protection for the skin. One particular study by Rizwan *et al*., 2011, has investigated the protective effect of lycopene, an antioxidant found within red fruits and vegetables, particularly cooked tomatoes. This randomised clinical trial found that individuals on a diet rich in tomato paste were more protected from UVR-induced mtDNA damage compared to those not on the tomato-rich diet. In addition, the study showed more protection against erythema, a reduction in UVR-induced MMP-1 expression, abolished UVR-induced reduction in fibrillin-1 expression and an increased pro-collagen I deposition in the tomato paste supplemented subjects (Rizwan *et al.*, 2011).

Work within our laboratory has compared the effect of a panel of antioxidants on ROS induced damage in human skin cells, which showed a graded response. A particular

entity (Tiron) was found to provide complete protection and it was utilised for investigations in Chapter 6 (publication submitted).

1.8 Mitochondria

Mitochondria (Figure 1.5) are membrane-bound organelles found in most eukaryote cells, and which vary widely in size, shape and number. They are typically described as oval in shape, 3-4 µm in length and approximately 1 µm in diameter (Scheffler, 2008). However, when stained and examined with a light microscope, mitochondria are viewed as elongated and threadlike, and are not static but active, with continuing cycles of fission and fusion. Mitochondria are characterised by two membranes, the outer and the inner, which separate the inter-membrane compartment and the inner matrix compartment. The outer membrane is smooth and creates a boundary from the cytosol of the cell. The surface area of the inner membrane is increased by protruding into the matrix in multiple invaginations known as cristae (Wojtczak and Zablocki, 2008).

The main function of mitochondria is to produce the majority of the cells energy in the form of adenosine triphosphate (ATP) by oxidative phosphorylation (OXPHOS) via the electron transport chain (ETC) (Birch-Machin, 2006; Wojtczak and Zablocki, 2008). Of the polypeptides required for the respiratory chain to work, 13 are encoded for by mtDNA, which is independent of nDNA (Chinnery and Schon, 2003; Birch-Machin, 2006). In addition, mitochondria also have a key role in cell death (apoptosis) regulation and ROS production (Paz *et al.*, 2008).

mtDNA encodes genes for 2 rRNAs, 22 tRNAs, and 13 protein subunits, which are key components of the mitochondrial ETC complexes, with the exception of complex II, which is entirely nuclear-encoded. Therefore, any damage to the mtDNA can lead to defects in the assembly of the ETC complexes, which can ultimately lead to the loss of mitochondrial respiration. This means that the UVR-induced mtDNA damage can cause a dysfunction of OXPHOS. UVR can also directly affect the ETC which will enhance the deterioration (Dranka *et al.*, 2011).

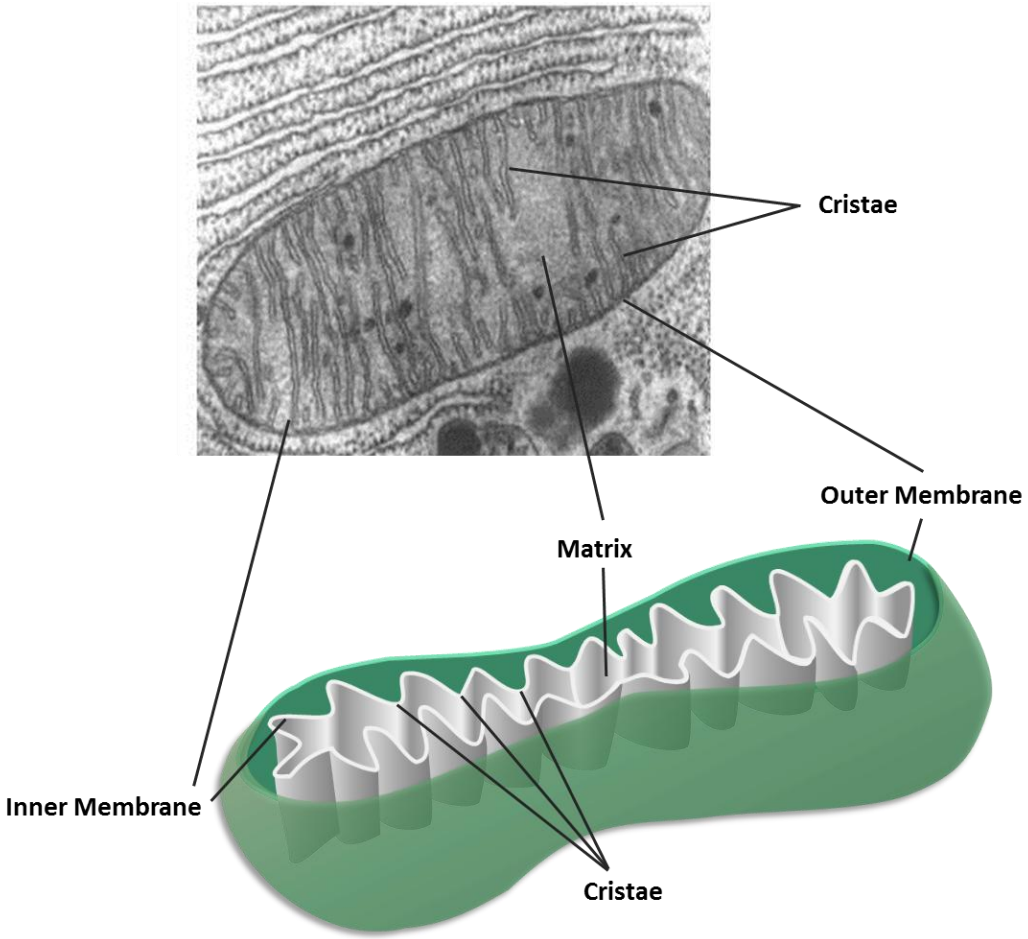

Figure 1.5: The Structure of a Mitochondrion. An electron micrograph of a mitochondrion adapted from (Fawcett, 1994) to identify the key structural components and a representative illustration.

1.8.1 Oxidative Phosphorylation

In the region of 90 % of the oxygen consumed by a eukaryote is used during OXPHOS, and this relates metabolic rate of a cell to mitochondrial function (Birch-Machin, 2006). For more information about the other cellular energy processes - glycolysis and the krebs cycle, please see the introduction to Chapter 5.

OXPHOS is a series of five protein complexes embedded within the inner mitochondrial membrane; these complexes are numbered I-V and are also named NADH-Q oxidoreductase, succinate-Q reductase, Q-cytochrome c oxidoreductase,

cytochrome c oxidase and ATP synthase respectively (Figure 1.6). Complexes I–IV represents the ETC and complex V is defined as the ATP synthase. Complex I and complex II receive electrons (e^-) from the krebs cycle and translocate these electrons to coenzyme Q, which then delivers the electrons to complex III. The electrons are then transferred to complex IV by the aid of cytochrome *c.* This is the final stage in the ETC and results in the reduction of oxygen (O_2) to water (H_2O). The energy created from this transfer of electrons is used to pump protons (H^+) across the inner mitochondrial membrane creating an electrochemical gradient, which is associated with complexes I, III, and IV. It is this resulting proton gradient that powers ATP synthesis, which condenses adenosine diphosphate (ADP) and inorganic phosphate (P_i) to form ATP (Wallace, 1992); this can be described as a coupling between the ETC and ATP synthesis. A translocation of protons from the intermembrane space to the mitochondrial matrix will lead to a dissociation of the ETC and ATP synthesis; a consequence of uncoupling proteins or other uncoupling mechanisms (Larsson, 2010).

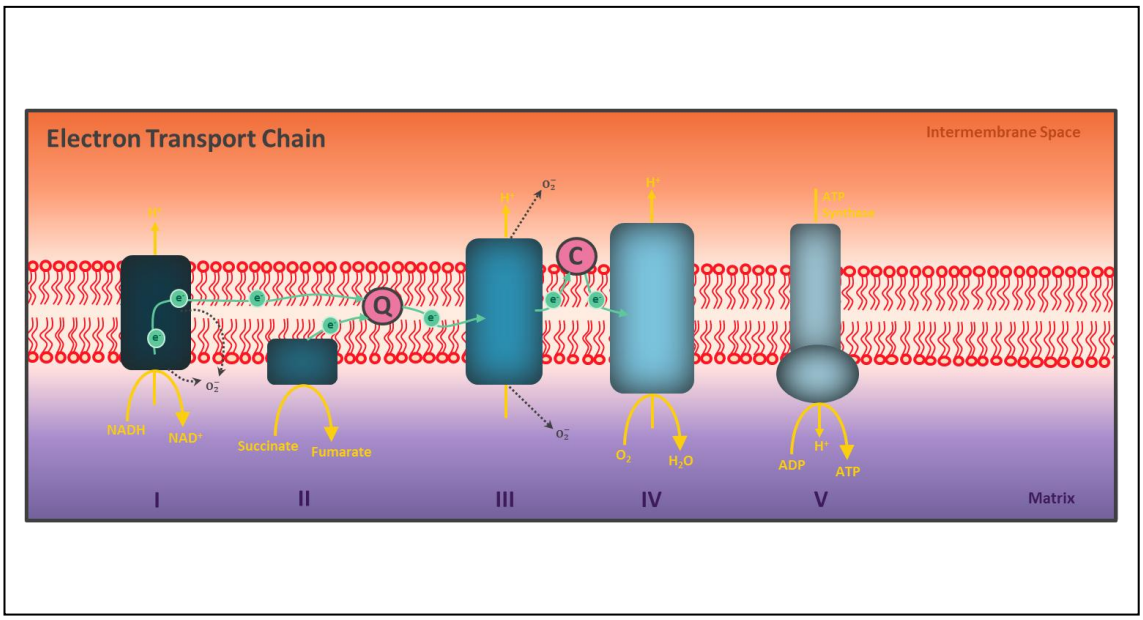

Figure 1.6: Oxidative Phosphorylation. OXPHOS takes place within the inner membrane of the mitochondria, and produces ATP by five multiple subunit enzyme complexes (I to V). The first four complexes make up the electron transport chain where electrons (e^-) are captured from donor molecules and are then transferred through the complexes I-IV. This is coupled with the pumping of hydrogen ions (H^+) to produce a gradient from which the potential energy is used by complex V (ATP synthase) to phosphorylate ATD to ATP. Q-coenzyme Q; C-cytochrome C.

Incomplete reduction of oxygen within the respiratory chain can cause the formation of the superoxide radical (O_2^-). This anion is charged and relatively unstable and is a key molecule in the initiation of pathways responsible for the production of ROS

(Birch-Machin, 2006; Shokolenko *et al.*, 2009). This molecule (O_2^-) is membrane-impermeable and is either released into the matrix compartment of the mitochondria or the inter-membrane space, depending upon the site in which it is produced. Due to the highly reactive state of (O_2^-), conversion to hydrogen peroxide (H_2O_2) is quick, either spontaneously or aided by superoxide dismutases. H_2O_2 is relatively stable and membrane permeable and freely diffuses throughout the cell, where it is the main mediator of oxidative stress. H_2O_2 generates the hydroxyl radical ($^{\bullet}HO$) by the Fenton reaction, which is a highly reactive molecule (Shokolenko *et al.*, 2009).

The mitochondrial respiratory chain is a major source of ROS production, but in normal metabolism ROS is only generated at low levels (Birch-Machin, 2006), and at these levels ROS have important roles as second messengers in activating transcription factors and promoting cell growth and differentiation (Paz *et al.*, 2008). The level of ROS is ordinarily regulated in a living cell with different stimuli controlling the expression of various antioxidant enzymes, including superoxide dismutase, glutathione peroxidase and catalase. It is when the antioxidant response is overwhelmed by high levels of ROS (as initiated by UVR) that damage to DNA and other vital entities occur (Paz *et al.*, 2008).

UVA and UVB have also been associated with the generation of the reactive nitrogen species (RNS), nitric oxide (NO). NO is an inducer of various physiological and pathological processes and has the ability to react with (O_2^-) and generate peroxinitrite (ONOO-), a strong oxidant and reactive substance. This molecule is able to cause distinct cytotoxicity of the cell by inducing protein nitration and nitrosylation, which adjusts the function of different crucial enzymes. NO is also able to reversibly inhibit cytochrome oxidase, complex IV of the respiratory chain, which plays an important role in the regulation of mitochondrial physiology (Poderoso *et al.*, 1996; Aitken *et al.*, 2007; Paz *et al.*, 2008).

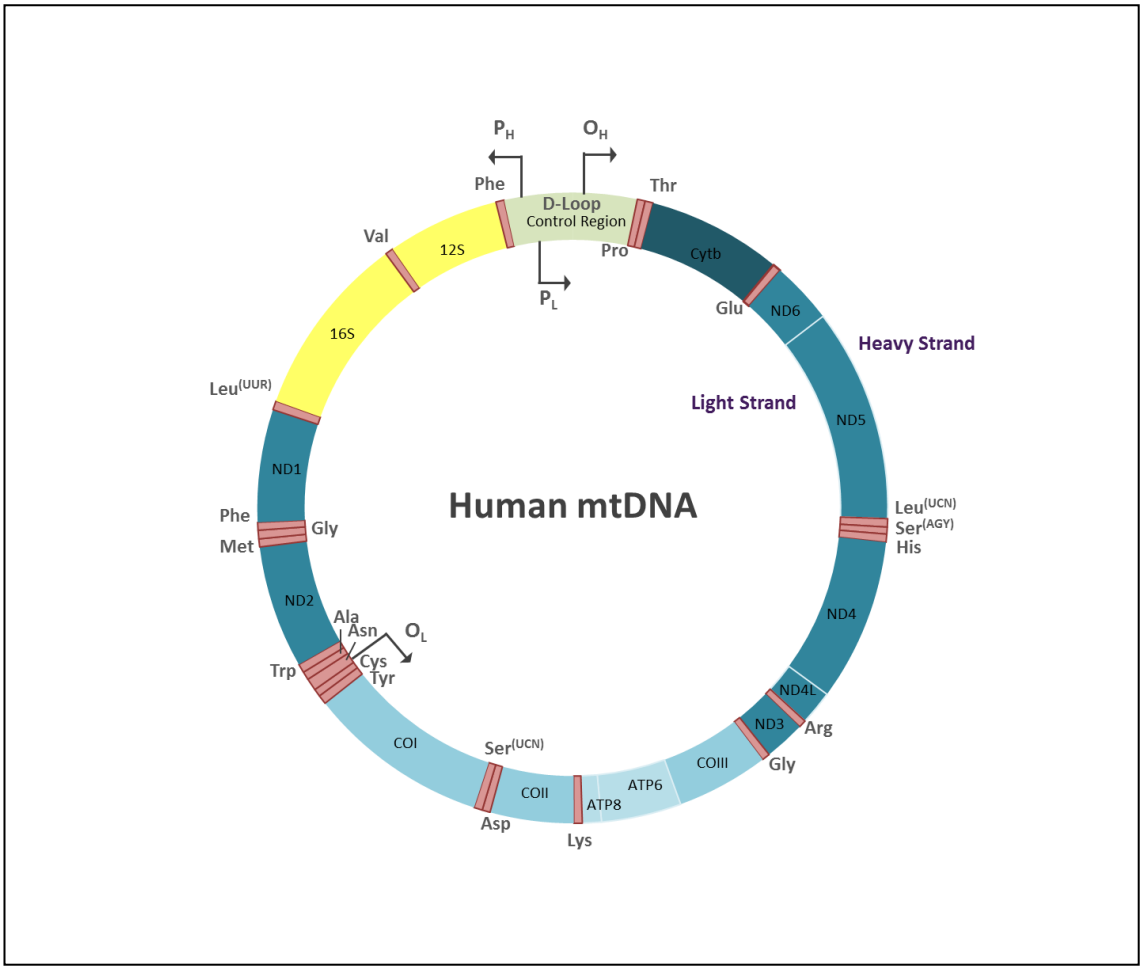

Figure 1.7: Human Mitochondrial (mt) DNA. Independent from nDNA, mtDNA is found in multiple copies per cell. Human mtDNA encodes for 13 subunits of the mitochondrial respiratory chain and are represented as follows: seven subunits of Complex I (ND1-6 and ND4L), one subunit of Complex III (Cytb), three subunits of Complex IV (COXI–III) and two subunits of Complex V (ATP6 and ATP8). Additionally mtDNA encodes for two rRNAs (12S and 16S, yellow), and 22 tRNAs required for the translation of these subunits (pink). The tRNAs are abbreviated to indicate the corresponding amino acid and are positioned on the strand which encodes it; light stand or heavy strand. O_H, origin of heavy strand replication; O_L, origin of light strand replication; P_H, promoter of heavy strand transcription; P_L, promoter of light strand transcription (Birch-Machin and Swalwell, 2010).

1.8.2 mtDNA

mtDNA (Figure 1.7) is present in multiple copies (10^3 – 10^4) per cell (Shadel and Clayton, 1997), they are double stranded, closed, circular in shape and 16,569-bp (Wallace, 1992). As well as encoding for the essential 13 polypeptides necessary for the complexes of the respiratory chain, mtDNA also encode 22 tRNAs and 2 rRNAs required for mitochondrial protein synthesis (Chinnery and Schon, 2003; Birch-Machin, 2006). Proteomic studies have estimated that, in general, mitochondria contain over 1000 distinct proteins; the additional proteins are encoded for by the nDNA and then imported into the mitochondria. These proteins include the remaining subunits

required for the respiratory chain, and those needed for mtDNA replication, transcription, translation and for mitochondrial maintenance (Scheffler, 2008; Birch-Machin and Swalwell, 2010).

Within the mitochondrial genome, there can be a mixture of both wild-type and mutant mtDNA; this occurrence is known as heteroplasmy (Birch-Machin, 2006). The performance of the cell is not altered because any detrimental effects created by mutated mtDNA can be compensated for by the wild-type mtDNA. However, a threshold level (50-60 % for deletions and 60-90 % for point mutations) does exist, and if this threshold is exceeded then cellular dysfunction occurs (Birch-Machin and Swalwell, 2010).

1.9 mtDNA Damage

Various mtDNA mutations are progressively being reported which are associated with mitochondrial disease (Chinnery and Turnbull, 2000), a number of which are involved with cancer and ageing (Chomyn and Attardi, 2003; Birch-Machin, 2006; Shokolenko *et al.*, 2009). Of these, there are several deletions and tandem mtDNA duplications which are associated with exposure to UVR (Birch-Machin, 2006).

1.9.1 Deletions

Deletions associated with mtDNA range in size from 2 kb up to almost 11 kb. Most of them can be found located in the major arc of the mitochondrial genome, between two proposed origins of replication (O_H and O_L); and they are never in the H-strand origin of replication (Krishnan *et al.*, 2008). The majority of these deletions are flanked with nucleotide repeats (5 to 18); only an approximate 15-25 % of the deletions are not associated with such repeats (Krishnan *et al.*, 2008; Tonska *et al.*, 2012).

The mechanism of the formation of mtDNA deletions is thought to be due to either replication or the activity of repair mechanisms. The likely cause is because of replication; two main hypotheses exist, a strand-asynchronous (strand-displacement) mode of replication, and a coupled leading-lagging strand replication (Krishnan *et al.*, 2004). The mechanism involving an intra-genomic recombination event via slipped strand mispairing, occurring due to direct repeats of DNA sequences flanking the

deletions, has been most commonly suggested (Schon *et al.*, 1989; Shoffner *et al.*, 1989; Berneburg *et al.*, 1999; Krishnan *et al.*, 2004). The proposal for the generation of deletions identifies that the direct DNA repeats renders the DNA to a susceptibility to bend. This facilitates the misannealing of these repeats and a loop formation of single-stranded DNA to open (Krishnan *et al.*, 2004). The mechanism for loop exclusion is thought to be ROS mediated SSB in the looped DNA (Berneburg *et al.*, 1999).

Some mtDNA deletions have been identified in sun-exposed human skin at higher levels than that of sun-protected skin (Schroeder *et al.*, 2008; Birch-Machin and Swalwell, 2010). The 4977 bp deletion, flanked by a 13 bp DNA repeat, is a major one of these deletions and is often termed the "common" deletion. The presence of this deletion in the mtDNA causes the removal of four genes for subunits of complex I, one gene for complex IV, two genes for complex V, as well as five genes for tRNAs (Shoffner *et al.*, 1989) (Figure 1.8)). The removal of these genes corresponds to the respiratory enzymes affected in the mitochondrial myopathy most associated, Kearns-Sayers syndrome; a rare neuromuscular disorder. The 4977 bp deletion is also common to various other mitochondrial disorders (Wallace, 1992; Birch-Machin *et al.*, 1998), and in approximately 50 % of single deletion cases, the 4977 bp is detected (Tonska *et al.*, 2012).

Another UVR associated deletion is the 3895 bp deletion, flanked by a 12 bp DNA repeat (Krishnan *et al.*, 2004), which has been connected with mitochondrial muscular disorders (Moraes *et al.*, 1992). This deletion has been found to be significantly increased in skin that had been exposed frequently to UVR, as opposed to skin that had been only occasionally exposed. Furthermore the 3895 bp deletion has been found at a greater frequency in samples from patients with NMSC when compared with the 4977 bp deletion (Krishnan *et al.*, 2004). The positioning of the 3895 bp is within the minor arc of the mitochondrial genome, an area less related with deletions. However, reasoning for the majority of deletions occurring in the major arc has been proposed as attributable to there being more possible deletion sites than the minor arc; i.e. more incidence of a direct repeat (Krishnan *et al.*, 2008). The genes affected by the presence of the 3895 bp deletion are two genes for complex I, two genes for rRNAs and five genes for tRNAs (Figure 1.8).

Other deletions have been linked with photo-ageing; the so called 3715 and 6278 bp deletions, for example, have been found at a similar level as the 4977 bp deletion in photo-aged skin (Eshaghian *et al.*, 2006). Yang *et al.*, 2004 have also identified a 7436 bp deletion as more prevalent in skin cancer and photo-aged skin than non photo-aged skin (J. H. Yang *et al.*, 2004).

The frequency of deletions in human skin (particularly the often reported 4977 bp and 3895 bp deletions) provides a desirable biomarker for cumulative UVR exposure.

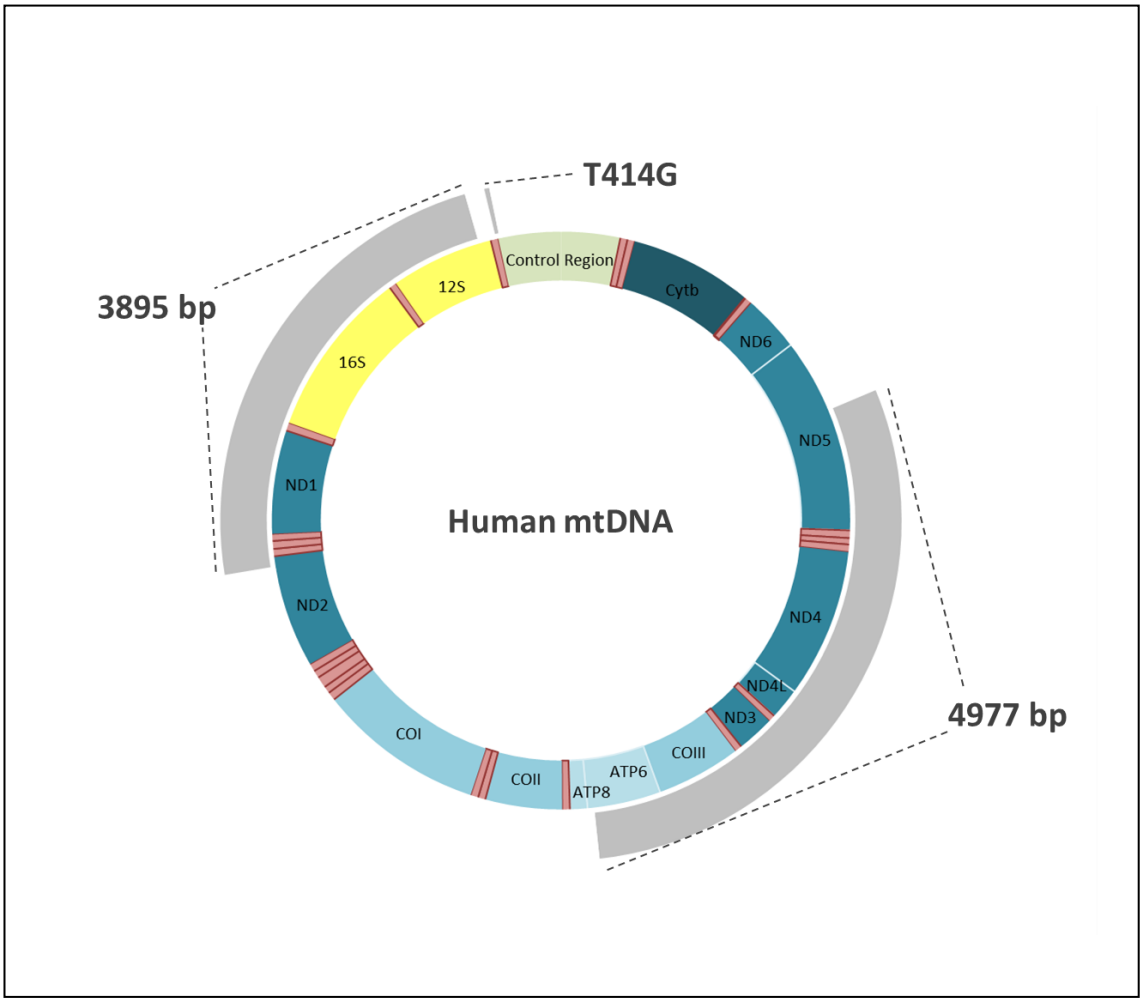

Figure 1.8: The Positioning of UVR-Induced Damage within Human mtDNA. The most common markers of UVR-induced mtDNA damage are illustrated in this figure. The figure also shows the sections of mtDNA affected by the deletions.

1.9.2 Point Mutations

Point mutations found within mtDNA have been identified in numerous tumour types (Polyak *et al.*, 1998; Eshaghian *et al.*, 2006). A link with mtDNA deletions and ageing has also been acknowledged; Michikawa *et al.*, 1999 initially recognised a particular

T414G mutation found within the control region of mtDNA (Figure 1.8) (Michikawa *et al.*, 1999). They found the T414G mutation in the dermal fibroblasts of more than 50 % of 14 genetically unrelated individuals over the age of 65 year of age. Such mutations were originally thought to be generated by means of ROS exposure and therefore the notion that they could be induced by UVR exposure was not unreasonable. Indeed, Birket *et al*., 2007 found this to be the case (Birket and Birch-Machin, 2007). However, in a follow up study, they found that this mutation was not related to ROS production in dermal fibroblasts, nor a consequence of mtDNA copy number (Birket *et al.*, 2009).

1.9.3 Strand Breaks

A major effect of UVR exposure is the formation of SSB and DSB. Furthermore, both of these types of DNA strand breaks have been implicated in the initiation and the progression of tumours. (Helleday *et al.*, 2007). The foremost initiator of the formation of direct SSB is ROS. SSB, as well as production of lesions such as photoproducts, can instigate the generation of DSBs post replication. A DSB can lead to the loss of a large amount of genetic material (Helleday *et al.*, 2007; Rastogi *et al.*, 2010). With this in mind, the quantification of strand breaks can therefore provide a good indication of the integrity of the genome. This type of UVR-induced damage is more easily detected *in vitro* than deletions, which are often less prevalent and require a repeated pattern of UVR exposure (Passos *et al.*, 2007).

1.9.4 mtDNA Damage Detection

Quantitative real-time polymerase chain reaction (QPCR) has been used successfully to determine genomic damage in multiple species and cell types. The assay works because any damage to DNA, such as that created by UVR (strand breaks, base modifications, bulky adducts, cross-links), will block DNA polymerase progression. This means damaged DNA will not be amplified, and therefore the amount of PCR product is inversely proportional to the amount of DNA damage. A downside to this method is that the type of DNA lesion is undistinguishable, and the amount of damage detected is only relative to the control sample. This is because the extent of endogenously generated DNA lesions is unknown (Jarrett *et al.*, 2013). This study uses various QPCR

methods to detect UVR-induced mtDNA damage; more specific details of which can be found in the introduction to Chapter 4.

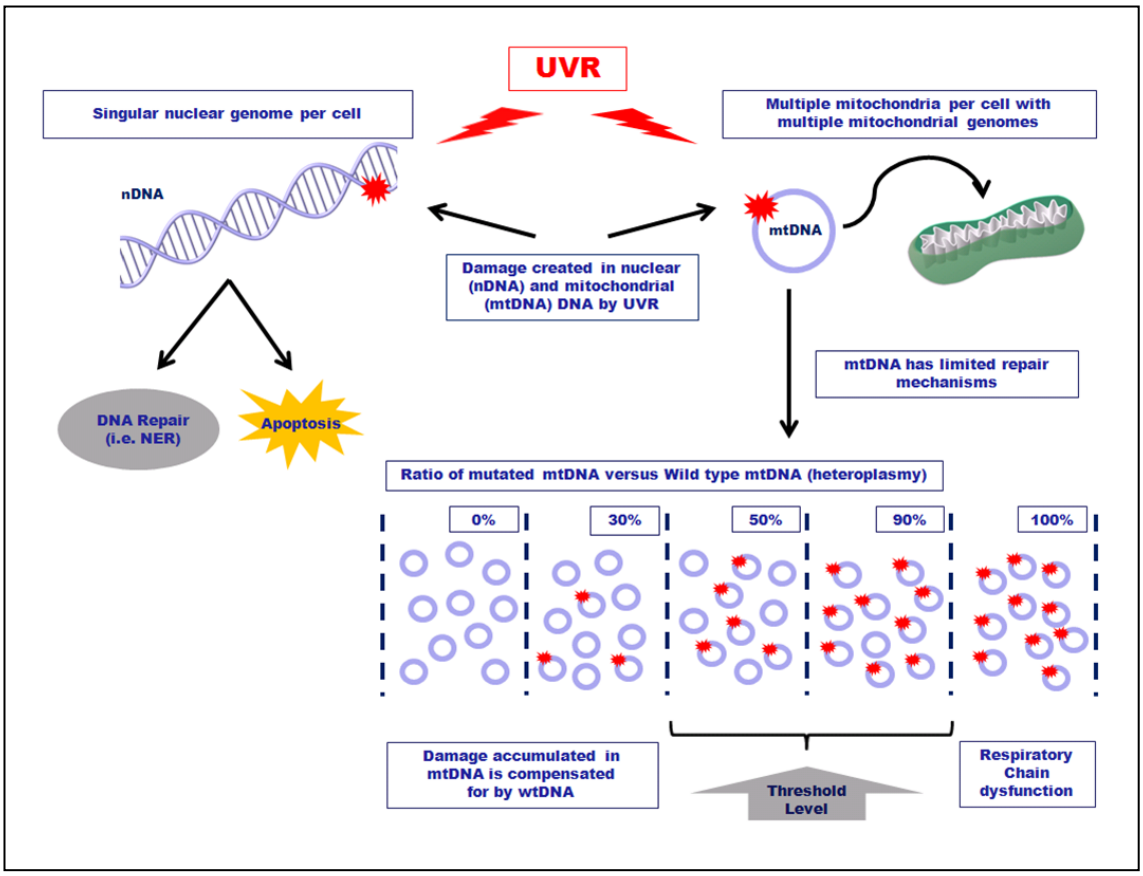

Figure 1.9: Damage to Cellular DNA by UVR and its Repair. UVR damage in nDNA can be repaired (in particular DNA photoproducts can be repaired by nucleotide excision repair (NER)), or if too severe will cause the initiation of pathways leading to cell death. In comparison to nDNA, mtDNA has limited repair mechanisms (i.e. no NER), and therefore damage in mtDNA can be accumulated over time and exposure. However, because there are multiple mitochondrial genomes within the mitochondrial reticular complex, any mutated mtDNA is compensated for by wild type mtDNA. The ratio of damaged to wild type mtDNA is an occurrence known as heteroplasmy and can range from 0-100 %. As the damage increases a threshold level for mutations is reached (50-60 % for deletions and 60-90 % for point mutations) and respiratory chain dysfunction occurs (Birch-Machin, 2000).

1.9.5 What makes mtDNA a Reliable Biomarker?

Unlike those found in nDNA, mtDNA has limited repair mechanisms and is therefore unable to repair UVR-induced damage such as photoproducts (Birch-Machin and Swalwell, 2010). This limited ability to repair, coupled with the ability to harbour mutated mtDNA without altering the function of the cell, is what makes mtDNA a reliable biomarker of UVR-induced damage (Birch-Machin and Swalwell, 2010). Figure 1.9 illustrates this incidence in more detail.

The production of ROS and RNS by UVR irradiation efficiently damages DNA, and due to the close proximity of the respiratory chain to mtDNA, damage here is hypothetically pronounced. Any mutations of mtDNA can progressively lead to dysfunction of the respiratory chain a consequence of which could lead to further production of ROS, resulting in further mtDNA damage. This is a vicious cycle, and in theory escalates levels of mtDNA mutations, which in turn causes a deficiency in the respiratory chain, which can lead to reduced energy production and, ultimately, tissue ageing (Schroeder *et al.*, 2008; Shokolenko *et al.*, 2009). The hypothesis, although a controversial theory, is strengthened by the research showing the increased incidence of mtDNA mutations in photo-aged skin (Birch-Machin *et al.*, 1998; Schroeder *et al.*, 2008).

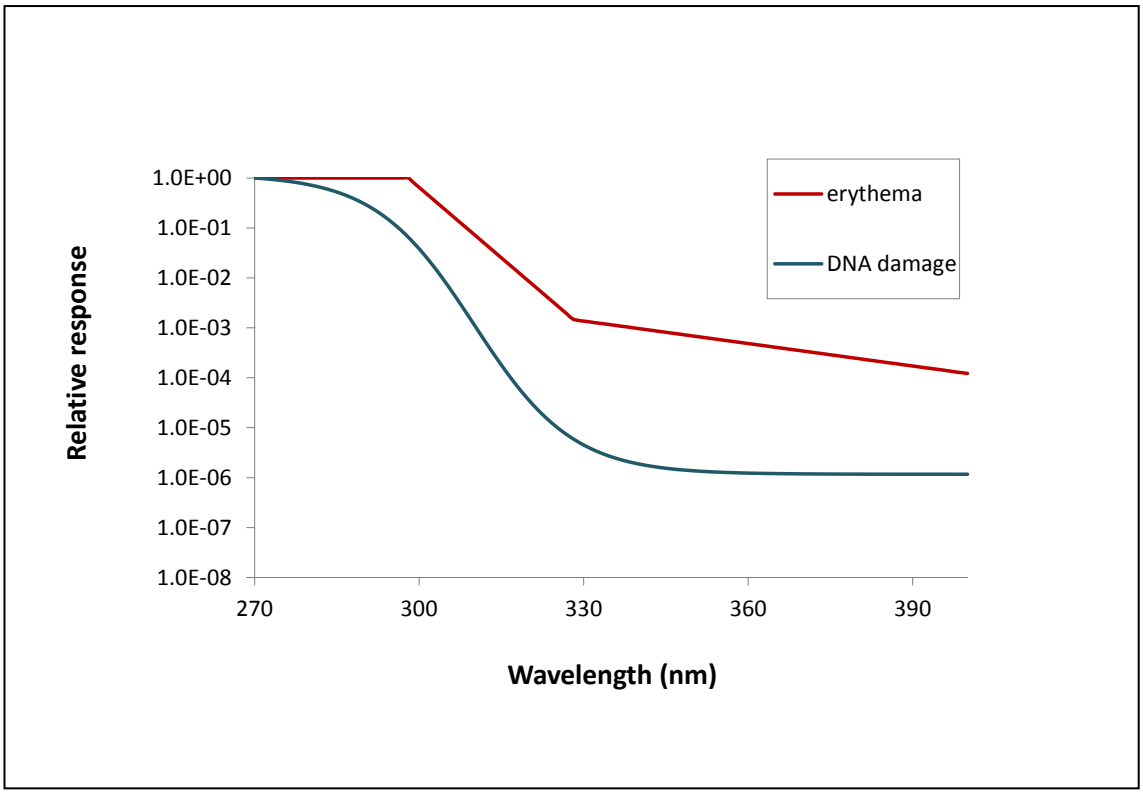

Figure 1.10: Action Spectra of UVR-Induced Erythema and nDNA Damage. The action spectra of UVR-induced erythema and nDNA damage are illustrated in this figure for reference. The image is adapted from (McKinlay and Diffey, 1987) and (Setlow, 1974) respectively.

1.10 What is an Action Spectrum?

An action spectrum shows the effectiveness of the different wavelengths of light which cause a given biological effect (Degruijl *et al.*, 1993; Lloyd, 2006). The various detrimental effects of UVR on the skin are largely related to wavelength. However UVR

also has therapeutic potential and is used in the successful clearing of the skin disorder psoriasis, an effect that is dependent on wavelength. It is therefore important to determine wavelength specific responses (Flockhart *et al.*, 2008).

The action spectrum of UVR-induced nDNA damage (Setlow, 1974) and erythema (McKinlay and Diffey, 1987) have previously been determined and are illustrated in Figure 1.10. Various other UVR wavelength dependencies associated with the skin have been verified, such as those related to non-mammalian carcinogenesis (Degruijl *et al.*, 1993), later predicting its relevance to human carcinogenesis (de Gruijl and Van der Leun, 1994). Further interest has included an investigation comparing the wavelengths involved in nDNA damage with those associated with erythema induction (Young *et al.*, 1998).

To determine an action spectrum, various light emissions (for this study UVR) are required, to account for wavelength differences. A monochromator only emits specific narrow wavelengths of radiation, and therefore may seem like the obvious choice for studying the effects of individual wavelengths. However a 5 nm distribution is still present with emissions of a monochromator, this shows a lack of complete specificity; furthermore the irradiance of a monochromator is very low. Although the use of a monochromator is entirely acceptable, due to the associated narrow and low irradiance, this method proves extremely time consuming. A more efficient method has been validated by Flockhart *et al*., 2008 who were interested in determining the action spectrum of UVR-induced NFAT (nuclear factor of activated T-cells) activity (Flockhart *et al.*, 2008). This method encompasses various UVR-emitting lamps, which overlap and cover the entire UVA and UVB spectrum. Although lamps emitting UVR are not very selective in terms of wavelength, the spectral irradiance of each UVR-emitting lamp can be measured. A graph of this sort can then be used to specify a particular distribution of the emitted radiation (B. L. Diffey, 2002). Figures taken from the Flockhart study, for reference, are shown in Figure 1.11. This data shows the extent of a particular biological effect from a particular UVR source (A) and the same effect plotted as an action spectrum (B) (Flockhart *et al.*, 2008). The combination of the known UVR-spectral distribution and the proposed action spectrum can be used to predict a biological response. The difference between the experimentally observed response and the predicted response can be used to refine the proposed action

spectrum. Further interactions can minimise these differences in order to obtain an action spectrum that explains the observed data. The resolution and stability of the solution depends on the choice of lamps, the size of experimental error and the degree of smoothing in the solution.

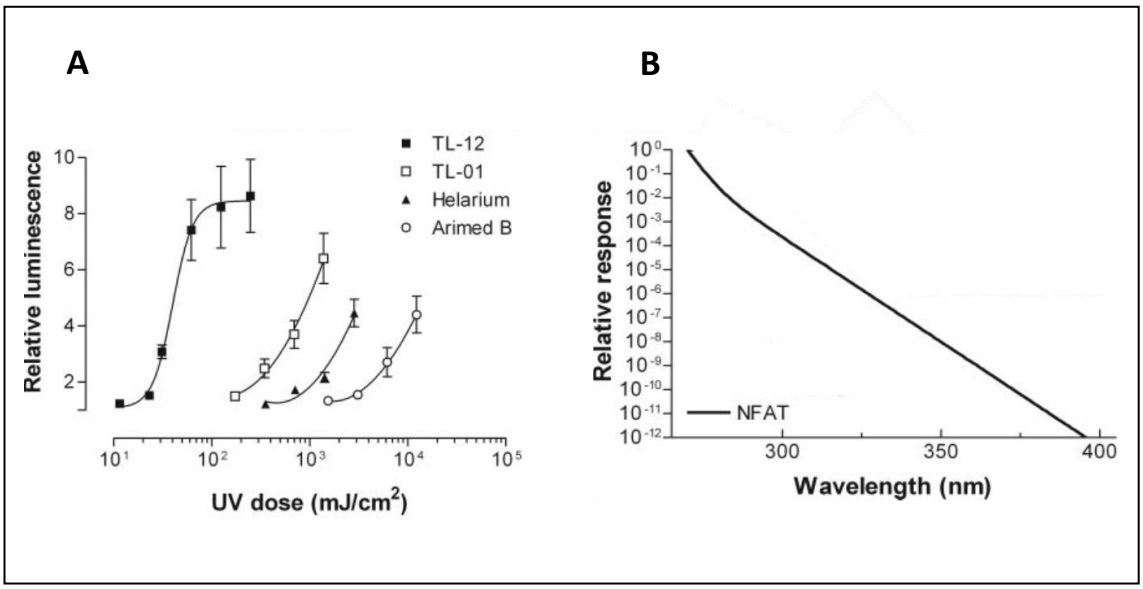

Figure 1.11: Determination of an Action Spectrum. The extent of a particular biological effect (in this case transcriptional activity of NFAT) from a particular UVR dose (A) can be used to plot the action spectrum (B). This shows the effectiveness of the different wavelengths of UVR radiation which cause a given biological effect (Flockhart *et al.*, 2008). TL12,TL01, Helarium and Arimed B are all UVR sources which emit different wavelengths of light, and of which are also utilised within this thesis.

1.11 Aims

The action spectra of UVR-induced detriment of various skin associations have largely been investigated. However the action spectrum of UVR-induced mtDNA damage has not been studied. Knowledge of this kind would be desirable due to the fact that damage within mtDNA is an established marker of UVR exposure in skin. The major aim of this thesis is therefore to determine the action spectrum of UVR-induced mtDNA damage. This will entail the fitting of a correct model which will best describe the data.

This study will aim to provide important information about the mechanism of this damage, for its use as an aid tool for UVR exposure and to help monitor the long-term safety of UVR photo-therapy. It will also assist in the evaluation of the efficacy of actives in cosmetics that serve to modulate sun damage. Furthermore, identification of

specifically damaging wavelengths could lead to alterations in how we protect our skin from the sun.

Subsequent aims to this were to identify other UVR-induced cellular effects in human skin such as nDNA damage and changes in cellular respiration. These differential effects could produce quantitative assessment of detrimental UVR effects. Such methods are necessary for the evaluation of UVR-protecting/UVR damage modifying treatments. Therefore the usefulness of these assays for this type of investigation will be evaluated by the utilisation of potential actives.

Chapter 2

Materials and Methods

Chapter 2 Materials and Methods

The methods found within this chapter are described as general, and are applicable throughout this thesis. More chapter specific methods are presented in individual method sections within each data chapter.

2.1 Cell Culture

2.1.1 HaCaT and HDFn Cells Lines

The immortalized human skin keratinocyte cell line (Boukamp *et al.*, 1988), HaCaT (a kind gift from Dr. N. E. Fusenig), and the human neonatal dermal fibroblast cell line, HDFn (Invitrogen, UK), were maintained in Dulbecco's modified eagles medium (DMEM; Lonza, UK) containing 10 % fetal calf serum (FCS; Lonza, UK) and 1 % penicillin;streptomycin (Lonza; UK), at 37 °C with 5 % CO_2. The cells were passaged every 3-4 days (HaCat) or 6-7 days (HDFn), when they reached 80-90 % confluence.

2.1.2 Primary Keratinocyte Cells

Human Primary Keratinocyte cells were obtained from patient samples from the RVI, Newcastle. Cells were maintained in EpiLife medium (Gibco, UK) supplemented with 0.2 % Human Keratinocyte Growth Supplement (HKGS; Gibco, UK) and 1 % penicillin;streptomycin (Lonza, UK) at 37 °C with 5 % CO_2. The cells were used experimentally at passages 1-3.

2.1.3 Long Term Storage of Cells

For long term storage cells were trypsinised and then re-suspended in DMEM, centrifuged at 300 RCF for 5 min and supernatant was removed. Cells were then re-suspended in a solution of 10 % dimethylsulphoxide (DMSO) diluted in FCS and transferred to 2 ml cryovials (Helena Biosciences, UK). Cells were then stored at -80 °C for short term and before long term storage in liquid nitrogen.

Following long term storage, cells were thawed rapidly before transfer to 10 ml DMEM heated to 37 °C in a tissue culture flask. Cells were incubated at 37 °C with 5 % CO_2 for 24 h and then DMEM was replaced. Cells were cultured for a minimum of one week before any experimental procedures.

2.2 Irradiation Methods

Except where otherwise stated, 24 h prior to irradiation cells were seeded into 60 mm dishes where they were grown to confluent monolayers. Cell lines were grown in phenol red free DMEM (Lonza, UK) supplemented with 10 % FCS and penicillin;streptomycin and Primary Keratinocytes were grown in their normally supplemented EpiLife medium; at 37 °C with 5 % CO_2.

2.2.1 Acute Dose

Prior to irradiation, medium was removed and cells were washed with phosphate buffered saline (PBS). Then either phenol red free DMEM – FCS (cell lines) or PBS (Primary Keratinocytes) was added and the lids of the dishes were removed. For the mock control, cells were covered in aluminium foil and placed under the lamps for the same duration as the irradiated cells. The cells were irradiated with various UVR sources, as follows: Germicidal, TL12, UV6, TL01, Helarium, Arimed B, Cleo ± filter (a more detailed description of each source can be found within Chapter 3). The dose ranges used, expressed as total UVR, were approximate as follows: 0.005-0.2 J/cm^2 (Germicidal), 0.01-3 J/cm^2 (TL12), 0.1-4 J/cm^2 (UV6), 0.1-14 J/cm^2 (TL01), 0.3-30 J/cm^2 (Helarium), 1-73 J/cm^2 (Arimed B), 4-74 J/cm^2 (Cleo – filter) and 3-37 J/cm^2 (Cleo + filter). Following UVR treatment medium was removed and the cells were washed with PBS before further analysis.

2.2.2 Repeat Dose

Repeated UVR exposure was required to induce mtDNA specific deletions. Various regimes were undertaken, the most successful of which is outlined in this section. HaCaT and HDFn cells were utilised for these investigations. When not irradiated, cells were kept under normal cell culture conditions (with the exception of media; phenol

red free DMEM + FCS was used) and samples were intermittently taken during ordinary cell passage. Mock control cells were subjected to the same conditions only they were covered in aluminium foil when placed under the lamps. Prior to each irradiation cells were washed with PBS and then, due to short irradiation exposures, were irradiated in PBS. The cells were irradiated on alternate days with various UVR sources and doses, expressed as total UVR, as follows: ~0.2 J/cm^2 TL01, ~0.5 J/cm^2 Helarium, ~2 J/cm^2 Arimed B, ~7.5 J/cm^2 Cleo – filter and ~19 J/cm^2 Cleo + filter. With the Cleo + filter UVR source, a single dose of 19 J/cm^2 proved too harsh; therefore this dose was split into three smaller doses per each alternate day. Following irradiation PBS was replaced with phenol red free DMEM + FCS.

2.3 DNA Extraction

Following treatment cells were trypsinised and removed by scraping. DNA was extracted using QIAamp DNA mini kit as per manufacturer's instructions (Qiagen, UK).

2.4 Quantification of DNA

The total concentration of DNA in each sample was quantified using the Nanodrop ND-100 (Nanodrop technologies, UK). Each DNA sample (1 ul) was pipetted onto the spectrophotometer. Dilutions of each sample were made up in high molecular grade water (Sigma, UK).

2.5 Quantitative PCR of 11 kb Amplicon

The degree of damage created by the differing amounts and types of UVR was investigated by PCR amplification of an 11 kb amplicon of mtDNA. The PCR was performed in 50 µl reactions containing: 200 ng template DNA, 10 mM buffer, 10 µM of each primer, 5 x SYBR Green, 10 mM dNTP (deoxyribonucleotide), 3.75 units of Expand Long Template enzyme (Roche, UK) and made up to the required volume with high grade PCR water. The primers used are found in Table 2-1 (Kleinle *et al.*, 1997). The cycling conditions were 94 °C for 2 min, 10 cycles of 15 sec denaturation at 94 °C, 30 sec annealing at 60 °C and 9 min extension at 72 °C; then 25 cycles of 15 sec

denaturation at 94 °C, 30 sec annealing at 60 °C and 8.5 min extension (+10 sec/cycle) at 68 °C (Passos *et al.*, 2007).

The analysis of the reactions was carried out on either the MJ Chrom4 (Bio-Rad) and the ABI Prism 7900HT (Applied Biosystems) PCR machines, which have been previously shown within our group to give comparable results.

Table 2-1: Long PCR Primers for Damage Detection within an 11 kb Amplicon.

Target	Name	Oligonucleotide Sequence (5' → 3')
11 kb	D1B	5'-ATG ATG TCT GTG TGG AAA GTG GCT GTG C-3' (282-255)
11 kb	OLA	5'-GGG AGA AGC CCC GGC AGG TTT GAA GC-3') (5756-5781)

Detection was via SYBR Green technology. Primers purchased from MWG, UK.

2.6 Analysis of mtDNA Damage

Cycle threshold (Ct) values were obtained by PCR analysis. Differences in Ct value compared to the control were calculated and expressed as a percentage. These values were obtained for each UVR dose received, and were then combined to produce dose curves of damage which were fitted in excel with a three parameter sigmoid plot of the form:

$$Ct = \frac{a}{1 + \exp - ((Log10\ dose - EC50)/\ b)}$$

Where a = maximum effect and b = slope.

The solver function within excel was used to find the minimum sum of the squared differences between the data and the fit.

Chapter 3

Results 1 - Optimisation

Chapter 3 Results 1 - Optimisation

3.1 Introduction

This chapter focuses on preliminary and optimisation experiments required to ensure accuracy, determine doses and discover potential variables associated with the future experiments. Within this thesis, various UVR emitting sources were used and these are commonly defined as “UVA lamps”, “UVB lamps” or “UVC lamps”. This is not an accurate or adequate description because UVR sources, although generally predominant in one of the UVR divisions, will as a majority emit a mixture UVA and UVB, and even UVC. The correct way to specify the emitted radiation is therefore by determining the spectral output (B. L. Diffey, 2002). Taking this in to consideration as well as the need for determining specific wavelength effects, a major aim of this chapter was to ascertain the spectral output of the UVR sources utilised in the bulk of the experiments within this thesis. Measuring the spectrum of radiation emitted by a particular source uses a procedure known as spectroradiometry. Spectroradiometry differs from radiometry (measurement of total radiant energy emitted by the source) and photometry (measurement of the visible spectrums radiant energy (380-780 nm)) as it is more precise in its measurements of the radiant energy emitted by measuring the individual wavelengths of the source (Schneider and Young, 1998). The spectral characteristics of the particular source can be illustrated in a graph where intensity is plotted against wavelength. To gather these measurements the spectroradiometer separates radiation into the wavebands of which the source is made up, and the individual bands are measured separately. A common way of achieving this is by use of a prism which is well known to be able to split visible light passed through it into its constituent wavebands which are detected by the eye as bands of coloured light. A diffraction grating is more commonly used in spectroradiometers to split radiation when measuring UVR (Anon, 1997).

Four integral units make up a spectroradiometer; the input optics, a monochromator, a detector and a control and logging system (Figure 3.1). The input optics is what gathers radiation from the specified source and delivers it to the monochromator.

When measuring short wavelength UVR, glass is inadequate and therefore quartz lenses, optical fibres and Teflon diffusers are commonly used in this process. The monochromator is what, as previously discussed, separates the radiation into its component wavelengths. If minimal stray levels of the radiation are necessary, the spectroradiometer will include a double monochromator, where two single-ruled diffraction gratings are used in tandem (Figure 3.1) - this study incorporates the use of a double monochromator. The detector measures the intensity of the radiation at each wavelength emitted by the source. The type of detector used is dependent upon the wavelength range of the source as well as the sensitivity required of the measurements. Photomultiplier tubes, combined with a photocathode encompassing an appropriate spectral response are most popular. The individual wavelengths of radiation are quantified in radiometric units and the control and logging system is what defines and stores this data. For robust accuracy of a spectroradiometer, calibration of the instrument is also necessary (Anon, 1997; B. L. Diffey, 2002).

This project utilises both spectroradiometry and radiometry. Once the spectral radiance of the individual UVR sources is determined a radiometer calibrated to the spectral reading was used on a more frequent basis to calculate the UVR dosage. For a detailed account of UVR sources and radiometric terminology please see Chapter 1.

Another key requirement of this chapter was to determine what effect the different sources of UVR had on mtDNA content. This would establish how the further assays on mtDNA damage could be utilised. To determine mtDNA content in the cell this study encompassed a QPCR method which has previously been described by Koch *et al*., 2001. For their study, these authors used the assay to determine any differences in mtDNA content between patient samples, data relevant for our investigations (Koch *et al.*, 2001). Furthermore, this assay has also been incorporated into a study where it was able to detect depleted mtDNA in immortalized (hTert) human fibroblasts by means of ethidium bromide exposure (Schroeder *et al.*, 2008). Throughout this chapter this assay will be identified as the 83 bp assay because a small 83 bp segment of mtDNA is amplified (Figure 3.2). The principle of the assay is that this small segment of mtDNA is not located in any major/well documented deletion site and therefore amplification of this product is comparable to mtDNA amount.

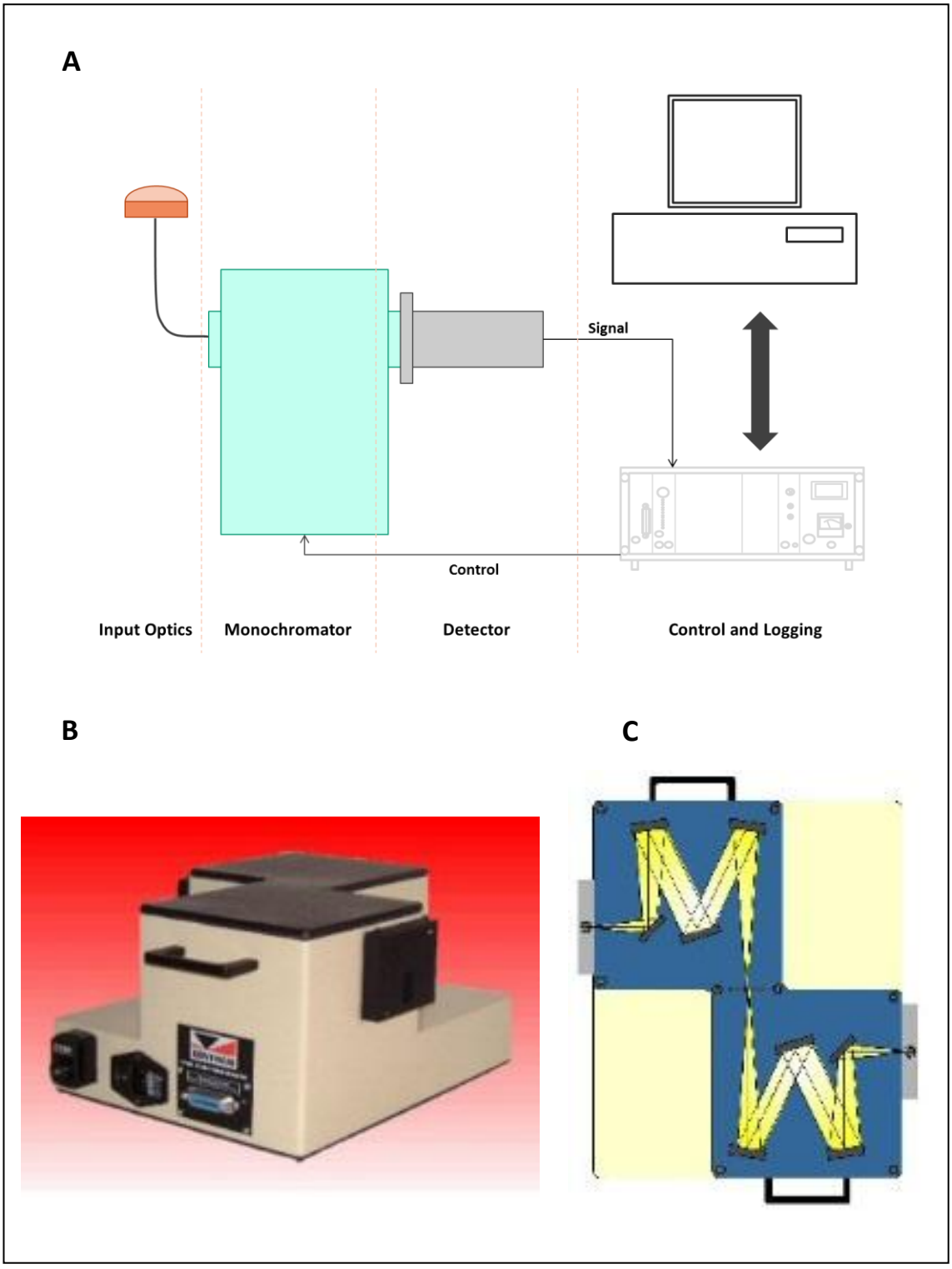

Figure 3.1: Image and Schematics of a Spectroradiometer. A spectroradiometer is made up of four units; the input optics, a monochromator, a detector and a control and logging division (A). In this study the Bentham double monochromator was used (B) and an illustration shows the internal workings of this double monochromator. Images taken/adapted from (Anon, 1997).

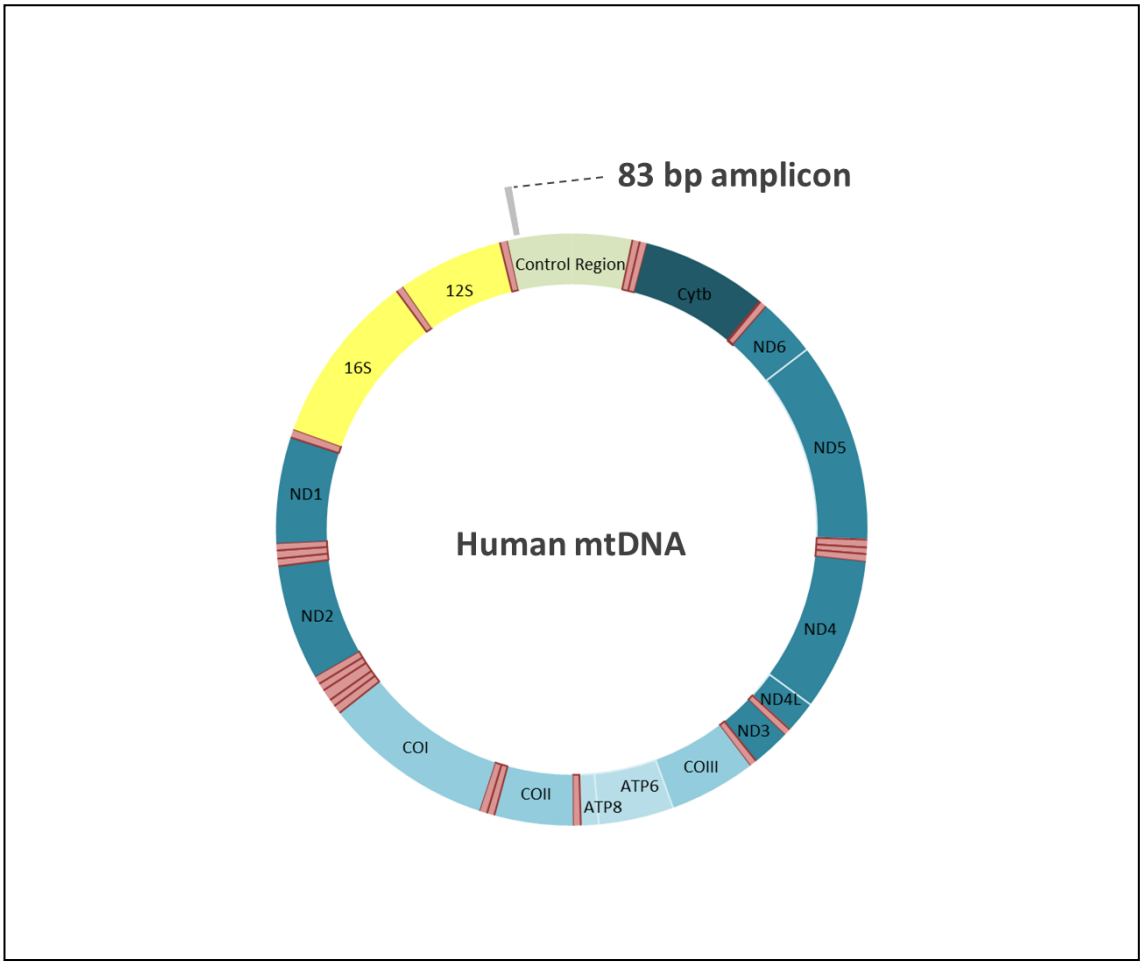

Figure 3.2: Location of the 83 bp Amplicon. This image illustrates the location of the 83 bp amplicon in the mtDNA which is amplified by QPCR in the 83 bp assay. This assay enables the determination of mtDNA content.

The final crucial requirement of this chapter was to verify cell viability in response to increasing doses of the different UVR sources. Viability of cells exposed to UVR has been assessed previously however, differences have only been determined between the divisions of UVR (UVA, UVB and UVC). It was important to assess the viability of the cells that were used in this study when they were exposed to all the sources of UVR encompassed in the remainder of this thesis.

3.1.1 Aims

The aims of this study are therefore to optimise experimental procedures and discover any hindrances which could affect future investigations. This should minimise errors and reduce time spent on unnecessary procedures.

3.2 Methods

The methods shown here are specific for this chapter; for general methods including cell culture techniques, UVR irradiations and the 11 kb PCR please refer to Chapter 2.

3.2.1 Calibration of UVR Lamps

The spectral irradiance was measured for the following 2 ft fluorescent lamps: LT 18W/UV-C (Germicidal), Philips TL 20W/12RS (TL12), Philips TL 20W/01 RS (TL01), Helarium R1.01 (Helarium), Helarium B1-12-40W (Arimed B), Philips TL 20W/09 RS with/without a glass filter (TL09 ± Filter). Measurements were taken at approximately 20 cm from the midpoint of a solarium containing four of each lamp and were taken from 250 to 400 nm in steps of 1 nm with a portable spectroradiometer (Bentham Instruments Ltd, Reading; model DMc150FC). The spectral irradiance was measured for the following 6 ft fluorescent lamps: Waldmann F85/100W-UV6 (UV6), iSOLde Cleo performance 100W-R with/without a glass filter (Cleo ± Filter). Measurements were taken at approximately 20 cm from the midpoint of a solarium containing four and seven (respectively) of each lamp and were taken from 250 to 400 nm in steps of 1 nm with a portable spectroradiometer. The monochromator was fixed with a bandwidth of 1 nm and the wavelength calibration was achieved using a low-pressure mercury discharge lamp (253.7 nm and 435.8 nm). Prior to calibration a spectral sensitivity calibration of the instrument was determined by reference to a calibrated deuterium spectral irradiance standard (National Physical Laboratory, UK (NPL 2003 irradiance scale)). The input optic for two other meters (to be used to measure irradiance on a daily basis) was placed as close as possible to the input of the spectroradiometer and the reading on each radiometer was noted at the midpoint of the spectroradiometer scan. Correction factors were applied so the correct irradiance could be measured for the various meter/lamp combinations. Total UVR, UVA, UVB and UVC was calculated by integrating the spectral irradiance curve and the erythemally weighted irradiance was calculated by combining the spectral irradiance with the erythemal action spectrum (CIE standard CIE S 007/E – 1998. Erythema Reference Action Spectra and Standard Erythema Dose).

3.2.2 Distribution of UVR Emitted from the 2 ft and 6 ft UVR Sources

An area of 56 cm by 32 cm was considered for assessment of the distribution of the UVR emitted from the 2 ft and the 6 ft UVR sources. The variation in emissions, related to distance from the light source origin, was also evaluated. To record the irradiance along the length and width of the considered area the radiometer was moved in 4 cm intervals. To measure the irradiance relative to its distance from the source the radiometer was moved in 2 cm intervals away from the source. The UVR sources used were the TL12 and UV6 for the 2 ft and 6 ft sources, respectively. Variation in irradiance due to the number of lamps used was taken in to account for the 2 ft UVR source where the recordings were repeated for two and four lamps.

3.2.3 Temperature Emitted from the UVR Sources over Time

A thermometer was placed under the UVR sources and temperature measurements were taken at 0, 0.5, 1, 2, 3, 4, 5 and 6 h. The temperature emissions of the UVR sources, where irradiations to create mtDNA damage were lengthy, were assessed; these included the Helarium, Arimed B, TL09 and Cleo lamps. A second experiment was also undertaken where the thermometer was covered with foil to mimic the condition that the control cells were exposed to.

3.2.4 Heating of Cells without Irradiation

HDFn cells were seeded at 5 x 10^6 cells/60 mm clear dish in phenol red free DMEM + FCS and were incubated at 37 °C for approximately 24 h. Following this medium was removed and cells were washed with PBS. Phenol red free DMEM - FCS (4 ml) was added to the cells and they were then placed in a water bath set to 48 °C for 0.5, 1 and 2 h. Control cells remained in the incubator set to 37 °C. mtDNA damage was assessed using the 11 kb QPCR assay described in Chapter 2.

3.2.5 TL12 Medium Investigation

Prior to irradiation, medium was removed and cells were washed with PBS. Phenol red free DMEM ± FCS or PBS (4 ml) was added to the cells and the lids of the dishes were removed. For the mock control the cells were covered in aluminium foil and placed

under the lamps for the same duration as the cells receiving the highest dose of UVR. The cells were irradiated for seven increasing doses of UVR ranging from approximately 7 to 1600 mJ/cm^2 (absolute UVR, equivalent to approximately 0.2 to 40 SED). Following UVR treatment medium was removed and the cells were washed with PBS. Cells were trypsinised and removed by scraping. DNA was extracted using QIAamp DNA mini kit (Qiagen, UK) as per manufacturer's instructions. mtDNA damage was assessed using the 11 kb QPCR assay described in Chapter 2.

3.2.6 Viability of Skin Cells Following UVR Exposure

Cell viability was assessed using the MTS Assay (CellTiter-96 Aqueous, Promega, UK). MTS [3-(4,5-dimethylthiazol-2-yl)-5-(3-carboxymethoxyphenyl)-2-(4-sulfophenyl)-2H-tetrazolium, inner salt] is a tetrazolium salt which is reduced to a coloured formazan product by NADPH or NADH in metabolically active cells only. This colour production is used to quantitate cell proliferation and cytotoixcity. Either HaCaT, Primary Keratinocytes or HDFn Cells were seeded (5x10^3 cells/well) into a 96-well plates leaving column 1 blank and were then incubated at 37 °C with 5 % CO_2 for 24 h. Cells were then treated with the designated UVR treatment, determined by altering exposure time by covering cells with foil, and then were assessed for cell viability by addition of 20 µl MTS. The cells were then incubated at 37 °C for 5 h. Absorbance was measured at 490 nm using the Spectromax 250 microplate reader (Molecular Devices, UK).

3.2.7 mtDNA Copy Number Analysis (83bp PCR)

The mtDNA content was investigated by QPCR amplification of an 83 bp section of mtDNA. The PCR was performed in 25 µl reactions containing: 50 ng DNA sample, 5 µM of each primer, 225 nm of the probe, 300 µM dNTP, 1 x TaqMan Universal PCR Mastermix (Invitrogen, UK) and was made up to the required volume with high grade PCR water. The primers and the probe used (Koch *et al.*, 2001), can be found in Table 3-1. The cycling conditions were 40 cycles of 15 s at 95 °C and 1 min at 60 °C. Analysis was performed on the StepOne PCR machine (Applied Biosystems, UK).

Table 3-1: TaqMan Primers and Probes for Detection of mtDNA Content (83 bp Assay).

Target	Name	Oligonucleotide Sequence (5' → 3')
mtDNA content	IS1 Forward	5'-GAT TTG GGT ACC ACC CAA GTA TTG-3' (16042-16066)
	IS2 Reverse	5'-AAT ATT CAT GGT GGC TGG CAG TA-3' (16125-16102)
	IS probe	5'-CAC CCA TCA ACA ACC GCT ATG TAT TTC GTA CA-3'VIC (16069/16101)

The primer and probe set were purchased from MWG, UK.

3.2.8 Statistical Analyses

Statistical evaluation was performed by a one-way ANOVA with either Bonferroni or Dunnett's correction post-hoc analysis test for comparison to the control. P-values below 0.05 were considered significant. For evaluation of mtDNA content a linear regression was performed, for comparison to the control P-values below 0.05 were considered significant.

3.3 Results

3.3.1 Measuring the Spectral Output of UVR Sources

The spectral irradiance for each of the UVR sources required for use in this study was measured and plotted as relative irradiance against wavelength (Figure 3.3). All the lamps with the exceptions of the Germicidal and the TL01 lamp emitted a broadband spectrum; this was shown as a broad peak of irradiance covering multiple wavelengths. The Germicidal and the TL01 lamps are narrowband and only covered a small section of the UVR spectrum which was clearly seen as narrow peaks centred at 254 and 311 nm, respectively. Figure 3.4 compares two sources used and expected to create the same effect (e.g. damage). These were the TL09 and Cleo both ± a glass (UVB) filter. Both lamps produced a similar broadband spectral output.

From the spectral irradiance of each lamp, the percentage amount of UVA, UVB and UVC emitted was calculated and is shown in Table 3-2. This table also contains the full names and manufactures of all the UVR sources used and also an abbreviated name devised for future use within this thesis.

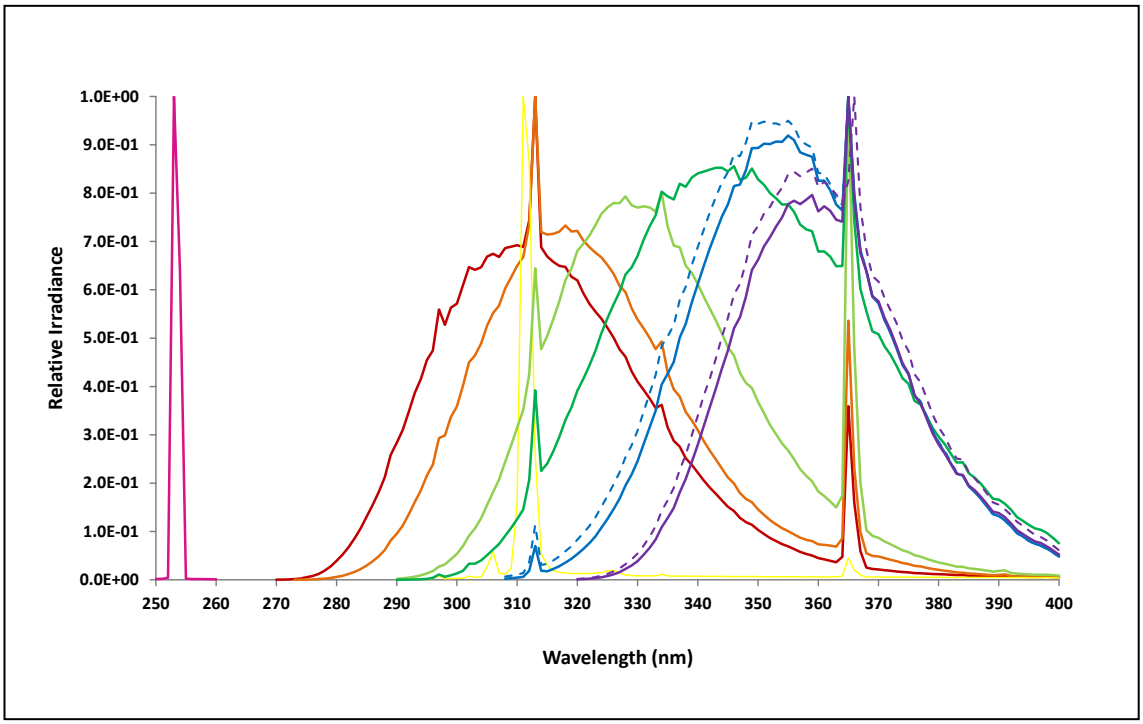

Figure 3.3: Spectral Chart. This figure shows the spectral output of the different UVR lamps used in the study. The various UVR sources, from left to right are as follows: Germicidal (-), TL12 (-), UV6 (-), TL01 (-), Helarium (-), Arimed B (-), TL09 – filter (-), TL09 + filter (-), Cleo – filter (--), Cleo + filter (--). For a magnified image please refer to Appendix I.

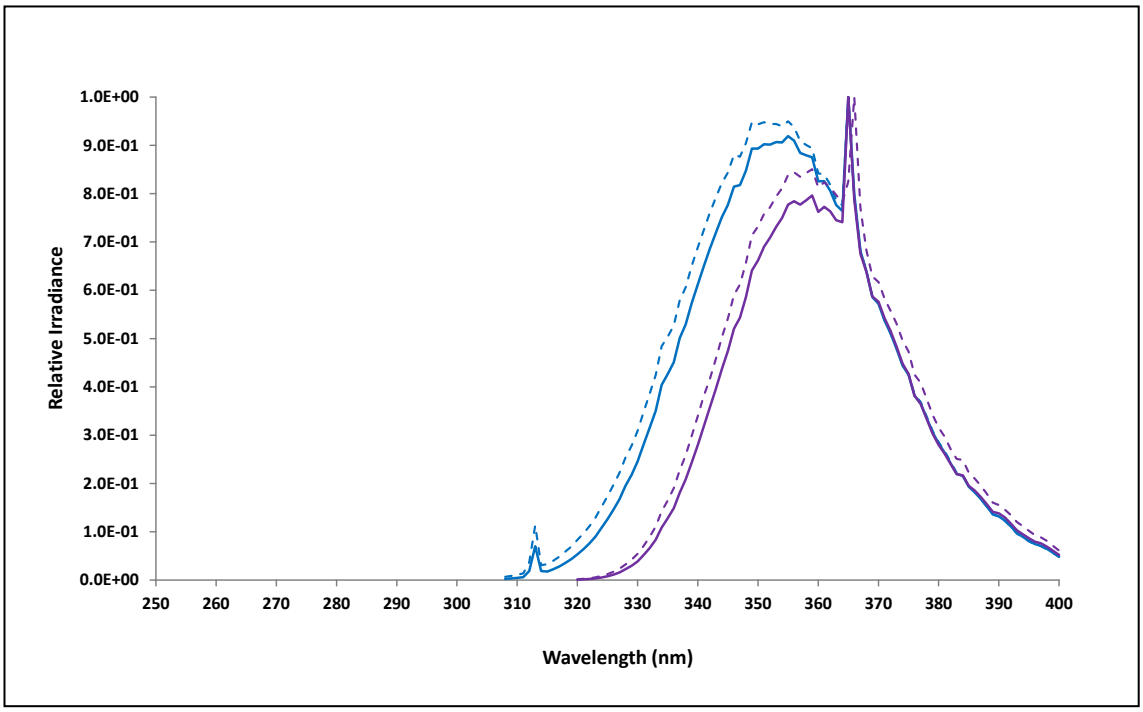

Figure 3.4: Comparison of the TL09 and the Cleo UVR Lamps. This figure shows the differences in the spectral output of the UVR lamps TL09 – filter (-), TL09 + filter (-), and Cleo – filter (--), Cleo + filter (--).

Table 3-2: Percentage UVA, UVB and UVC Emitted from the Various UVR Lamps.

Lamp name	Abbreviated lamp name	Percentage UVR emitted		
		UVA	UVB	UVC
T 18W/UV-C (Lamp Specs LLP, UK)	Germicidal	2	2	96
Philips TL 20W/01 RS	TL01	22	78	0
Philips TL 20W/12 RS	TL12	48	52	0
Waldmann F85/100W-UV6	UV6	63	37	0
Helarium R1.01	Helarium	88	13	0
Wolff System Helarium B1-12-40W/BPIN	Arimed B	96	4	0
Philips TLK 40W/09R	TL09 – filter	99.6	0.4	0
Philips TLK 40W/09R (filtered by glass)	TL09 + filter	100	0	0
iSOLde Cleo performance 100W-R	Cleo – filter	99.3	0.7	0
iSOLde Cleo performance 100W-R (filtered by glass)	Cleo + filter	100	0	0

This table shows the full name and the manufactures of the various UVR lamps used in this study and the percentage of UVA, UVB and UVC which is emitted from each. The abbreviated names (which are how each lamp is referred to throughout this thesis) are also included.

3.3.2 Evaluation of the Distribution of UVR from the Source

The purpose of the evaluation of UVR distribution was to standardise the methodology used for this study and to remove any varying factors found through the positioning of the cells. The radiation emitted spreads from its source and varies, and it was therefore necessary to assess and determine the differences in radiation dependent on the positioning of any entity which was to be evaluated. The distribution of UVR emitted from the 2 ft and the 6 ft UVR source over a 56 by 32 cm area was measured and is shown in Figure 3.5. The difference in emissions related to distance from the source was also considered. A consistent increase in irradiance was seen towards the centre of the 2 ft UVR source as opposed to the outlying edges and this trend was independent of lamp number. A large increase in irradiance (0.996 mW/cm^2 ± 0.065) was seen when lamp number was increased from 2 to 4 independent of positioning. The percentage difference in emissions was 44 % for 4 lamps and 46 % for 2 lamps when measurements were taken from left to right, and 19 % for 4 lamps and 32 % for

2 lamps when measurements were made from front to back. The emissions from the 6 ft UVR source were more consistent with just a 3 % difference in emissions when measurements were taken from left to right and 9 % when measurements were made from front to back.

3.3.3 Assessment of Temperature Emitted from UVR Sources over Time

UVR sources which would require long irradiation time periods in impending experiments were assessed only. Figure 3.6 shows that only the emissions from the TL09 source (with or without the foil cover) caused a temperature increase of above that of incubator conditions. The maximum temperature reached with this UVR source was 48 °C independent of the foil cover. The foil cover caused a reduction in the temperature emitted from all the UVR sources of 1.75 ± 0.25 °C in Helarium and Arimed B, 3.13 ± 0.48 °C in Cleo and 1.63 ± 0.42 °C in TL09.

3.3.4 Damage Created in HDFn Cells Heated to 48 °C

HDFn cells were placed in a water bath set to 48 °C for up 2 h. This temperature was chosen as this was the maximum temperature emission created by the UVR sources. Damage was assessed by inhibition of the amplification of an 11 kb amplicon of mtDNA by QPCR which is shown as an increase in Ct value. This data shows that there was no increase in Ct value in HDFn cells heated at 48 °C for up to 2 h when compared with the control which had remained at 37 °C. Heating of the cells to 48 °C for over 2 h saw a large compromise in cell viability; data not shown.

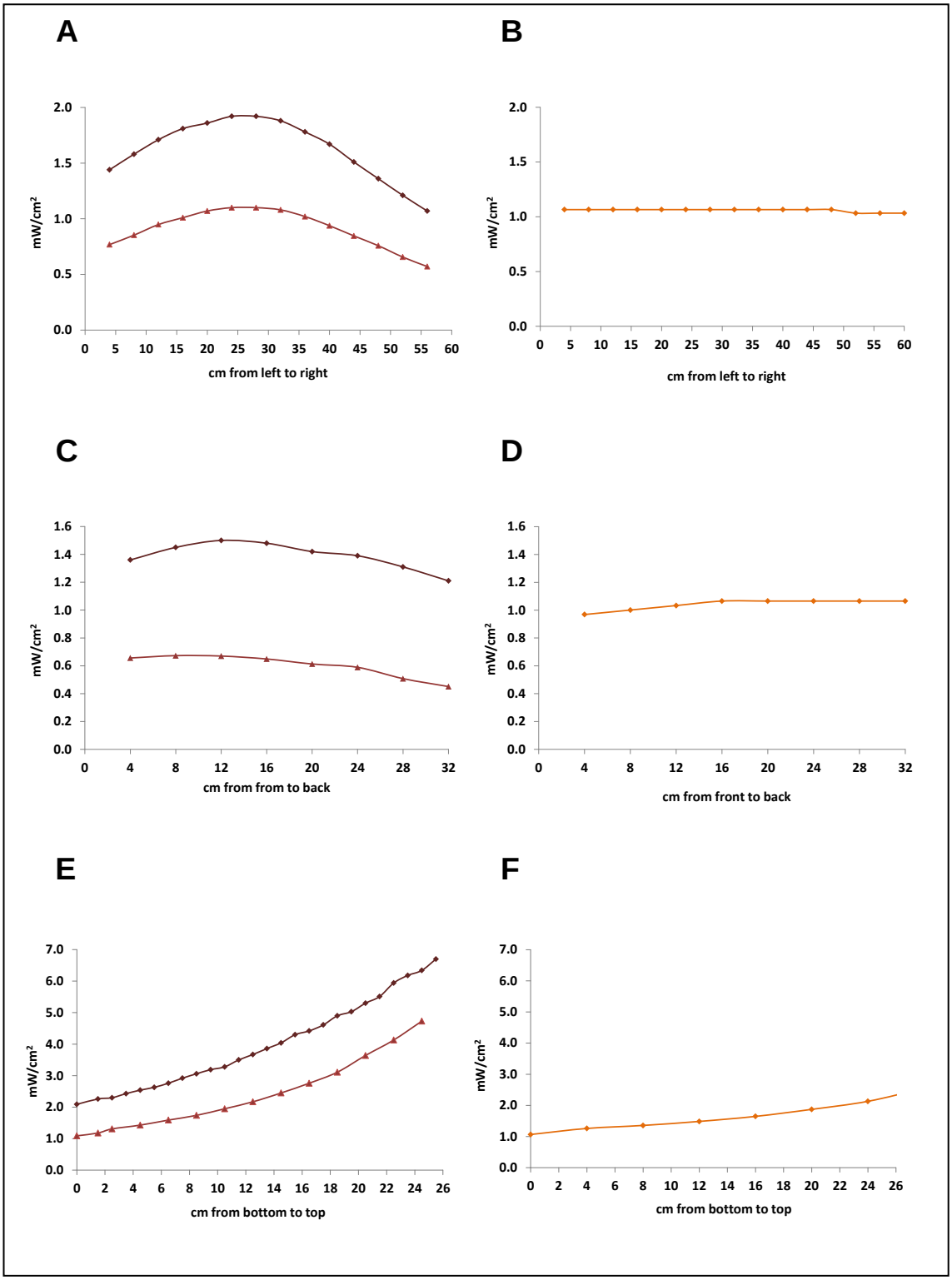

Figure 3.5: Comparing the Differences in the Distribution of Irradiance. The irradiance of two different UVR sources were compared; a 2ft light box containing TL12 lamps (A, C, E) and a 6ft sun-bed containing UV6 lamps (B,D,F). Irradiation was measured in 4 cm intervals along the length (A, B) and the width (C, D) of a 56 by 32 cm area under the lamps of interest, and irradiation was measured in 2-4 cm intervals moving towards the source when positioned in the centre of the 56 by 32 cm area (E, F). Lamp number was also evaluated as follows; 4 lamps (♦) and 2 lamps (▲).

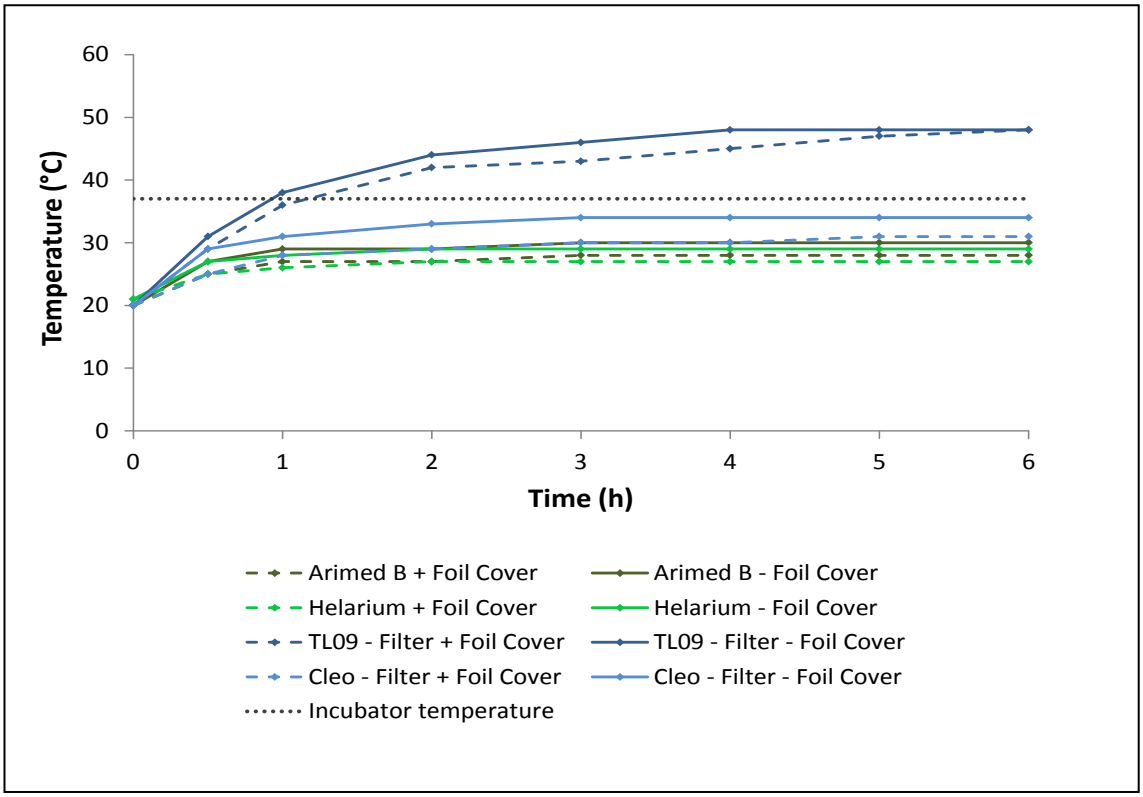

Figure 3.6: Temperature Emissions from Various UVR Sources. A thermometer either covered in foil or left uncovered was placed centrally under the various UVR sources and temperature was measured at 0.5, 1, 2, 3, 4, 5 and 6 h.

Table 3-3: The Effect of Heat on the mtDNA of HDFn cells using the 11 kb QPCR.

Sample Name	Ct	Mean Ct
Blank	Undetermined	
Blank	Undetermined	
Blank	Undetermined	N/A
0 h (Control)	10.22	
0 h (Control)	10.42	
0 h (Control)	10.29	10.31
0.5 h	10.30	
0.5 h	10.32	
0.5 h	10.10	10.24
1 h	10.60	
1 h	10.34	
1 h	10.01	10.31
2 h	10.22	
2 h	10.55	
2 h	10.15	10.31

This table shows the results of 11 kb QPCR assay of samples of DNA extracted from HDFn cells which were exposed to 48 °C in a water bath for 0.5, 1 and 2 h. Control cells remained in the incubator at 37 °C.

3.3.5 UVR-Induced mtDNA Damage, Dependent on Irradiation Media

Both HaCat (Figure 3.7) and HDFn (Figure 3.8) cells were irradiated using the TL12 UVR source in either PBS or DMEM ± FCS (n=3). The mtDNA damaged investigated, was determined by QPCR amplification of an 11 kb amplicon of mtDNA. Characteristic dose effect curves were produced and the maximum effects were seen when cells were exposed to a dose of approximately 400 mJ/cm^2 (the equivalent of approximately 10 SEDs), in both cell lines and for all irradiation media.

For each curve the EC_{50} (the dose of UVR needed to create 50 % cell death) was calculated and mean values were determined. These values were plotted into bar charts and compared statistically by one way ANOVA with Bonferroni's post hoc correction to determine any differences in EC_{50} dependent on irradiation media. A small increase in EC_{50} was seen when HaCat cells were irradiated in DMEM + FCS in comparison to being irradiated in PBS or DMEM - FCS. With HDFn cells there was a small increase in EC_{50} from cells irradiated in PBS to those irradiated in DMEM - FCS, and a further increase was seen when cells were irradiated in DMEM + FCS. For all of these differences the P value was found to be >0.05 and was therefore not found to be statistically significant. Mean values were also determined for the maximum response of each curve and again plotted as bar chart and compared statistically by one way ANOVA with Bonferroni's post hoc correction. In the HaCaT cell line there was a varying result. When irradiated in DMEM - FCS a mean maximum response of 78 % (increase in Ct value) which is much less than when cells were irradiated in DMEM + FCS and PBS where the maximum response was 95 and 125 % respectively. With the HDFn cells the maximum response was more consistent with mean maximum responses as follows 113 % (DMEM - FCS), 115 % (PBS) and 125 % (DMEM + FCS). As with the differences in EC_{50} for all of these differences the P value was found to be >0.05 and was therefore not found to be statistically significant.

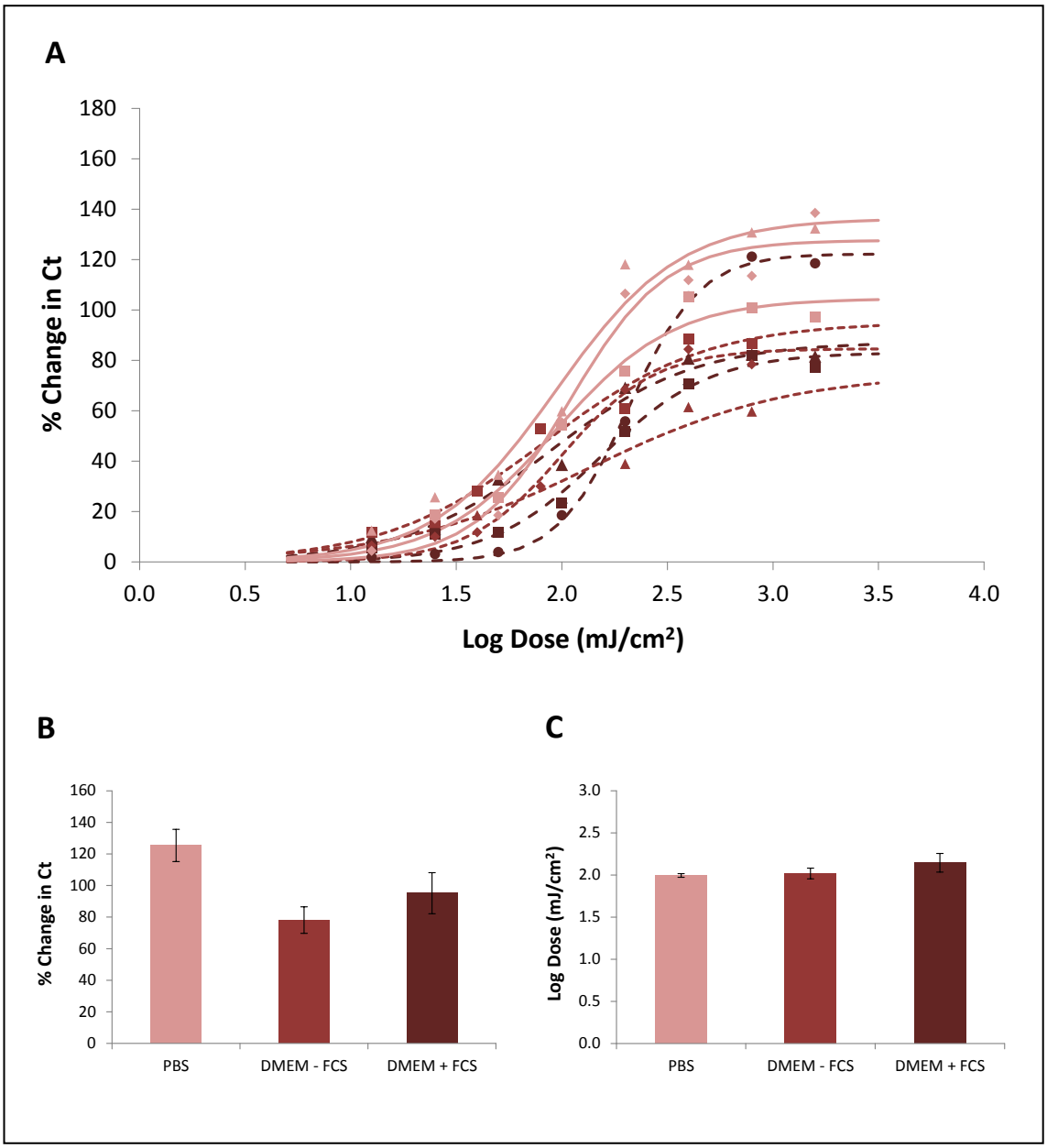

Figure 3.7: mtDNA Damage in the HaCat Cell Line Dependent on Irradiation Media. On (A) each curve represents a series of experiments repeated singularly. For the technical repeats of this experiment n=3. Cells were irradiated in PBS (-), DMEM – FCS (-), or DMEM + FCS (-). The maximum mtDNA damage (B) and mean EC_{50} values (C) were calculated from these curves. The y-axis (A+B) shows damage represented by an increase in ct compared to the control (considered un-damaged) calculated as a percentage increase. Therefore 0 % signifies no damage. For all irradiations the TL12 UVR source was used and differences were non-statistically significant, n=3 ± SEM.

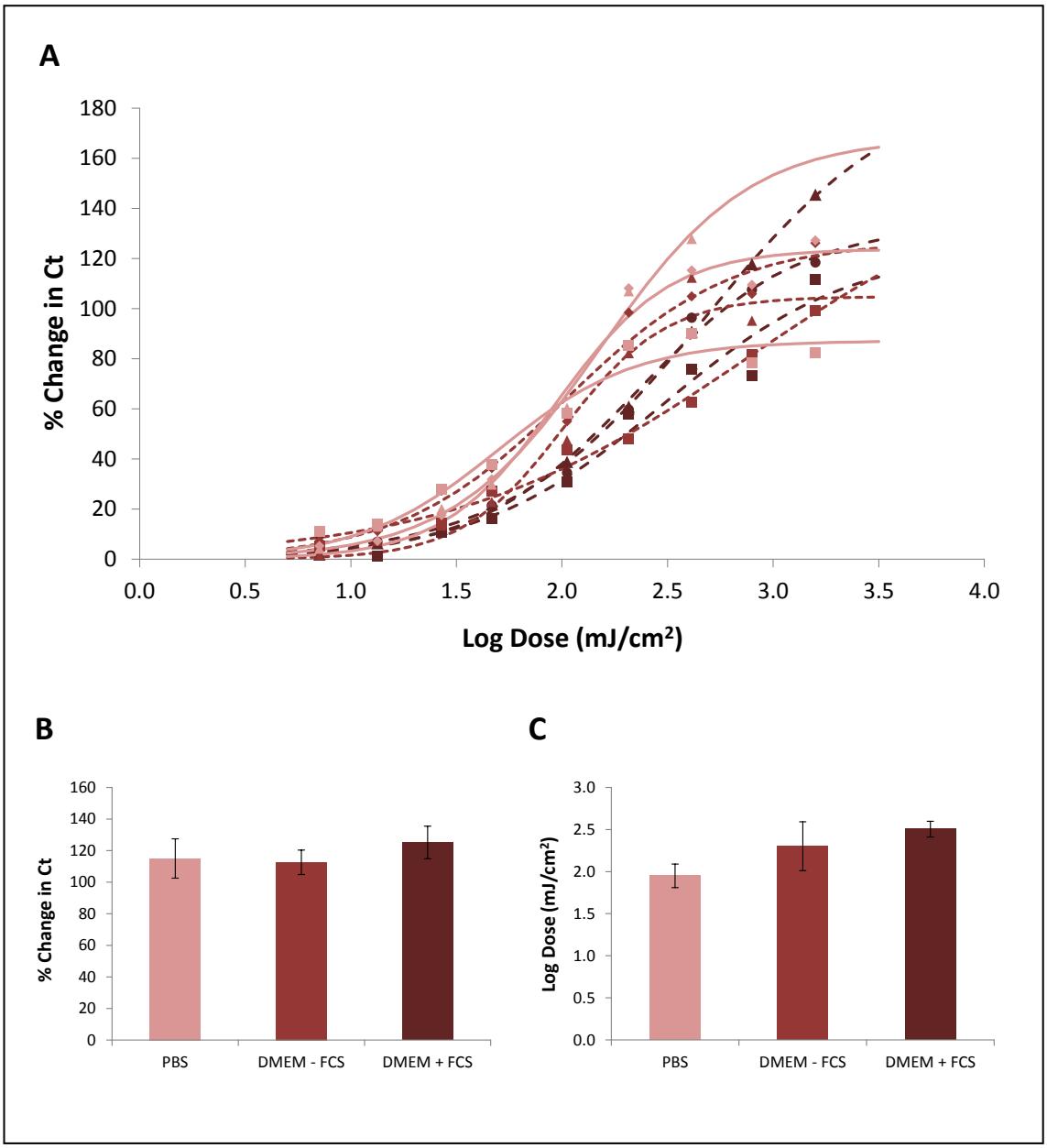

Figure 3.8: mtDNA Damage in the HDFn Cell Line Dependent on Irradiation Media. On (A) each curve represents a series of experiments repeated singularly. For the technical repeats of this experiment n=3. Cells were irradiated in PBS (-), DMEM – FCS (-), or DMEM + FCS (-). The maximum mtDNA damage (B) and mean EC_{50} values (C) were calculated from these curves. The y-axis (A+B) shows damage represented by an increase in ct compared to the control (considered un-damaged) calculated as a percentage increase. Therefore 0 % signifies no damage. For all irradiations the TL12 UVR source was used and differences were non-statistically significant, n=3 ± SEM.

3.3.6 Assessment of the Viability of Skin Cells Exposed to Various UVR Sources

The viability of HaCaT cells, Primary Keratinocytes and HDFn cells when exposed to increasing doses of the various UVR sources was assessed using the MTS assay. The different UVR sources investigated was as follows: Germicidal (Figure 3.9), TL12 (Figure 3.10), UV6 (Figure 3.11), TL01 (Figure 3.12), Helarium (Figure 3.13), Arimed B (Figure 3.14), Cleo – Filter (Figure 3.15) and Cleo + Filter (Figure 3.16). The trend shows that the viability of all the skin cells decreased with increasing doses of all the UVR sources, and these decreases were statistically significant at all of the higher doses. To make this data more comprehensible EC_{50} values as a dose of mJ/cm^2 for all the UVR sources were calculated and various useful entities from these values were also calculated such as LOG_{10}, SED and the irradiation time required to achieve the particular dose. This data has been outlined in Table 3-4 and it shows that, as a general rule, the longer the wavelengths the UVR source emits (see Figure 3.3) the higher the dose required to cause 50 % cell death. This was coupled with an increase in irradiation time, as well as a reduction in SED. An observation from this table was that there was a trend for the susceptibility to cell death dependent on cell type. This saw that the HaCaT cells for, the majority, were consistently the least susceptible, HDFns and Primary Keratinocytes were differentially vulnerable dependent on UVR source.

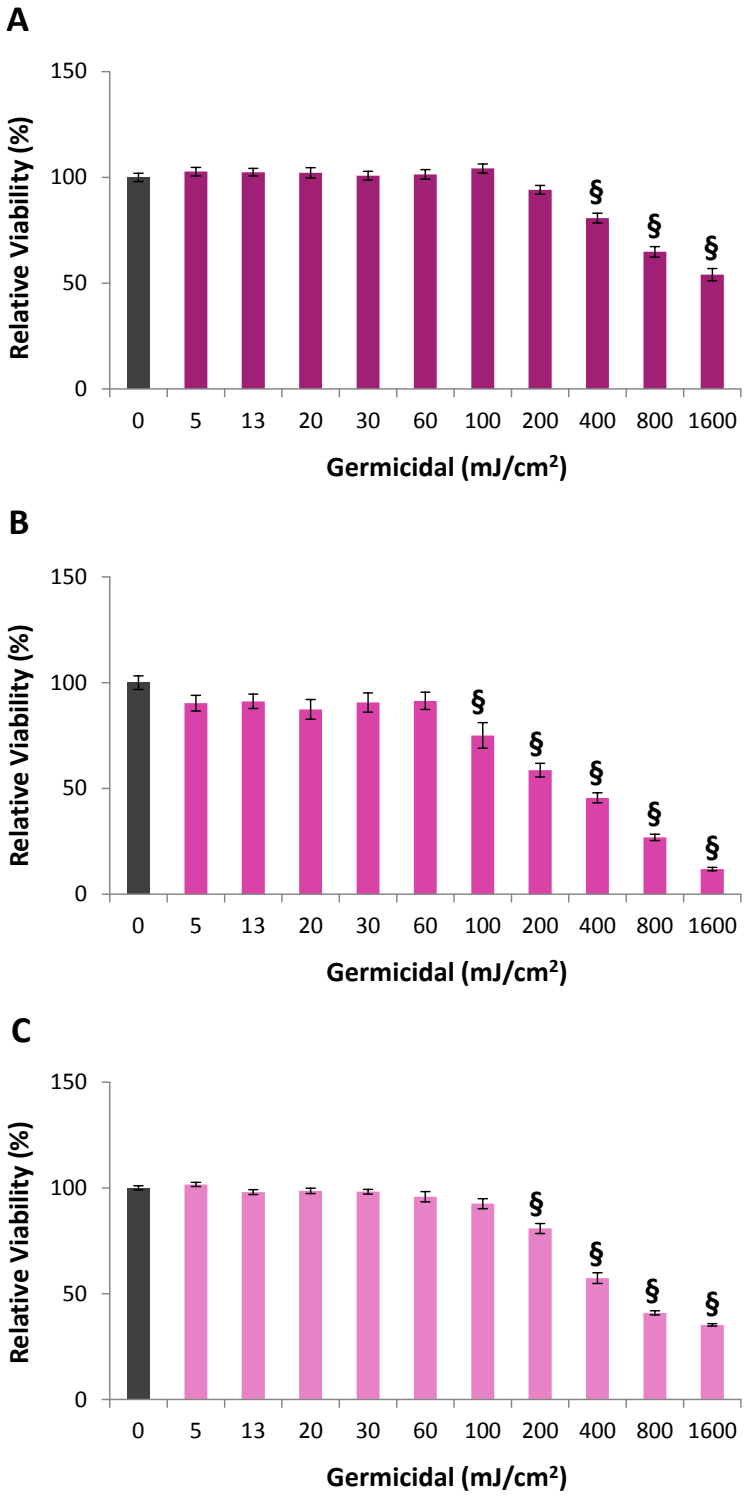

Figure 3.9: Viability of Skin Cells Exposed to the Germicidal UVR Source. HaCaT (A), Primary Keratinocytes (B) and HDFn cells (C) were exposed to increasing doses of the Germicidal UVR source and then assessed for viability using the MTS assay. Absorbance was measured at 490 nm. Data represents the mean value of 8 technical replicates, n=3 ± SEM, §P<0.001 compared to the control.

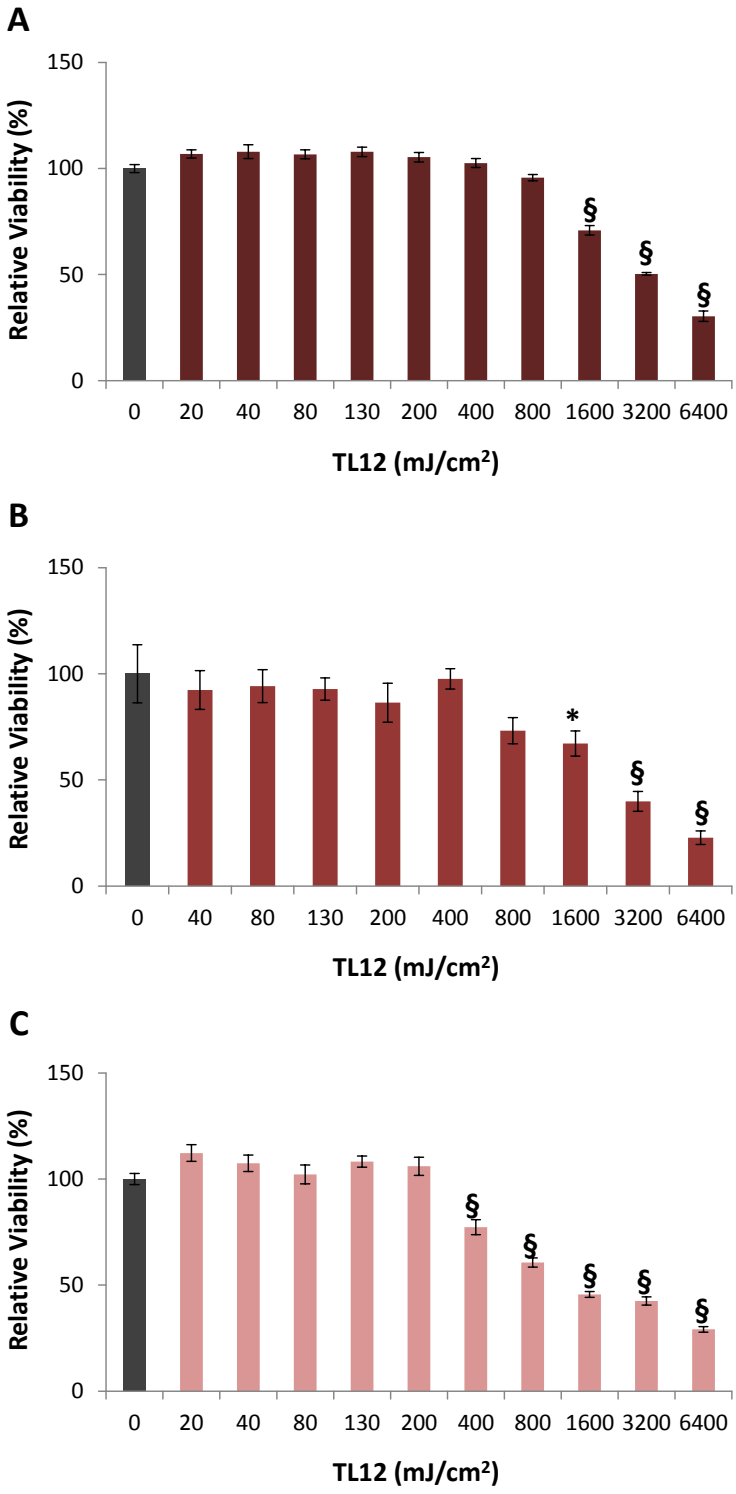

Figure 3.10: Viability of Skin Cells Exposed to the TL12 UVR Source. HaCaT (A), Primary Keratinocytes (B) and HDFn cells (C) were exposed to increasing doses of the TL12 UVR source and then assessed for viability using the MTS assay. Absorbance was measured at 490 nm. Data represents the mean value of 8 technical replicates, n=3 ± SEM, *P<0.05, §P<0.001 compared to the control.

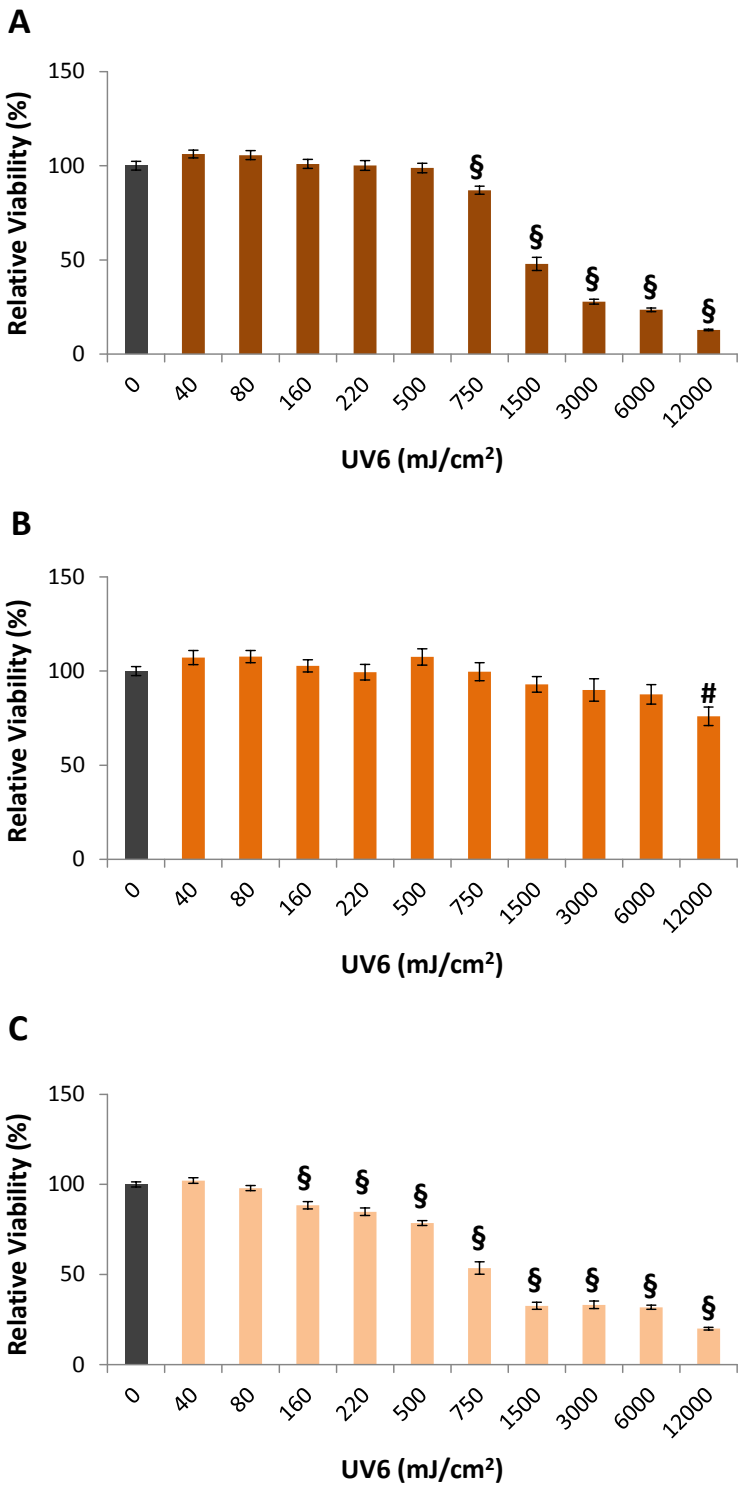

Figure 3.11: Viability of Skin Cells Exposed to the UV6 UVR Source. HaCaT (A), Primary Keratinocytes (B) and HDFn cells (C) were exposed to increasing doses of the UV6 UVR source and then assessed for viability using the MTS assay. Absorbance was measured at 490 nm. Data represents the mean value of 8 technical replicates, n=3 ± SEM, #p<0.01, §P<0.001 compared to the control.

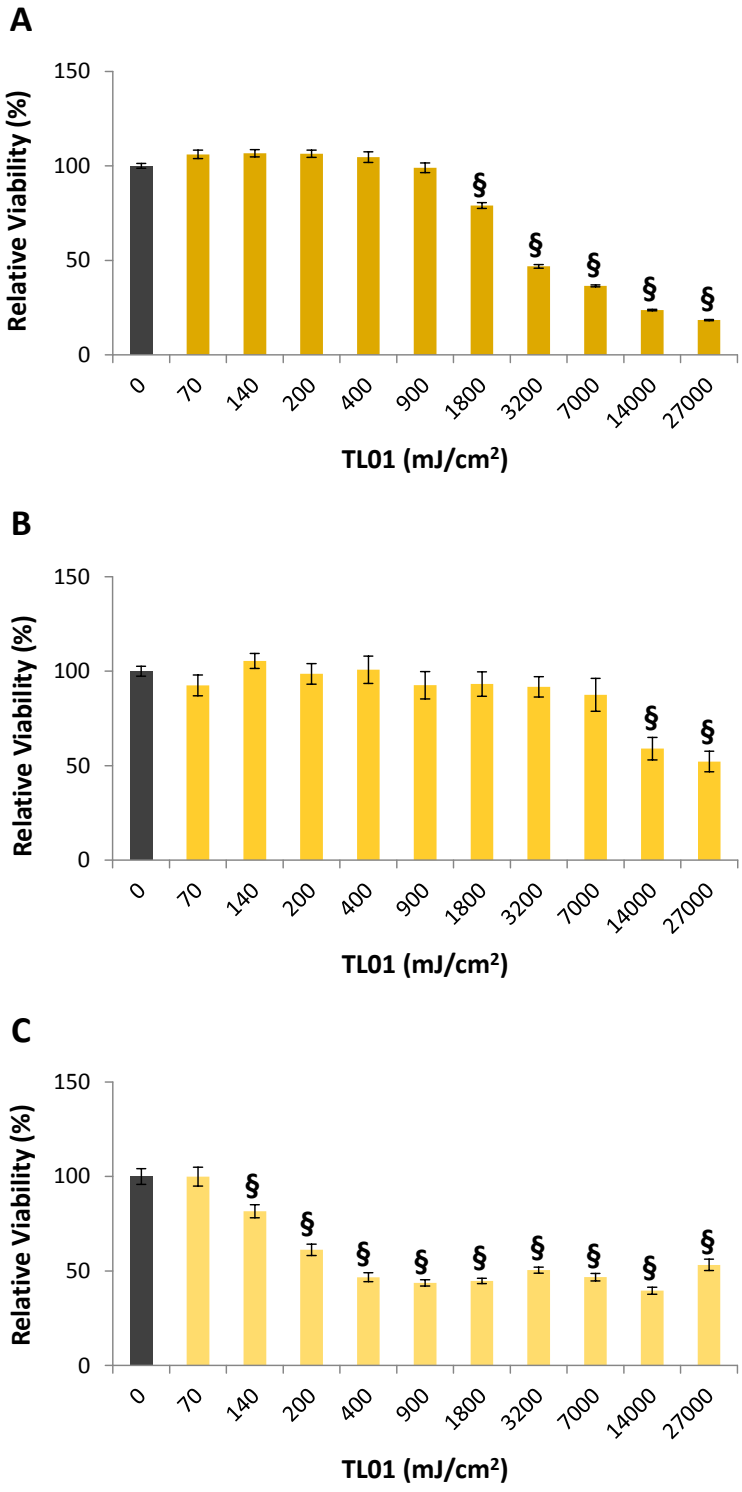

Figure 3.12: Viability of Skin Cells Exposed to the TL01 UVR Source. HaCaT (A), Primary Keratinocytes (B) and HDFn cells (C) were exposed to increasing doses of the TL01 UVR source and then assessed for viability using the MTS assay. Absorbance was measured at 490 nm. Data represents the mean value of 8 technical replicates, n=3 ± SEM, §P<0.001 compared to the control.

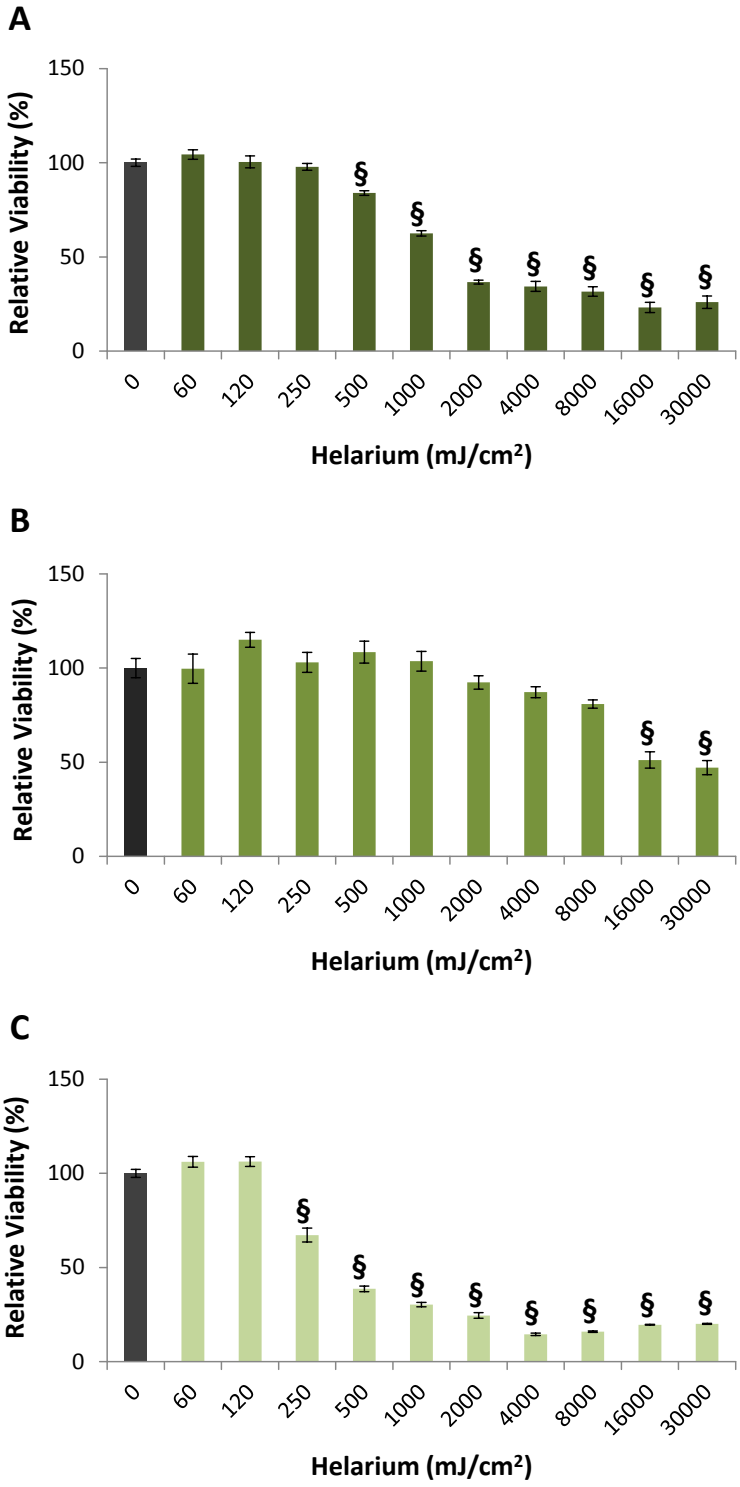

Figure 3.13: Viability of Skin Cells Exposed to the Helarium UVR Source. HaCaT (A), Primary Keratinocytes (B) and HDFn cells (C) were exposed to increasing doses of the Helarium UVR source and then assessed for viability using the MTS assay. Absorbance was measured at 490 nm. Data represents the mean value of 8 technical replicates, n=3 ± SEM, §P<0.001 compared to the control.

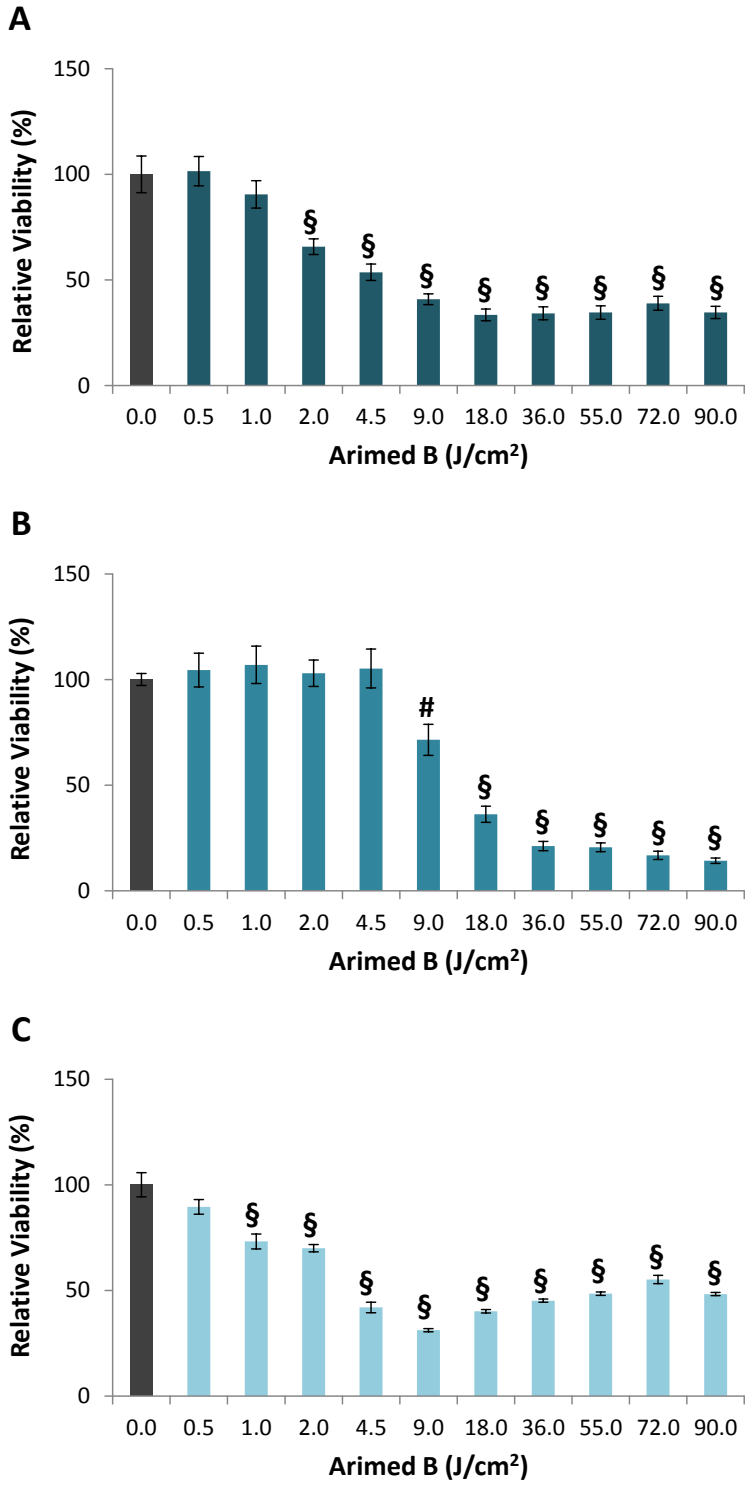

Figure 3.14: Viability of Skin Cells Exposed to the Arimed B Source. HaCaT (A), Primary Keratinocytes (B) and HDFn cells (C) were exposed to increasing doses of the Arimed B UVR source and then assessed for viability using the MTS assay. Absorbance was measured at 490 nm. Data represents the mean value of 8 technical replicates, n=3 ± SEM, #p<0.01, §P<0.001 compared to the control.

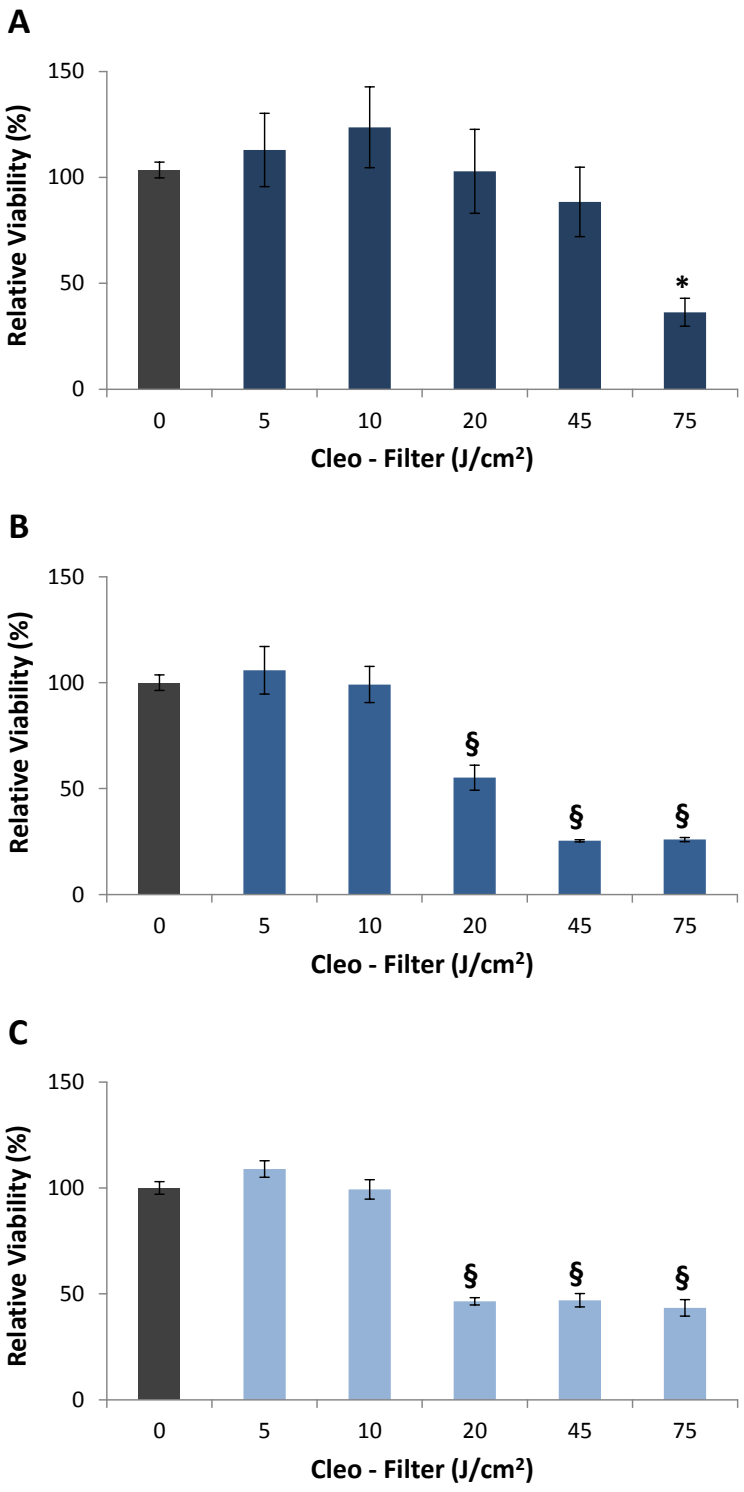

Figure 3.15: Viability of Skin Cells Exposed to the Cleo - Filter UVR Source. HaCaT (A), Primary Keratinocytes (B) and HDFn cells (C) were exposed to increasing doses of the Cleo - Filter UVR source and then assessed for viability using the MTS assay. Absorbance was measured at 490 nm. Data represents the mean value of 8 technical replicates, n=3 ± SEM, *P<0.05, §P<0.001 compared to the control.

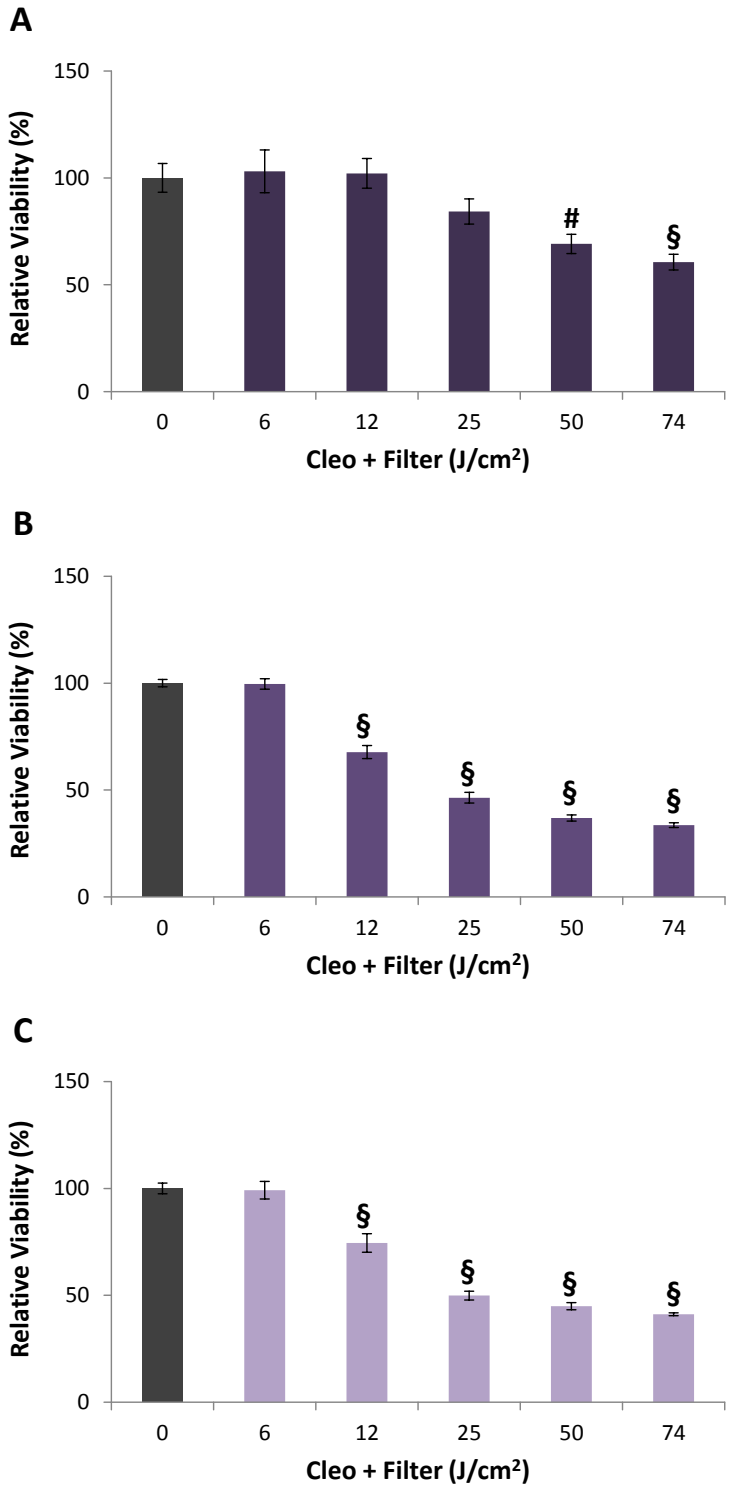

Figure 3.16: Viability of Skin Cells Exposed to the Cleo + Filter UVR Source. HaCaT (A), Primary Keratinocytes (B) and HDFn cells (C) were exposed to increasing doses of the Cleo + Filter UVR source and then assessed for viability using the MTS assay. Absorbance was measured at 490 nm. Data represents the mean value of 8 technical replicates, n=3 ± SEM, #P<0.01, §P<0.001 compared to the control.

Table 3-4: EC_{50} Values Calculated from the Viability Data of Cells Irradiated with the Various UVR Sources.

HaCaT Cells				
Lamp	**mJ/cm^2**	**LOG$_{10}$**	**SED**	**Min**
UVC	1533.70	3.19	150	15
TL12	4202.41	3.62	103	32.5
UV6	5008.33	3.70	65	79
TL01	12024.87	4.08	70	89
Helarium	11223.81	4.05	23	92
Arimed B	38774.46	4.59	22	128
Cleo - Filter	71192.96	4.85	10	138
Cleo + Filter	86803.50	4.94	5	209
Primary Keratinocytes				
Lamp	**mJ/cm^2**	**LOG$_{10}$**	**SED**	**Min**
UVC	654.45	2.81	65	6.5
TL12	3466.35	3.54	86	27
UV6	21835.09	4.34	270	330
TL01	25153.06	4.40	145	185
Helarium	23887.87	4.38	47	190
Arimed B	38315.41	4.58	22	126
Cleo - Filter	41580.21	4.62	6	80
Cleo + Filter	43118.47	4.63	2	105
HDFn Cells				
Lamp	**mJ/cm^2**	**LOG$_{10}$**	**SED**	**Min**
UVC	981.77	2.99	94	9.5
TL12	3540.91	3.55	87	27.5
UV6	4650.48	3.67	59	72
TL01	16387.76	4.21	94	120
Helarium	5317.76	3.73	11	45
Arimed B	58180.46	4.76	33	190
Cleo - Filter	53360.67	4.73	7	103
Cleo + Filter	50215.47	4.70	3	122

This data shows values of EC_{50} displayed as mJ/cm^2 for doses from the various UVR sources calculated from the previous viability data for the three different cell types. From this, further values of LOG$_{10}$, SED and the irradiation time (min) have also been calculated and are presented.

3.3.7 Determination of mtDNA Content of Skin Cells Following UVR Exposure

HaCaT cells (Figure 3.17), Primary Keratinocytes (Figure 3.18) and HDFn cells (Figure 3.19) were exposed to increasing doses of the various UVR sources. A repeated pattern of UVR exposure was also assessed in HaCaT cells (Figure 3.20) and HDFn cells (Figure 3.21). Following irradiations mtDNA content was investigated using the 83 bp assay by amplifying a short amplicon of mtDNA using a QPCR. The majority of this data shows that mtDNA content in skin cells was not altered when exposed to acute doses of the various UVR sources. Exceptions to the rule were minimal gradients of the linear line which were found to be statistically significant. These were in HaCaT cells exposed to increasing doses of the TL12 ($P<0.004$) and UV6 ($P<0.02$), in Primary Keratinocytes exposed to increasing doses of TL12 ($P<0.04$) and TL01 ($P<0.01$) and in HDFn cells exposed to increasing doses of TL01 ($P<0.05$) and Helarium ($P<0.03$). When the cells were exposed repetitively the linear regression did not statistically significantly deviate from the control.

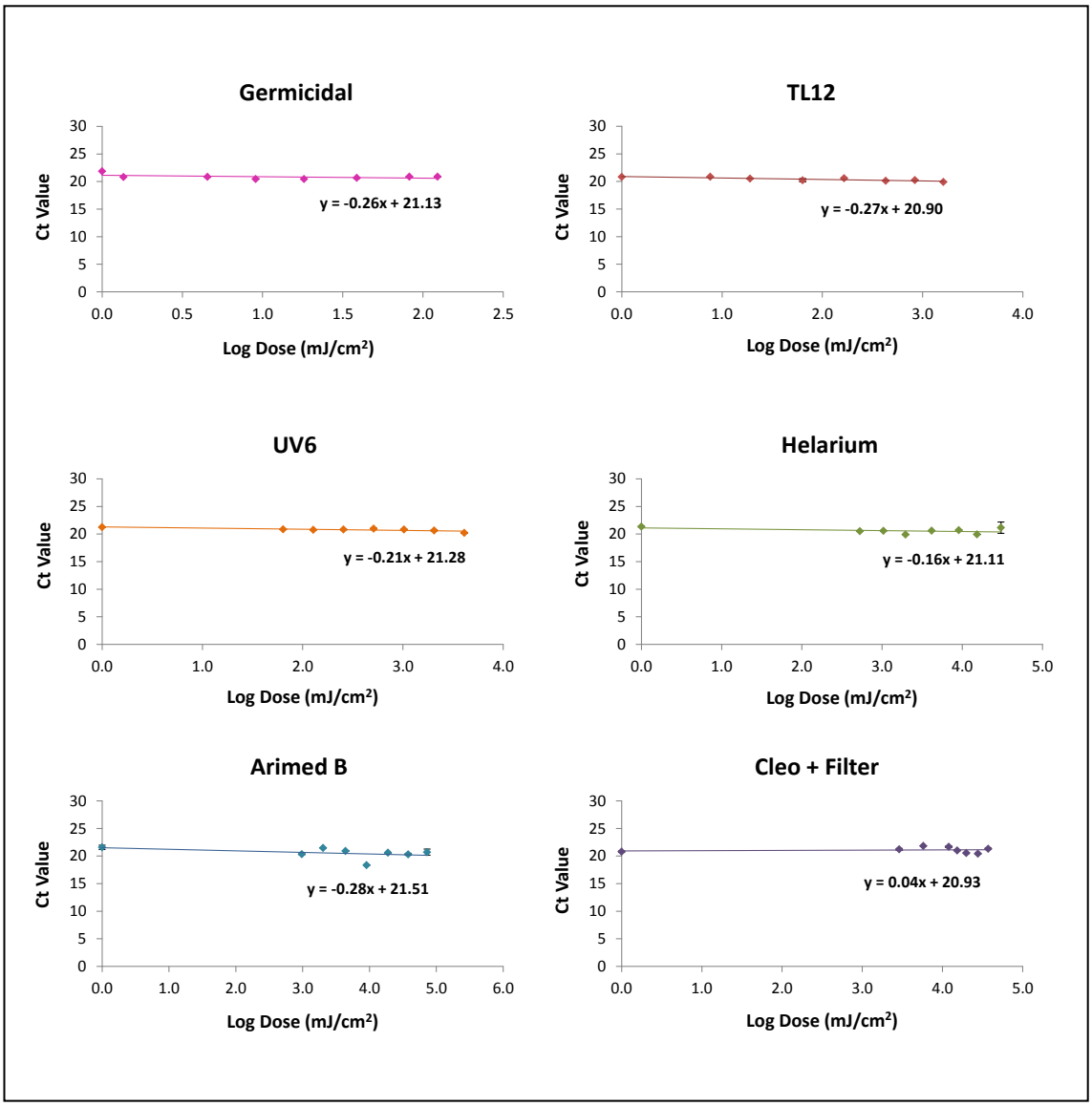

Figure 3.17: Determination of mtDNA Content in HaCaT Cells Following UVR Exposure. HaCaT cells were exposed to increasing doses of the various UVR sources. mtDNA content was assessed using a QPCR method to amplify an 83 bp section of mtDNA. Data expressed as the mean n=3 ± SEM. Linear regression analysis of this data showed no statistically significant deviation from control (P>0.05) with the exception of irradiation TL12 (P<0.004) and UV6 (P<0.02).

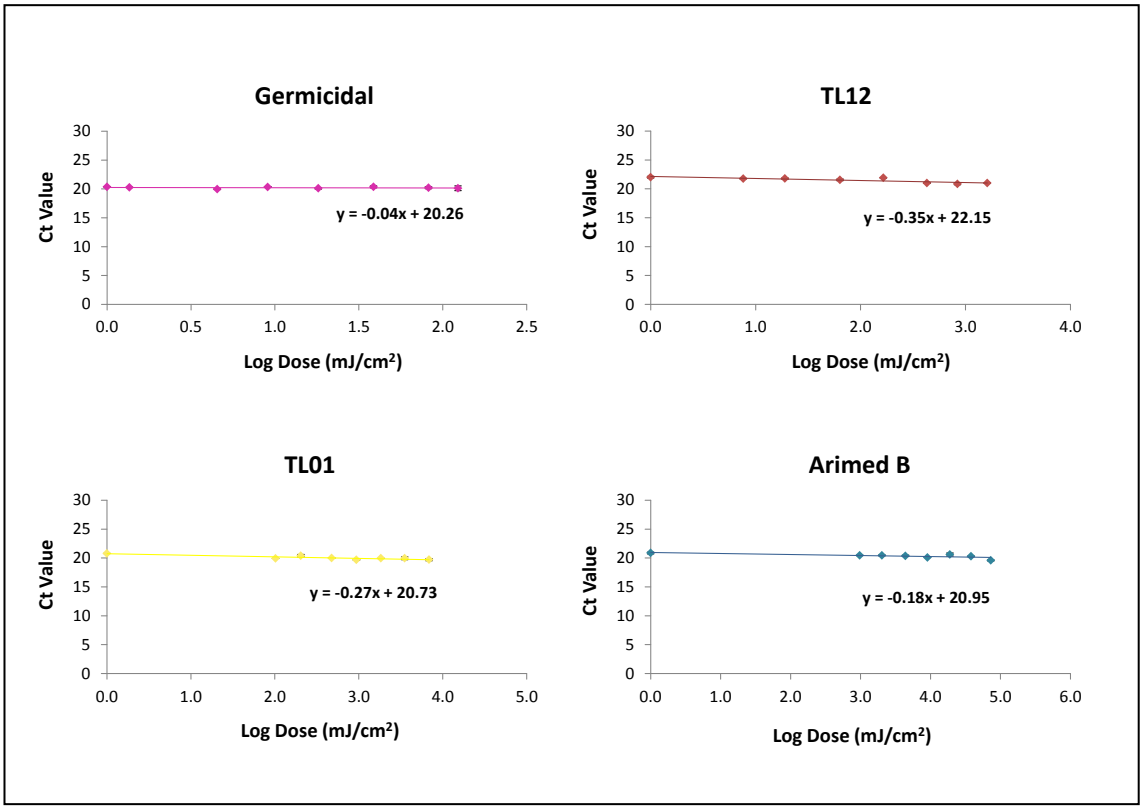

Figure 3.18: Determination of mtDNA Content in Primary Keratinocytes Following UVR Exposure. Primary Keratinocyte cells were exposed to increasing doses of the various UVR sources. mtDNA content was assessed using a QPCR method to amplify an 83 bp section of mtDNA. Data expressed as the mean n=3 ± SEM. Linear regression analysis of this data showed no statistically significant deviation from control ($P>0.05$) with the exception of irradiation with TL12 ($P<0.04$) and TL01 ($P<0.01$).

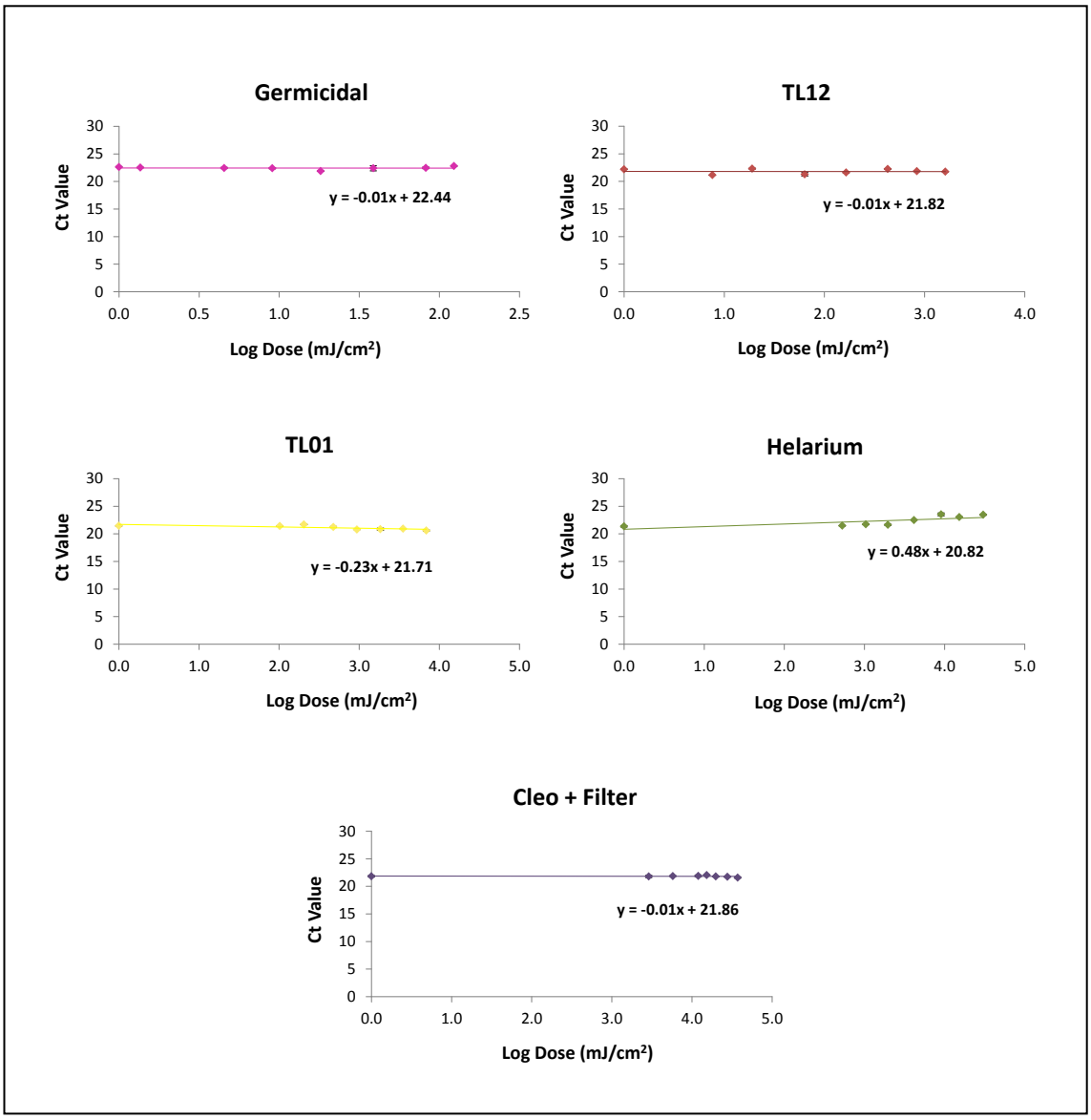

Figure 3.19: Determination of mtDNA Content in HDFn Cells Following UVR Exposure. HDFn cells were exposed to increasing doses of the various UVR sources. mtDNA content was assessed using a QPCR method to amplify an 83 bp section of mtDNA. Data expressed as the mean n=3 ± SEM. Linear regression analysis of this data showed no statistically significant deviation from control ($P>0.05$) with the exception of irradiation with TL01 ($P<0.05$) and Helarium ($P<0.03$).

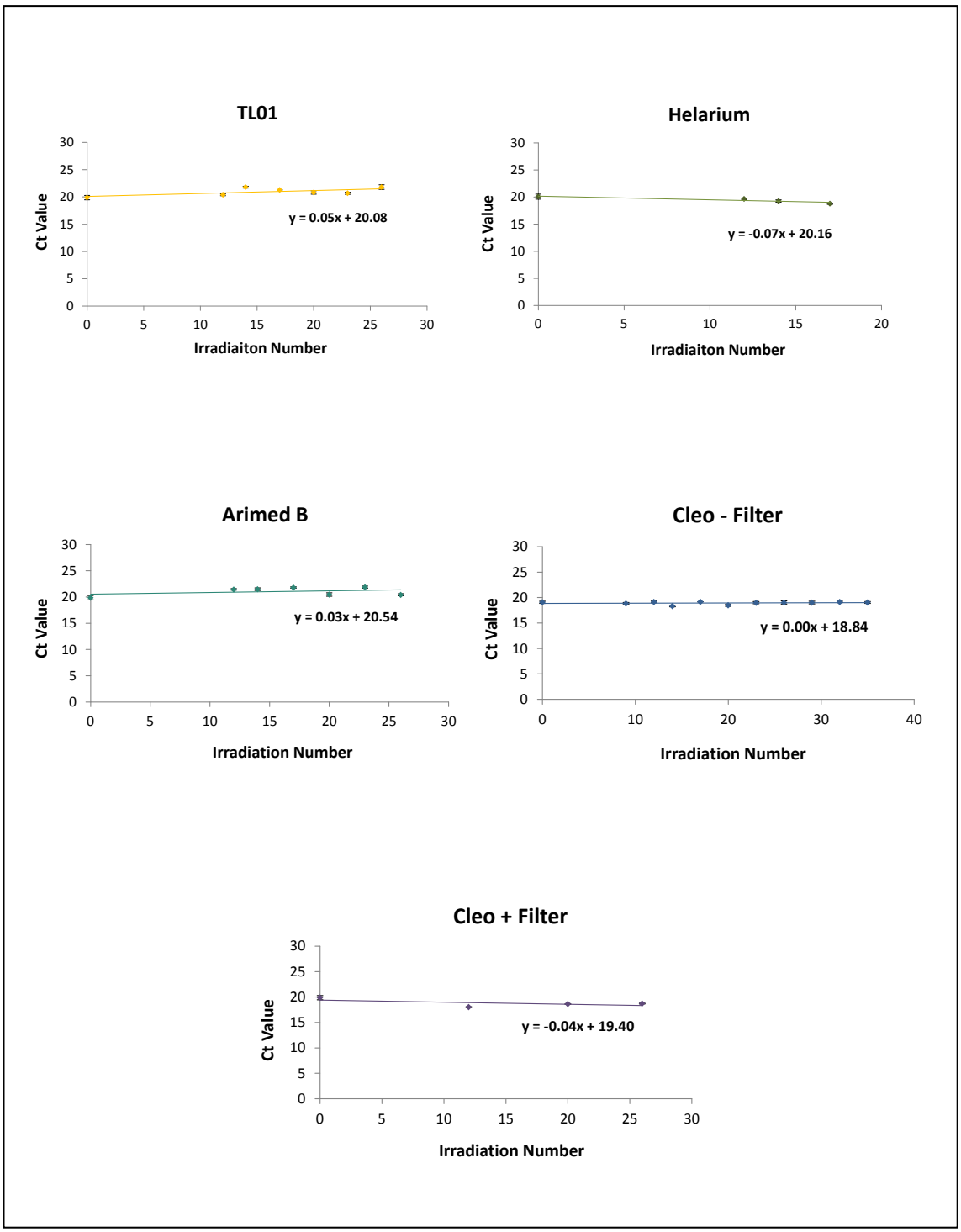

Figure 3.20: Determination of mtDNA Content in HaCaT Cells Following Repeated UVR Exposure. HaCaT cells were exposed to 1 SED of the various UVR sources every other day for up to 35 exposures (irradiation number). mtDNA content was assessed using a QPCR method to amplify an 83 bp section of mtDNA. Data expressed as the mean n=3 ± SEM. Linear regression analysis of this data showed no statistically significant deviation from control (P>0.05).

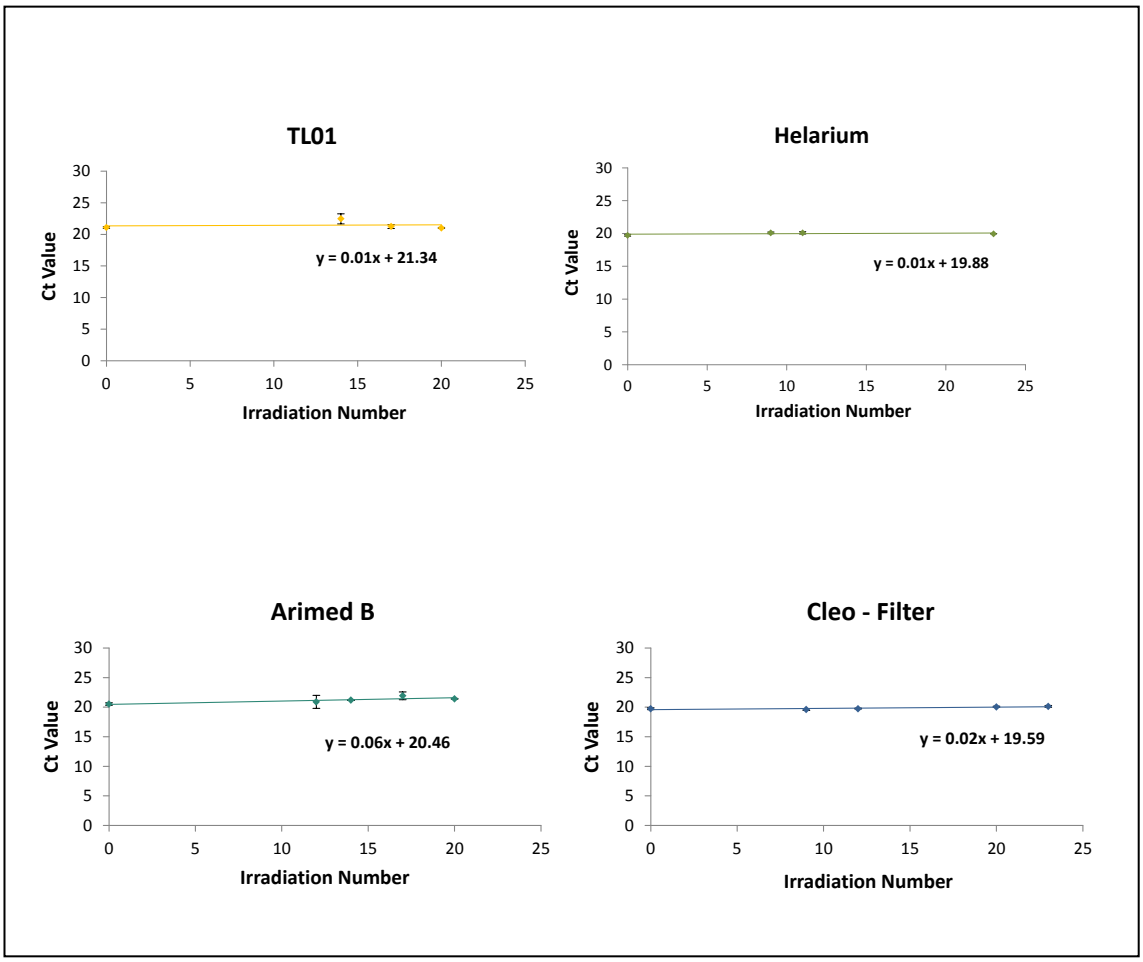

Figure 3.21: Determination of mtDNA Content in HDFn Cells Following Repeated UVR Exposure. HDFn cells were exposed to 1 SED of the various UVR sources every other day for up to 35 exposures (irradiation number). mtDNA content was assessed using a QPCR method to amplify an 83 bp section of mtDNA. Data expressed as the mean n=3 ± SEM. Linear regression analysis of this data showed no statistically significant deviation from control (P>0.05).

3.4 Discussion

3.4.1 The Spectral Output of UVR Sources

On all the spectral charts narrow peaks can be seen at approximately 313 nm and 365 nm. These peaks are characteristic lines of the low pressure mercury vapour that is contained in the fluorescent lamps.

The UVR sources used for this study were specifically selected to give a range of wavelengths within the UVR spectrum. The Germicidal and the TL01 lamps covered a narrowband emission spectrum giving emission which were mainly UVC (96 %) and UVB (78 %) respectively (see Table 3-2) which were seen as sharp peaks at 254 nm and 311 nm. All the remaining lamps had a broadband emission spectrum, the TL12 lamps emitted an even spread across the entire spectrum whereas the TL09 and the Cleo lamps + filter provided an entirely UVA source. The Arimed B lamp was the closest match to natural sunlight with 4 % UVB and 96 % UVA (sunlight is 6 % UVB and 94 % UVA; (B. L. Diffey, 2002)). The remaining UV6 and Helarium lamps provided an intermediary between TL12 and Arimed B. Interestingly the TL12, UV6 and the TL01 lamps are routinely used in the treatment of psoriasis, and it is therefore interesting to see any detrimental effects associated with these particular lamps. The UVR sources chosen all had unique spectrums which enabled particular sections of the UVR spectrum to be analysed in future experiments. For example, any damaged caused by the TL09/Cleo lamp - filter that was not caused by the TL09/Cleo lamp + filter was assumed to be due to the UVR wavelengths between ~315 – 330 nm. The irradiance emitted from the TL09 lamp was low, and to deliver the high doses needed to determine the entire UVR damaging effects, a long irradiation time at a high temperature was required. This proved difficult without causing substantial cell death and therefore the Cleo UVR source was obtained in an aim to combat these difficulties. Figure 3.4 shows that the difference in the spectra of the two lamps ± filter is minimal and that either lamp could be used interchangeably.

3.4.2 Evaluation of the Distribution of UVR from the Source

An important aspect of this study was to determine any differences in irradiance from the lamps dependent of the position beneath the lamps. The results show that there is an uneven distribution of irradiance emitted from the 2 ft UVR source and this highlights the importance for measuring irradiance from the UVR source based on position for each individual experiment. As expected there was a large decrease in emissions from the lamps in the 2 ft light source when they were reduced in number from 4 to 2. The percentage error of distribution is higher when using 2 lamps (46 and 32 %) opposed to 4 (44 and 19 %) and this should be taken in to account. As well as this, the emissions vary more when closer to the source than when further away, this is seen by the curve 'flattening' as it moves further away from the source. When measuring the irradiance from left to right a flattening is seen in the centre which shows no error across the plate and therefore cells should be positioned as close to the centre as possible. A similar flattening is seen towards the front of the canopy where plates can be positioned so that there is only 1 % error across the 6 cm dishes used. The results show a much larger difference in distribution when using the 2 ft light source as opposed to the 6 ft light source.

3.4.3 Temperature Emissions are Greatest from the TL09 UVR Source

It has been discussed that temperature emitted from light sources may contribute to the negative effects measured in previous studies. This has been of particular debate when investigating the effects of IRR (Piazena and Kelleher, 2010; Jung *et al.*, 2012). The fluctuation in temperature during irradiations was a necessary variable and it was therefore important to investigate the temperature emissions produced by the UVR sources used in this study. Temperature emissions were measured from the UVR sources which required lengthy irradiation periods in order to deliver the large doses required to create mtDNA damage. These sources include Helarium, Arimed B, TL09 and Cleo. Temperature was measured over a 6 h time period, with and without the mimicking of the foil cover used to protect control experiments from UVR. Results showed that the addition of the foil cover created a small reduction in the temperature emitted from all of the UVR sources assessed. However, with the

exception of the TL09 UVR source, all the UVR source temperature emissions measured were found to be below that of which the cells would ordinarily be acclimatised to within the incubator (37 °C). Therefore any damage seen cannot be equated to 'heating' effects, and a reduction in temperature effects would be accounted for by use of the control. The large increase in temperature emitted from the TL09 UVR source was of some concern which was a problem easily solved by use of the Cleo UVR source in its place.

3.4.4 No Damage Created in HDFn Cells Heated to 48 °C

The TL09 source had already been utilised for various studies (not all included in this thesis). So it was therefore of interest to see whether the high temperature emitted from this lamp could actually cause damage in the mtDNA by means of measuring the reduction of amplification of a large section of the mitochondrial genome (11 kb QPCR assay). For this experiment no UVR was used, and instead the cells were exposed to a high temperature (48 °C) by use of a water bath. Following analysis, no mtDNA damage was seen (in comparison to control cells) in the cells exposed to the high temperature. So although for the majority of this study the Cleo UVR source was favoured over the TL09 it was reassuring to discover that the damage created (when assessed using the 11 kb assay) by this source was from the UVR and not the heat it emits.

3.4.5 Damage Dependent on Irradiation Media was not found to be Statistically Significant

On-going work in our group has shown that constituents of the culture media can modulate the performance of oxidative stress probes as inducers of oxidative stress (Boulton *et al.*, 2011). In light of this it was important to investigate any effects of culture media (i.e. DMEM $\pm$ FCS, PBS) on UVR induced mtDNA damage. This was due to prospect of irradiating the cells in DMEM - FCS in an aim to reduce the potential death of cells irradiated in PBS for long time periods (e.g. with TL09 irradiations).

A profile of UVR dose effect curves, over a range of 7 to 1600 mJ/cm^2 (absolute UVR, equivalent to approximately 0.2 to 40 SED), using the TL12 UVR source to irradiate either HaCaT or HDFn cells, were plotted (Figure 3.7 and Figure 3.8 respectively). Each

of these 'individual' curves represented a series of experiments used to make up an individual data point. The mean maximum response was plotted to show any extensive differences dependent on irradiation media. With HaCaT cells, the mean maximum response was much less in DMEM ± FCS than when cells were irradiated in PBS alone which suggested that DMEM could be acting protectively on the cells. However, this trend was not seen in the HDFn cells where the highest mean maximum effect was seen when cells were irradiated in DMEM + FCS. In addition to this no statistical significance between the mean maximum effects, dependent of irradiation media, was seen in either of the cell lines. As well as the mean maximum response, the mean EC_{50} was also plotted. With the HDFn cells a clear stepwise increase in EC_{50} was seen from PBS, DMEM - FCS and DMEM + FCS which was also reflected in the HaCaT cells, but the increases were much smaller. This again suggests that the DMEM could be acting protectively on the cells and more so with the addition of FCS. Nevertheless this effect was again not found to be statistically significant in either cell line. An increase in the number of experiments assessed may uncover some differences in the effect of UVR on cells dependent of irradiation media, but any variance is likely to be small. Further experiments therefore encompassed DMEM - FCS as the irradiation media used in cell line experiments. Due to possible confounding effects in Primary Keratinocyte cells cultured in DMEM, PBS was the irradiation media used for these cells.

3.4.6 UVR-Induced Skin Cell Death is Wavelength Dependent

The majority of the reported cell viability to UVR exposure data involves the crude separation of UVA and UVB. Little data exists on the more specific different UVR sources effects and it is therefore difficult to compare previous literature to this study. As a general entity, UVA at a dose of 10 J/cm^2 has been found to cause minimal cell death in dermal fibroblasts (M. J. Petersen *et al.*, 1992; Hoerter *et al.*, 2008). Furthermore 100 mJ/cm^2 UVB has been found to not significantly decrease human keratinocyte viability (M. J. Petersen *et al.*, 1992). This UVB source only covered wavelengths 280 to 320 nm, and therefore represents a source unlike those used within this study. Although discrepancies in the experimental procedure exist of the previously reported and this study, similarities in the result are present. For example, when using the Cleo + filter UVR source (the source most closely resembling that used

in previous studies for UVA) no statistically significant cell death was seen with a dose of 10 J/cm^2. Also, following an approximate dose of 100 mJ/cm^2 of various UVB emitting sources (TL12, UV6 and TL01) no statistically significant reduction in cell viability was seen. These similar tendencies for cell death support the MTS assay as an adequate measure for cell viability, as does its ability to detect a dose-dependent effect for the greater part.

The cell viability data shows decreases when the skin cells were exposed to increasing doses of all the UVR sources. The summary presented in Table 3-4 illustrates that as a general rule, the longer the wavelengths the UVR source emits the higher the dose required to cause 50 % cell death. This was coupled with an increase in irradiation time, as well as a reduction in SED. This could suggest that the time the cells are irradiated for may affect viability, which would be understandable as the cells are removed from their optimum environment. This data was considered in the analysis of future experiments as irradiation time could lead to confounding effects. Nonetheless the trend for shorter wavelengths of UVR to cause more cell death is well reported in various cell types (Andley *et al.*, 1994; Aoki *et al.*, 2004).

An observation from this data saw a trend for the HaCaT cells to be the most resistant to UVR exposure, independent of UVR source type. This effect has been shown previously, where keratinocytes achieved better survival rates following UVR exposure than dermal fibroblasts (Otto *et al.*, 1999). However, although more resilient to several of the different UVR source exposures, Primary Keratinocytes did not consistently follow this pattern. For some if the different UVR exposures these cells proved more sensitive than the HDFn cells. Possible suggestions for these differences could be owed to the greater variability seen in Primary Keratinocytes; potentially due to donor differences.

3.4.7 mtDNA Content of Skin Cells is not Affected by UVR Exposure

mtDNA can vary between individual subjects as well as between an individual's tissues and can also differ with the age of the sample (Venegas *et al.*, 2011). Therefore as a rule in our laboratory all samples investigated for mtDNA damage first undergo determination of mtDNA content by use of the 83 bp assay. This is to ensure that the

same amount of mtDNA is used in mtDNA damage assays (as DNA amount is a confounding factor in PCR analysis). For the experimental work in this thesis, cell lines and Primary Keratinocytes were utilised. There could be differences between mtDNA content, between the different donors used to obtain the Primary Keratinocytes, and also possibly between different passage numbers of the cell lines. However a difference between the cells was obsolete as comparisons were made to a control of the exact same cells. What was of interest was any difference in mtDNA content created by irradiation as this could over/under estimate any damage recorded. Therefore samples of the three different cells types exposed to a selection of lamps covering all UVR wavelengths were analysed for mtDNA content (Figure 3.17, Figure 3.18 and Figure 3.19). As well as this, mtDNA content in HaCaT and HDFn cells exposed to a repeated pattern exposure of the various UVR sources was also determined (Figure 3.20 and Figure 3.21). The data for mtDNA content was conflicting, showing that some of the lamps created a difference in mtDNA in some cells but not others. For example the UV6 UVR source was found to cause differences in mtDNA content in HaCaT cells but not Primary Keratinocytes or HDFn cells and the Helarium lamp in HDFn cells but not HaCaT cells. Further to this, lamps emitting similar wavelengths caused differences. An example of this was shown by the TL12 lamp, which emits the exact same wavelengths as the TL01, causing no difference in mtDNA content in HDFn cells, whereas the TL01 lamp did. PCR is sensitive to various parameters and to determine differences in mtDNA content a consistent dose-dependent difference should have been seen. Instead the Ct values tended to remain at 20-22 Ct, with minor fluctuations causing alterations in the gradient of the linear regression due to the stringent data. If UVR was to cause an effect on mtDNA content then this effect would most certainly be dose-dependent which is commonly associated with a sigmoidal plot, as seen in Figure 3.7 and Figure 3.8. Although some significant differences in mtDNA were seen, these differences were not consistent across cell type or UVR source and the regression was quite linear rather than the expected sigmoidal plot. Therefore it was concluded that the increasing doses of UVR did not alter mtDNA content.

3.4.8 Summary

The spectral outputs of the UVR sources used in this study were varied so that they generally overlap and cover the entire UVA and UVB spectrum. The Germicidal lamp was utilised to add completion to the data by means of a UVC dimension. Further to this, the TL09 lamp and the Cleo lamp had a mirroring spectral output and these two lamps were found to be able to be used interchangeably.

The distribution of UVR from the 6 ft UVR source was more consistent than the 2 ft UVR source. This highlighted the need for accurate cell placement when using the 2 ft UVR source.

The TL09 UVR source emitted a temperature above incubator conditions of 48 °C, however this temperature was not found to create damage in mtDNA when using the 11 kb assay.

The media the cells were irradiated in had no statistically significant effect on the amount of mtDNA damage that was created by the TL12 lamp when assessed using the 11 kb assay.

UVR sources emitting a large number of long UVR wavelengths as opposed to short UVR wavelengths needed a higher dose to create the same amount of cell death.

Increasing doses of UVR had no effect on mtDNA content and therefore the same amount of cellular DNA could be used in future QPCR experiments to measure UVR-induced damage.

Chapter 4

Results 2 - Determining the Action Spectrum of UVR-Induced mtDNA Damage

Chapter 4 Results 2 – Determining the Action Spectrum of UVR Induced mtDNA Damage

4.1 Introduction

QPCR has the ability to effectively quantify both damage and repair in nDNA and mtDNA which has been shown in various cell and tissue types after exposure to numerous genotoxins (Santos *et al.*, 2006). This chapter describes the use of QPCR to measure the damage created in mtDNA by UVR.

A method previous to the use of QPCR for the calculating of mtDNA deletions (disease, ageing and toxin associated) was Southern hybridization with a probe composed of the whole mitochondrial sequence or of the D-loop region (Kleinle *et al.*, 1997; Tonska *et al.*, 2012). With this approach the occurrence of false positives was minimal, however the method was laborious. Further negatives for this method was the requirement for a substantial DNA sample (10-50 µg) and the resulting sensitivity was quite poor (Kleinle *et al.*, 1997; Tonska *et al.*, 2012). Another method identified for this type of analysis is by multiplex ligation probe-dependent amplification (MLPA), where >40 genomic copy-number changes such as deletions or duplications can be semi-quantitatively targeted in one assay. Although quite recently introduced and reportedly successful, Tonska *et al.*, 2012 found that it had a lower sensitivity compared to a carefully optimised PCR. They went on to suggest that MLPA could be of benefit for high-throughput molecular diagnosis of patients when complemented with PCR (Tonska *et al.*, 2012). Consequently the most common and most sensitive approach is by various PCR methods, making for speedy analysis and requiring a smaller sample size (ng DNA). These focus on the use of short segment PCR for the determination of specific deletions and long PCR methods which are able to amplify 10-25 kb of DNA and can therefore cover the majority of the mitochondrial genome (Kleinle *et al.*, 1997; Santos *et al.*, 2006).

As the aim of this chapter was not to scan the samples for many mtDNA deletions, but instead to quantify the occurrence of specifically selected deletions and overall

damage in response to UVR-irradiation, it was decided that QPCR was the most purposeful method.

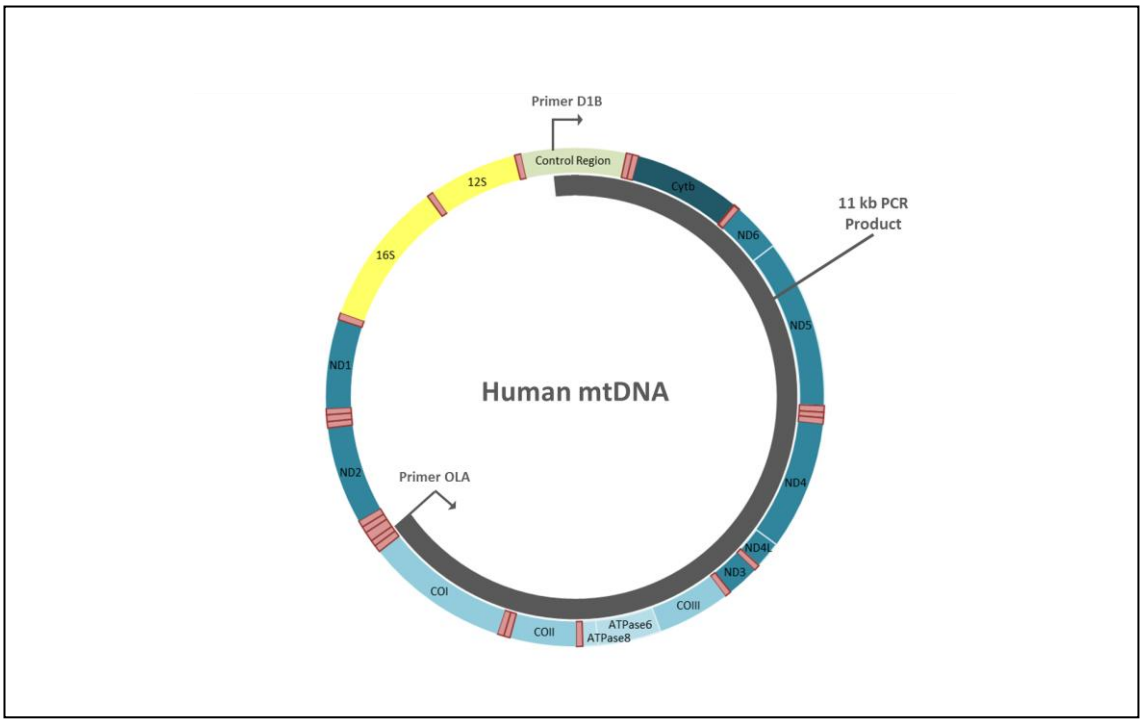

Figure 4.1: Positioning of the 11 kb Section of mtDNA Amplified by the Long QPCR Method. This figure illustrates where the primer set used for this QPCR method anneal, and where the 11 kb section they amplify is positioned within mtDNA. More information detailing the primer sequences for this assay can be found in Chapter 2.

A major QPCR assay used within this study was utilised in an aim to quantify total mtDNA damage by means of the previously discussed long PCR. The basis of this assay is that various DNA lesions and breaks will hinder the progression of DNA polymerase. This means that DNA with minimal damage will amplify more efficiently and to a greater extent than DNA with maximal damage. Furthermore this assay is useful in the measuring of DNA repair kinetics (Santos *et al.*, 2006). The particular assay used in this study amplifies an 11,095 bp segment of the mtDNA which is found in the major arc, the "hotspot" area for mtDNA deletions (Tonska *et al.*, 2012). A similar method has been described by Santos et al., 2006, which was further optimised to the one utilised in this investigation by Passos *et al*., 2007, who were interested in age related increases in mtDNA damage (Santos *et al.*, 2006); (Passos *et al.*, 2007). Our group has also recently published this method for its use in determining UVR-induced damage within the mitochondrial genome (Swalwell *et al.*, 2012). The position of the primers used in this assay and the location of the product formed is depicted in Figure 4.1.

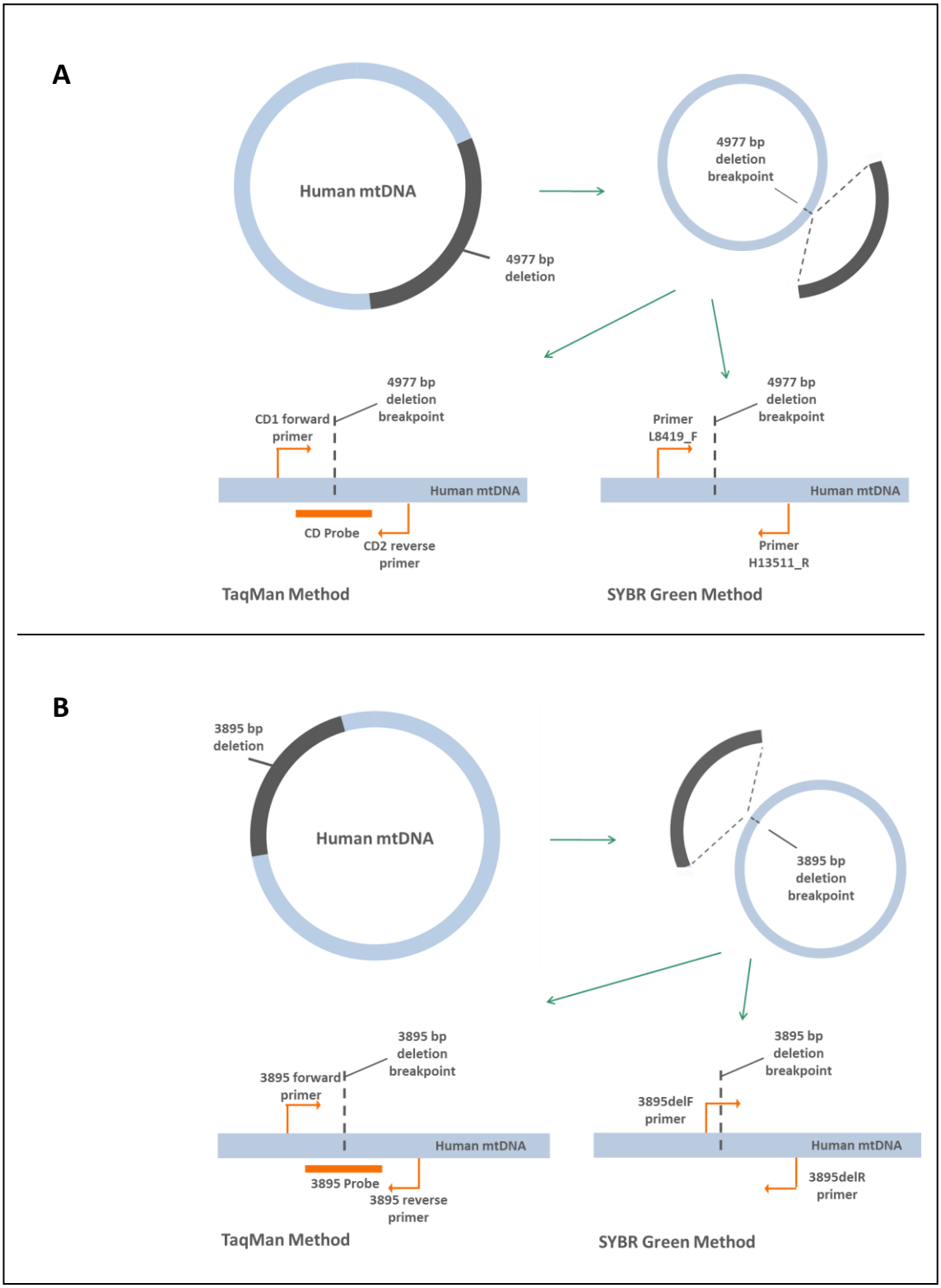

Figure 4.2: Illustration of Different QPCR Methods used to Detect Specific mtDNA Deletions. This figure depicts the differences between the TaqMan and SYBR Green methods used to detect for the mtDNA specific deletions; the 4977 bp (A) and the 3895 bp (B). For detection of both of the deletions, the TaqMan method encompasses a probe which spans the breakpoint of the deletion with the primer set annealing either side. This allows for specific deletion detection. For the detection of the 4977 bp deletion the SYBR Green method utilises a primer set which anneals either side of the breakpoint. This method incorporates a short extension time during PCR cycling to ensure only the deletion is amplified. With detection of the 3895 bp deletion, the SYBR Green method uses a primer set, the forward primer of which spans the breakpoint and the reverse primer anneals outside of the breakpoint, only allowing for amplification of DNA carrying the deletion. Both the previously validated and the modified primer sets for 3895 bp SYBR Green detection follow this method.

The two UVR associated specific mtDNA deletions, identified as particularly relevant to this study, were the 4977 bp and the 3895 bp. A detailed explanation of these two deletions is found in Chapter 1. In brief both have been found to be more prevalent in sun-exposed skin as opposed to sun-protected and they have both been reportedly induced by artificial UVR exposure in cell cultures (Berneburg *et al.*, 1999; Krishnan *et al.*, 2004; Schroeder *et al.*, 2008). This chapter uses various QPCR methods to determine the induction of these two deletions by UVR in skin cells. These methods include both SYBR Green and TaqMan chemistries, some of which have been published. The principle of these QPCR methods is for the primer or probe to span the break-point of the deletion, thereby only amplifying mtDNA which contains the specific deletion. A detailed illustration of how the different methods are utilised to detect the specific deletions is shown in Figure 4.2.

4.1.1 Aims

The primary aim of this chapter was to determine an action spectrum of UVR-induced damage. Assessment of damage was three-fold; by a long QPCR method to measure total damage within an 11 kb segment of the mitochondrial genome and by means of more specific short QPCR to identify the induction of two different UVR-induced mtDNA deletions.

4.2 Methods

The methods shown here are specific for this chapter; for general methods including cell culture techniques, UVR irradiations and the 11 kb PCR please refer to Chapter 2.

4.2.1 Action Spectrum Modelling

From the dose curves of mtDNA damage created by the TL12, UV6, TL01, Helarium, Arimed B, Cleo – filter and Cleo + filter UVR sources, a consistent value was obtained. This value was the UVR dose required to create a 10 % increase in mtDNA damage from the control. From this data a dose per unit effect for each of the UVR sources was calculated (observed effect).

A three-exponential model was then fitted based on the previously determined action spectrum of UVR-induced erythema. This model encompassed two points fixed at 270 and 400 nm and incorporated two inflection points. The trend function within excel was then used to fit straight lines between the points. Based on this initial curve, a relative dose per unit effect for each of the UVR sources was obtained (modelled effect).

The action spectrum for UVR-induced mtDNA damage was then predicted using the solver function within excel to find the minimum sum of the squared differences between the observed effect and the modelled effect. For reference a screen shot of the excel worksheet used for analysis can be found in Appendix II.

4.2.2 Positive Controls

A small sample of patient DNA harbouring the 4977 bp deletion was a kind gift from Professor Robert Lightowlers. To increase the quantity for regular positive control analysis this deletion was amplified using both primer sets found in Table 4-1. The PCR was performed in 50 µl reactions containing: 50 ng DNA sample, 1x PCR master (Roche, UK), 200 nM of each primer and made up to the required volume with high grade PCR water. The Amplification conditions were 94 °C for 2 min, and then 40 cycles of 15 sec at 94 °C, 30 sec at either 60 °C (TaqMan primers) or 52.3 °C (SYBR Green primers) and 45 sec at 72 °C. A final extension at 72 °C for 7 min was also performed. The Cycling was carried out on the GeneAmp PCR system 9700 (Applied Biosystems, UK).

Samples m63d and m61e were positive and negative for the 3895 bp deletion respectively. These samples were perilesional skin samples excised from the face of male outpatients from the RVI, Newcastle. The labelling of these samples was numerical for subject, m denotes male, d is dermis and e is epidermis.

4.2.3 4977 bp Deletion SYBR Green PCR

The PCR was performed in 25 µl reactions containing: 50 ng DNA sample, 1x Platinum SYBR Green qPCR SuperMix-UDG with added 1 mM M_gCl_2, 1 µl 1/20 BSA (Invitrogen, UK), 200 nM of each primer and made up to the required volume with high grade PCR

water. The primers and method used were previously optimised and kindly shared by the mitochondrial research group, see Table 4-1. The Amplification conditions were 95 °C for 10 min, and then 40 cycles of 15 sec at 95 °C, and 1 min at 52.3 °C; melt curve analysis performed at 50 °C-105 °C, reading every 0.5 °C. The analysis of the reactions was carried out on the StepOne PCR machine (Applied Biosystems, UK).

Table 4-1: Primers and Primer/Probe Sets for Deletion Detection.

Target	Name	Oligonucleotide Sequence (5' → 3')
4977 bp	L8419_F	5'- TAC ACT ATT CCT CAT CAC CC -3' (8419-8438)
	H13511_R	5'- TTG GAG TAG AAA CCT GTG A -3' (13511-13493)
4977 bp (Koch *et al.*, 2001)	CD1 forward primer	5'- ACC CCC ATA CTC CTT ACA CTA TTC C -3' (8405-8429)
	CD2 reverse primer	5'- AAG GTA TTC CTG CTA ATG CTA GGC T -3' (13465-13489)
	CD probe	5'- ACA CAA ACT ACC ACC TAC CTC CCT CAC CA-3'FAM (8485/13459)
3895 bp (Harbottle *et al.*, 2010)	3895delF	5'-CTG CTA ACC CCA TAC CCC GAA AAT GTT G-3' (527–535 ⁄4431–4449)
	3895delR	5'-GAA GGA TTA TGG ATG CGG TTG CTT GCG TGA G-3' (4680)
3895 bp	3895del_mod_F	5'- CCG CTG CTA ACC CCA TAC CCC GAA AAT GTT G -3' (524-535/4431-4449)
	3895del_mod_R	5'- A GAA GGA TTA TGG ATG CGG TTG CTT GCG TGA G -3' (4681)
3895 bp (Harbottle and Birch-Machin, 2006)	3895 Forward	5'-CAA CCC TCG CCC ATC CTA-3' (491-508)
	3895 Reverse	5'-CCT GCA AAG ATG GTA GAG TAG ATG AC-3' (4516-4489)
	3895 Probe	5'-TGC TAA CCC CAT ACC CCG AAA ATG TTG G-3'FAM (527/4450)

Primers and primer/probe sets for the 4977 bp and the 3895 bp deletions are listed. Detection was either via SYBR Green (un-shaded) or TaqMan (shaded) technology. All primers and primer/probe sets were purchased from MWG, UK.

4.2.4 4977 bp Deletion TaqMan PCR

The PCR was performed in 25 µl reactions containing: 50 ng DNA sample, 300 nM of each primer, 200 nM of the probe, 300 nM dNTP, 1 x TaqMan Universal PCR Mastermix (Invitrogen, UK) and was made up to the required volume with high grade PCR water. The primers and the probe used (Koch *et al.*, 2001), can be found in Table 4-1. The cycling conditions were 95 °C for 10 min followed by 40 cycles of 15 s at 95 °C and 1 min at 60 °C. Analysis was performed on the StepOne PCR machine (Applied Biosystems, UK)

4.2.5 3895 bp deletion SYBR Green PCR

The PCR was performed in 25 µl reactions containing: 1x QuantiTect SYBR Green Mastermix (Qiagen, UK), 350 nM of each primer and made up to the required volume with high grade PCR water. The primers used were either a pair published (Harbottle *et al.*, 2010) or a similar pair with minor modifications, see Table 4-1. The modified pair differed from the previously validated pair by the addition of the (CCG) sequence at the 5' end of the forward primer and the addition of an (A) at the 5' end of the reverse primer which equalized the melting temperatures (Tms) of the pair. The Amplification conditions were 95 °C for 15 min, and then 40 cycles of 15 sec denaturation at 94 °C, 30 sec annealing at 64 °C and 30 sec extension at 72 °C; analysis performed at 50 °C-105 °C, reading every 0.5°C. The analysis of the reactions was carried out on the ABI Prism 7900HT or StepOne (both Applied Biosystems, UK) PCR machines.

4.2.6 3895 bp Deletion TaqMan PCR

The PCR was performed in 25 µl reactions containing: 50 ng DNA sample, 300 nM of each primer, 200 nM of the probe, 300 nM dNTP, 1 x TaqMan Universal PCR Mastermix (Invitrogen, UK) and was made up to the required volume with high grade PCR water. The primers and the probe used (Harbottle and Birch-Machin, 2006), can be found in Table 4-1. The cycling conditions were 95 °C for 10 min followed by 40 cycles of 15 s at 95 °C and 1 min at 60 °C. Analysis was performed on the StepOne PCR machine (Applied Biosystems, UK)

4.2.7 Concentration Curves

Concentration curves to show the efficiency of the primers utilised to measure induction of the 4977 bp deletion were determined using a positive DNA ranging from 10 – 5000 pg. The concentration curves for the SYBR Green primers used to amplify the 3895 bp deletion were produced using negative and positive DNA samples with a concentration range of 100 – 100000 pg. For the TaqMan method used to detect the 3895 bp deletion a concentration curve was produced using negative and positive DNA samples with a concentration range of 1000 - 100 pg.

4.2.8 Agarose Gel

Amplified PCR products were loaded on a 1 % w/v agarose (Gibco BRL, UK), dissolved in 40 mM tris-acetate 1 mM EDTA (1x TAE) gel, stained with ethidium bromide (0.25 μg/ml; Sigma, UK). A DNA molecular weight marker (Hyperladder 1) was also loaded and ran along-side the samples. Electrophoresis was performed in 1x TAE at 100-150 V for approximately 1 h. The gel was visualised using the FluroChem UV transilluminator (Alpha Innotech, UK) and was photographed as necessary.

4.2.9 Statistical Analysis

For evaluation of mtDNA deletion detection a linear regression was performed for comparison to the control, P-values below 0.05 were considered significant.

4.3 Results

4.3.1 UVR-Induced mtDNA Damage

The initial damage created in mtDNA was determined by the occurrence of strand breaks/lesions within an 11 kb section of the genome. This was quantified by the reduction in efficiency of the amplification of this product by QPCR in the damaged DNA. Damage was created by increasing the dosage of a particular UVR source, and when analysed, this data could be manipulated to produce a dose curve of damage. Figure 4.3 (A) shows a representative example of such a dose curve, the data is of the damage created by the TL01 lamp in HDFn cells. Each data point on this curve is for a

minimum of three biologically independent experiments, each technically repeated three times; therefore each point shows the mean of a minimum of nine sets of data. Each dose curve generally shows eight data points that represent 24 biologically independent experiments, an accumulation of 72 technical repeats. Further to this, each dose curve was repeated for the three different cell types investigated. For reference, an example of the dose curves of damage created by the TL01 lamp in the three different cell types has been plotted together; this is shown in Figure 4.3 (B). The dose curves on this figure mirror each quite closely, showing little difference. Observations made from this figure are that the HDFn cells are the most susceptible to damage followed by the Primary Keratinocytes then the HaCaTs.

The complete set of the dose curves of damage created by the various UVR sources in HaCat, Primary Keratinocytes and HDFn cells is recorded in Figure 4.4; A, B, and C respectively. The dose ranges used were approximate as follows, 0.005-0.2 J/cm^2 (Germicidal), 0.01-3 J/cm^2 (TL12), 0.1-4 J/cm^2 (UV6), 0.1-14 J/cm^2 (TL01), 0.3-30 J/cm^2 (Helarium), 1-73 J/cm^2 (Arimed B), 4-74 J/cm^2 (Cleo – filter) and 3-37 J/cm^2 (Cleo + filter); this equates to maximum SED values of 20, 80, 50, 80, 60, 40, 10 and 2 respectively.

The damage was calculated as a percentage increase when compared to UVR-protected control cells. Characteristic dose effect curves could be plotted for all the UVR sources in all the cell types. A trend showed a shift to the right of the dose curve when the UVR source emitted more long wavelengths (UVA). The maximum damage created by the different UVR sources differed. A particular observation of this was with irradiation with the Cleo ± filter where the maximum damage was much lower across cell types but mainly seen with HaCaT and HDFn cells. Further to this, little difference was seen in the slopes of the two curves created by the Cleo – filter and Cleo + filter in HaCaT cells. A similar observation was made in the HDFn cells where the slope of the curves created by the TL01 and the Helarium UVR sources are similar.

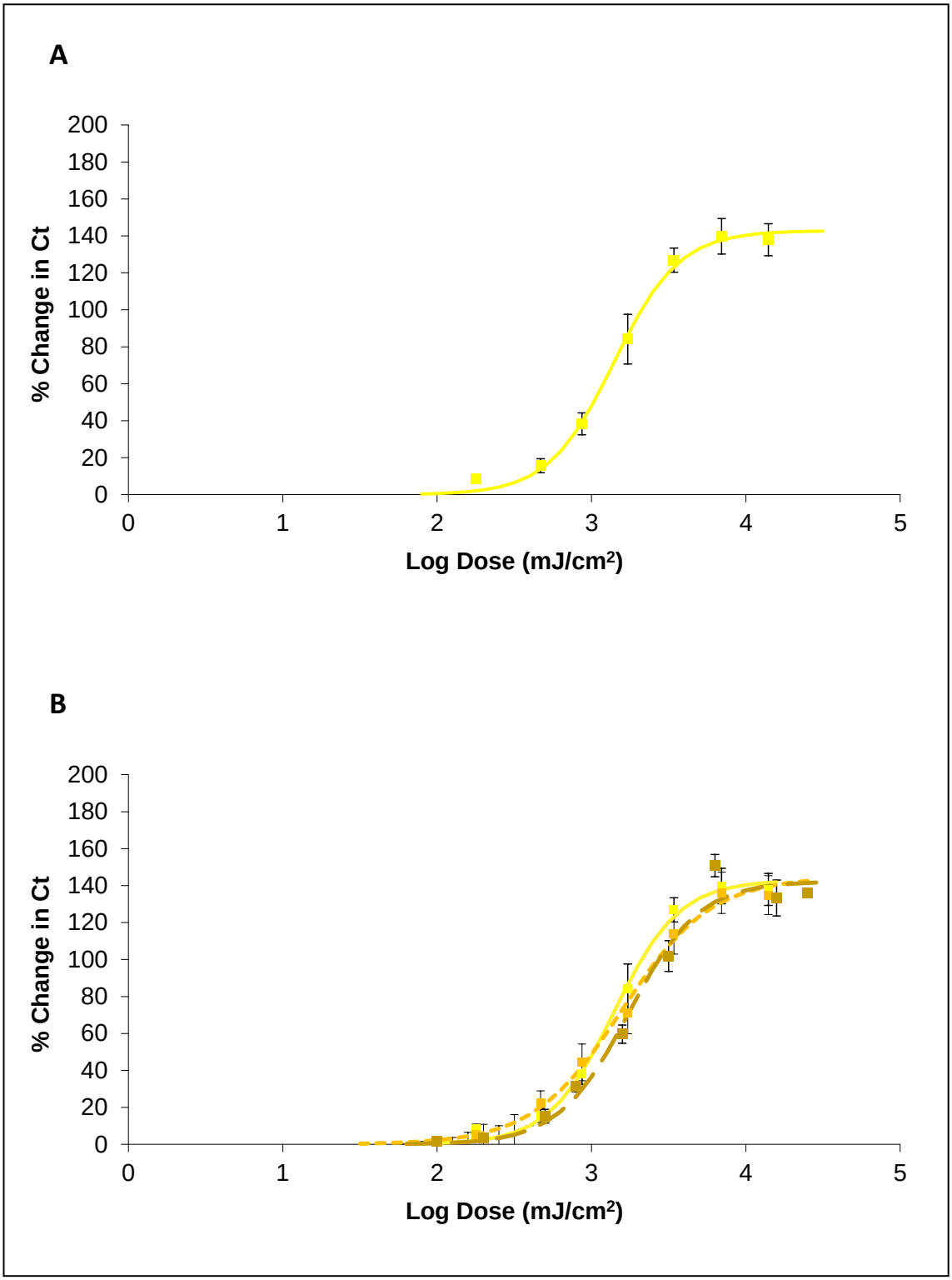

Figure 4.3: TL01-Induced Dose Curves of Damage. For reference, (A) shows the individual effect on increasing doses of TL01 of HDFn cells. This data is combined in (B) to compare the difference in cell type effect, from left to right; HDFn (—), Primary keratinocyte (- -) and HaCaT (——). Damage was assessed by a reduction in amplification of an 11 kb product by QPCR (increase in ct) and is expressed as a percentage increase when compared to control (UVR protected) cells Therefore 0 % signifies no damage (n≥3 ±SEM).

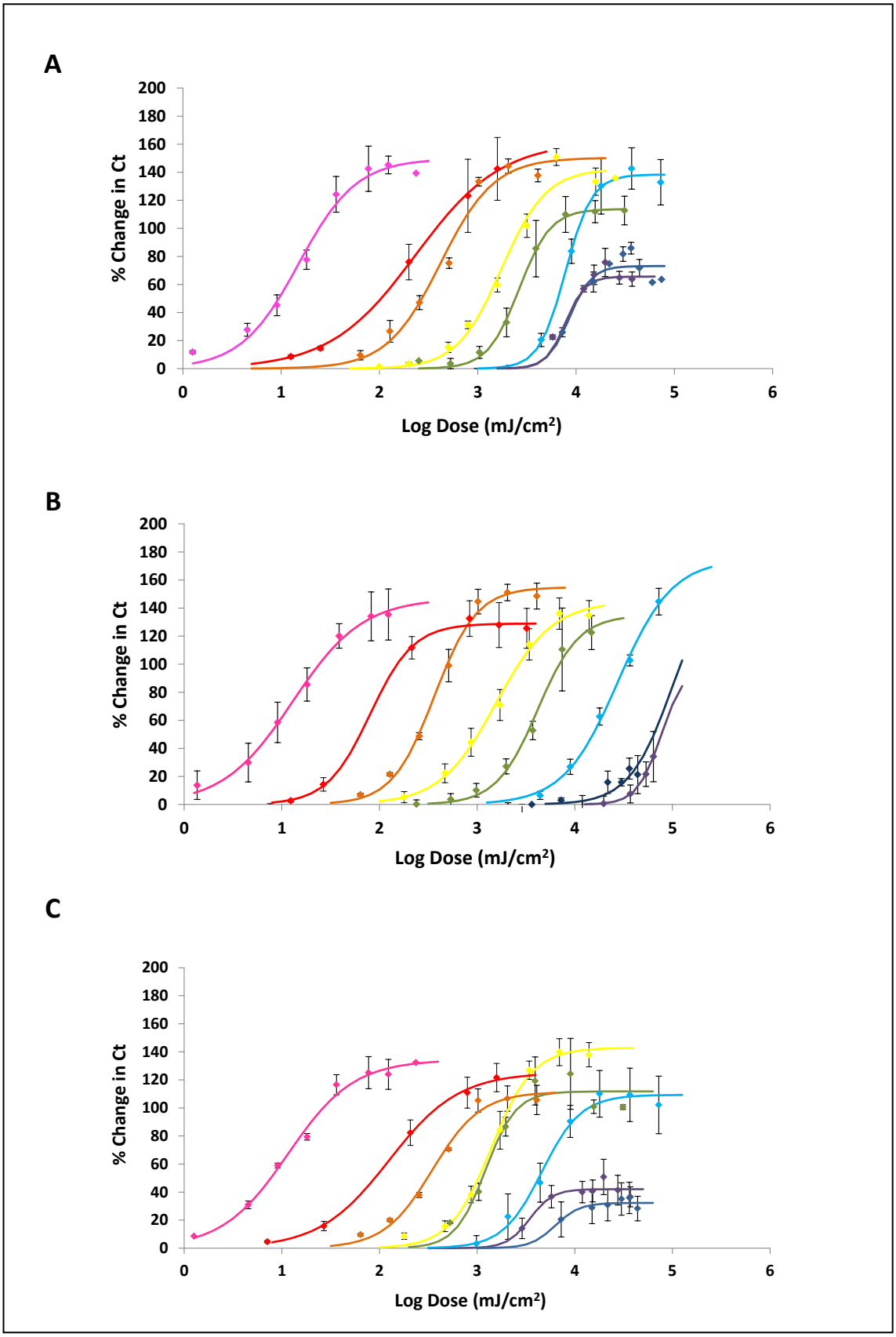

Figure 4.4: UVR-Induced Dose Curves of Damage. HaCaT (A), Primary Keratinocyte (B) and HDFn (C) cells were irradiated with increasing doses of (from left to right) the Germicidal (-), TL12 (-), UV6 (-), TL01 (-), Helarium (-), Armed B (-), Cleo – filter (-) and Cleo + filter (-) UVR sources. Damage was assessed by a reduction in amplification of an 11 kb product by QPCR (increase in ct) and is expressed as a percentage increase when compared to control (UVR protected) cells Therefore 0 % signifies no damage (n≥3 ±SEM).

4.3.2 The Action Spectrum of UVR-Induced mtDNA Damage

Following the plotting of the dose curves created by the various UVR sources, data could be utilised to calculate an action spectrum for each cell type. The action spectra for each individual cell type were fitted to a three-exponential model and are shown in Figure 4.5. For comparison, these were also plotted together on Figure 4.6, along with the previously determined action spectra for erythema induction and nDNA damage.

The action spectra for all three cell types followed a similar trend. The shortest wavelengths (270) were consistently the most detrimental. From this point the wavelength effects reduced with an increase in length until ~325 nm (HDFn), ~330 nm (HaCaT and Primary Keratinocytes). From these wavelengths in the HDFn and HaCaT mtDNA the detrimental effect seemed to increase with further decreasing wavelengths shown by the soft incline. From these wavelengths the little difference was seen in the damage to mtDNA in the Primary Keratinocytes.

The damaging effect of UVR on the mtDNA of HDFn cells was consistently higher than the other two cell types. This was particularly apparent between wavelengths 320-340 nm.

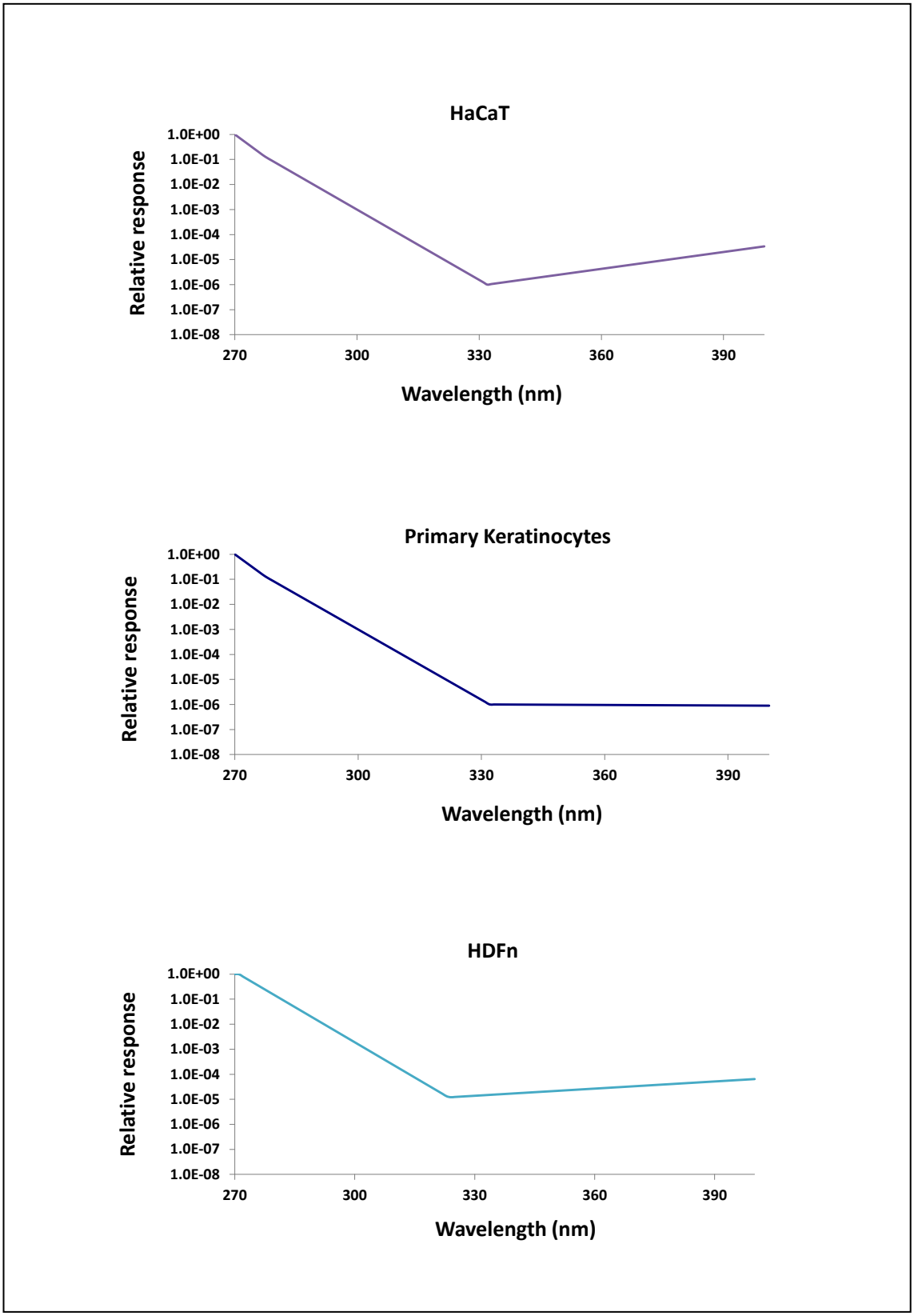

Figure 4.5: Action Spectrum of UVR-Induced mtDNA Damage. Utilising the data in Figure 4.4, action spectra of UVR-induced mtDNA damage were estimated using a method known as de-convolution. The action spectra for damage in an 11 kb section of mtDNA in HaCaT, Primary Keratinocyte and HDFn cells are plotted (n≥3).

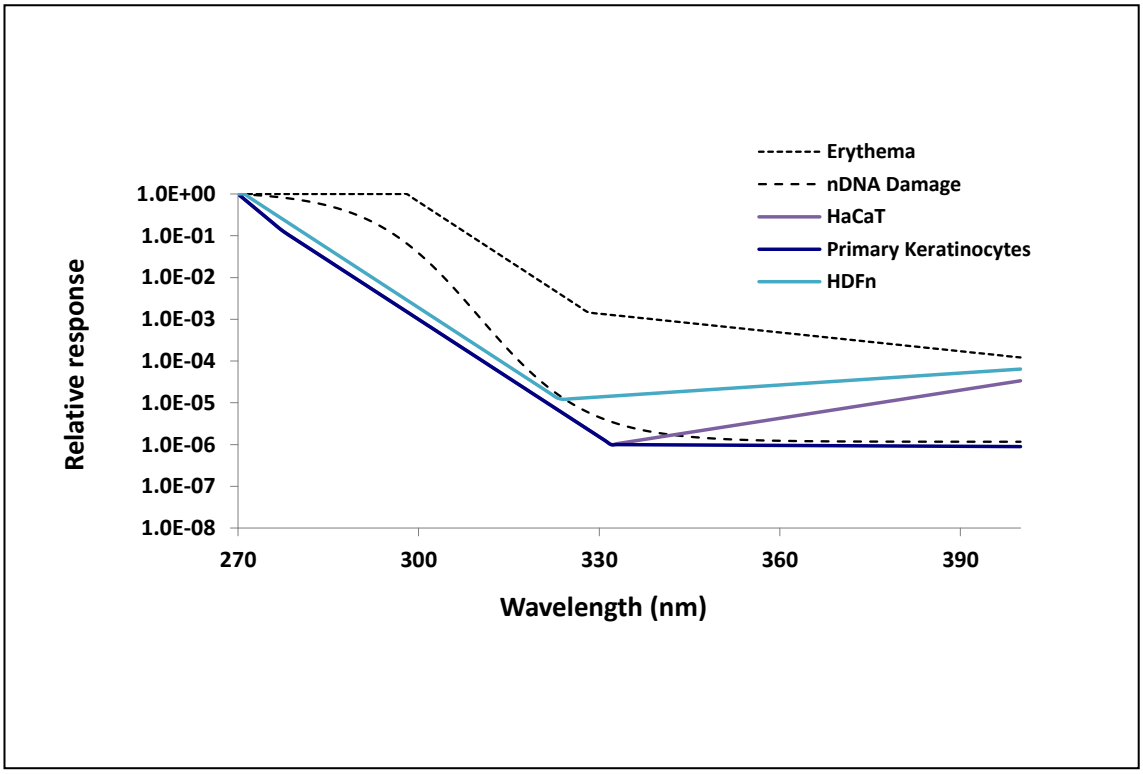

Figure 4.6: Comparison of Action Spectra. This figure compares the estimated action spectra for mtDNA damage of the different skin cell types. Previously determined action spectra for Erythema induction (McKinlay and Diffey, 1987) and nDNA damage (Setlow, 1974) are also plotted for reference.

4.3.3 Comparison of SYBR Green and TaqMan Technology to Detect the 4977 bp Deletion

Two different methods for detection of the 4977 bp deletion were initially utilised. The SYBR Green method was taken from the mitochondrial research group and the TaqMan method was previously published (Koch *et al.*, 2001). For analysis, a positive control from a patient sample known to harbour the deletion was amplified in an aim to increase the quantity for future use.

A clear single peak at ~78 °C was obtained when the dissociation curve was run following amplification of the desired product by the SYBR Green method (Figure 4.7). This was a necessary procedure with the SYBR Green method and ensured that only the single product desired had been amplified. The amplified PCR products (from both the SYBR Green and TaqMan methods) were then ran on a typical agrose gel and this showed the presence of a single band of the expected size (Figure 4.8). It also showed that the re-amplified could be detected (lanes 6+7).

Figure 4.9 shows a standard curve for the two primer sets; SYBR Green (A) and TaqMan (B). For these curves the positive control was serially diluted as follows: 5000, 500, 100, 50, 10 pg. With this data analysis typically a minimum Ct value corresponded with the highest DNA concentration. A strong linear correlation of 0.92 was seen with the SYBR Green method; however linearity was higher with the TaqMan method (0.99).

4.3.4 UVR-Induced 4977 bp Deletion

After determining the most valid PCR method to use in the detection of the 4977 bp deletion, a series of experiments were undertaken in an aim to create the deletion in skin cells. Vast optimisation based on previous literature and group knowledge took place in an aim to determine a repeat dose that did not substantially reduce cell viability. The main aim of these experiments was to ultimately produce an action spectrum of damage, therefore requiring the irradiation by various UVR sources. This meant a daily dose chosen must somehow connect the UVR sources and to achieve that a consistent SED of 1 was chosen. The doses were then given on alternate days to allow the cells time to recover. An SED of 1 was a high amount of UVR when irradiating with the Cleo + filter UVR source so to account for this the dose from this lamp was split into three equal daily doses on the irradiation days. The Germicidal UVR source was considered too damaging and un-related and was not used in this study. Following just two 1 SED irradiations from the TL12 UVR source a large effect on viability was seen and therefore irradiations with this source were abandoned.

Due to the repetitive nature of this experiment Primary Keratinocytes were not considered for analysis as differentiation of these cells renders them redundant to use following approximately four passages.

The QPCR TaqMan method was utilised to determine the induction of the 4977 bp deletion. Following amplification, many of the samples were producing un-determined Ct values. This indicated that the deletion was not present in these samples; however it meant that the data for these samples could not be used in the analysis. Consequently these values were corrected to 35, as were any values above this number. This enabled a value to be determined that indicated no deletion which was

consistent with the blank sample (no DNA) and the negative control. An UVR-protected control sample was taken at the beginning and end of each experiment for comparisons (represented by a [-]). The irradiation number was related to the amount of times the cells had been irradiated with 1 SED of each UVR source. Variations in the samples irradiation number were seen due to cell viability and growth.

The data for this experiment is shown in Figure 4.10-Figure 4.14. With this investigation values obtained for blank and negative samples remained consistently high. The positive sample was reliable in its amplification producing Ct values of 16.12 ± 0.5. These observations confirmed the rigidity of the assay. Following amplification of both the cell type samples, irradiated with all of the various UVR sources, a trend for a high Ct was seen. This was frequently in the 35 Ct region with only minor fluctuations from this; an observation independent of irradiation number. The most notable fluctuation was with the HDFn cells irradiated with Helarium (Figure 4.11; B). With this result, Ct values of 28.48 ±3.3 and 28.28 ±1.0 were seen in samples which had been exposed to 12 and 23 repeat irradiations of Helarium, this is compared to a Ct >35 seen in samples where cells had only been exposed to 9 irradiations. However, the UVR-protected cell sample taken at the beginning of that experiment produced a Ct value of 32.32 ±2.7. Another fluctuation was seen with HaCaT cells irradiated with the Cleo – filter UVR source (Figure 4.13; A). With this experiment a small dose-dependent decrease in Ct was visible following 26 repeat irradiations and up until 32 irradiations with the Cleo - filter. However, a sample taken following just 9 irradiations with this UVR source saw a low value of 32.38 Ct a value similar to that following the higher number of irradiations.

The data was analysed by linear regression; the control values obtained from the beginning and the end of each experiment were combined for each experiment. Despite earlier observations, with this analysis no statistically significant deviation from control was seen across experiments. There were exceptions to this however; both cell types irradiated with Arimed B saw a statistically significant increase in regression of $P<0.02$ in HaCaT cells and $P<0.03$ in HDFn cells from the control.

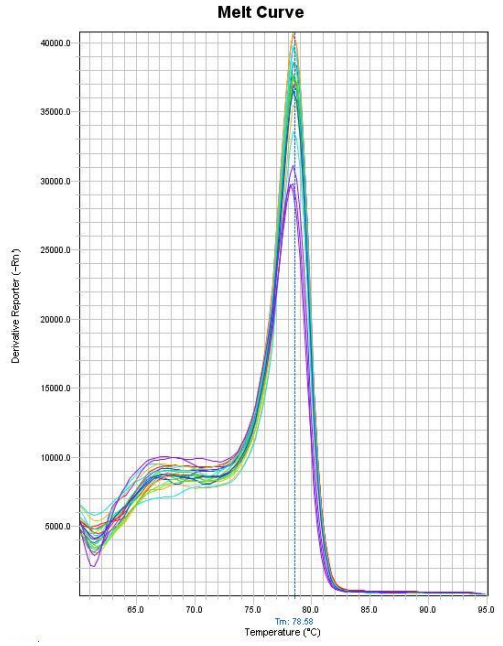

Figure 4.7: PCR Dissociation Curve After Amplification of the 4977 bp Deletion Using the SYBR Green Assay. The dissociation curve shows the melting temperature of the product and ensures that only the desired amplicon was detected.

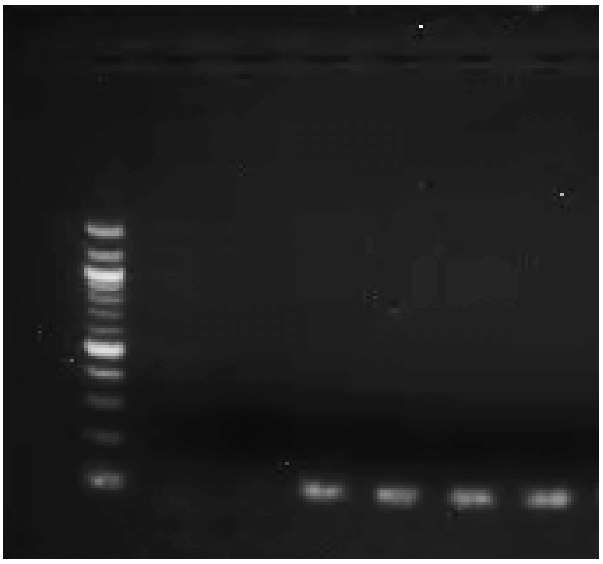

Figure 4.8: Determination of the Amplified 4977 bp Deletion Assay Product. A patient sample with mitochondria harbouring the 4977 bp deletion was amplified using two primer pairs to create a positive control for further analysis. The products obtained were 107 bp when using the TaqMan assay primers and 97 bp when using the SYBR Green assay primers. The sample layout for the gels was as follows: lane 1-hyperladder 1, lanes 2+3-control (no deletion present; using TaqMan and SYBR Green primers respectively), lanes 4+5-product amplified directly from patient sample (using TaqMan and SYBR Green primers respectively), lanes 6+7-product re-amplified (using TaqMan and SYBR Green primers respectively).

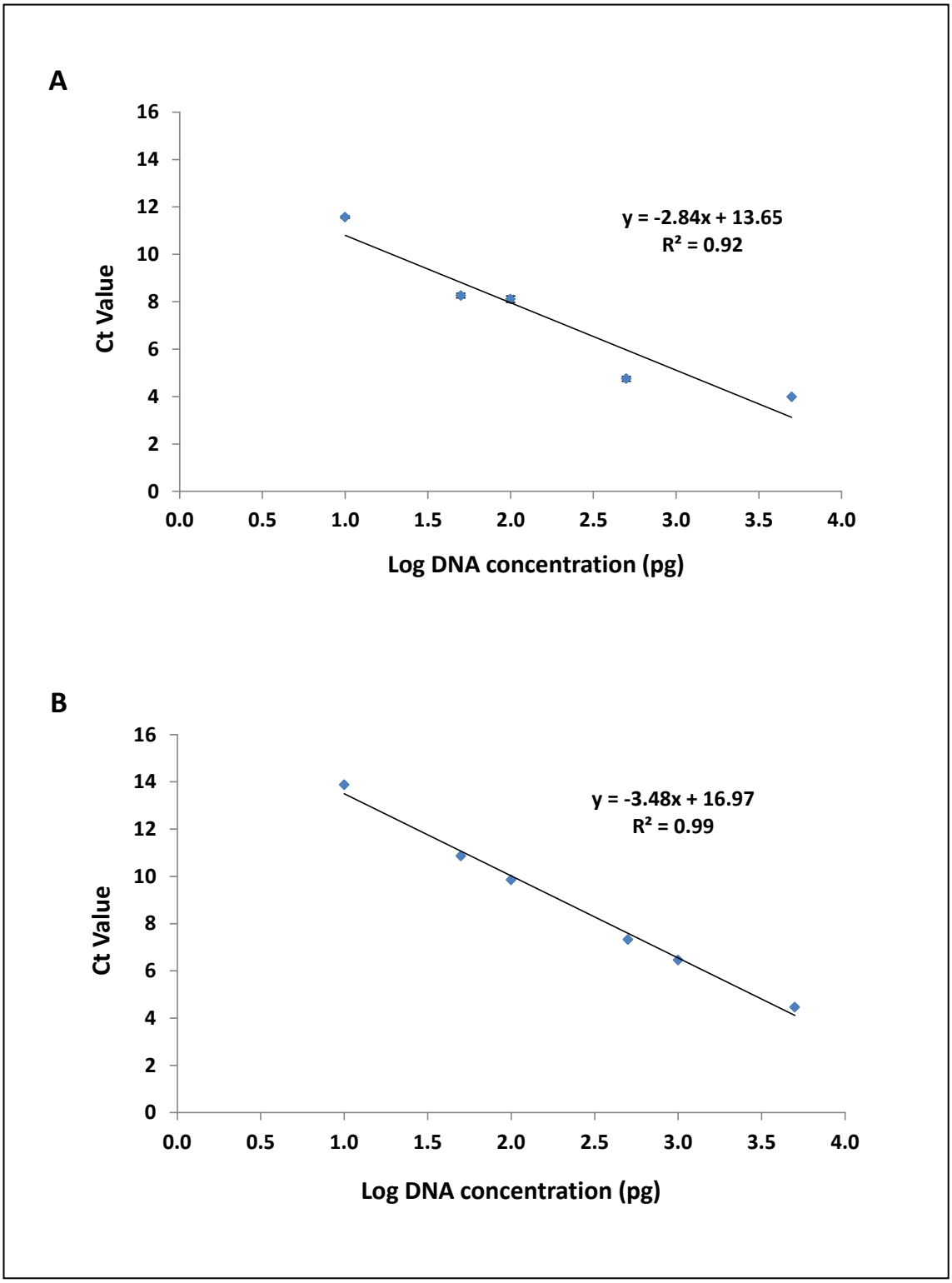

Figure 4.9: Standard Curve of Various Primers Used to Detect the 4977 bp Deletion. Ct values measured following serial dilutions of DNA samples using either SYBR Green QPCR (A) or using a TaqMan method (B). The sample was a 4977 bp positive sample.

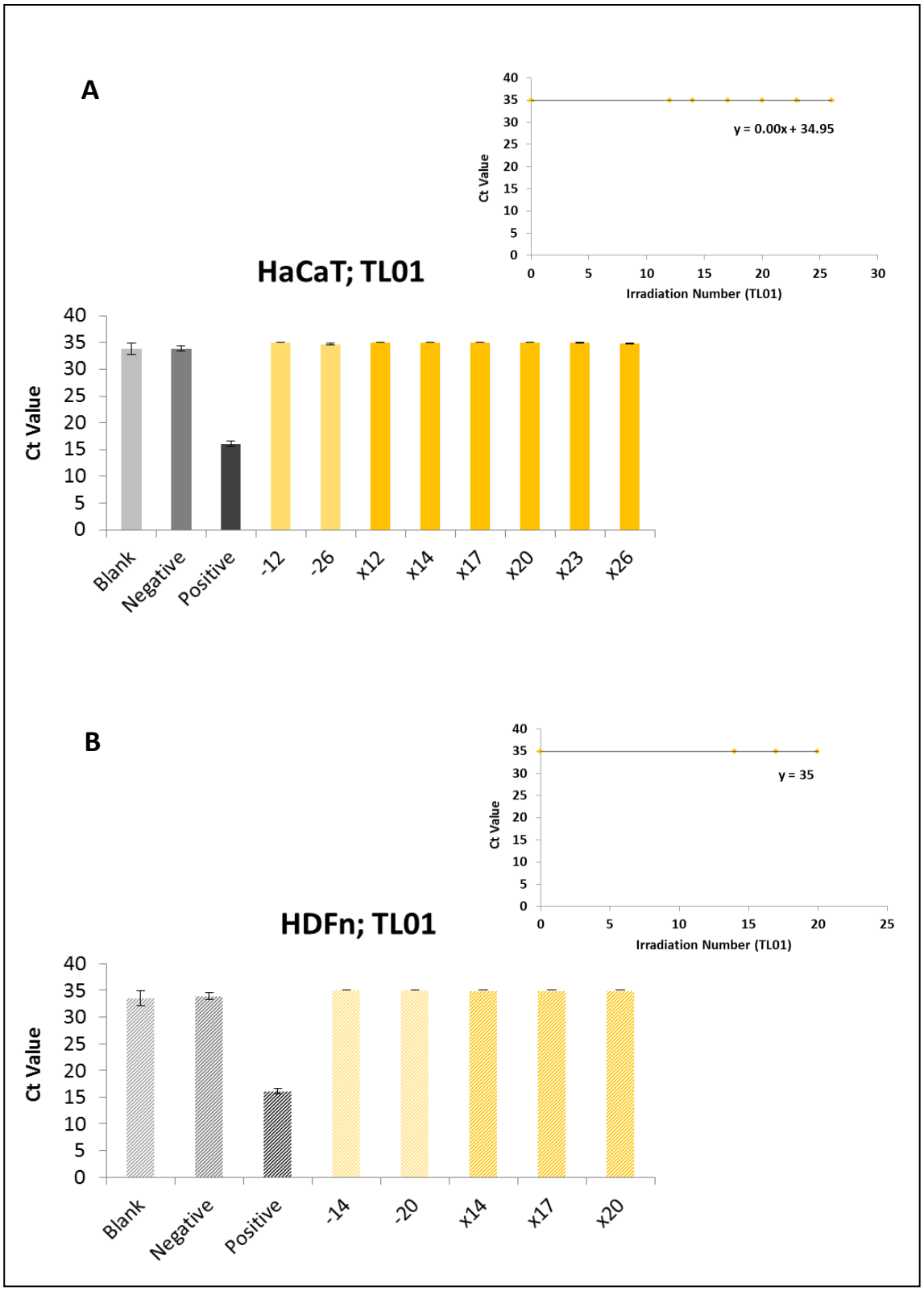

Figure 4.10:Presence of the 4977 bp Deletion in Either HaCaT or HDFn Cells Irradiated with TL01. Both HaCaT (A) and HDFn (B) cells were irradiated on alternate days with 1 SED (~0.2 J/cm^2) TL01. Samples were taken at regular intervals and are represented by the number of irradiations delivered (where [+] indicates exposed and [–] indicates the un-exposed control). The length of the study was determined by cell viability. Induction of the 4977 bp deletion was determined using a TaqMan QPCR method. To enable analysis un-determined Ct values and those >35 were expressed as 35. Positive and negative controls were used for comparison. Direct comparison was made to the control using linear analysis which showed no statistically significant deviation (P>0.05; n=3 ± SEM).

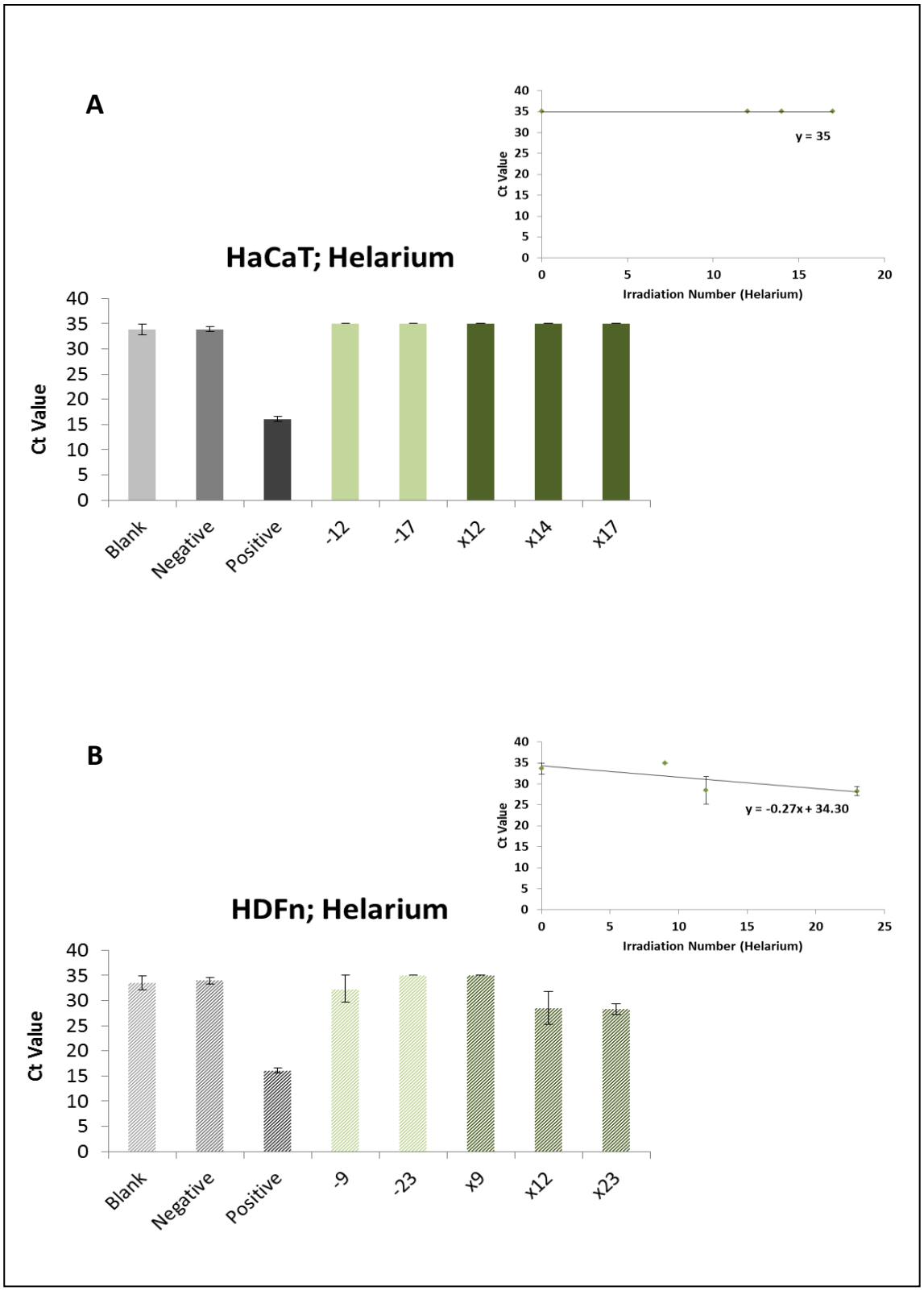

Figure 4.11: Presence of the 4977 bp Deletion in Either HaCaT or HDFn Cells Irradiated with Helarium. Both HaCaT (A) and HDFn (B) cells were irradiated on alternate days with 1 SED (~0.5 J/cm^2) Helarium. Samples were taken at regular intervals and are represented by the number of irradiations delivered (where [+] indicates exposed and [–] indicates the un-exposed control). The length of the study was determined by cell viability. Induction of the 4977 bp deletion was determined using a TaqMan QPCR method. To enable analysis un-determined Ct values and those >35 were expressed as 35. Positive and negative controls were used for comparison. Direct comparison was made to the control using linear analysis which showed no statistically significant deviation (P>0.05; n=3 ± SEM).

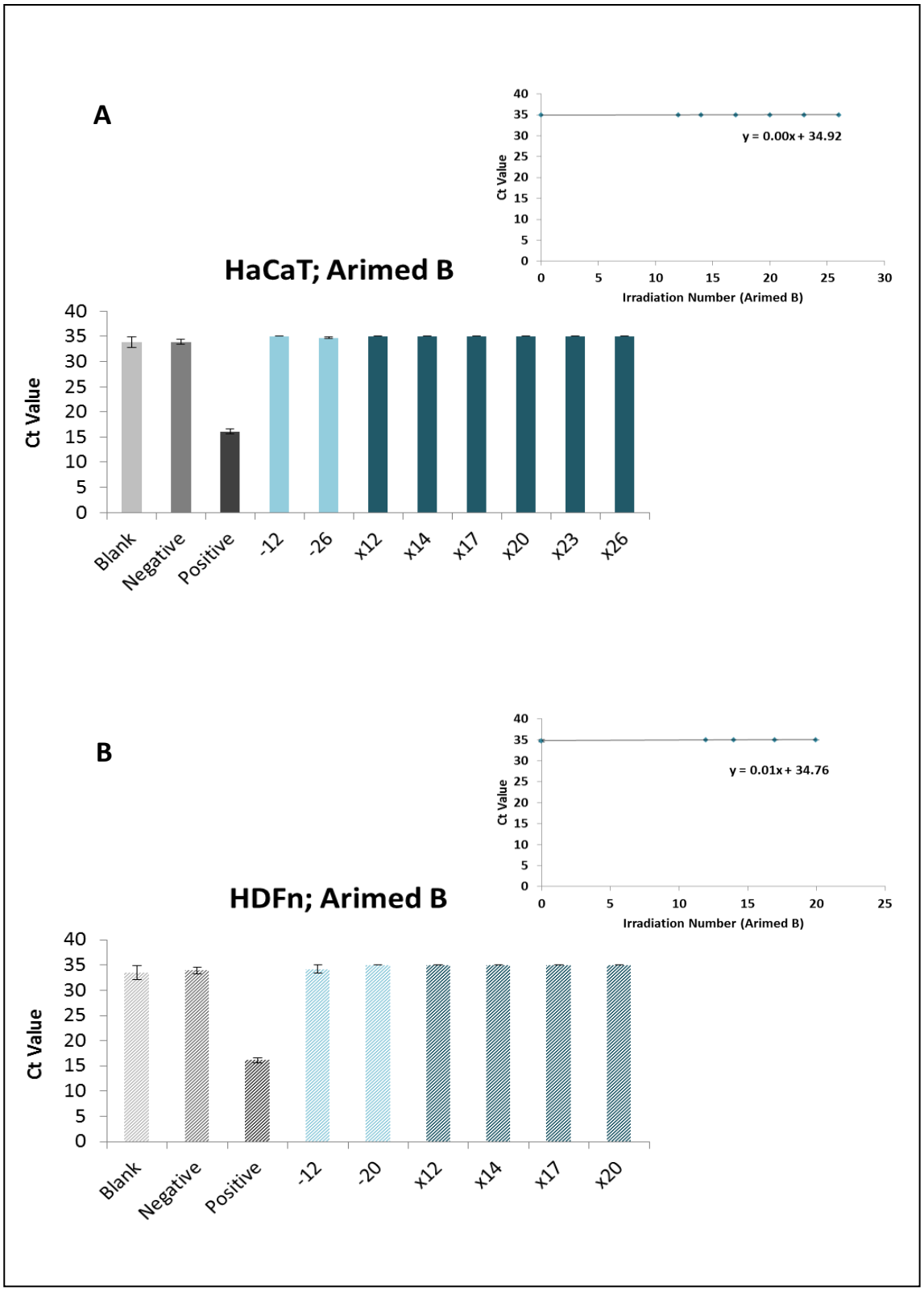

Figure 4.12: Presence of the 4977 bp Deletion in Either HaCaT or HDFn Cells Irradiated with Arimed B. Both HaCaT (A) and HDFn (B) cells were irradiated on alternate days with 1 SED (~2 J/cm^2) Arimed B. Samples were taken at regular intervals and are represented by the number of irradiations delivered (where [+] indicates exposed and [–] indicates the un-exposed control). The length of the study was determined by cell viability. Induction of the 4977 bp deletion was determined using a TaqMan QPCR method. To enable analysis un-determined Ct values and those >35 were expressed as 35. Positive and negative controls were used for comparison. Direct comparison was made to the control using linear analysis which showed a statistically significant increase of $P<0.02$ and $P<0.03$ for HaCaT and HDFn cells respectively (n=3 ± SEM).

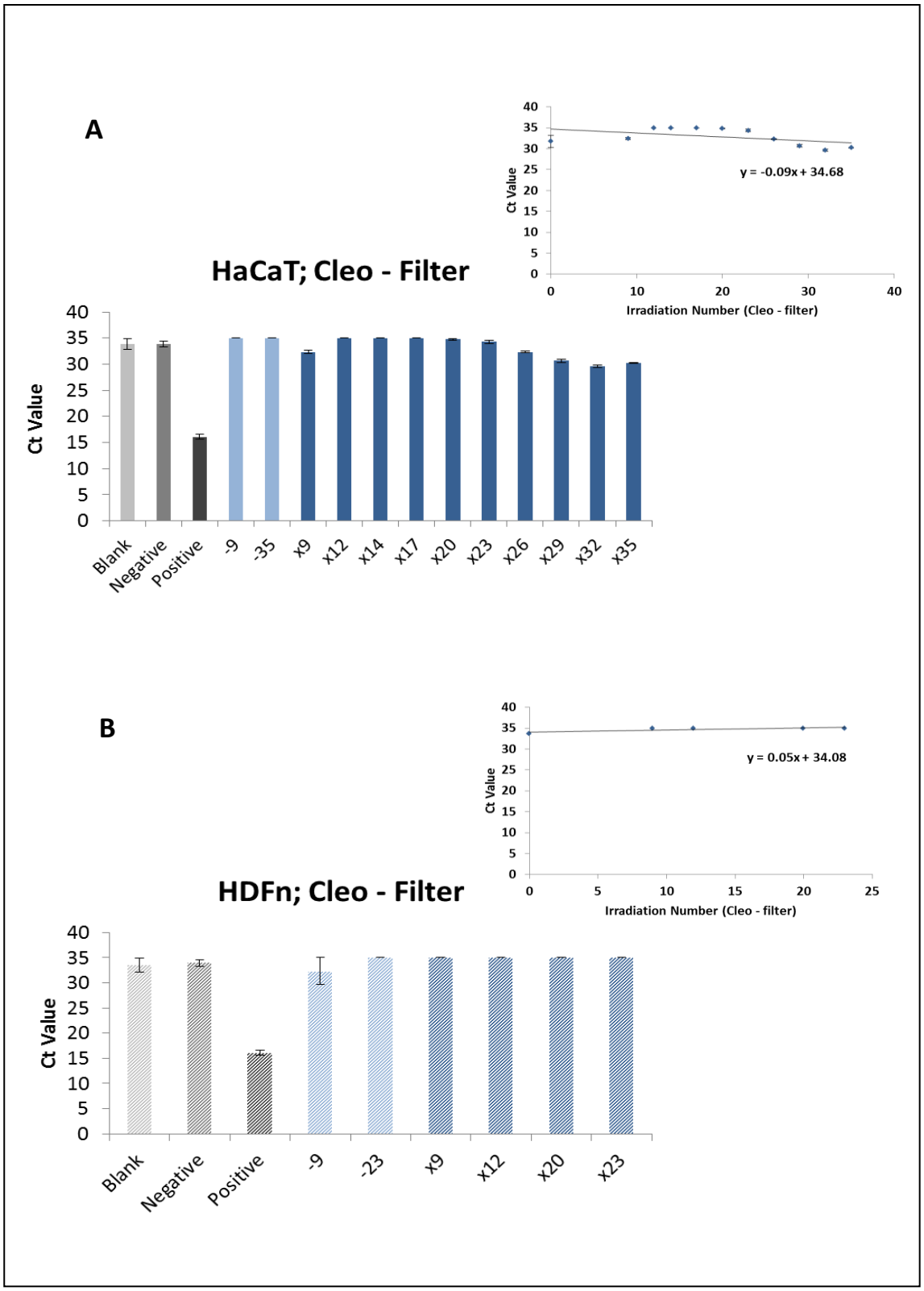

Figure 4.13: Presence of the 4977 bp Deletion in Either HaCaT or HDFn Cells Irradiated with Cleo - filter. Both HaCaT (A) and HDFn (B) cells were irradiated on alternate days with 1 SED (~7.5 J/cm^2) Cleo - filter. Samples were taken at regular intervals and are represented by the number of irradiations delivered (where [+] indicates exposed and [–] indicates the un-exposed control). The length of the study was determined by cell viability. Induction of the 4977 bp deletion was determined using a TaqMan QPCR method. To enable analysis un-determined Ct values and those >35 were expressed as 35. Positive and negative controls were used for comparison. Direct comparison was made to the control using linear analysis which showed no statistically significant deviation (P>0.05; n=3 ± SEM).

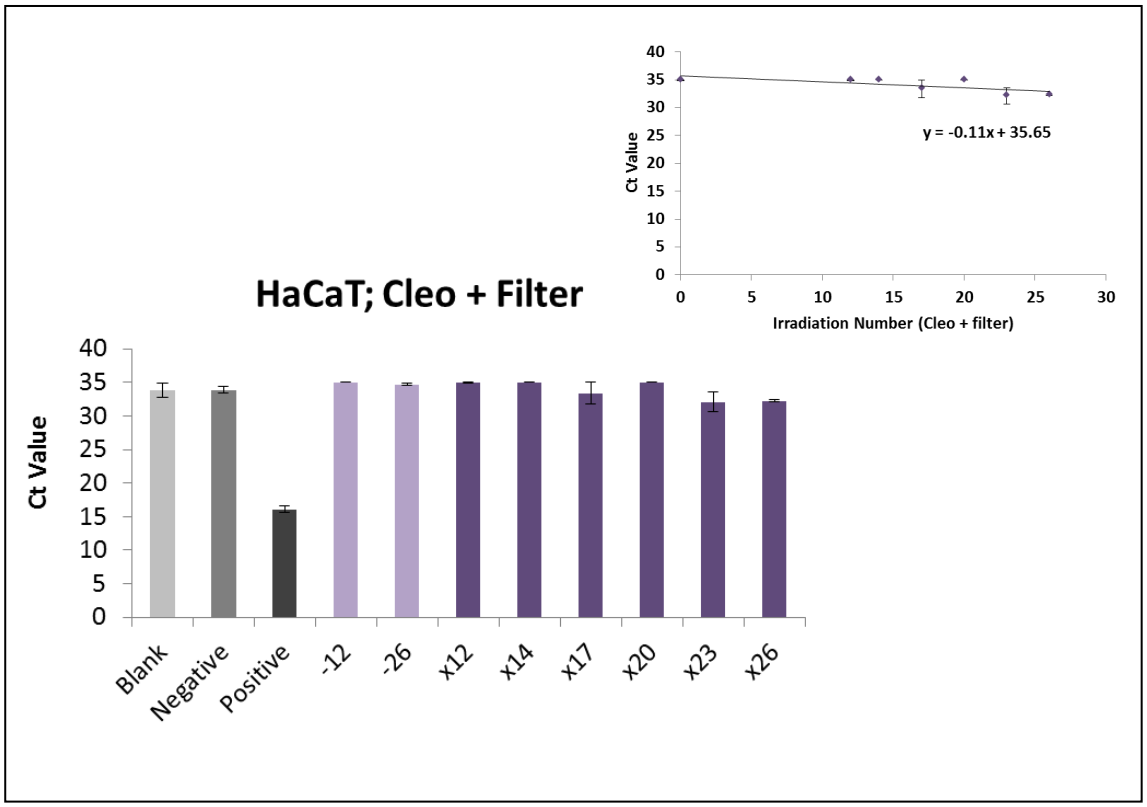

Figure 4.14: Presence of the 4977 bp Deletion in HaCaT Cells Irradiated with Cleo + filter. HaCaT cells were irradiated on alternate days with 1 SED (~19 J/cm^2) Cleo + filter. With this lamp the dose was split and given as three smaller doses per day. Samples were taken at regular intervals and are represented by the number of irradiations delivered (where [+] indicates exposed and [–] indicates the un-exposed control). The length of the study was determined by cell viability. Induction of the 4977 bp deletion was determined using a TaqMan QPCR method. To enable analysis un-determined Ct values and those >35 were expressed as 35. Positive and negative controls were used for comparison. Direct comparison was made to the control using linear analysis which showed no statistically significant deviation (P>0.05; n=3 ± SEM).

4.3.5 Comparison of SYBR Green and TaqMan Technology to Detect the 3895 bp Deletion

As with the 4977 bp deletion, two different methods for detection of the 3895 bp deletion were utilised. Both the SYBR Green and the TaqMan method had been previously published (Harbottle and Birch-Machin, 2006; Harbottle *et al.*, 2010). Further comparison was also made between the previously published SYBR Green method and that of some modified primers. Initially analysis used un-irradiated and irradiated cellular DNA as the negative and positive controls. For TaqMan analysis sun-exposed patient samples were used as negative and positive controls, and this work was performed in collaboration with Dr Nina Beadle.

A clear single peak at 80 °C was obtained when the dissociation curve was run following amplification of the desired product by the SYBR Green method (Figure 4.15). Again this necessary procedure ensured that only the product desired had been amplified. With this PCR run, samples were amplified with both the previously published primers and the modified primers, and this curve therefore shows a similar product. The amplified PCR products (from both the SYBR Green method) were then ran on a typical agrose gel and this showed the presence of a single band of the expected size (Figure 4.16).

Figure 4.17 shows a standard curve for the published SYBR Green method (A), the modified SYBR Green method (B) and the published TaqMan method (C). For the SYBR Green methods, negative (un-irradiated) and positive (6 x 2.3 J/cm^2 TL09 + filter) HaCaT sample DNA was diluted as follows: 100000, 50000, 10000, 5000, 1000, 500 and 100 pg. A strong linear correlation of 0.99 and 0.98 was seen with the published and modified SYBR Green primers to amplify the positive control respectively. However a similar correlation of 0.96 (published) and 0.99 (modified) when the same primers were used to amplify the negative control.

For the TaqMan method, negative and positive for the 3895 bp deletion patient DNA samples were diluted as follows: 10000, 7500, 5000, 2500 and 1000 pg. Observations of this data indicate a high correlation of 0.99 when the primers were used to detect the deletion in the positive control samples, where a minimum Ct value corresponded with the highest DNA concentration. Conversely when used to detect the deletion in the negative sample a low correlation of 0.4 was seen and little difference was seen in the Ct value with alterations of DNA quantity.

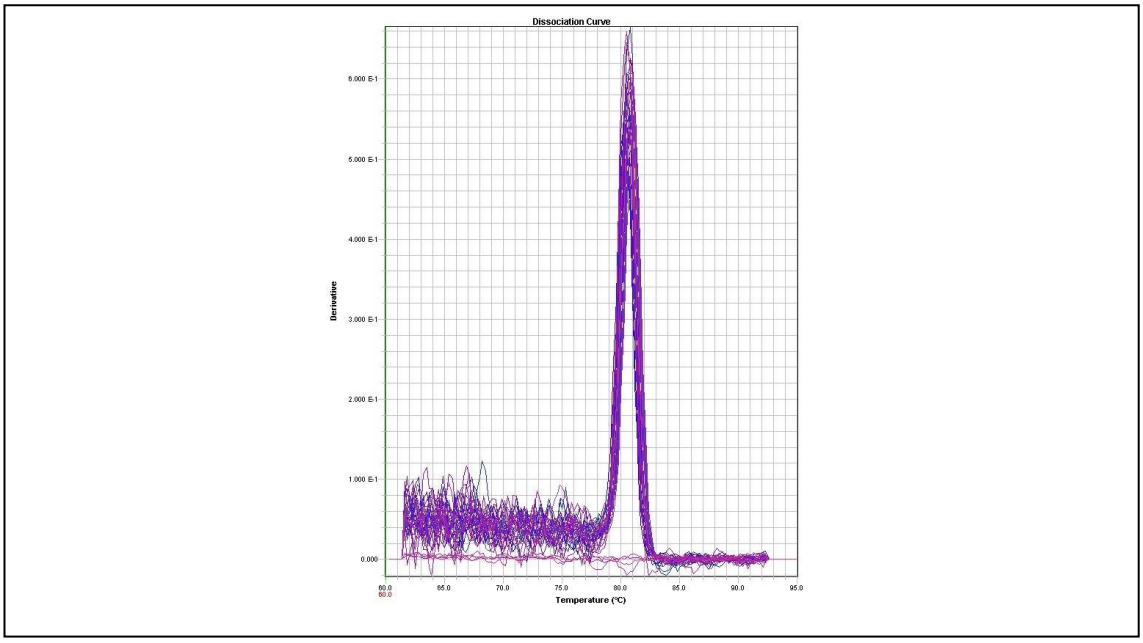

Figure 4.15: PCR Dissociation Curve Following Amplification of the 3895 bp deletion using the SYBR Green Assay. The dissociation curve shows the melting temperature of the product and ensures that only the desired amplicon was detected.

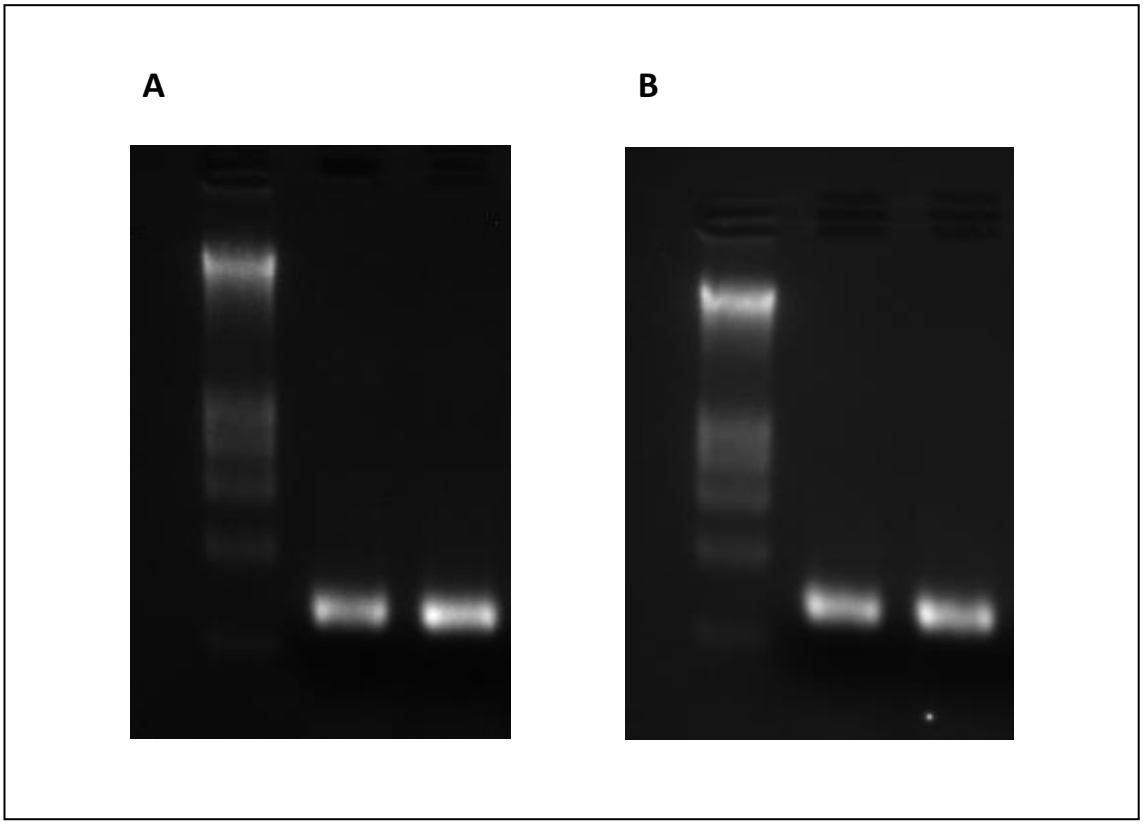

Figure 4.16: Determination of the Amplified 3895 bp Deletion Product in HaCat Cell Line. Samples were amplified using either previously validated primers (A) or modified primers (B) were run to obtain the required product (261 bp and 265 bp respectively). The sample layout for both gels was as follows: lane 1 – hyperladder 1, lane 2 – control (UVR protected), lane 3 – UVR irradiated (6 x 2.3 J/cm^2 TL09 + filter).

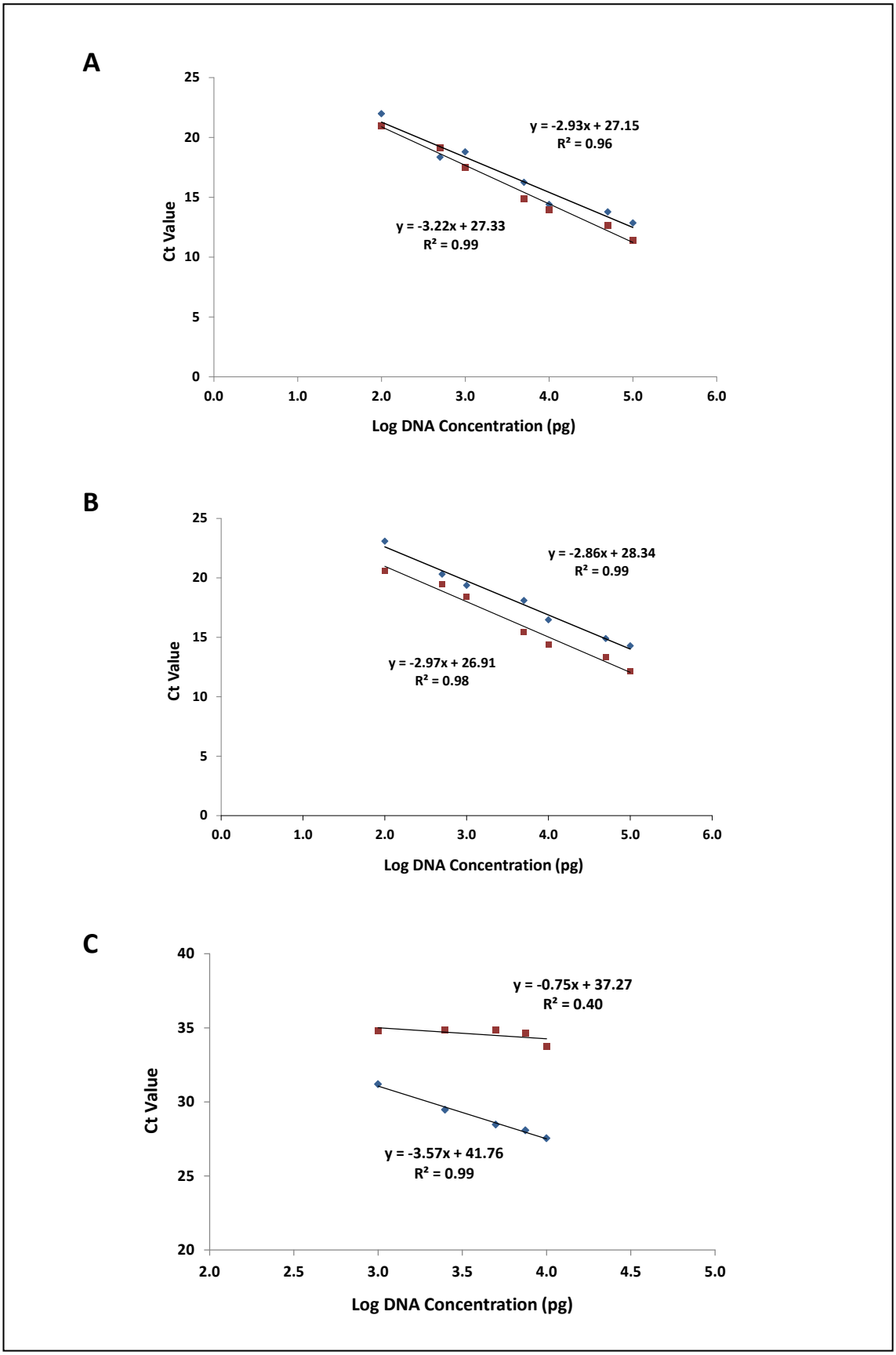

Figure 4.17: Standard Curve of Various Primers Used to Detect the 3895 bp Deletion. Ct values measured following serial dilutions of DNA samples using either SYBR Green QPCR using previously validated primers (A) and modified primers (B) or using a TaqMan method (C). The samples amplified were as follows: control HaCaT cells (UVR protected) (♦; A+B), UVR irradiated HaCaT cells (6 x 2.3 J/cm^2 TL09 + filter ■; A+B), 3895 bp positive sample (m63d; ♦; C) and 3895 bp negative sample (m61e; ■; C).

4.3.6 UVR-Induction of the 3895 bp Deletion

Following determination of the most valid PCR method to use in the detection of the 3895 bp deletion, a series of experiments were undertaken in an aim to create the deletion in skin cells. As with the production of the 4977 bp deletion, a vast optimisation based on previous literature and group knowledge took place, with the objective to determine a repeat dose that did not substantially reduce cell viability. Again, the main purpose of these experiments was to ultimately produce an action spectrum of deletion production, this therefore required irradiation by various UVR sources. This meant the daily dose chosen must somehow connect the UVR sources; to achieve this, a dose of an SED of 1, consistent with 4977 bp deletion production, was chosen. Experimental methods and analysis were the same as that used to determine 4977 bp induction, so for more information on this please refer to section 4.3.4 .

The data for this experiment is shown in Figure 4.18-Figure 4.22. The values obtained for blank and negative samples remained consistently high. The positive sample was reliable in its amplification producing Ct values of 26.42 ± 0.2. These observations confirmed the rigidity of the assay. Following amplification of both the cell type samples, irradiated with all of the various UVR sources, a trend for a high Ct was seen. Although quite variable, this was frequently in the 35 Ct region and this observation was independent of irradiation number. One notable experiment that deviated from this trend was with the HDFn cells irradiated with Helarium (Figure 4.19; B). With this result, following the repeat irradiations Ct values similar to the positive control were seen. These were 27.24 ± 0.4, 27.66 ± 0.2 and 27.49 ± 0.2 in samples which had been exposed to 9, 12 and 23 repeat irradiations of Helarium, respectively. However, the UVR-protected cell samples were also low, producing Ct values of 31.20 ± 1.6 and 29.43 ± 3.3 for samples taken at the beginning and the end of the experiment respectively.

The data was analysed by linear regression where the control values obtained from the beginning and the end of each experiment were combined for each experiment. Despite the observation with HDFn cells exposed to the Helarium UVR source, with this analysis, no statistically significant deviation from control was found in any of the experiments.

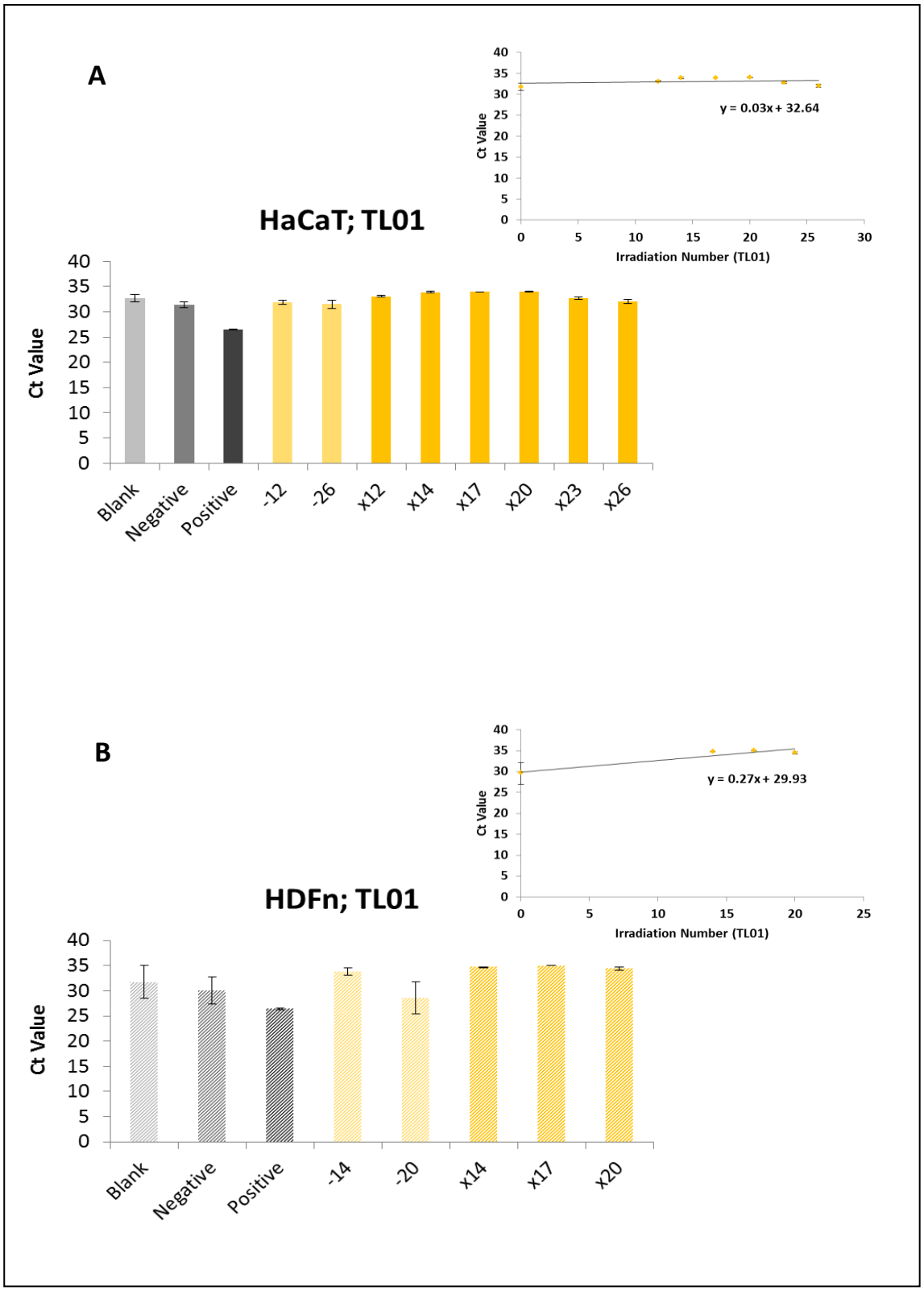

Figure 4.18: Presence of the 3895 bp Deletion in Either HaCaT or HDFn Cells Irradiated with TL01. Both HaCaT (A) and HDFn (B) cells were irradiated on alternate days with 1 SED (~0.2 mJ/cm^2) TL01. Samples were taken at regular intervals and are represented by the number of irradiations delivered (where [+] indicates exposed and [–] indicates the un-exposed control). The length of the study was determined by cell viability. Induction of the 3895 bp deletion was determined using a TaqMan QPCR method. To enable analysis un-determined Ct values and those >35 were expressed as 35. Positive and negative controls were used for comparison. Direct comparison was made to the control using linear analysis which showed no statistically significant deviation (P>0.05; n=3 ± SEM).

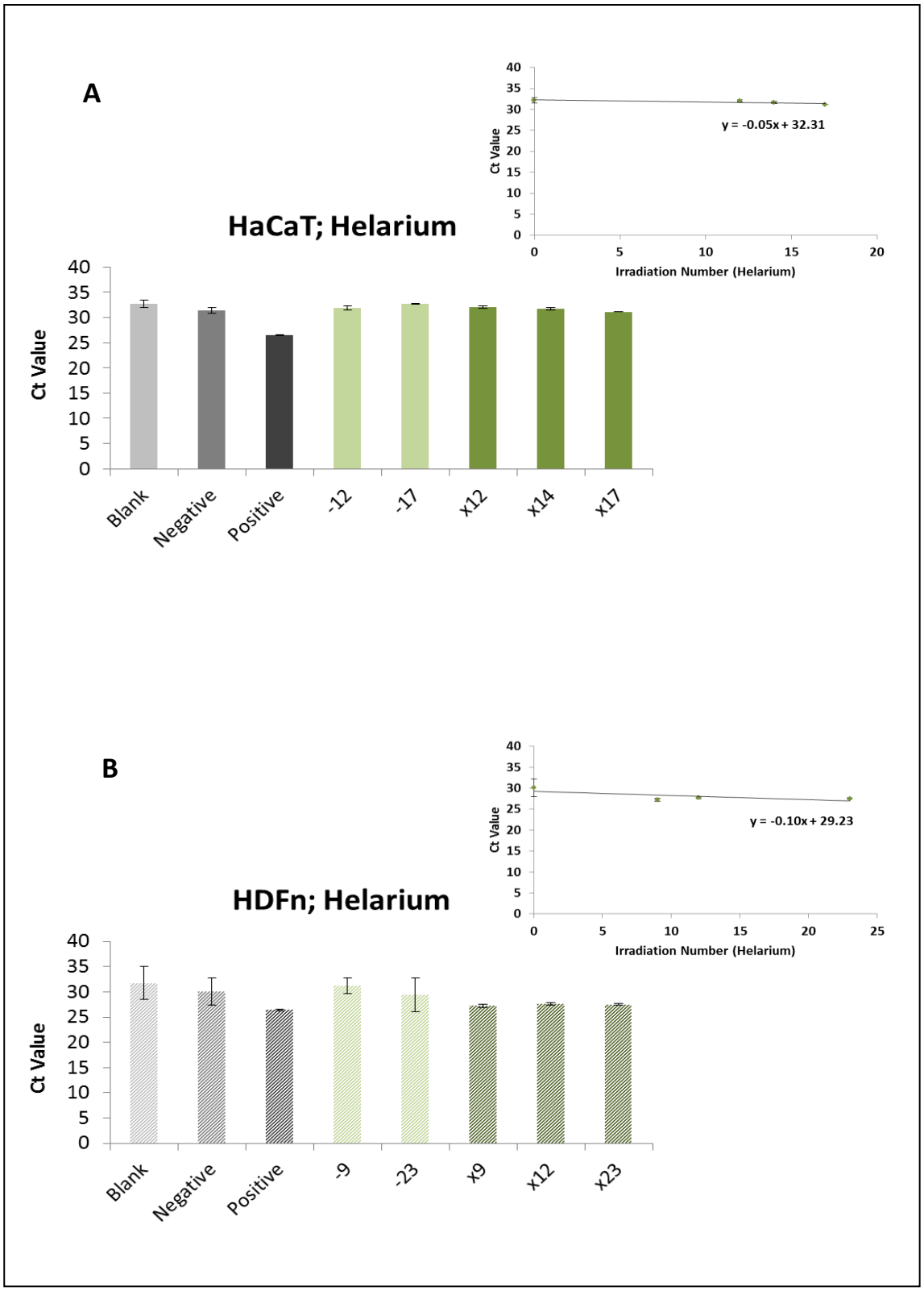

Figure 4.19: Presence of the 3895 bp Deletion in Either HaCaT or HDFn Cells Irradiated with Helarium. Both HaCaT (A) and HDFn (B) cells were irradiated on alternate days with 1 SED (~0.5 J/cm^2) Helarium. Samples were taken at regular intervals and are represented by the number of irradiations delivered (where [+] indicates exposed and [–] indicates the un-exposed control). The length of the study was determined by cell viability. Induction of the 3895 bp deletion was determined using a TaqMan QPCR method. To enable analysis un-determined Ct values and those >35 were expressed as 35. Positive and negative controls were used for comparison. Direct comparison was made to the control using linear analysis which showed no statistically significant deviation (P>0.05; n=3 ± SEM).

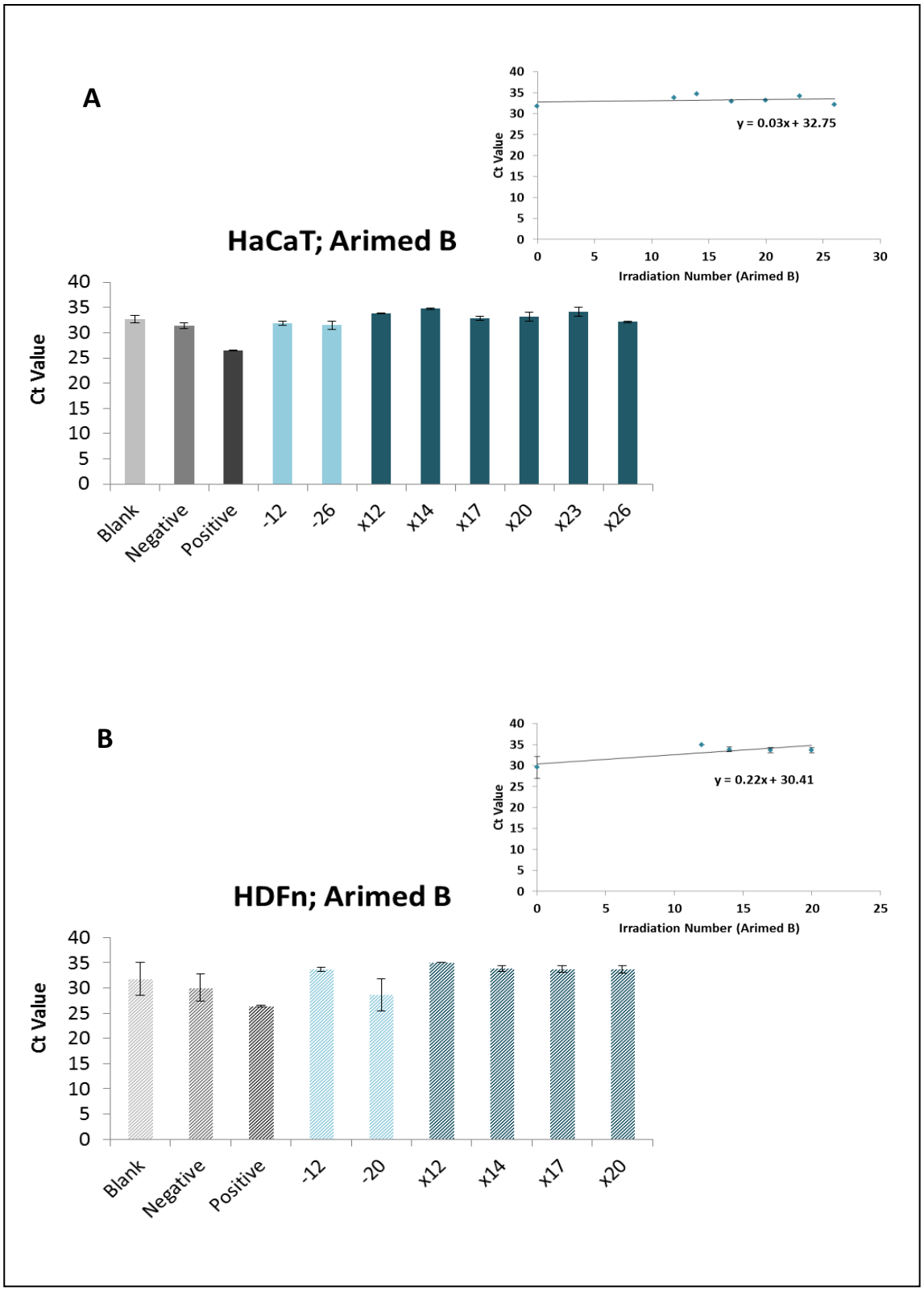

Figure 4.20: Presence of the 3895 bp Deletion in Either HaCaT or HDFn Cells Irradiated with Armed B. Both HaCaT (A) and HDFn (B) cells were irradiated on alternate days with 1 SED (~2 J/cm^2) Armed B. Samples were taken at regular intervals and are represented by the number of irradiations delivered (where [+] indicates exposed and [–] indicates the un-exposed control). The length of the study was determined by cell viability. Induction of the 3895 bp deletion was determined using a TaqMan QPCR method. To enable analysis un-determined Ct values and those >35 were expressed as 35. Positive and negative controls were used for comparison. Direct comparison was made to the control using linear analysis which showed no statistically significant deviation (P>0.05; n=3 ± SEM).

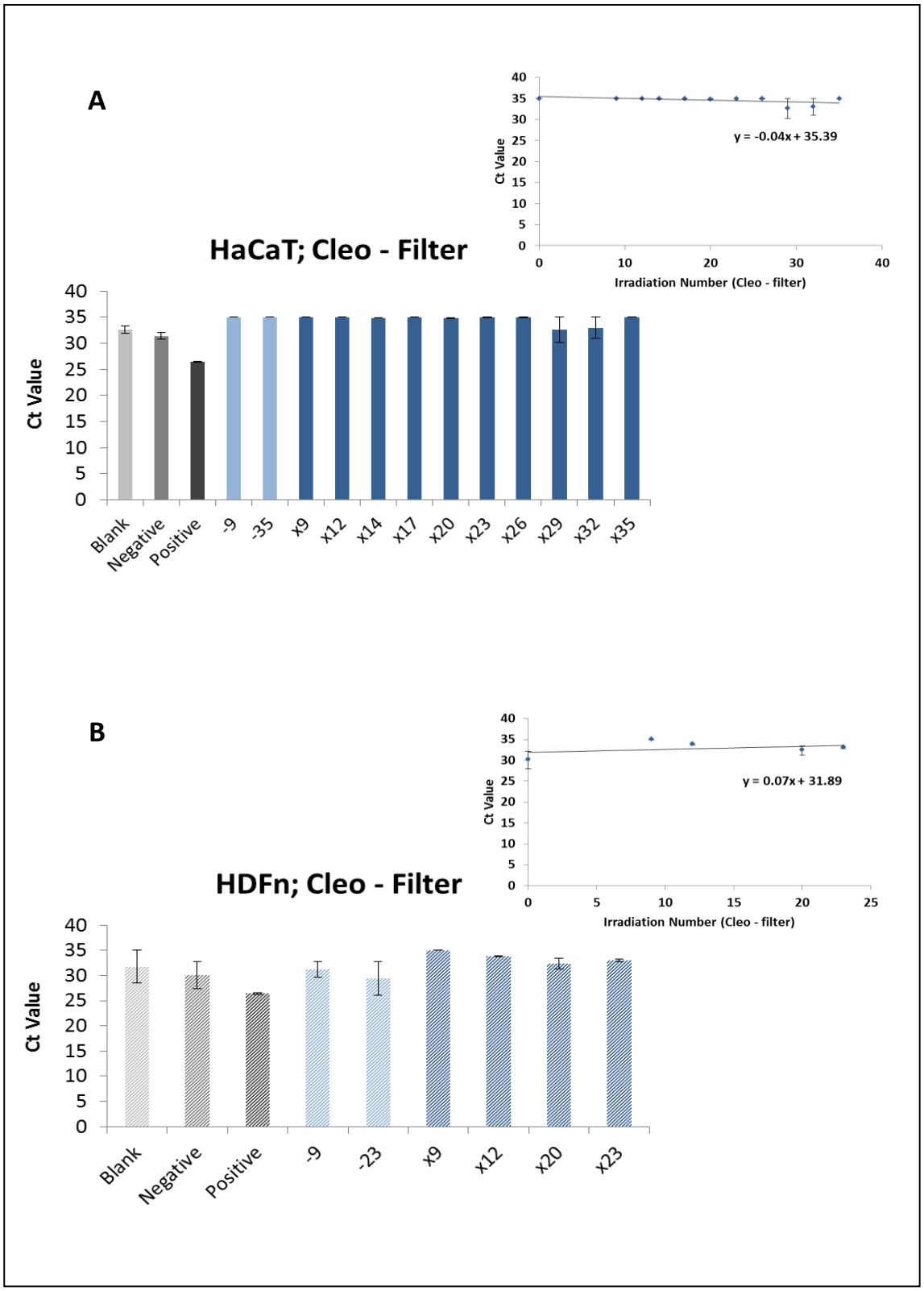

Figure 4.21: Presence of the 3895 bp Deletion in Either HaCaT or HDFn Cells Irradiated with Cleo - filter. Both HaCaT (A) and HDFn (B) cells were irradiated on alternate days with 1 SED (~7.5 J/cm^2) Cleo - filter. Samples were taken at regular intervals and are represented by the number of irradiations delivered (where [+] indicates exposed and [–] indicates the un-exposed control). The length of the study was determined by cell viability. Induction of the 3895 bp deletion was determined using a TaqMan QPCR method. To enable analysis un-determined Ct values and those >35 were expressed as 35. Positive and negative controls were used for comparison. Direct comparison was made to the control using linear analysis which showed no statistically significant deviation (P>0.05; n=3 ± SEM).

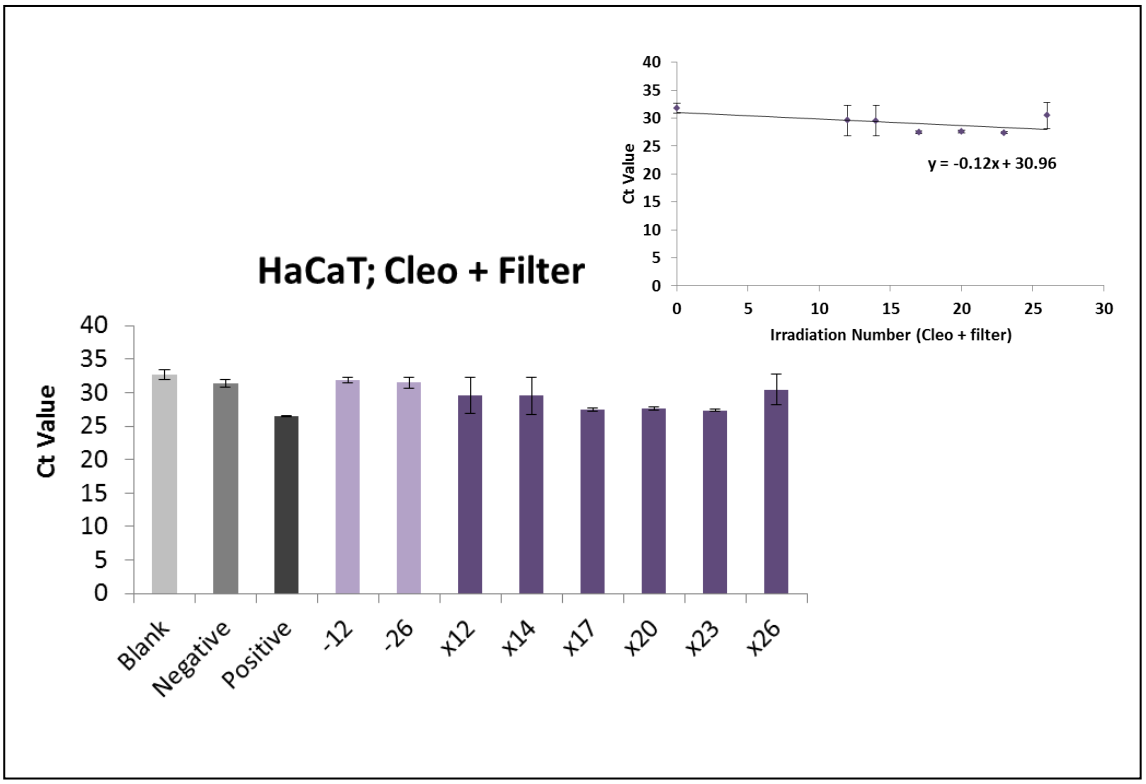

Figure 4.22: Presence of the 3895 bp Deletion in HaCaT Cells Irradiated with Cleo + filter. HaCaT cells were irradiated on alternate days with 1 SED (~19 J/cm^2) Cleo + filter. With this lamp the dose was split and given as three smaller doses per day. Samples were taken at regular intervals and are represented by the number of irradiations delivered (where [+] indicates exposed and [–] indicates the un-exposed control). The length of the study was determined by cell viability. Induction of the 3895 bp deletion was determined using a TaqMan QPCR method. To enable analysis un-determined Ct values and those >35 were expressed as 35. Positive and negative controls were used for comparison. Direct comparison was made to the control using linear analysis which showed no statistically significant deviation (P>0.05; n=3 ± SEM).

4.4 Discussion

4.4.1 UVR Wavelength Dependence of mtDNA Damage within an 11 kb Segment

Initially cells were irradiated with the TL09 - filter UVR source. The doses ranged approximately from 0.9 to 106 J/cm^2 (0.1 to 10 SED). The higher irradiations of the TL09 – filter UVR source produced extremely low yields of DNA, hindering further analysis. This was primarily identified as a problem due to large cell death from long irradiation time periods (the highest dose took 5 h 40 min). In our group, previous assessment of the viability of cells exposed to the TL09 – filter UVR source by Propidium Iodode and fluorescence activated cell sorting (FACS) analysis found 80 % cell death after 5 h of irradiation (Data obtained by Dr Helen Swalwell). Further investigations, shown in Chapter 3, have recognised heating properties associated with

this lamp which could have contributed to this high amount of cell death. To further facilitate with my investigations an additional UVR lamp was sourced (Cleo). The Cleo UVR source had a higher UVR output allowing for shorter irradiation periods, and furthermore, the temperate emissions from this lamp were much lower.

This primary investigation sought to determine UVR-induced mtDNA damage by establishing the occurrence of strand breaks/lesions within an 11 kb section of the genome. This assay is well validated (Kleinle *et al.*, 1997; Passos *et al.*, 2007; Swalwell *et al.*, 2012) and damage was quantified by the reduction in efficiency of the amplification of this product by QPCR in the damaged DNA.

The UVR-induced damage was clearly and consistently found to be entirely dose-dependent in all the skin cell types investigated. This enabled well-structured characteristic dose curves of damage to be plotted. The dose ranges used were approximate as follows, 0.005-0.2 J/cm^2 (Germicidal), 0.01-3 J/cm^2 (TL12), 0.1-4 J/cm^2 (UV6), 0.1-14 J/cm^2 (TL01), 0.3-30 J/cm^2 (Helarium), 1-73 J/cm^2 (Arimed B), 4-74 J/cm^2 (Cleo – filter) and 3-37 J/cm^2 (Cleo + filter); this equates to maximum SED values of 20, 80, 50, 80, 60, 40, 10 and 2 respectively.

A trend showed a shift to the right of the dose curve when the UVR source emitted more long wavelengths (UVA). For example, the Germicidal UVR source (emitting the shortest wavelengths; highest energy) required a lower dose than the Cleo + filter (emits the longest wavelengths; lowest energy) to create the same amount of damage. With only minimal discrepancies this observation was consistent across cell type with all UVR sources.

An observation of this data saw differences in the maximum damage created by the different UVR sources. This was a possible consequence of the high doses of UVR required to achieve maximum damage. Some of the doses used by particular UVR sources were necessary to achieve complete dose curves, and do not represent biologically relevant exposures. This was further supported by the viability data reported in Chapter 3. It is likely that some of the high doses were creating cell death before the maximum damage could be created. This effect seems to be specific to UVR source, as well as cell type. This effect was taken into account when plotting the action

spectrum detailed in the following section. It resulted in values of damage produced by lower doses being utilised. These differences may also be due to differences in the way the different wavelengths of UVR create damage.

The reasoning for the lower doses received by the cells (by means of SED), when irradiated with the Cleo ± filter, was simply due to effect on cell viability and irradiation length. This resulted in less defined dose curves.

4.4.2 The Action Spectrum of UVR-Induced mtDNA Damage

To minimise any confounding effects due to cell death, a consistent value of a 10 % increase in mtDNA damage was utilised for action spectrum prediction. This allowed for minimal cell death but was also taken when the curve was in its exponential phase. From these values relative differences between the UVR-sources were calculated. Similar values were obtained from the predicted action spectrum, and then the solver function in excel was used to minimise the differences between the model and the observed data. An example excel-worksheet, as well as raw values showing the differences in relative effects, can be found in Appendix II. The data obtained using the Germicidal UVR source was omitted from determination of the action spectra. This was because this UVR source only covered a narrowband of chiefly UVC, peaking at 252 nm, leading to an uncertainty of the effect of the wavelengths between 255-270 nm. The effect of UVC is not biologically relevant as its wavelengths do not reach the earth's surface (Lloyd, 2006) and therefore the exclusion of the Germicidal lamp data from the action spectrum was no considered detrimental to the overall aim. Observations from Figure 4.4 show that the Germicidal UVR source is the most detrimental of sources utilised, and it is therefore hypothesised that the short wavelengths it emits would have been shown to have caused the greatest effect.

Initially modelling of the action spectra incorporated the use of two-exponential curve. Although this curve fitted well, it was not very flexible, which meant a lot of "smoothing" of the data occurred. This is because with this type of model only one point varies and therefore a model with more varying points would be more compliant, and represent the data better; this lead to action spectrum prediction using a three-exponential model. Support for this decision was the fact that the previously

determined action spectrums (for UVR-induced erythema and nDNA damage; used for comparison in this thesis) were fitted to a model with two inflection points which decrease exponentially. This meant that the data in this thesis could be better compared to those previously determined if a three-exponential model was employed.

The action spectra for all three cell types followed a similar trend with the shorter wavelengths being the most detrimental; showing a reduction in effect with an increase in wavelength. At ~325 nm (HDFn) and ~330 nm (HaCaT) this reduction in damage then began to increase with an increase in wavelength. This effect was not mirrored in the Primary Keratinocytes; instead from ~330 nm the increasing wavelength did not appear to have an effect on mtDNA damage. Further observations saw that the HDFn cells appeared most sensitive to all the wavelengths of UVR. This was particularly apparent with the wavelengths 320-340 nm. As well as this, the mtDNA of all the cell types seemed more vulnerable to wavelengths 270-~320 nm than nDNA. Similarly the wavelengths from ~330 nm looked as though they were more damaging to the mtDNA of the HDFn and HaCaT cells.

A higher sensitivity of dermal fibroblasts to UVR has been previously reported; Marionnet *et al*., 2010 found that there was a greater oxidative response in dermal fibroblasts in comparison to keratinocytes. This was shown by a more rapid induction of associated gene expression when irradiated with a UVR source predominant in the longer, UVA associated, wavelengths (Marionnet *et al.*, 2010). Bernerd and Asselineau, 1998 have also suggested differential cell type sensitivity to UVA supporting that dermal fibroblasts are less resistant to UVA. This was seen in skin equivalents exposed to 30 J/cm^2 UVA1 (Bernerd and Asselineau, 1998). One suggestion for this phenomenon was that keratinocytes contain higher levels of ferritin, an entity involved in oxidative stress response. Ferritin has a protective effect by chelating iron which can be induced by UVA, and is damaging because it can catalyse the formation of hydroxyl radicals (Qian and Van Houten, 2010). Interestingly work within Chapter 6 investigates the effect of a particular exogenesis antioxidant (Tiron) which mimics ferritins iron chelating capabilities. Therefore this increase in ferritin levels could increase the resistance of keratinocytes to UVA. A further suggestion for keratinocytes increased resistance is possibly due to the superficial nature of keratinocytes, and their exposed vulnerability, Bernerd and Asselineau hypothesised that they could be programmed for

stress resistance. For example, the high presence of keratins along with the differentiation and consequential production of the cornified envelope could perhaps provide keratinocytes with a physical barrier to UVR. This hypothesis, of increased resistance in keratinocytes due to the high prevalence of keratin, has been further suggested by Otto *et al*., 1999 who reported better survival rates in UVR exposed keratinocytes than UVR exposed dermal fibroblasts (Otto *et al.*, 1999).

The difference in damage to the mtDNA of HaCat and Primary Keratinocytes was perhaps due to the heterogeneity of the Primary Keratinocytes. Furthermore, although HaCaTs are well known as a good substitute for normal human keratinocytes in skin related experiments, differences between these cell types are present. For example some molecular defects involving the NF-kB (nuclear factor kappa-light-chain-enhancer of activated B cells) signalling pathway are associated with HaCaT cells (Neuner *et al.*, 1996; Syed *et al.*, 2012).

There is a possibility that the differences seen between the three cell types could be due to variation between experiments; i.e. irradiation media and heating effects. However, the optimisation experiments shown in Chapter 3 indicate that any such effects were likely to be insignificant. Within Chapter 3, experiments included irradiation using a broadband UVR source, which emitted both UVA and UVB (TL12), and confirmed that irradiation media did not affect mtDNA damage. This chapter also shows that heating does not affect mtDNA damage; a finding required for a recent publication (Swalwell *et al.*, 2012).

The action spectra for UVR-induced mtDNA damage in all three cell types seemed more sensitive to the shorter wavelengths of UVR compared to the nDNA damage action spectrum (Setlow, 1974). However not too many conclusions can be drawn from this because the action spectrum of UVR-induced nDNA damage was not performed in skin cells, and the data for the action spectra predicted in this thesis vary, which emphases cellular differences. Nonetheless, the action spectrum for UVR-induced mtDNA damage in HDFn and HaCaT cells does not entirely follow the trend of that previously seen. Instead they suggest that the wavelengths in the UVA range may be more detrimental as the wavelengths increase in length. This could possibly be due to the close proximity of mtDNA to the ETC, a major source of ROS which is exacerbated

by UVA. This could emphasise the impact of UVA, the damaging effects of which are largely due to ROS production. Further modelling of the action spectra, which would include the addition of error, would be advantageous and may increase the certainty of this data.

This work was limited by the available technology. A large part of this work involved the sourcing of adequate UVR emitting lamps. A higher number of lamps with unique UVR spectra would have created more data points which would have increased the reliability of the data. Furthermore it would have been of benefit if the lamps which emitted largely UVA wavelengths had higher irradiation emissions. This would have reduced experimental time, consequently minimising cell death and variability between UVR exposures.

4.4.3 Data Support the TaqMan Method for Detecting the 4977 bp Deletion

Although the TaqMan method had been previously published (Koch *et al.*, 2001), and the utilisation of a SYBR Green method was investigated due to the lower experimental costs associated with this technology. The first experimental procedure encompassed the amplification of a patient DNA sample known to harbour the 4977 bp deletion. The aim of this procedure was to increase the quantity of this small sample amount for future positive control analysis. Electrophoresis analysis determined that both PCR methods could successfully amplify the 4977 bp deletion, and furthermore re-amplification produced comparable products. Dissociation curve analysis, following the SYBR Green method, saw a clear single peak at ~78 °C clarifying that only the single product desired had been amplified and was detected.

However, following standard curve analysis a correlation of just 0.92 was seen with the SYBR Green method compared with the high linearity of 0.99 seen with the TaqMan method. When determining primer accuracy, the coefficient of correlation obtained from the standard curve should be ≥0.99 (Invitrogen, 2013). Therefore the TaqMan method was utilised for further investigations of 4977 bp deletion induction.

4.4.4 4977 bp was not Induced Following Repeat UVR Irradiation

The aim of this investigation was to determine an action spectrum of the UVR-induced 4977 bp deletion. This deletion cannot be created by one off acute doses and instead requires a repeated irradiation regime. Initial optimisation experiments were sought in an aim to determine a method which allowed for repeat irradiation of cells without causing substantial cell death. A necessity, as repetitive doses of the same dose of acute UVR can cause an increase in cell death, an observation noted by Merwald *et al*., 2005, in UVA irradiated human squamous cell carcinoma cells (Merwald *et al.*, 2005).

Koch *et al*., 2001 found that a dose of 2 J/cm^2 UVA delivered just three times was sufficient enough to cause induction of the 4977 bp deletion in human neonatal keratinocytes. They also found an increase in incidence increased with dose. To maintain consistency across lamp type a dose of 1 SED was chosen, this was a daily dose of ~19 J/cm^2 with the Cleo + filter (100 % UVA) (Koch *et al.*, 2001). With this lamp the dose was split into three doses across the day of ~6.3 J/cm^2, similar to the mid-range dose recorded by Koch *et al* (7 J/cm^2). Therefore this dose regime, based on the previous reports should have created the 4977 bp deletion after just three repeat irradiations. However we did not see induction of the deletion at this stage, an observation consistent with Berneburg *et al*., 1999. Berneburg *et al* exposed human dermal fibroblasts to 8 J/cm^2 three times a day, a dose initially used for this present study but found to be too harsh for the cells used. They also exposed their cells every day (Berneburg *et al.*, 1999), again a condition found to cause a large amount of death in this present study. With these conditions the Berneburg group did not see induction of the common deletion until cells had been exposed to 26 exposures. This shows conflict between the published data and therefore careful considerations were taken into account with this investigation. Differences between this investigation and that performed by the Berneburg group are distinct. The 100 % UVA (Cleo + filter; UVR source most similar to that used by Berneburg) dose used in this study was just approximately 79 % of that used by Berneburg and my doses were delivered on alternate days, not every day. This was necessary for these present experiments because, when Berneburg's regime was followed substantial cell death hindered the

progression. For ease of analysis between the different UVR sources, the number of irradiations were represented as the number of 1 SED irradiations (all lamps with the exception of the Cleo + filter received one daily dose of 1 SED). This means that with the Cleo + filter (100 % UVA) HaCaT cells received a total of 78 repeat doses of ~6.3 J/cm^2. HDFn cells suffered in viability with this dose and consequently no data is available for this cell type when irradiated with 100 % UVA.

Due to lack of investigations of the induction of the 4977 bp deletion with any UVR source, except those emitting 100 % UVA, it was difficult to determine an acceptable repeat dose to use when irradiating with the other UVR sources. This was why a consistent dose of 1 SED was utilised. Initial experiments found that with the UVR sources, with the exception of the Cleo + filter, this dose could be delivered on alternate days without creating substantial cell death. For further explanation for this dose choice please refer to section 4.4.6 . Not all of the available UVR sources were used in these investigations; the Germicidal and TL12 UVR sources were considered or proved too damaging when exposure was of a repetitive nature. Furthermore, all experiments were continued until cell death, due to either the UVR exposure or otherwise, caused the termination.

When both cell types were exposed to repeat irradiations of the Arimed B UVR source (Figure 4.12) linear regression analysis of the data saw a statistically significant increase. This indicates that the deletion was reduced with UVR exposure. However this observation is most certainly down to how the analysis was conducted. When the QPCR analysis gave values of “un-determined” or >35 (indicating no deletion) they were amended to 35 (the value associated with a lack of deletion presence). When both cells were irradiated with Arimed B values were >35 and were therefore corrected to 35, this meant that all values associated with this lamp had no value for error. A larger variation, perhaps due to a higher number of samples, in the control was seen. These values for the control samples were very close to 35, at 34.89 ± 0.1 in the HaCaT cells and 34.73 ± 0.3 in HDFn cells. It is therefore the lack of error seen in the positive samples which caused an increase in detection of the deletion, and careful examination of the data it has dismissed this finding.

Figure 4.11 (B) saw that when HDFn cells were irradiated with Helarium the deletion could have possibly been induced shown by a decrease in the Ct value of 28.48 ± 3.3 and 28.28 ± 1.0 following 12 and 23 repeat irradiations. A similar potential induction was seen when HaCaT cells were irradiated with the Cleo – filter UVR source (Figure 4.13; A) where a, possible, small dose dependent decrease in Ct was seen following 26 to 32 irradiations. However variation seen in the control samples and an inconsistency relating dose to induction meant that no statistical deviation from the control was seen when analysed by linear regression.

Based on the findings by Koch *et al*, induction of the 4977 bp deletion should have been early on the investigation with the 100 % UVA source (Cleo + filter). However this finding did conflict with the Berneburg *et al*, who supported my lack of induction of the deletion in the primitive stage of the experiment. Berneburg and his group did manage to induce the deletion, but using a regime found to be too harsh for the cells used in this study, and therefore quite unrealistic. It is perplexing how the Berneburg group were able to deliver such a high dose, and this thesis suggests methods were not complete or entirely available within the published data. Using a less severe regime, but with a higher number of repeat irradiations I was unable to duplicate these findings. Berneburg *et al* did suggest that their finding was cell type specific, and that the deletion was mainly identifiable within the dermal layers. This could be one possible reason for why the deletion could not be induced within this present study. The UVR dose regime when using the 100 % UVA source was too severe for the dermal fibroblasts utilised here, meaning the results were based on keratinocyte irradiations with this UVR source. Again this questions the dosing regimen that Berneburg *et al* reported. Furthermore, fibroblasts experiments were completed when exposed to all the other UVR sources used. Both the Cleo – filter and Arimed B UVR sources encompass similar wavelengths to that of the Cleo + filter and theoretically should have initiated a similar response. As well as this, it has been proposed within our group that the common deletion is only found in supernatant cells which are therefore dead.

Experiments were discontinued due to a lack of induction of the 4977 bp deletion, and the lengthy nature of investigation. The action spectrum of UVR-induced 4977 bp production was not determined due to an inability to successfully create the deletion.

4.4.5 Data Support the TaqMan Method for Detecting the 3895 bp Deletion

The 3895 bp deletion has been found to be more prevalent in sun exposed skin compared with sun protected skin and is therefore an important specific of mtDNA damage to evaluate (Krishnan *et al.*, 2004). Investigations in to the induction of the 3895 bp deletion used a QPCR method to amplify a section of the mtDNA specifically harbouring the deletion and quantified by the efficiency of this amplification. The theory of this assay means that an increase in the efficiency of the product amplified means there is an increase in occurrence of the 3895 bp deletion and therefore mtDNA damage.

Initially validation was of a SYBR Green method and entailed modification of a pair of primers previously published (Harbottle *et al.*, 2010), and comparison between these two distinct primers sets. The reason for modifying the previously validated set of primers was in an attempt to make them more efficient and also to provide myself with experience of this technique. Both these primers were designed to anneal at either side of the deletion, with the forward primer spanning the break point. This meant that the products amplified all contained this deletion. The positive control sample used was HaCat cells irradiated 6 x 2.3 J/cm^2 TL09 + filter over two days.

The dissociation curve (Figure 4.15) ran at the end of the PCR showed a single peak which confirmed amplification of the single amplicon desired and the absence of contamination. This was further strengthened by visualisation of single bands of the required size by DNA electrophoresis. However a band was also visible in the un-irradiated samples where no deletion should have been present.

For further analysis of these primer sets the Ct values obtained after PCR amplification were evaluated dependent on DNA concentration and plotted into a standard curve. A correlation of 0.99 and 0.98 was seen with the published and modified SYBR Green primers to amplify the positive control respectively. This indicates that the accuracy of the primers was slightly reduced due to modifications. Irrespective of this, a similar correlation of 0.96 and 0.99 was seen with the published and modified SYBR Green primers to amplify the negative control respectively. This linearity was associated with

a DNA concentration dependent slope indicating that both primers detected the 3895 bp deletion in samples where it should not be present.

These key observations lead to the investigation of a previously published TaqMan method for the detection of the 3895 bp deletion (Harbottle and Birch-Machin, 2006). For this experiment negative and positive were obtained from patient samples known to harbour the 3895 bp deletion. The standard curve data saw a high and accurate correlation of 0.99 when this method was used to detect the deletion in the positive control sample. With this result the slope DNA concentration dependent where a minimum Ct value corresponded with the highest DNA concentration. When the same method was used to detect the deletion in the negative control no slope, dependent on DNA concentration, was seen which was demonstrated by a low correlation of 0.4. The Ct values obtained by this method for detection in the negative control were all high, approximately 35, the ordinary cut off showing absence of detection. This means that the TaqMan method was accurate in its measurement of the 3895 bp deletion as it had high correlation in samples known to harbour the deletion but most importantly could not detect the deletions in samples known not to harbour it.

The fact that the both SYBR Green methods detected the 3895 bp deletion in un-irradiated cells could have possibly been due to the cells used having a high background level of the 3895 bp deletion. This could have possibly been explained by the high passage number of these cells of (~70-80). However experimental work in the following section utilised the TaqMan method in these same cells, and was unable to detect any pre-existing deletions.

This investigation confirmed that the TaqMan method was most accurate in the detection of the 3895 bp deletion and was therefore the assay of choice in succeeding explorations.

4.4.6 3895 bp was not Induced Following Repeat UVR Irradiation

The ultimate aim of this investigation was to determine an action spectrum of the UVR-induced 3895 bp deletion. As with the 4977 bp deletion, this deletion cannot be created by one off acute doses and, also, instead requires a repeated irradiation regime. The initial optimisation experiments sought in an aim to determine a method

which allowed for repeat irradiation of cells without causing substantial cell death was the same as that detailed in section 4.4.4 .

No previous data reports the induction of the 4977 bp deletion with UVR sources other than those emitting 100 % UVA. Due to this fact doses for deletion induction using the other various UVR sources were chosen based on a study by Krishnan *et al*., 2004. This study, from our group, found that the 3895 bp deletion was induced following 17 alternate day irradiations of HaCaT cells with the Helarium lamp of 1 SED (~0.5 J/cm^2) (Krishnan *et al.*, 2004). Therefore 1 SED was deemed a verifiable dose to use across the lamps.

Observations from this data saw that the amplification of the 3895 bp deletion was more variable than that seen with the 4977 bp deletion. Still, following amplification of both the cell type samples, irradiated with all of the various UVR sources, a trend for a high Ct was seen. Figure 4.19 (B) represents the data obtained from HDFn cell irradiated with the Helarium UVR source. It shows that following 9, 12 and 23 repeat irradiations low Ct values of 27.24 ± 0.4, 27.66 ± 0.2 and 27.49 ± 0.2 were respectively reported. These values were similar to the positive control and indicate an induction of the deletion. This induction, although apparent, was not dose-dependent. Furthermore more careful observations noted that the UVR-protected controls also obtained low Ct values. This meant that following analysis by linear regression no deviation of the occurrence of the 3895 bp deletion from the control was seen.

This was a puzzling finding as it conflicted with that previously seen within our own group. One explanation for this inconsistency was the difference in the method used for analysis. Krishnan *et al* used a different PCR primer set than what was used in this investigation, and analysis was via conventional PCR and gel visualisation (Krishnan *et al.*, 2004). This study used more recently validated primers described by (Harbottle and Birch-Machin, 2006; Harbottle *et al.*, 2010) and analysis was by QPCR. The primers encompassed in this study are well established detectors for the 3895 bp deletion in human skin for the detection of UVR-induced damage. They are possibly not, however, sensitive enough to detect induction of the deletion in cell culture.

Experiments were discontinued due to a lack of induction of the 3895 bp deletion, and the lengthy nature of investigation. The action spectrum of UVR-induced 3895 bp production was not determined due to an inability to successfully create the deletion. To produce an action spectrum successfully a well-defined dose-dependent response is required. Therefore small inconsistent differences would make this task impossible, and it was perhaps an ambitious aim.

4.4.7 Summary

UVR irradiation causes dose-dependent increases in damage in an 11 kb section of the mitochondrial genome. The induction of damage is wavelength dependent, with UVR sources emitting shorter wavelengths being the most detrimental.

Differences between the action spectra of UVR-induced mtDNA damage in HDFn, HaCaT and Primary Keratinocytes were observed. A consistent increase in the sensitivity of HDFn cells to all the wavelengths of UVR was seen compared to HaCaT and Primary Keratinocytes. This is possibly due to a keratinocyte increased resistance related to their exposed positioning in the skin. The action spectra of UVR-induced mtDNA damage in HDFn and HaCaT cells, showed an increase in damage with wavelengths >320 nm. This suggests an increase in the vulnerability of mtDNA to these wavelengths than nDNA.

The TaqMan technology was decided the most accurate for determination of both the 4977 bp and 3895 bp mtDNA specific deletions. However these deletions were not induced *in vitro* in keratinocytes or fibroblasts following various UVR source exposures and regimes. This was contrary to previous findings and was possibly due to a difference in the methods utilised.

Chapter 5

Results 3 – The Effect of UVR on Cellular Respiration

Chapter 5 Results 3 – The Effect of UVR on Cellular Respiration

5.1 Introduction

Cellular respiration is a series of processes which ultimately leads to the generation of cellular energy in the form of ATP. The two main metabolic pathways in ATP production are glycolysis and OXPHOS. Glycolysis takes place in the cytoplasm and is the breakdown of one molecule of glucose to two molecules of pyruvate the process of which yields two net molecules of ATP. Pyruvate is then further metabolised to lactic acid, which completes the glycolysis cycle and is also known as anaerobic respiration. However in the presence of oxygen pyruvate is oxidatively decarboxylated to acetyl CoA, this then enters the Krebs cycle which is located in the mitochondrial matrix. On entering the Krebs cycle acetyl CoA is then further reduced to CO_2 and NAD is reduced to NADH – which is required for the ETC. More information about the ETC can be found in Chapter 1, but in brief the ETC is a series of five protein complexes embedded within the inner mitochondrial membrane; these complexes are numbered I-V. Electrons are captured from donor molecules and are then transferred through the protein complexes I-IV; this is coupled with the pumping of hydrogen ions to produce a gradient from which the potential energy is used by complex V (ATP synthase) to phosphorylate ADP to ATP. This process of ATP production is also termed aerobic respiration and is much more efficient than glycolysis as it produces 36 net molecules of ATP per glucose molecule (Figure 5.1).

Cells have the flexibility to switch which of these energy producing processes is predominant. A particular example of this is the Warburg effect a phenomenon of some tumours where mitochondrial respiration is decreased leading to an increase in the conversion of glucose to lactic acid even when there is oxygen present (Qian and Van Houten, 2010). As well as this, mitochondria are implicated in various chronic pathologies associated with energy production; this is mainly because an insufficiency in energy production is linked to processes in the cell which require energy to function. Namely ion pumping and molecular motors, but most relevant for this study is the energy consumed in the activation of cellular repair pathways. These pathways are

activated when there is an accumulation of ROS/RNS induced damage in cellular components such as DNA and proteins. An increase in ROS/RNS flux can also initiate pathways which utilise NADPH leading to an increase in metabolic demand (Dranka *et al.*, 2011).

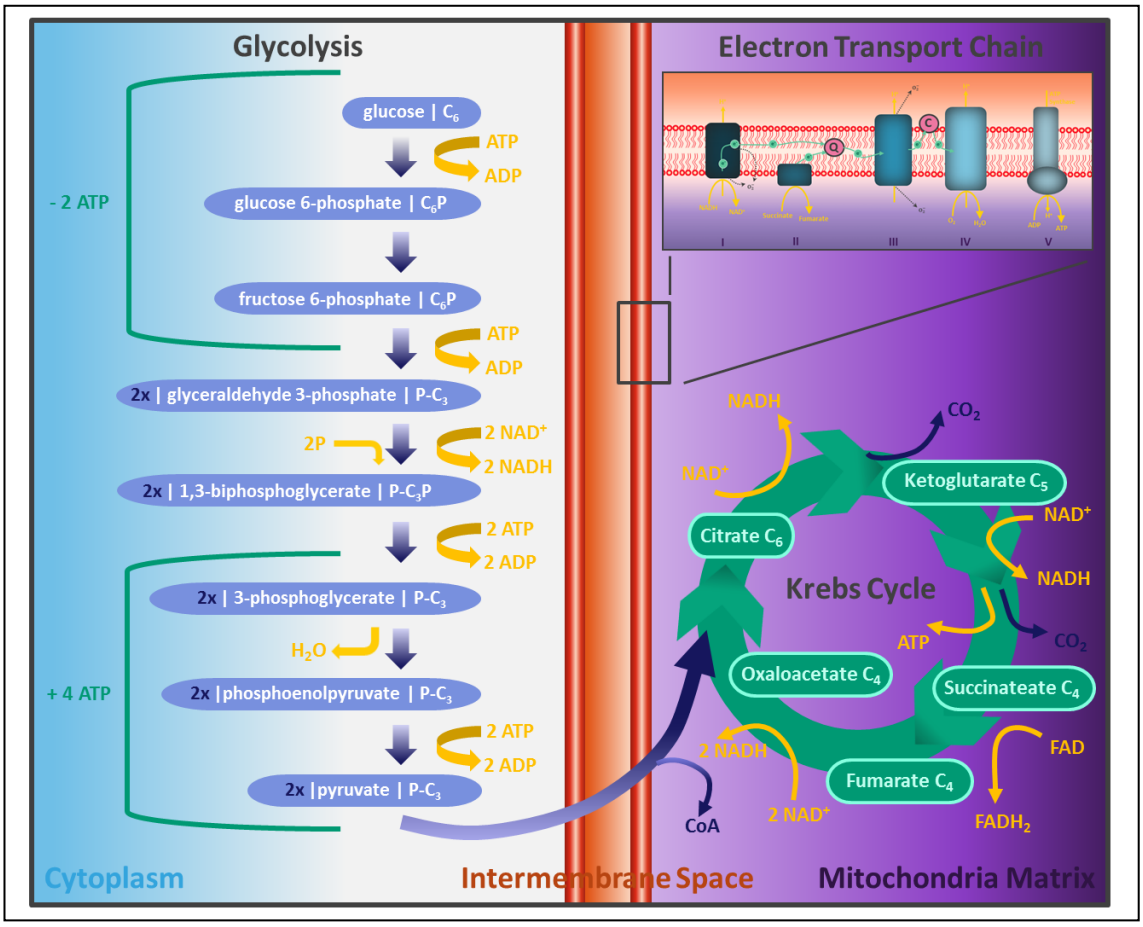

Figure 5.1: Cellular Respiration Including Glycolysis, the Krebs Cycle and the ETC. Glycolysis takes place in the cytoplasm yielding two net molecules of ATP in the absence of oxygen and is known as anaerobic respiration. Aerobic respiration requires the consumption of oxygen and comprises of the Krebs cycle, which is located in the mitochondrial matrix, and the ETC which is a series of five protein complexes embedded within the inner mitochondrial membrane. This process produces 36 net molecules of ATP per glucose molecule. For a more magnified illustration of the ETC please see chapter1.

Due to the fact that mtDNA encodes for key components of the mitochondrial ETC complexes, any damage to the mtDNA can lead to defects in the assembly of these complexes which can ultimately lead to the loss of mitochondrial respiration. This means that the UVR-induced mtDNA damage that was determined in previous chapters can cause a dysfunction of OXPHOS. UVR can also directly affect the ETC which will enhance the deterioration. Thus, mitochondria produce oxidants but at the same time they are a target for oxidative damage. This theory is termed the "vicious cycle" illustrating that an increase in ROS/RNS (for example, caused by UVR)

will damage mitochondria that, in turn, will exacerbate ROS production (Dranka *et al.*, 2011).

The quantification of oxygen consumption in cultured cells has previously, most frequently, been performed using Clark-type electrodes. This electrode uses a catalytic platinum surface to measure oxygen concentration and this technology has been shown to be accurate with a high reproducibility rate. However this assay only investigates individual samples of which it requires a large amount and, furthermore, with this technology the cells are removed from their cultured environment and suspended in a stirred, buffer solution (Dranka *et al.*, 2011; Jarrett *et al.*, 2013). There is a possible detriment of this detached condition and this is known as anoikis – a form of apoptosis that is induced in cells that are ordinarily adherent-dependent and therefore, when suspended, interactions in the extracellular matrix are lost (Frisch and Francis, 1994; Frisch and Screaton, 2001). Anoikis is also incidentally linked with an increase in ROS flux and the associated mitochondrial damage. In addition to this, oxidative stress can also be increased as a result of the stirring mechanism, a phenomenon known as non-laminar shear. This means that the effect that ROS (such as that induced by UVR) has on mitochondrial respiration is difficult to accurately determine when using Clark-type electrode assays (Dranka *et al.*, 2011). A common piece of machinery used to measure glycolysis is the Cytosensor microphysiometer which measures extracellular pH. As well as the Clark-type electrode the Cytosensor microphysiometer is low-throughput, only measuring four samples at a time. For this only a small sample is needed but it requires a constant flow across a sensor perfusion chamber to determine its measurements (Jarrett *et al.*, 2013).

An alternative to Clark-type electrodes in the investigation of cellular respiration is an innovative technology - the Seahorse Extracellular Flux (XF) Analyzer (Seahorse Bioscience, North Billerica, MA, USA) an image of which can be found in Figure 5.2. Recent publications have directly compared the two methods and results have assessed the data obtained from the Seahorse XF Analyzer more positively than that gained from the Clark-type electrodes (Dranka *et al.*, 2011). The key positives of the Seahorse XF Analyzer is that it is high-throughput, measurements can be taken from both adherent and suspended cells, a measurement related to glycolysis is also determined – resulting in a more accurate assessment of cellular respiration and finally

this technology is not an end-point assay, meaning further analysis of the cells can take place following experiments i.e. cell viability or ATP production.

Another recently introduced piece of equipment capable of measuring OXPHOS is the Oroboros Oxygraph-2k (O2k). Horan *et al*., 2012 have extensively reviewed the use of both the O2k and the Seahorse XF Analyzer which is summarised in Table 5-1 (Horan *et al.*, 2012). They found that both machines could measure OXPHOS in *in vitro,* real-time experiments on isolated mitochondria, cultured cells and tissues. The data produced by the two machines has also found to be comparable as shown by Wang and Moraes, 2011 who were investigating the mitochondrial biogenesis of different human cancer cell lines (Wang and Moraes, 2011); (Horan *et al.*, 2012). The key advantages of the Seahorse XF Analyzer compared to the O2k is, as previously mentioned, its ability to produce a measurement associated with glycolysis as well as OXPHOS and also its high-throughput capability.

The Seahorse XF Analyzer technology enables accurate quantification of cellular respiration in intact cells. This machinery takes simultaneous repeated measurements of oxygen consumption rate (OCR) and extracellular acidification rate (ECAR) that are representative of oxidative OXPHOS and glycolysis respectively. OCR and ECAR are calculated by the changes in oxygen and proton (pH) concentration over a specified time period, measured in real-time by sensors in the cell medium (specialised un-buffered medium is required to accurately measure ECAR) just 200 µm above the cells surface. These measurements are taken non-invasively which allows for follow up end point assays. The Seahorse XF Analyzer is bench-top machinery available in both a 24-well and a 96-well format that produces high-throughput measurements, and it also allows for real-time injection of compounds to aid in the analysis of cellular respiration measurements.

Table 5-1: Comparison of the Oroboros Oxygraph 2k and the Seahorse XF Extracellular Flux Analyzer.

Equipment Specifics	Oroboros O2k	Seahorse XF Extracellular Flux Analyser
Cost of equipment*	$50k (~£32k)	$200k (~£130k)
Automated	No	Yes
Labour intensity	High (needs constant operator input)	Minimal (system is fully automated)
Internal Calibration	No	Yes
Respiratory measurements	OXPHOS	OXPHOS/glycolysis/CO_2
Assay Format	2 chamber based	24- or 96-well plate based
High-resolution sensitivity	Yes (polarographic sensors)	Yes (fluorescent sensors)
High-throughput capability	No (2 samples per sun)	Yes (24-96 samples per run)
Time per sample assay	Slow ~1 h for two samples	Fast ~90 min for up to 96 samples
Controlled temperature range	Yes (4-45 °C)	Yes, but ambient temperature needs to be 8 °C lower than desired temperature
Background correction per assay	No (separate assay per chamber)	Yes (background control wells on plate)
Tissue types analysed	mitochondria/cells/permeabilised fibers	Mitochondria/cells/pancreatic islets/ muscle fibres/ hippocampal slices
MMP analysis[¥]	Yes	No
Substrates injected per assay	Unlimited	Limited to four
Injection of Oxygen[#]	Yes	No
Cost per assay[§]	Cheap – (regents/substrates required)	Expensive – reagents/substrates plus a new fluorescent plate per assay

This table shows technical specifications and respiratory specifics, taken from (Horan *et al.*, 2012). *Approximate U.S.dollars, ¥mitochondrial membrane potential, #analysis to determine if the respiration rate alters between high and low oxygen concentrations, §cost is relative because the experimental design using the Oroboros O2k may prove to be equally or more expensive in the longer term, e.g. constantly monitoring operator usage.

For this study the 24-well format for the Seahorse XF Analyzer was used. The cell culture plate is organised in the same way as a normal 24-well plate, with rows labelled A-D and columns 1-6. However the plates look very different and the seeding surface area of each well is only that of a typical 96-well plate. Each plate comes with a disposable top lid which contains a probe for each well at the bottom of which are two fluorescent biosensors (oxygen and pH), and these are paired with fibre-optic waveguides which transfer fluorescent signals through optical filters to sensitive photo-detectors (Qian and Van Houten, 2010). The fluorescence biosensors for oxygen and pH are excited at 530 nm and 470 nm, respectively, and emissions are produced at 650 nm and 530 nm, respectively, which are detected by photo-detectors (Brand and Nicholls, 2011). The top lid also encompasses four ports (labelled A-D) per well which enables reagents to be injected in real-time into the assay. Figure 5.2 shows an illustration of how the Seahorse XF Analyzer works and shows an image of the specialised 24-well plate. The ability to inject compounds into the assay in real-time is particularly useful for experiments investigating the respiratory profile of a cell, where specific metabolic modulators are administered at fixed time points in order to determine different parameters of respiratory activity.

A specific experiment used for this study encompassed the subsequent injections of oligomycin, carbonyl cyanide-ptrifluoromethoxyphenylhydrazone (FCCP) and a combination of rotenone and antimycin A; this is illustrated in Figure 5.3. Firstly oligomycin inhibits complex V, and this causes a reduction in OCR and a build-up of the inner mitochondrial membrane potential proton gradient. Adding oligomycin gives us a measure for the leakage of H^+ from the inter-membrane space of the mitochondria to the matrix (proton leak). This enables us to calculate the level of oxygen consumption required for ATP turnover (production) by subtracting this from the basal respiration value. The second injection is FCCP, an uncoupling agent, which depolarises the inner mitochondrial membrane potential. To compensate for this the mitochondria increase their flux through the ETC in an aim to restore the proton gradient. This leads to a rapid consumption of energy and oxygen, without the generation of ATP giving a measure of (maximal) respiratory capacity. This allows us to determine a further measurement for respiratory reserve (capacity) by subtracting basal respiration from respiratory capacity. Finally a combination of rotenone and antimycin A is injected.

Rotenone inhibits complex I preventing potential energy (NADH) from being converted to usable energy (ATP) and antimycin A inhibits complex III which consequently inhibits ATP production by disrupting the formation of the proton gradient across the inner membrane (Barbi de Moura *et al.*, 2012; Jantzen *et al.*, 2012; Jarrett *et al.*, 2013). The measurement of OCR following the final injection is related to oxygen consumed from non-mitochondrial events such as cell surface oxygen consumption and oxidase enzymes within the cytoplasm (Nadanaciva *et al.*, 2012).

The literature on the effects of UVR on human skin cells is somewhat limiting. The general consensus is that OXPHOS decreases with UVR exposure (Djavaheri-Mergny *et al.*, 2001). From my investigations of the literature, the relationship between OXPHOS and glycolysis in cells exposed to UVR does not seem to have been established; and especially not using the innovative Seahorse XF Analyzer. With this in mind, this chapter aims to observe any changes in cellular respiration due to UVR exposure enabling a better understanding of the interplay between OXPHOS and glycolysis. A secondary aim was to optimise a method with this technology which P&G could continue to use in their research. A requirement of the assay was to be able to measure any beneficial effects of specific potential cosmetic product actives when applied prior/following UVR exposure.

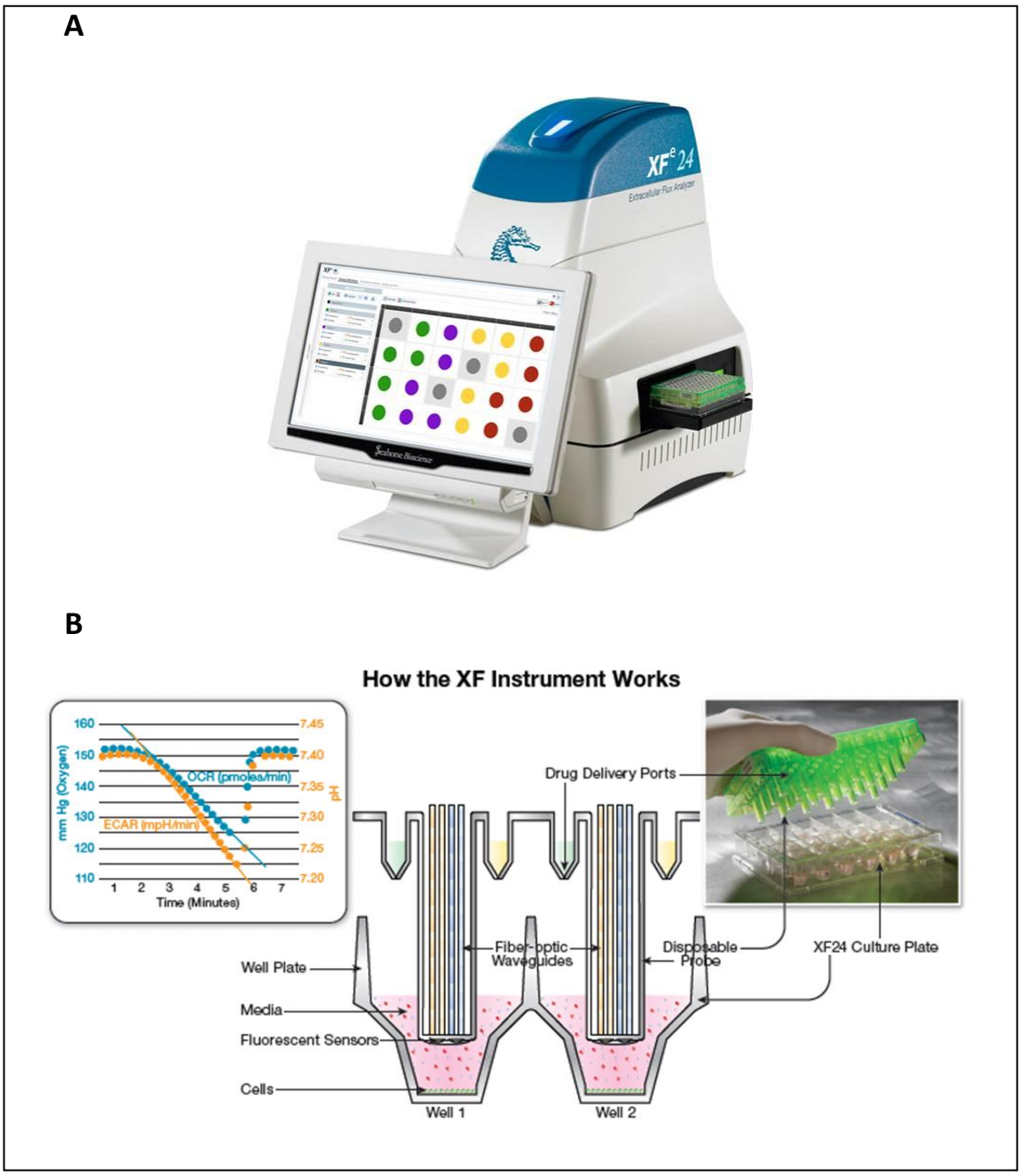

Figure 5.2: An Image of the Seahorse XF Analyzer machinery and an Illustration of How it Works. (A) shows an image of the Seahorse XF Analyzer. (B) on the left shows how OCR and ECAR are calculated, in the middle illustrates the working Seahorse XF Analyzer plate which is shown in the image on the right.

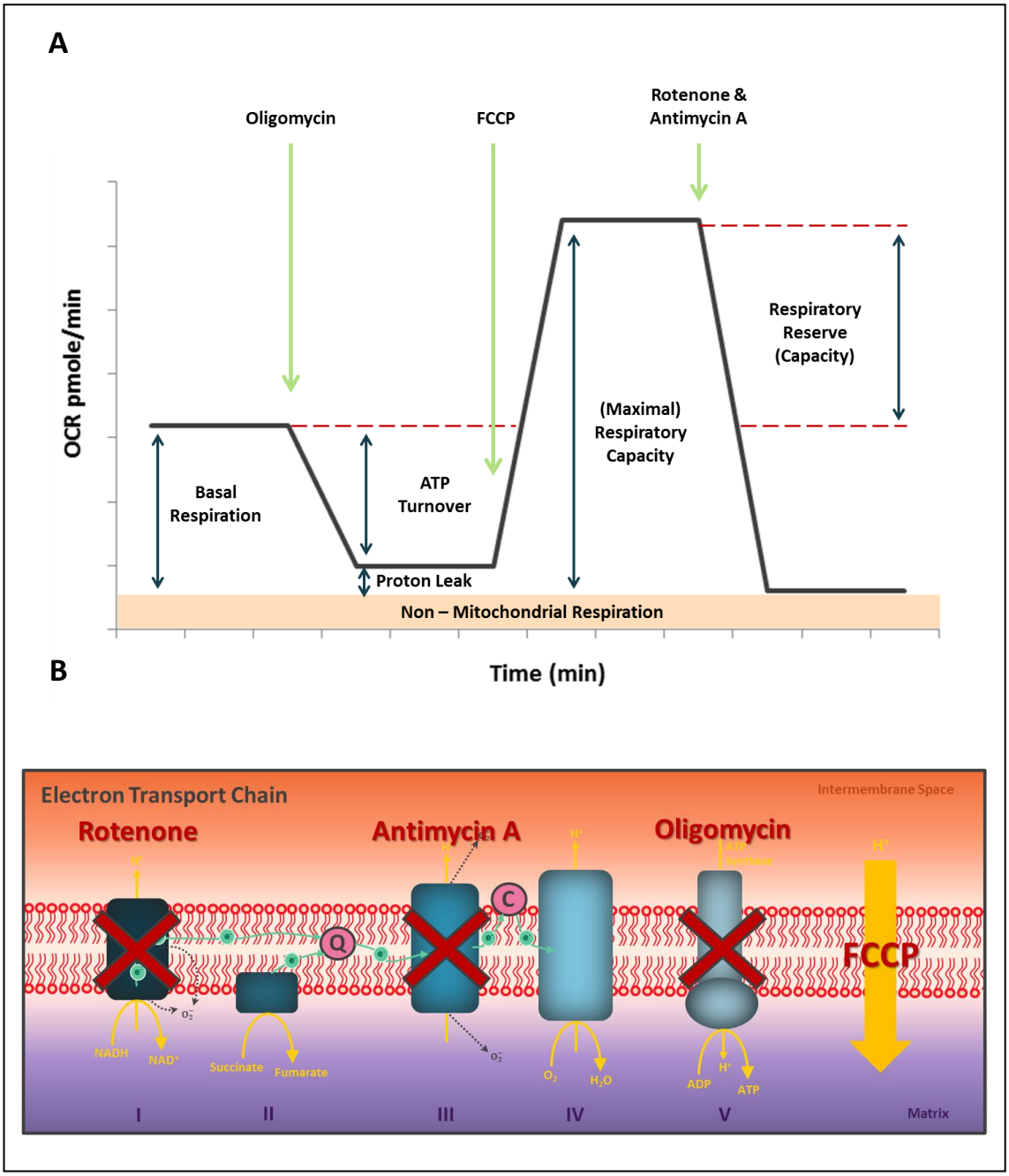

Figure 5.3: An Illustration of the Respiratory Profile of a Cell and how the Modulators which are used to Create it Work Illustration (A) demonstrates the effect oligomycin, FCCP and the combination of rotenone and antimycin A should have on the respiratory profile of a particular cell. Illustration (B) shows which parts of the electron transport chain each modulator effects. Oligomycin inhibits complex V, FCCP depolarises the inner mitochondrial membrane potential, rotenone inhibits complex I and antimycin A inhibits complex III.

Recently in the cosmeceutical market Elizabeth Arden introduced a product (Prevage^{TM}) publicised as an anti-ageing treatment which contains 0.5 % of a compound called idebenone (Wempe *et al.*, 2009). For this study we enlisted the use of this interesting entity to validate the optimised assay. Idebenone (6-(10-hydroxydecyl)2,3-dimethoxy-5-methyl-1,4-benzoquinone) is a synthetic derivative of ubiquinone (CoQ_{10}) and was initially patented by Takeda Chemical

Industries, Osaka, Japan (Figure 5.4). In 1986 it was introduced to the market in Japan where it was initially suggested to aid in deficiencies of brain function associated with an age-dependency (such as Alzheimer's Disease) (Zs -Nagy, 1990; Geromel *et al.*, 2002). It is now currently being investigated for benefit in the treatment of various mitochondrial and neuromuscular diseases which are associated with respiratory chain dysfunction (Carbone *et al.*, 2012). Idebenone differs in structure from CoQ_{10} by means of a shorter carbon side chain as it possess an alkyl chain with a terminal polar hydroxyl group whereas CoQ_{10} contains ten isoprenoid repeats (Haefeli *et al.*, 2011). This means idebenone has a lower molecular weight (approximately 60 % smaller) subsequently increasing its solubility, characteristics of which should assist in the penetration of idebenone in the skin in comparison to CoQ_{10} (McDaniel *et al.*, 2005a). CoQ_{10} is naturally found within the human body and is a key molecule within the ETC where it aids the transfer of electrons from complexes I and II to complex III. The similarity of the quinone structure that idebenone and CoQ_{10} share is what enables them to transfer electrons as well as to undergo reversible reduction/oxidation (redox) reactions. This means they both can act as effective antioxidants and electron carriers, and also increase the production of cellular ATP (Wempe *et al.*, 2009; Montenegro *et al.*, 2012). However at low oxygen concentrations (hypoxic; <15 %), such as in cellular stress, CoQ_{10} is inclined to oxidise itself and consequentially develop a pro-oxidant behaviour which leads to a surge in production of hydrogen peroxide, superoxide, and hydroxyl radicals. In contrast to this, under these same conditions, idebenone continues to protect against free radical formation and can retain normal ATP levels (McDaniel *et al.*, 2005a; Carbone *et al.*, 2012). Due to these antioxidant capabilities it has been suggested that idebenone could be valuable in the prevention of skin ageing by the protection of oxidative damage created from exposure to environmental insults such as UVR (Wempe *et al.*, 2009). Previous studies interested in the photo-protective effects of idebenone have been conflicting; McDaniel *et al.,*2005 found idebenone to be the most effective of a range of antioxidants (including CoQ_{10}) to offer oxidative protection which was linked with photo-protection in human keratinocyte cells (McDaniel *et al.*, 2005b). Conversely, Tournas *et al*., 2006 found idebenone offered little protection against the induction of erythema in human skin (Tournas *et al.*, 2006). However this study does not intend to investigate the protective effect that idebenone may offer but conversely as reversible treatment.

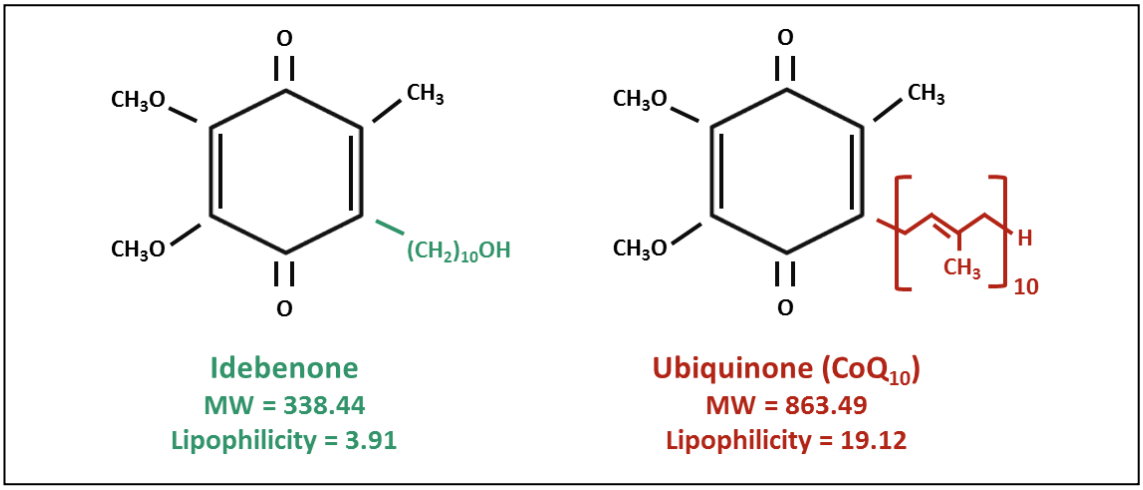

Figure 5.4: Differences of idebenone and ubiquinone (CoQ_{10}). This figure shows the structural, molecular weight (MW) and lipophilicity (the octanol:water partition coefficient) differences of idebenone on CoQ_{10}.

5.1.1 Aims

The main aim of this chapter is to investigate any changes in cellular respiration due to UVR exposure which will provide a better understanding of the interplay between OXPHOS and glycolysis in skin cells. A further aim is to provide an optimised method with the Seahorse XF analyzer technology of which P&G could continue to use in their research to measure any beneficial effects of specific potential cosmetic product actives when applied prior/following UVR exposure.

5.2 Methods

5.2.1 Cell Culture

5.2.1.1 BJ Skin Fibroblast Cell Line

The normal human neonatal dermal fibroblast cell line, BJ Skin fibroblasts (ATCC, USA) were maintained in Eagle's minimum essential medium (EMEM; ATCC, USA) containing 10 % FCS (ATCC, USA) and a 1 % gentamicin/amphotericin solution (Gibco, USA) at 37 °C with 5 % CO_2. The cells were passaged every 6-7 days when they reached 80-90 % confluence and medium was refreshed every 2-3 days.

5.2.1.2 HEKn Cells

Human neonatal epidermal keratinocytes (HEKn; Lots 988937 and 985750, Gibco, USA) were maintained in EpiLife medium (Gibco, USA) supplemented with 0.2 % HKGS

(Gibco, USA) and 1 % gentamicin/amphotericin solution (Gibco, USA) at 37 °C with 5 % CO_2. The cells were used experimentally at passages 1-2.

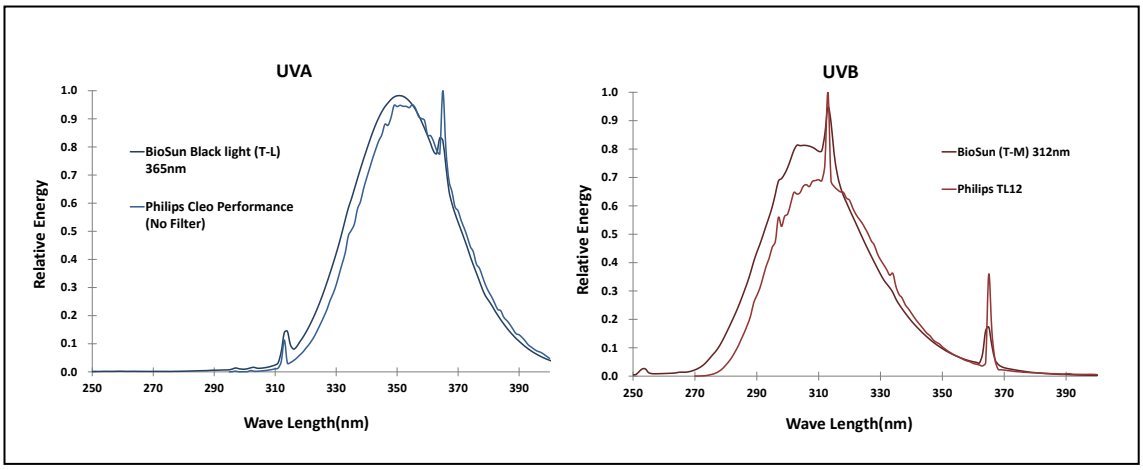

Figure 5.5: Comparison of the Spectra of the UVA and UVB Lamps of the BioSun Solar Simulator. This figure compares the spectra of the UVA lamp (BioSun black light (T-L) 365 nm) and the UVB lamp (BioSun (T-M) 312 nm) of the BioSun solar simulator with similar UVR lamps used in Newcastle University experiments. Namely the Philips Cleo Performance with no glass filters (UVA) and the Philips TL12 (UVB).

5.2.2 Irradiation Methods

Prior to irradiation, medium was removed and cells were washed with, and medium was replaced with PBS. For irradiations the lids of the dishes were removed and control cells were covered in aluminium foil but exposed to the same conditions as the irradiated cells. Doses of UVR were varied by the covering and uncovering of foil at the required time-points. The irradiation unit used was the BioSun Solar Simulator (Vilber Lourmat, France) calibrated in-house by P&G. The unit contained both UVA and UVB out-puts identified as the BioSun black light (T-L) 365 nm and the BioSun (T-M) 312 nm respectively. The out-put of these two lamps was comparable to the lamps used in all other investigations within Newcastle University – see **Figure 5.5**.The BJ Skin fibroblasts were irradiated with various doses of UVA ranging from 1-50 J/cm^2 and the HKEn cells were irradiated with various doses of UVB ranging from 7.5-30 mJ/cm^2. Following UVR treatment cells were assessed for cell viability, ATP production or cellular respiration.

5.2.3 Cell viability - CyQUANT® NF Cell Proliferation Assay

Cell viability was assessed using the CyQUANT NF Cell Proliferation Assay (Molecular Probes, USA). With this assay cellular DNA content is measured via fluorescent dye binding and this is proportional to cell number. Cells were first seeded ($10x10^3$ cells/well) into 96-well black clear bottomed plates (Thermo Scientific, USA) and then incubated at 37 °C with 5 % CO_2 for 24 h. Cells were then treated with the designated UVR treatment and assessed for cell viability either immediately or following a 24 h incubation at 37 °C with 5 % CO_2 in the cell specific growth media. For the assay irradiation/growth media was removed and replaced with 100 µl of the dye binding solution (prepared as per manufactures instructions) the plate was then protected from light and incubated at room temperature for 30 min. Fluorescence was measured by excitation at 485 nm and emission was detected at 530 nm using the Spectromax microplate reader (Molecular Devices, USA).

5.2.4 ATP Production - CellTiter-Glo® Luminescent Cell Viability Assay

The CellTiter-Glo assay (Promega, USA) was used to determine ATP production. With this assay the reagent caused both lyses of the cells and inhibition of endogenous ATPases. It also provided luciferase/luciferin which reacted with ATP ultimately leading to the release of a photon of light which was measured. As well as a measurement of ATP, the luminescence generated was proportional to the number of viable cells (Dranka *et al.*, 2011). Cells were first seeded into a 96-well plate ($10x10^3$ cells/well), which was black with a clear bottom (Thermo Scientific, USA). These cells were then incubated at 37 °C with 5 % CO_2 for 24 h. Cells were then treated with the designated UVR treatment, see section 5.2.2 , and assessed for ATP production either immediately or following a 24 h incubation at 37 °C with 5 % CO_2 in the cell specific growth media. For the assay 100 µl of the CellTiter-Glo reagent (prepared as per manufactures instructions) was added to 100 µl of irradiation/growth media already present in the well. The plate was then placed on a cell mixer and shook for 2 min and was then incubated at room temperature for 10 min. Luminescence was measured using the luminometer LUMIstar OPTIMA (BMG Labtech, USA).

5.2.5 Cellular Respiration – Seahorse Assay (Baseline)

Prior to cell seeding 24-well Seahorse tissue culture plates (Seahorse Bioscience, USA) were coated with 0.2 % gelatin (Sigma, USA) diluted in PBS. Cells were seeded at $1x10^5$ (BJ Skin fibroblasts) or $4x10^4$ (HKEn cells) cells/well (as optimised by Holly Rovito; P&G) and incubated at 37 °C with 5 % CO_2 for 24 h. The top sensor plate of the 24-well Seahorse plate was hydrated with XF Calibrant (Seahorse Bioscience, USA) to do this 1 ml of Calibrant was added to each well of a utility plate. This was then incubated at 37 °C, with no CO_2, for a minimum of 4 h. Cells were then treated with the designated UVR treatment and cellular respiration was investigated either immediately or following a 24 h incubation at 37 °C with 5 % CO_2 in the cell specific growth media. The irradiation/growth media was then removed and cells were washed with 1 ml of XF running media and 600 µl of XF running media was added. The running media for BJ Skin fibroblasts was Seahorse Media (Seahorse Bioscience, USA) with 25 mM of glucose (Sigma, USA) and 1 mM of pyruvate (Sigma, USA). The running media for HKEn cells was a special order of unbuffered EpiLife Medium (Gibco, USA #ME120155L1, Lot PAG11219101) with 10 ng/ml insulin (Gibco, USA), 10 ng/ml hydrcortisone (Sigma, USA), 60 µM calcium chloride (Gibco, USA), 10 mM of glucose (Sigma, USA), 1 mM of pyruvate (Sigma, USA) and 2 mM of glutamine (Gibco, USA). Both of these running media were altered to pH 7.4 prior to analysis. Following addition of the running media the 24-well Seahorse plate was incubated at 37 °C with no CO_2 for 60 min and the top sensor and utility plate were loaded into the Seahorse XF Instrument for calibration. After calibration was complete the utility plate was replaced with the 24-well Seahorse plate and assay was started. Typically the assay consisted of an equilibration period followed by several loops of a mixing period of 4 min, a 2 min pause and a measurement period of 3 min; the number of loops was determined by the requirements of the assay.

5.2.6 Cellular Respiration – Seahorse Assay (Compound Injection)

For several of the experiments compounds were injected into the assay in an aim to either alter the profile of respiration or determine any effects specific compounds had on the detrimental effects created by the different UVR treatments. Typically three loops of a mixing period of 4 min, a 2 min pause and a measurement period of 3 min

were used to determine baseline measurements prior to the first injection and a further three loops were performed following each compound injection. The assessment of the respiration profile required a series of three compound injections (Seahorse Bioscience, USA) which were 1.3 µM oligomycin, 0.5 µM FCCP and the combination of 1.0 µM rotenone and 5.0 µM antimycin A. Other compounds of interest included injections of 25 µM idebenone (Enzo Life Sciences, USA) or 1.0 mM niacinamide (Sigma, USA) which were administered once baseline values were established, either as standalone injections or prior to the assessment of the respiration profile.

5.2.7 Protein Concentration – BCA Assay

A BCA protein assay was performed following the Seahorse run for normalisation. For this assay standard dilutions and the working reagent were prepared as shown in assay protocol. The Seahorse media in each well was first replaced with 50 µl PBS. Following this 25 µl of each BCA standard dilution was added to the designated wells of a clear 96-well plate in duplicate. Next either 400 µl or 200 µl of the working reagent was administered to the 24-well seahorse plate and the 96-well plate respectively. Both plates were mixed thoroughly on a plate shaker for 30 sec they were then protected from light and incubated at 37 °C for 30 min. Plates were cooled to room temperature and then a duplicate of 225 µl from each well of the 24-well Seahorse plate was transferred to a designated well in the 96-well plate (i.e. x2 wells for each seahorse well). Absorbance was measured using the Spectromax microplate reader (Molecular Devices, USA) at 562 nm.

5.2.8 Statistical Analyses

Statistical evaluation was performed by a one-way ANOVA with Dunnett's correction for comparison to the control. P-values below 0.05 were considered significant.

5.3 Results

This chapter encompasses data obtained within P&G in the USA and therefore uses techniques, reagents and cells which differ from those in the main study. Many of the assays used were commonly used within P&G and had already been optimised in-house. Due to the time restraints of this particular study the BJ fibroblasts were exposed to UVA only and the HEKn cells were exposed to UVB only. These were seen as the most physiologically relevant divisions of UVR for the two different cell types to be exposed to.

5.3.1 Viability of BJ fibroblasts and HEKn cells exposed to UVR

It was necessary to determine the viability of the BJ fibroblasts and HEKn cells when exposed to UVR to determine the optimum dose of UVR to use for the cell respiration experiments. Cell viability was assessed using the CyQUANT NF Cell Proliferation Assay and cells not exposed to UVR were seen as 100 % viable. BJ fibroblast cells were exposed to 5, 30 and 50 J/cm^2 UVA and were then assessed for viability immediately. The results of this are shown in Figure 5.6 (A); they reveal that a dose of up to 30 J/cm^2 UVA had little effect on the immediate viability of BJ fibroblasts and that a dose of 50 J/cm^2 UVA caused a 9 % decrease from the control. However this decrease was not found to be significant. BJ fibroblasts were then assessed for viability 24 h after exposure to 1, 10, 20 and 30 J/cm^2 UVA. This data shows (Figure 5.6; B) that non-significant decreases of 10, 16 and 14 % viability from the control were seen in BJ fibroblasts 24 h following a 1, 10 and 20 J/cm^2 UVA irradiation respectively. A significant decrease ($P<0.01$) of 35 % from the control was seen in the viability of BJ fibroblasts 24 h following a 30 J/cm^2 UVA irradiation.Previous work within P&G had revealed that a dose of 30 mJ/cm^2 UVB caused a minimal effect on the viability of HEKn (data not shown). It was then determined what effect 7.5, 15 and 30 mJ/cm^2 UVB had on HEKn viability 24 h following irradiation. Figure 5.6 (C) shows that 7.5, 15 and 30 mJ/cm^2 UVB caused significant decreases of 13 ($P<0.05$), 14 ($P<0.05$) and 26 % ($P<0.001$) respectively in HEKn 24 h following irradiation.

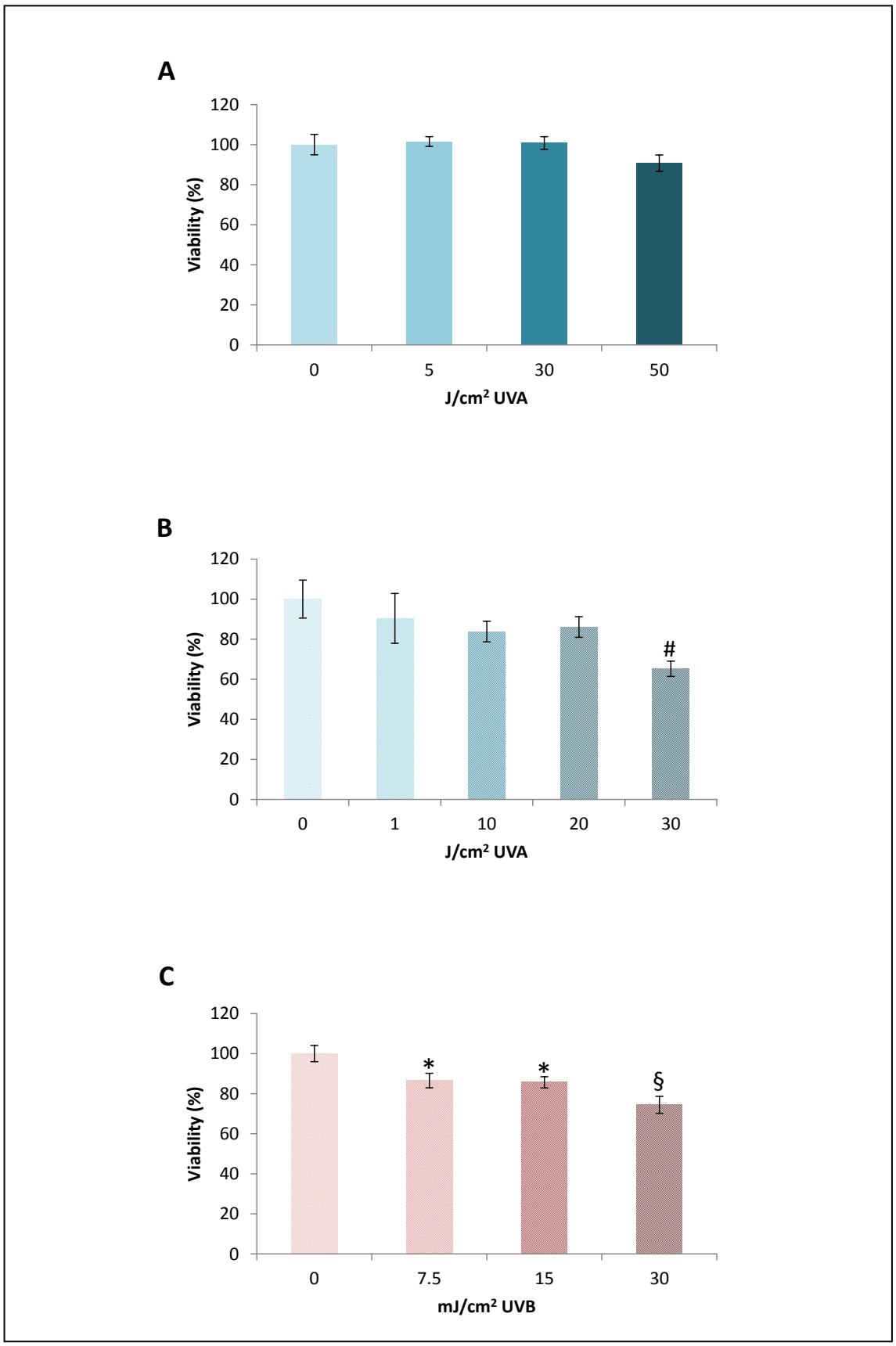

Figure 5.6: UVR-Induced Death of BJ Fibroblasts and HEKn Cells. BJ fibroblast cells were exposed to UVA and were assessed for viability either immediately (A) or following 24 h (B). HEKn cells were exposed to UVB and were assessed for viability following 24 h (C). Comparisons were made to an un-irradiated control. Cell viability was assessed using the CyQUANT NF Cell Proliferation Assay Fluorescence was measured by excitation at 485 nm and emission was detected at 530 nm (mean values n≥8 ± SEM, *P<0.05, #P<0.01, §P<0.001 compared to the control).

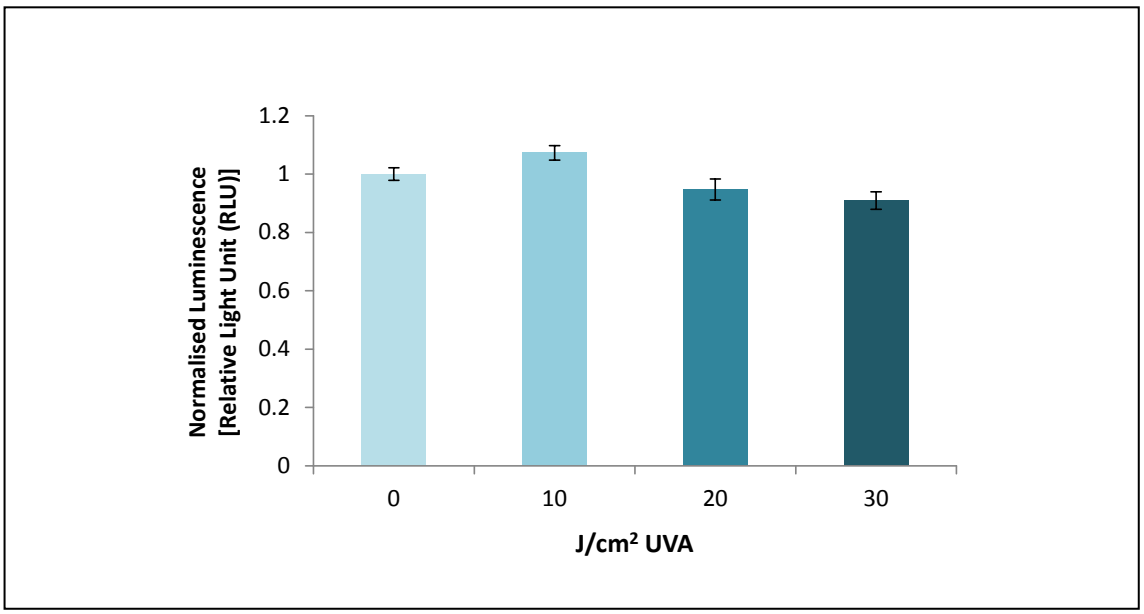

Figure 5.7: ATP Production in BJ Fibroblasts Following UVA Irradiation. Comparisons were made to an un-irradiated control. ATP production was determined using the CellTiter-Glo assay immediately following irradiation (n=2 mean ± SEM).

5.3.2 The Effect of UVA on ATP production in BJ Fibroblast cells

Based on the viability experiments shown in section 5.3.1 , doses of 10, 20 and 30 J/cm^2 UVA were used to determine the effect that UVA has on BJ fibroblast ATP production. The result of this, shown in Figure 5.7, indicates that UVA has a minimal effect on ATP production in BJ fibroblasts as none of the differences shown were found to be significant.

5.3.3 Differences in the BJ Fibroblasts Cells Baseline OCR and ECAR in Response to UVA Exposure

The effect of UVR on cellular respiration was further investigated using the 24-well Seahorse XF Analyzer. This machinery determined measurements of OCR and ECAR, simultaneously in real-time. Examples of the raw Seahorse traces are shown in Figure 5.8 (OCR) and Figure 5.9 (ECAR) illustrating the effect that doses of 1, 5, 10, 20 and 30 J/cm^2 UVA have on both baseline OCR and baseline ECAR in BJ fibroblasts. There was a dose-dependent effect of UVR on both OCR and ECAR in BJ fibroblasts and this was clearly depicted in the raw data. The real-time experiment was run for approximately 2 h (with the exception, 3.5 h for 20 J/cm^2 due to interesting findings) and therefore the analysis of this data encompassed measurements taken from the

beginning of the experiment (1 h – because the cells required a 1 h incubation period prior to analysis, see section 5.2.5) and the end (2 h, or 3.5 h for 20 J/cm^2). A further experiment explored the effect 1, 5 and 10 J/cm^2 UVA had on cellular respiration in BJ fibroblasts 24 h following irradiation and compared this with that seen in the 1 h trace. The data analysis for the effect on OCR can be found in Figure 5.10 and shows that there was a well-defined dose-dependent decrease in OCR observed at both 1 h and 2 h following UVA irradiations from 5 to 30 J/cm^2 which were statistically significant from 10 to 30 J/cm^2 when compared with the un-irradiated cells. A trend for the difference to be further decreased at 2 h as opposed to 1 h was also seen. The initial decrease in OCR created by 5 J/cm^2 UVA seemed to have recovered by 24 h, however with 10 J/cm^2 the initial decrease had further declined at 24 h by 100 % compared with the control ($P<0.001$). The data analysis for the effect of UVA on baseline ECAR can be found in Figure 5.11. Observations made from this figure determined a statistically significant dose-dependent increase in ECAR at doses 5 and 10 J/cm^2 at both 1 h and 2 h when compared to the control. With a dose of 30 J/cm^2 ECAR was reduced to below detectable levels at both 1 h and 2 h ($P<0.001$). When the cells were exposed to 20 J/cm^2 there was an initial statistically significant increase of 50 % ($P<0.001$) seen at 1 h when compared with the control. By 2 h this increase had reduced to 80 % of the control and by 3.5 h it had further reduced to just 30 % of the control ($P<0.001$). The initial increase, followed by the steady drop in ECAR was clearly visible during the progression of the assay and therefore this experiment was ran longer to get a clearer picture of the effects of this particular UVA dose. This effect seemed more prominent when looking at the raw trace shown in Figure 5.9. Due to the sharp decline in ECAR seen with both 20 and 30 J/cm^2 UVA at 2 h, only doses 1-10 J/cm^2 were assessed at 24 h (Figure 5.11). This data shows that with exposure to 10 J/cm^2 there is a statistically significant decrease in ECAR of 60 % from the control ($P<0.001$). With a dose of 1 and 5 J/cm^2 UVA ECAR was increased at 24 h to 26% more than the control ($P<0.01$ and $P>0.001$, respectively). This shows an increase with 1 J/cm^2 UVA which wasn't present at 1 h and 2 h; however the increase in ECAR with 5 J/cm^2 at 24 h is less than that seen at 1 h.

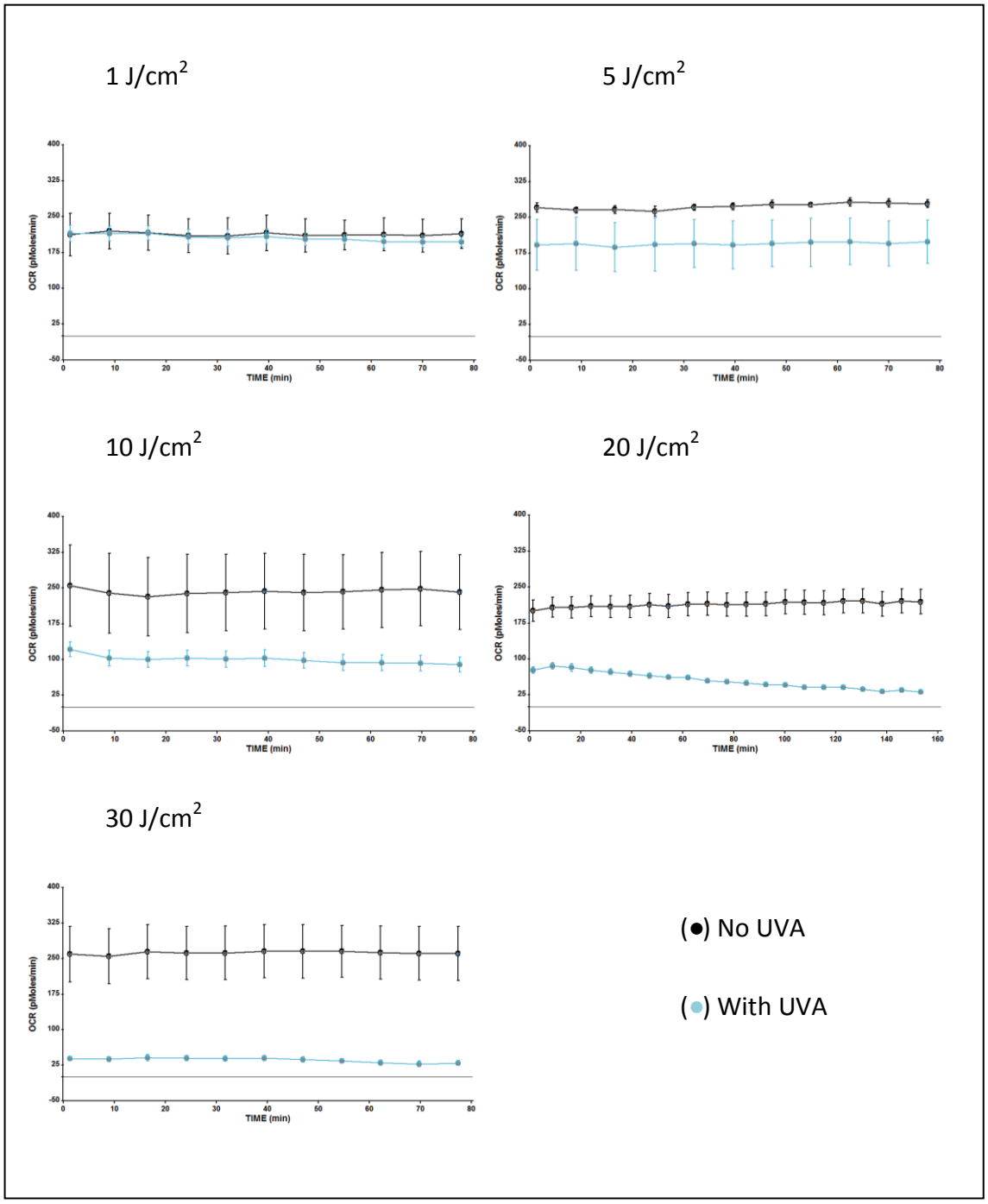

Figure 5.8: Seahorse Traces Showing Baseline Measurements of OCR in BJ Fibroblasts Following UVA Irradiation. Comparisons were made to an un-irradiated control. Each trace shows an example of an individual experiment; data shows the mean of a minimum of five replicates per experiment ± SEM.

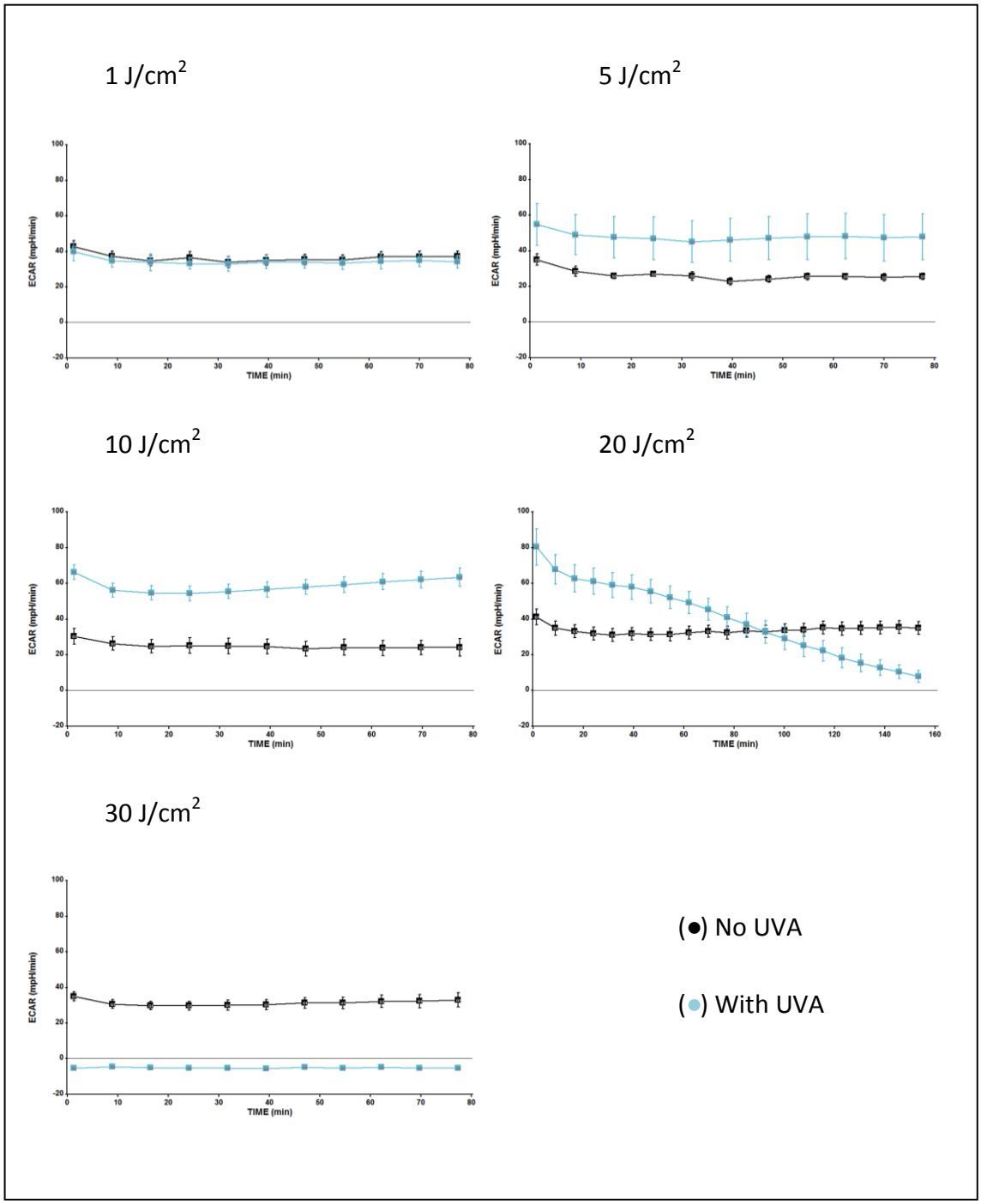

Figure 5.9: Seahorse Traces Showing Baseline Measurements of ECAR in BJ Fibroblasts Following UVA Irradiation. Comparisons were made to an un-irradiated control. Each trace shows an example of an individual experiment; data shows the mean of a minimum of five replicates per experiment ± SEM

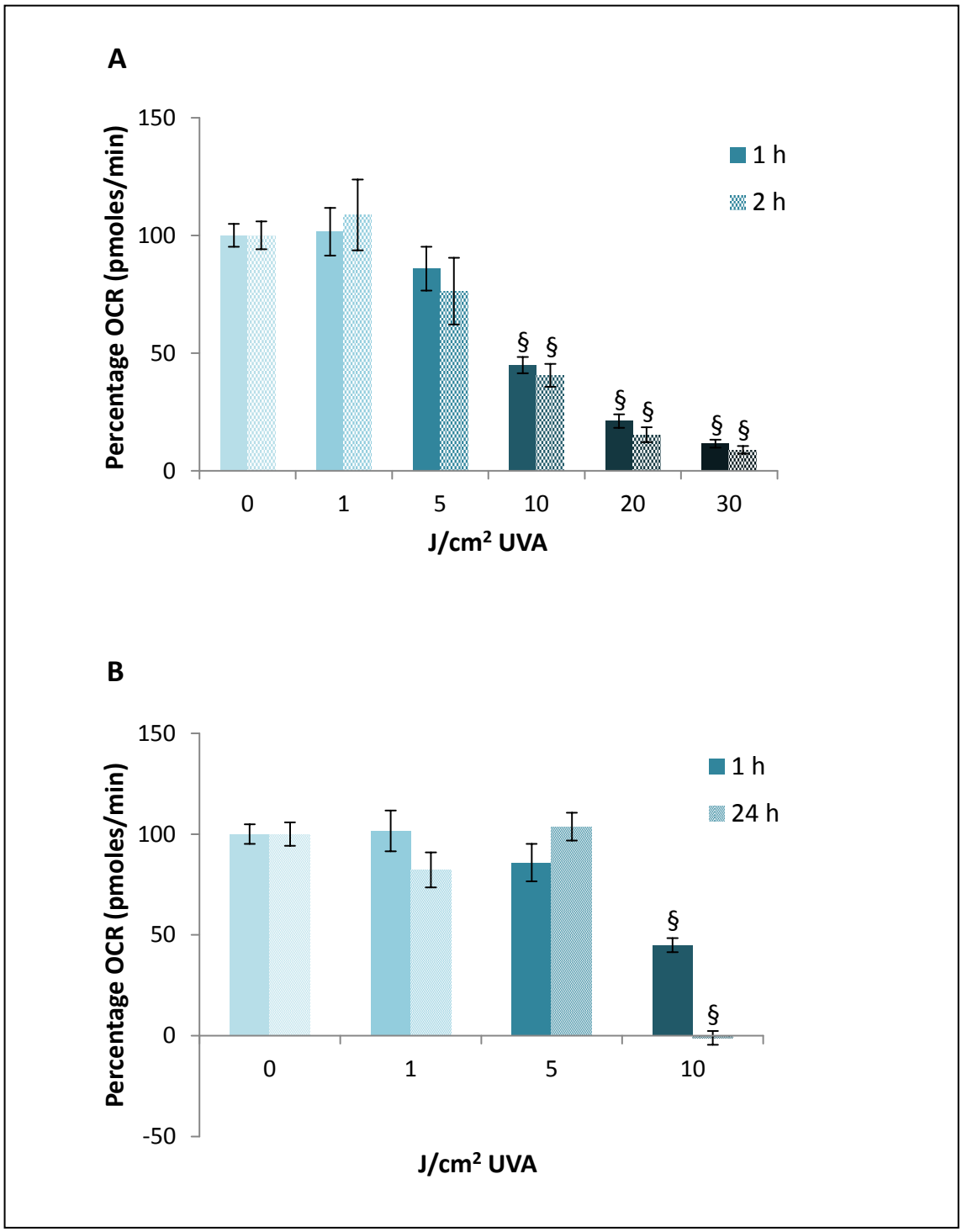

Figure 5.10: Baseline Oxygen Consumption Rates Following UVA Irradiation. BJ fibroblast cells were exposed to increasing doses of UVA and baseline measurements of OCR were taken at 1 h (A+B), 2 h (A) and 24 h (B) following irradiation using the 24-well Seahorse XF Analyzer. Comparisons were made to an un-irradiated control (mean values n>2 ± SEM, §P<0.001 compared to the control)

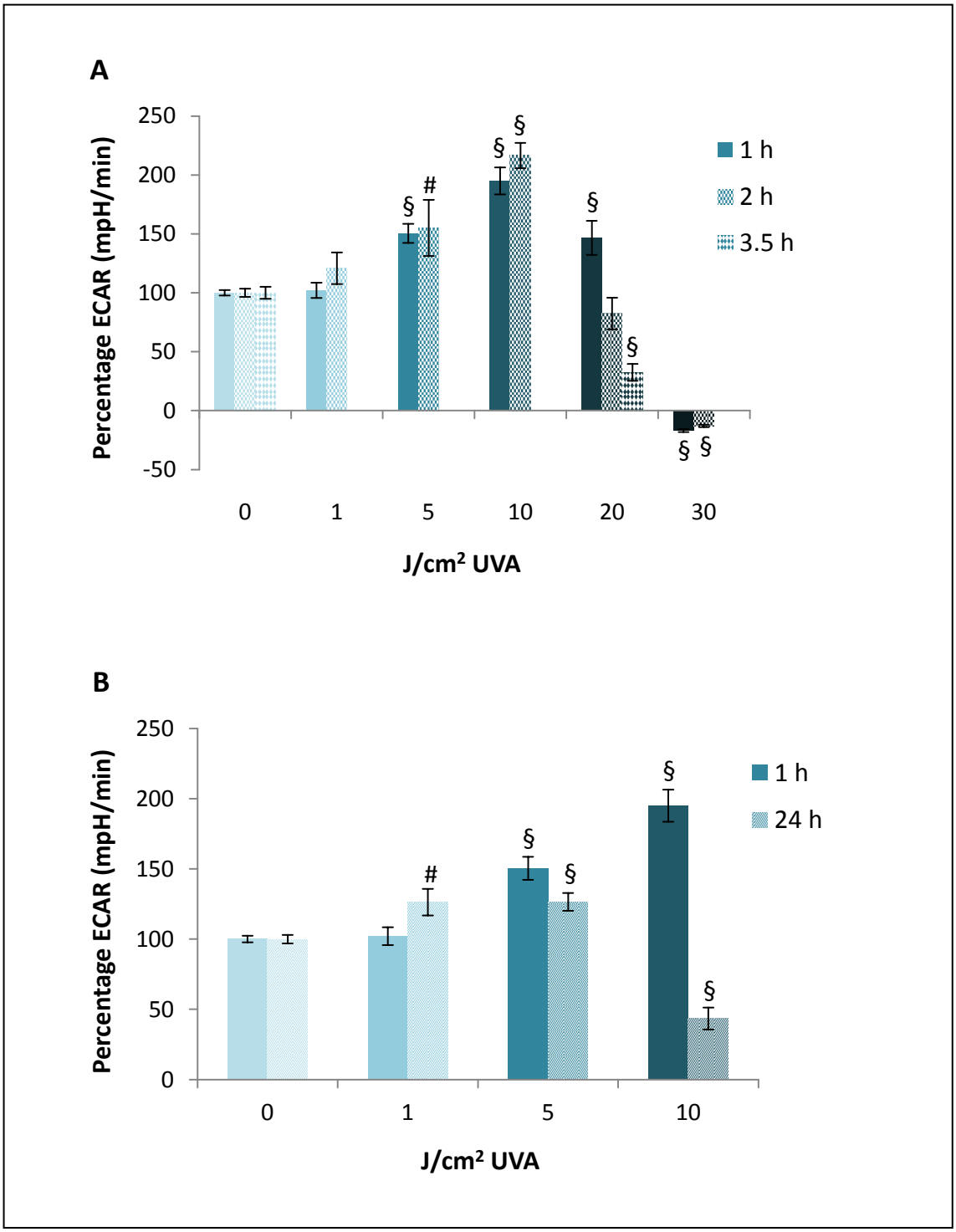

Figure 5.11: Baseline Extracellular Acidification Rates Following UVA Irradiation. BJ fibroblast cells were exposed to increasing doses of UVA and baseline measurements of ECAR were taken at 1, 2 and 3.5 h (A); 1 and 24 h (B) following irradiation using the 24-well Seahorse XF Analyzer. Comparisons were made to an un-irradiated control (mean values n>2 ± SEM, #P<0.01, §P<0.001 compared to the control).

5.3.4 Differences in the HEKn Baseline OCR and ECAR in Response to UVB Exposure

HEKn cells were subjected to doses of 7.5, 15 and 30 mJ/cm^2 UVB. Baseline measurements for OCR and ECAR were determined in real-time using the Seahorse XF Analyzer. The experimental time course (as described in section 5.3.3) was ran over approximately 2 h and therefore the analysis of this data encompassed measurements taken from the beginning of the experiment (1 h – because the cells required a 1 h incubation period prior to analysis, see section 5.2.5) and the end (2 h). A further experiment explored the effect that the same doses of UVB had on baseline respiration rates 24 h following irradiation and compared this with that seen in the 1 h trace. The data analysis for the effect on OCR can be found in Figure 5.12; this figure illustrates a decrease of OCR in HEKn when exposed to doses of 15 and 30 mJ/cm^2 at 1 h which had further decreased at 2 h, however, these decreases were not found to be statistically significant. Interestingly at 24 h exposure to 7.5, 15 and 30 mJ/cm^2 UVB had caused dose-dependent and statistically significant decreases of baseline OCR in HEKn (47 % $P<0.01$, 51 % $P<0.01$ and 73 % $P<0.001$, respectively). Figure 5.13 shows the effect that UVB exposure had on baseline ECAR in HEKn, which was very little at 1 h and 2 h. No change was seen with the high dose of 30 mJ/cm^2 UVB. As seen previously with baseline OCR, a decrease of baseline ECAR in HEKn exposed to all doses of UVB was seen at 24 h. This decrease was only statistically significant when the cells were exposed to the highest dose of 30 mJ/cm^2 UVB, where ECAR had decreased by 62 % of the control ($P<0.001$).

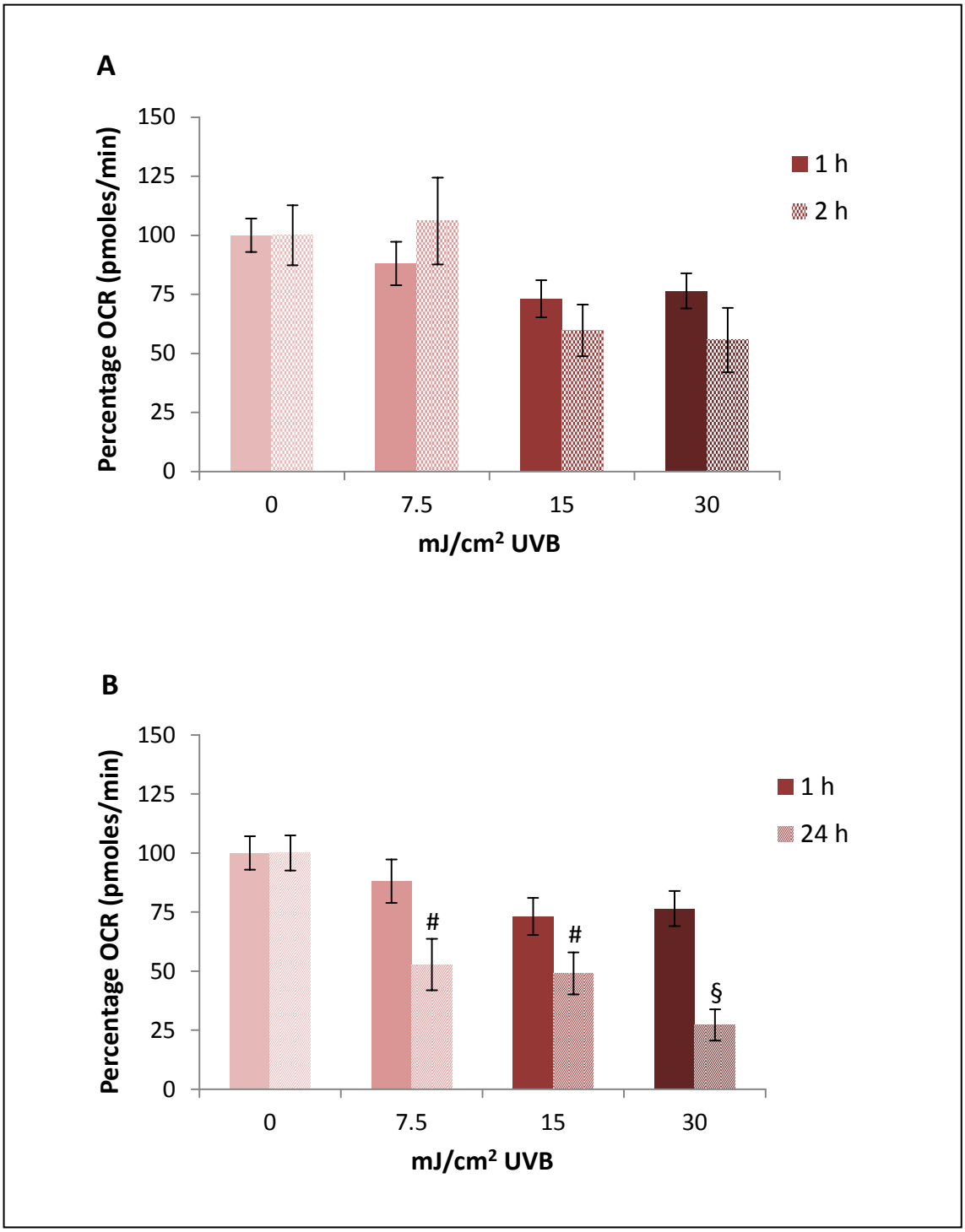

Figure 5.12: Baseline Oxygen Consumption Rates Following UVB Irradiation. HEKn cells were exposed to increasing doses of UVB and baseline measurements of OCR were taken at 1 h and 2 h (A) and 1 h and 24 h (B) following irradiation using the 24-well Seahorse XF Analyzer. Comparisons were made to an un-irradiated control (mean values n>2 ± SEM, #P<0.01, §P<0.001 compared to the control).

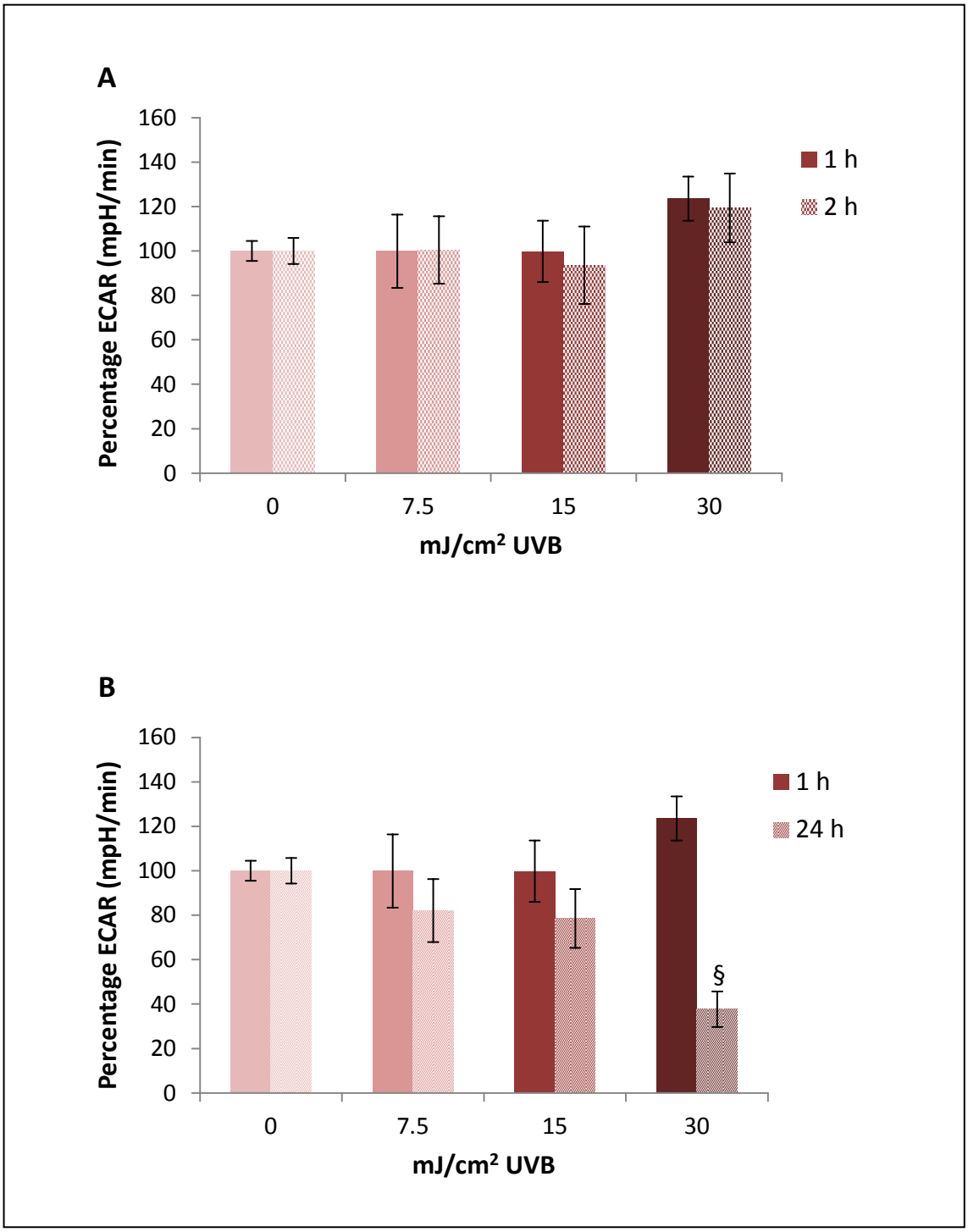

Figure 5.13: Baseline Extracellular Acidification Rates Following UVB Irradiation. HEKn cells were exposed to increasing doses of UVB and baseline measurements of ECAR were taken at 1 h and 2 h (A) and 1 h and 24 h (B) following irradiation using the 24-well Seahorse XF Analyzer. Comparisons were made to an un-irradiated control (mean values n>2 ± SEM, §P<0.001 compared to the control).

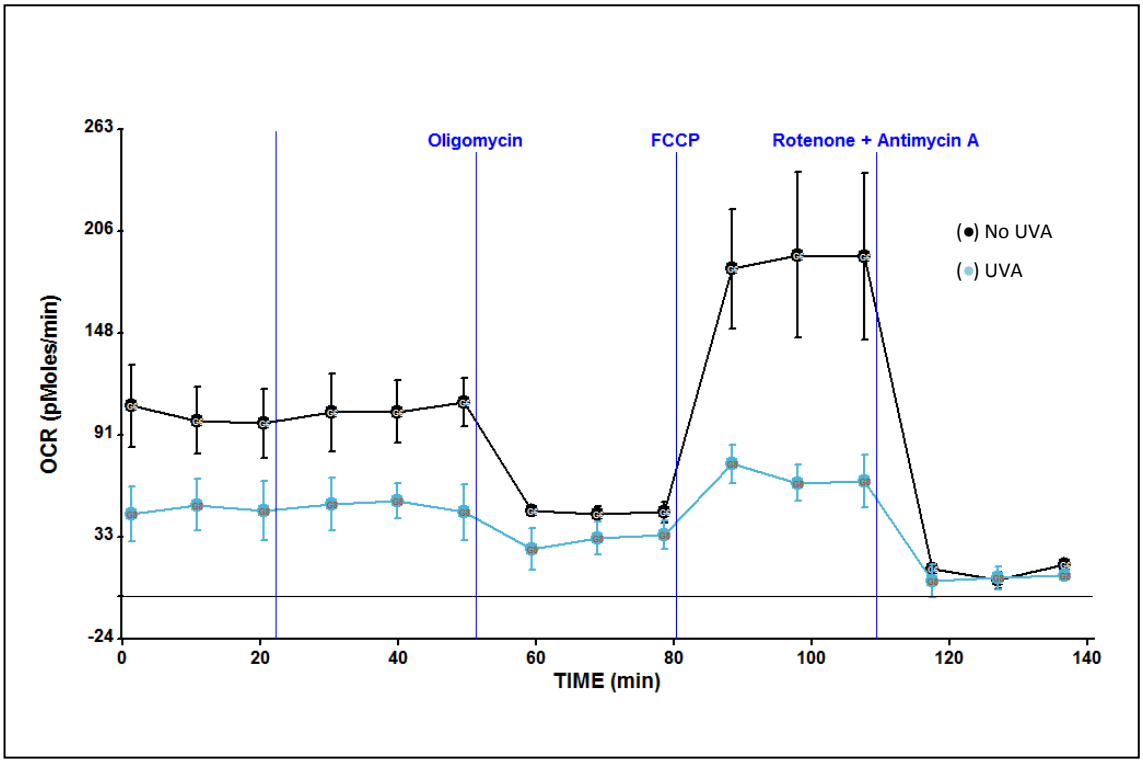

Figure 5.14: A Representative Example of the Respiration Profile of a Cell Altered by Specific Metabolic Modulators; with/without UVR Exposure. This Seahorse trace shows an example of an individual experiment of the real-time measurement of OCR in BJ fibroblasts following a 5 J/cm^2 UVA irradiation compared to an un-irradiated control. OCR was analysed using the 24-well Seahorse XF Analyzer during which specific metabolic modulators were administered at fixed time points in order to determine different parameters of respiratory activity. The compounds used for this were oligomycin (1.3 µM), FCCP (0.5 µM) and finally a combination of rotenone (1.0 µM) and antimycin A (5.0 µM). The data shows the mean of a minimum of five replicates ± SEM.

5.3.5 BJ Fibroblast Cell Respiratory Profile when Exposed to UVA

The experiments in section 5.3.3 determined which doses of UVA caused a "dampening" effect of baseline cellular respiration in BJ fibroblasts without drastically altering it. Following this discovery, these particular doses of UVA were used in experiments exploring the effect UVA exposure had on the respiratory profile of the BJ fibroblast cell. Figure 5.14 is a representative example of one of these particular experiments which incorporates three successive injections of metabolic modulators into the assay; firstly oligomycin, followed by FCCP and finally a combination of rotenone and antimycin A. The administration of these modulators gives measurements of mitochondrial function which encompass basal respiration, proton leak, ATP turnover, respiratory capacity and respiratory reserve (see section 5.1). The trace for the cells not subjected to UVA shows a typical profile of cells exposed to these metabolic modulators which is illustrated in **Figure 5.3**. It also shows the effect

that 5 mJ/cm^2 UVA had on this profile in BJ fibroblast cells, which as wells as a decrease in basal respiration there is also a clear decrease in the respiratory capacity of the BJ fibroblast cells. The analysis of the individual measurements of mitochondrial function is shown in Figure 5.15. For this experiment BJ fibroblast cells were exposed to 1, 5 and 10 J/cm^2 UVA and were then assessed for mitochondrial function 1 h and 24 h after irradiation. At 1 h 10 J/cm^2 caused a significant decrease ($P<0.001$) in all the measurements of mitochondrial function in BJ fibroblast cells with the exception of proton leak where no difference was seen when compared with the control. 1 and 5 J/cm^2 UVA had little effect on basal respiration, proton leak and therefore ATP turnover in BJ fibroblasts when compared to the control. These doses of UVA did however cause a statistically significant decrease in respiratory capacity and respiratory reserve of the cells $P<0.01$ and $P<0.001$ for 1 and 5 J/cm^2, respectively. By 24 h 1 and 5 J/cm^2 had no effect on the mitochondrial function of the BJ fibroblasts. 10 J/cm^2 on the other hand had caused complete inhibition of any mitochondrial function (to below detectable levels) which was found to be statistically significant for all measurements with the exception of the reserve capacity of the BJ fibroblast cells.

5.3.6 HEKn Cells Respiratory Profile when Exposed to UVB

The analysis of the individual measurements of mitochondrial function in HEKn cells exposed to UVB is shown in Figure 5.16. For this experiment the cells were exposed to 7.5, 15 and 30 mJ/cm^2 UVB and were then assessed for mitochondrial function 1 h and 24 h after irradiation. At 1 h, when the cells were exposed to 7.5 and 15 mJ/cm^2, no statistical difference was seen at any of the measurements of mitochondrial function although decreases were seen, with the exception of proton leak. When the cells were exposed to 30 mJ/cm^2 again no difference was seen when determining proton leak but decreases in function were seen at all other parameters measured which was statistically significant for ATP turnover, respiratory capacity and respiratory reserve ($P<0.001$, $P<0.05$ and $P<0.001$, respectively). When the cells were assessed at 24 h, all measurements for mitochondrial function had been decreased, on the most part dose-dependently, as well as statistically significantly when compared with the control (with the exception of reserve capacity when the cells were exposed to the lower dose of 7.5 mJ/cm^2).

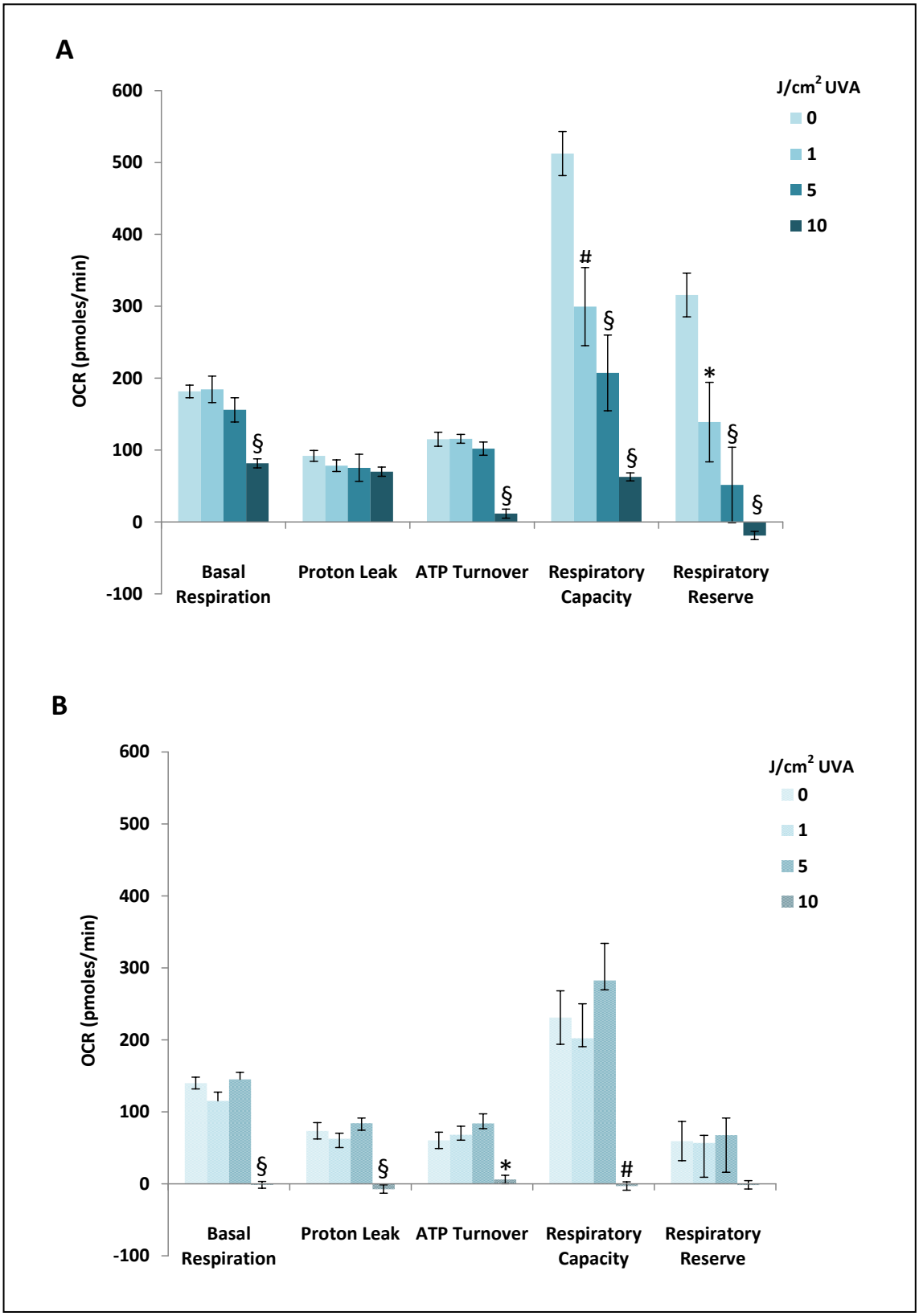

Figure 5.15: Mitochondrial Function in BJ Fibroblast Cells Exposed to UVA. BJ fibroblast cells were exposed to increasing doses of UVA and then assessed for mitochondrial function using the 24-well Seahorse XF Analyzer 1 h (A) and 24 h (B) following irradiation. Comparisons were made to an un-irradiated control. Mitochondrial function comprises basal respiration, ATP turnover, proton leak, respiratory capacity and respiratory reserve. These were determined using the following specific metabolic modulators, administered at fixed time points to alter OCR, oligomycin (1.3 µM), FCCP (0.5 µM) and a combination of rotenone (1.0 µM) and antimycin A (5.0 µM) (mean values n>2 ± SEM, *P<0.05, #P<0.01, §P<0.001 compared to the control).

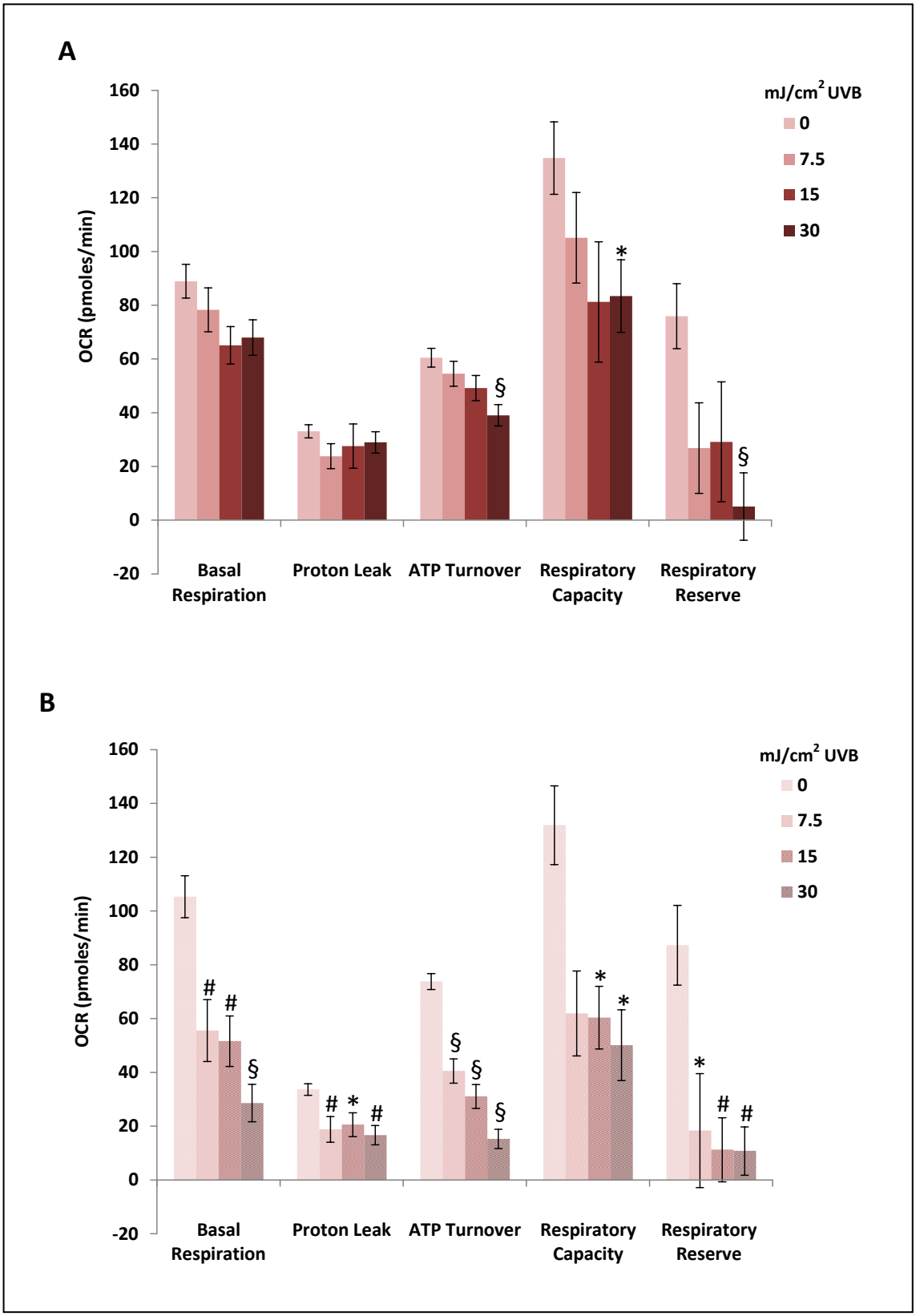

Figure 5.16: Mitochondrial Function in HEKn Cells Exposed to UVB. HEKn cells were exposed to increasing doses of UVB and then assessed for mitochondrial function using the 24-well Seahorse XF Analyzer 1 h (A) and 24 h (B) following irradiation. Comparisons were made to an un-irradiated control. Mitochondrial function comprises basal respiration, ATP turnover, proton leak, respiratory capacity and respiratory reserve. These were determined using the following specific metabolic modulators, administered at fixed time points to alter OCR, oligomycin (1.3 µM), FCCP (0.5 µM) and a combination of rotenone (1.0 µM) and antimycin A (5.0 µM) (mean values n>2 ± SEM, *P<0.05, #P<0.01, §P<0.001 compared to the control).

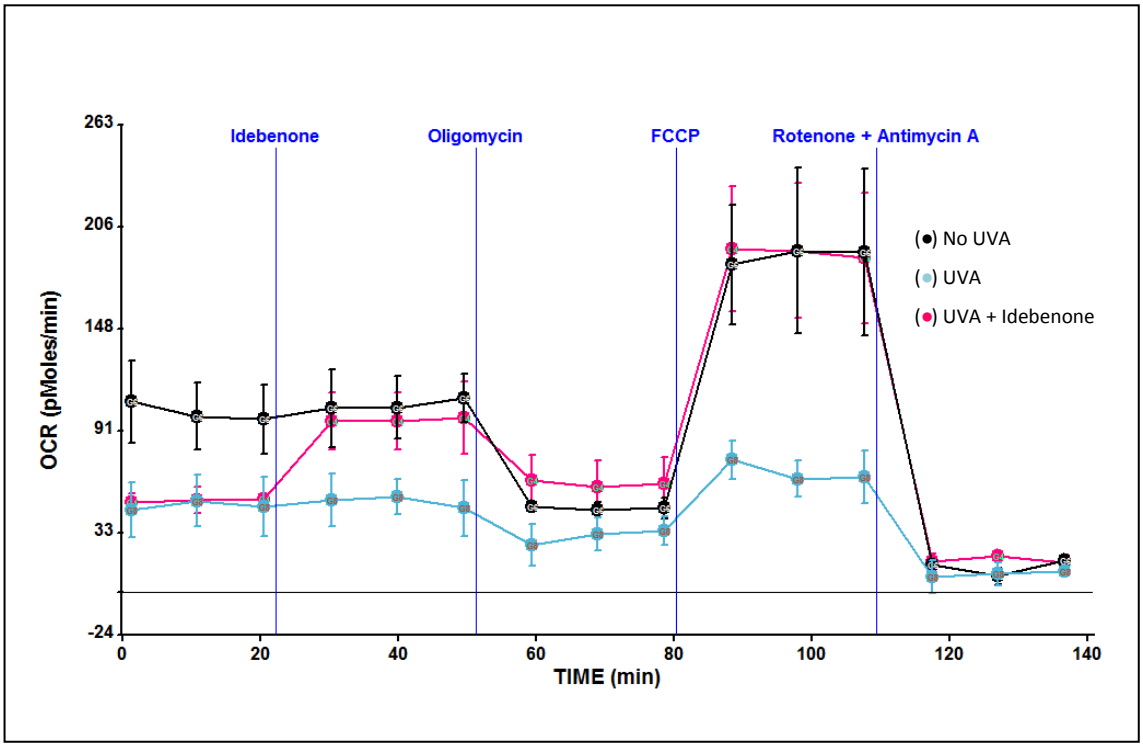

Figure 5.17: A Representative Example of the Effect of Idebenone on the Respiration Profile of a Cell Altered by Specific Metabolic Modulators; with/without UVR Exposure. This Seahorse trace shows an example of an individual experiment of the real-time measurement of OCR in BJ fibroblasts following a 5 J/cm^2 UVA irradiation compared to an un-irradiated control. OCR was analysed using the 24-well Seahorse XF Analyzer and during the analysis 25 µM idebenone was administered to the required cells. Following this, specific metabolic modulators were then administered at fixed time points in order to determine different parameters of respiratory activity. The compounds used for this were oligomycin (1.3 µM), FCCP (0.5 µM) and finally a combination of rotenone (1.0 µM) and antimycin A (5.0 µM). The data shows the mean of a minimum of five replicates ± SEM.

5.3.7 The Effect Idebenone had on the Respiratory Profile of UVA Exposed BJ Fibroblast Cells

Figure 5.17 is a representative example of an individual experiment interested in finding out the effect Idebenone had on BJ fibroblasts which had been exposed to UVA. The trace shows the respiratory profile used to give measures for mitochondrial function (as described in section 5.3.5) of control cells which were left un-irradiated and cells which had been exposed to 5 J/cm^2 UVA irradiation as well as cells which had been exposed to 5 J/cm^2 UVA followed by a treatment of 25 µM idebenone. Again the trace for the cells not subjected to UVA shows a typical profile of cells exposed to these metabolic modulators which is illustrated in Figure 5.3. It also shows that 5 mJ/cm^2 UVA caused a clear reduction in basal respiration as well as respiratory capacity in BJ fibroblast cells. Following treatment of 25 µM idebenone the effect that 5 mJ/cm^2 UVA seemed to have on the cells had reduced. When 25 µM idebenone was

added to un-irradiated cells an increase in basal respiration was also seen compared to the control; data not shown. Figure 5.18 shows the effect that 25 µM idebenone had on basal respiration (both OCR and ECAR) of un-irradiated cells and those exposed to 1 and 5 J/cm^2 UVA. From this figure it is clear that idebenone could increase baseline OCR to above control levels with or without UVA exposure and this increase was found to be statistically significant for the majority of cases. This trend is also true for baseline ECAR; where statistically significant increases initiated in cells following 1 J/cm^2 UVA (24 h) and 5 J/cm^2 UVA (1 h and 24 h) were further increased. The effect that 25 µM idebenone had on the mitochondrial function parameters of control and UVA exposed (5 J/cm^2) cells is displayed in Figure 5.19. Idebenone (in un-irradiated cells) caused a statistically significant increase in basal respiration ($P<0.001$) and proton leak ($P<0.05$) in comparison to the control cells. However in 5 J/cm^2 UVA irradiated cells, 25 µM idebenone ensured that no difference was seen with these cells when compared to the control at all measured parameters. This was particularly noticeable when measuring respiratory capacity where 5 J/cm^2 UVA exposed cells without the treatment of idebenone had caused a statistically significant decrease of approximately 60 % ($P<0.001$) of that of the control cells.

5.3.8 The Effect Idebenone had on the Respiratory Profile of UVB Exposed HEKn Cells

HEKn cells were either left un-irradiated or exposed to 30 mJ/cm^2 UVB; these cells were then either left un-treated or treated with 25 µM idebenone. Figure 5.20 is the data showing the basal respiration (both OCR and ECAR) of these different treatments. From this figure you can see that a treatment of 25 µM idebenone in un-irradiated cells caused a statistically significant increase of over 100 % ($P<0.001$) in baseline OCR levels in HEKn cells of that of the control. An increase in baseline OCR was also seen with 30 mJ/cm^2 UVB exposed cells treated with 25 µM idebenone when compared with the control, although this difference was not found to be statistically significant. Idebenone had a similar effect on the baseline measurements of ECAR in HEKn cells, where a statistically significant increase was seen in cells treated with idebenone independent of the UVB exposure variables. Figure 5.21 demonstrates the effect that 25 µM idebenone had on the mitochondrial function parameters of control and UVB

exposed (30 J/cm^2) cells. Idebenone (in un-irradiated cells) caused a statistically significant increase in basal respiration ($P<0.001$), proton leak ($P<0.001$) and respiratory capacity ($P<0.05$) in comparison to the control cells. The statistically significant decrease of ATP turnover and respiratory capacity, created with a 30 mJ/cm^2 UVB dose, was reduced by the addition of 25 µM idebenone to non-statistically different levels when compared to the control. This was not the case however for the measurement of respiratory reserve where levels were still statistically significantly reduced. Idebenone also caused similar increases of proton leak in 30 mJ/cm^2 UVB exposed cells from that seen in un-irradiated cells.

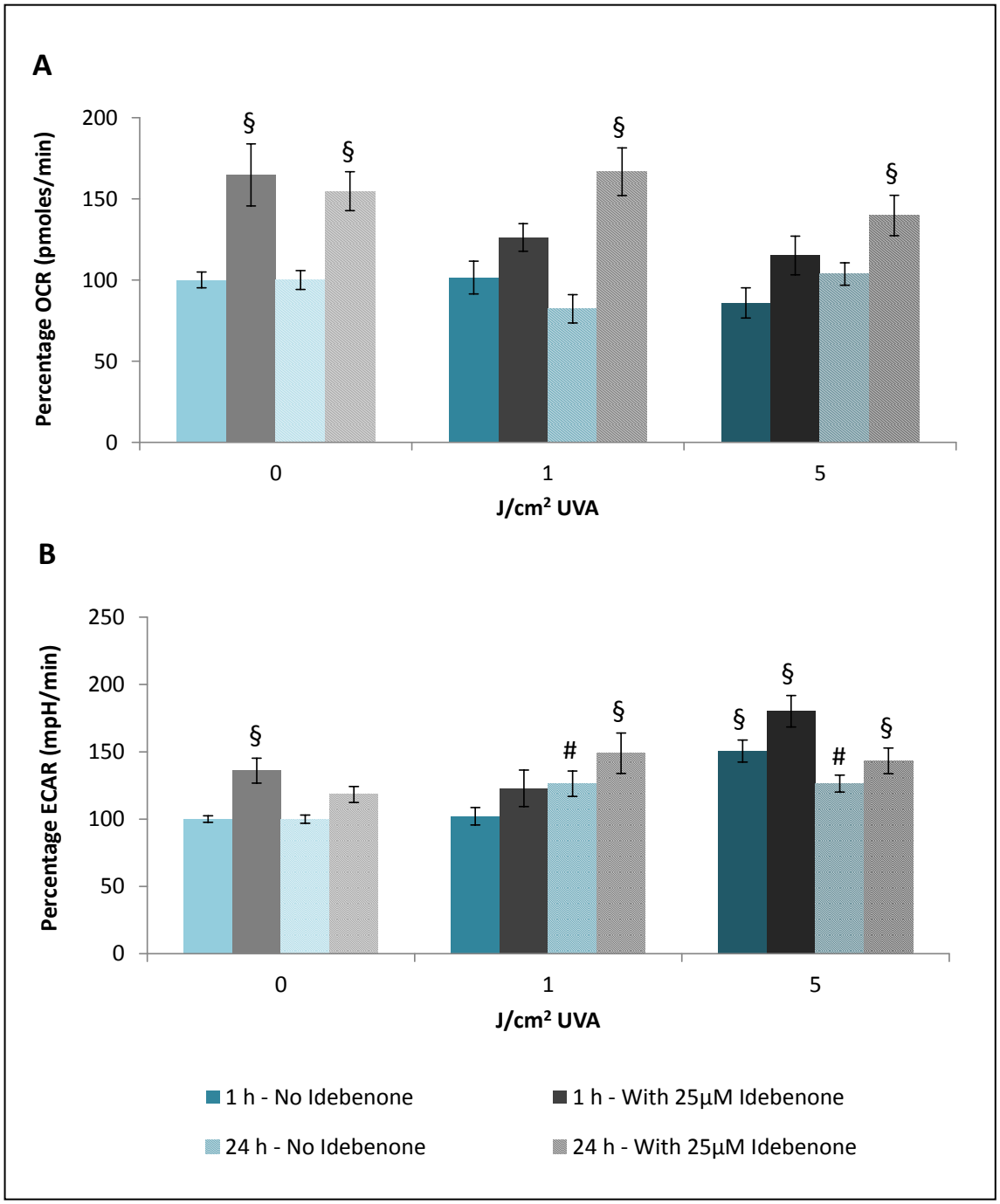

Figure 5.18: The Effect of Idebenone on Baseline Cellular Respiration of BJ Fibroblasts Following UVA Irradiation. BJ fibroblast cells were exposed to increasing doses of UVA and baseline measurements of OCR (A) and ECAR (B) were taken at 1 h and 24 h following irradiation using the 24-well Seahorse XF Analyzer. During the analysis 25 µM idebenone was administered to the required cells and comparisons were made to an un-irradiated control. (mean values n>3 ± SEM, #P<0.01, §P<0.001 compared to the control).

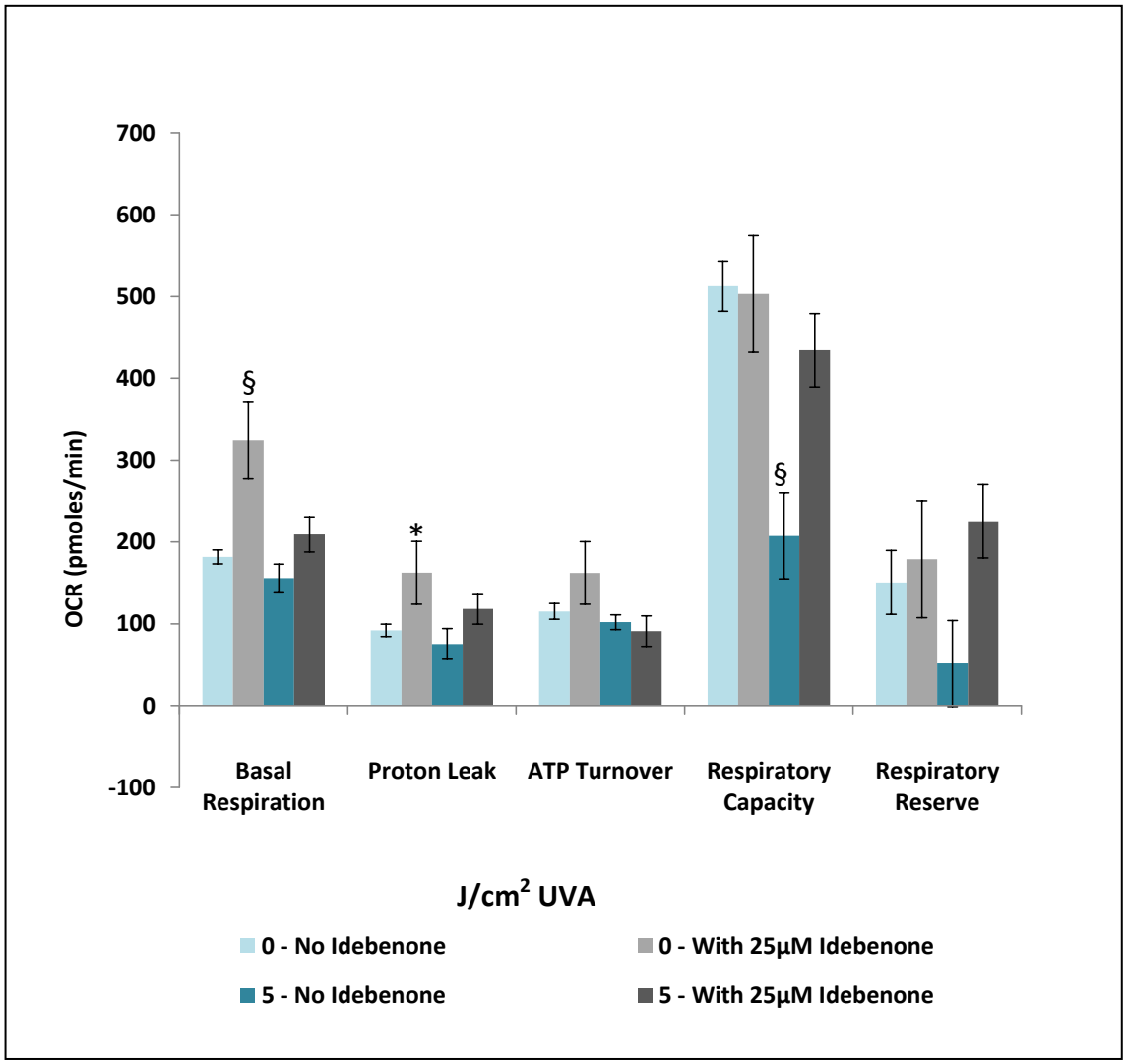

Figure 5.19: The Effect Idebenone had on the Mitochondrial Function of BJ Fibroblast Cells Exposed to UVA. BJ fibroblast cells were exposed to 5 J/cm^2 UVA and then assessed for mitochondrial function using the 24-well Seahorse XF Analyzer 1 h following irradiation. Comparisons were made to an un-irradiated control. Prior to mitochondrial function analysis 25 µM idebenone was administered to the required cells Mitochondrial function comprises basal respiration, ATP turnover, proton leak, respiratory capacity and respiratory reserve. These were determined using the following specific metabolic modulators, administered at fixed time points to alter OCR, oligomycin (1.3 µM), FCCP (0.5 µM) and a combination of rotenone (1.0 µM) antimycin A (5.0 µM) (mean values n=3 ± SEM, *P<0.05, #P<0.01, §P<0.001 compared to the control).

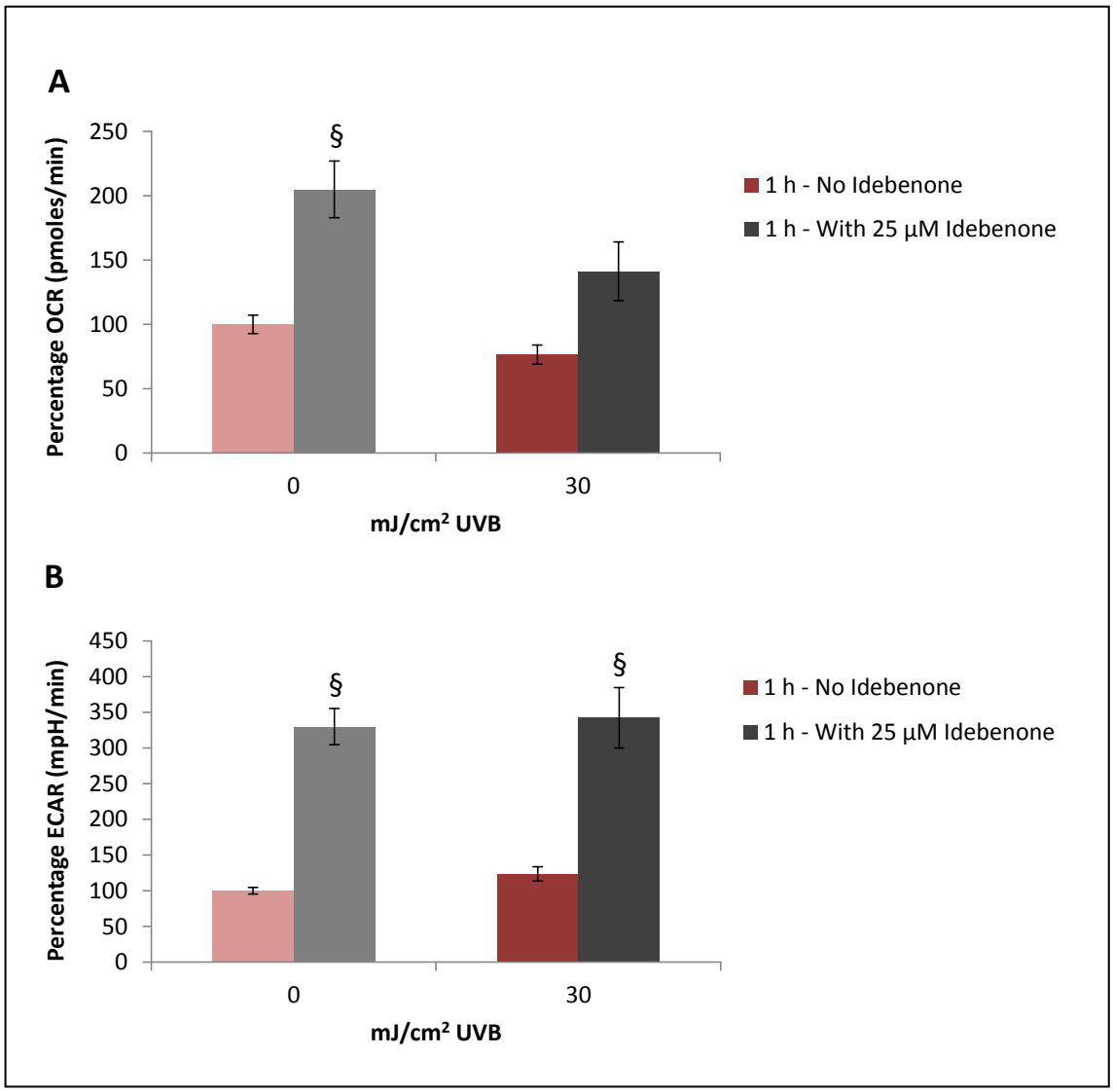

Figure 5.20: The Effect of Idebenone on Baseline Cellular Respiration of HEKn Following UVB Irradiation. HEKn cells were exposed to increasing doses of UVB and baseline measurements of OCR (A) and ECAR (B) were taken at 1 h and 24 h following irradiation using the 24-well Seahorse XF Analyzer. During the analysis 25 µM idebenone was administered to the required cells and comparisons were made to an un-irradiated control (mean values n>2 ± SEM, §P<0.001 compared to the control).

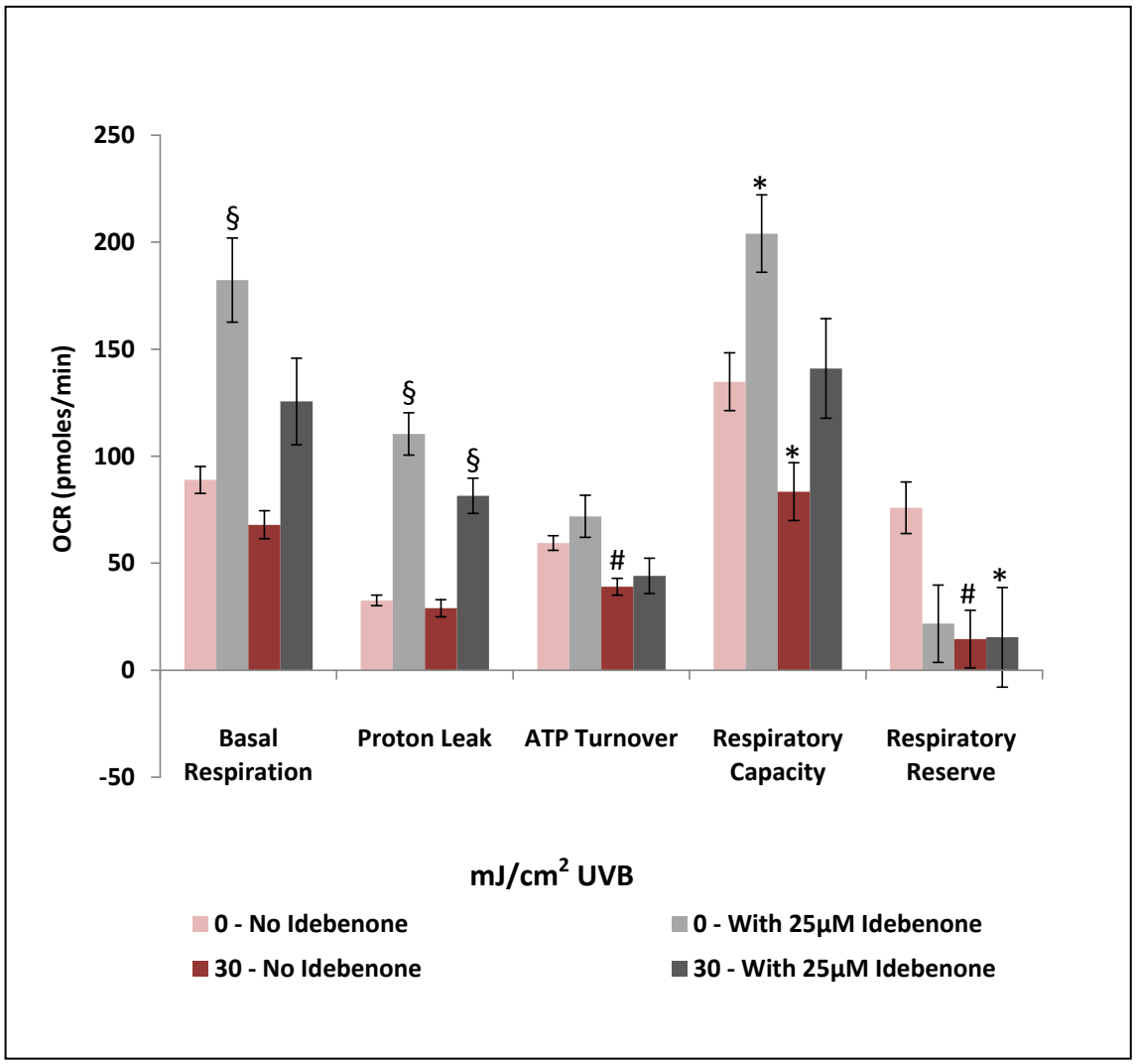

Figure 5.21: The Effect Idebenone had on the Mitochondrial Function of HEKn Cells Exposed to UVB. HEKn cells were exposed to 30 mJ/cm^2 UVB and then assessed for mitochondrial function using the 24-well Seahorse XF Analyzer 1 h following irradiation. Comparisons were made to an un-irradiated control. Prior to mitochondrial function analysis 25 µM idebenone was administered to the required cells Mitochondrial function comprises basal respiration, ATP turnover, proton leak, respiratory capacity and respiratory reserve. These were determined using the following specific metabolic modulators, administered at fixed time points to alter OCR, oligomycin (1.3 µM), FCCP (0.5 µM) and a combination of rotenone (1.0 µM) antimycin A (5.0 µM) (mean values n>2 ± SEM, *P<0.05, #P<0.01, §P<0.001 compared to the control.

5.4 Discussion

5.4.1 Viability of Cells Following UVR Exposure

When using new cells, reagents and techniques it is important not to rely on data previously obtained as the slightest difference can cause inaccuracies to occur. With this in mind, the first task of this study was to determine the dosage of either UVA or UVB needed for optimum effect on the respiration in fibroblast and keratinocyte cells, respectively (see section 5.3.1). It was found that up to dose of 50 J/cm^2 UVA had little effect on the viability of BJ fibroblasts, and this conflicted slightly with what was found in Chapter 3, where a decrease in the viability of HDFns exposed to the equivalent UVA was seen following a dose of just 15 J/cm^2. There are various factors which could have caused the differences seen, such as variances between the skin fibroblast cell line types, the slight dissimilarities between the spectra of the UVR source used, as well as differences in the cell viability assay used; all of which confirm the validity for performing this assay. The viability data between the two studies compares when assessing the effect of 10 J/cm^2 UVA, where minor non-statistically significant decreases in viability were seen. This finding related well to that found in the literature, where no statistical difference of the viability of human dermal fibroblasts following an approximate dose of 10 J/cm^2 UVA up to 24 h using various viability methods (M. J. Petersen *et al.*, 1992; Hoerter *et al.*, 2008). Petersen *et al*., 1992 also found human keratinocytes to be >90 % viable following an irradiation of 100 mJ/cm^2 UVB. This data is in keeping with what was discovered in Chapter 3 as well as that found previously at P&G. The differential effect of UVA on fibroblast viability as well as the viability of the cells 24 h following irradiations must be taken into account when assessing the effect of higher doses of UVA on cellular respiration.

5.4.2 UVA Caused a Dose-Dependent Decrease in OXPHOS of BJ Fibroblasts

It has been theorised that damage to mtDNA (by the exposure to UVR) has more importance in the deficiency of OXPHOS due to the fact that it encodes components of the ETC and thus controls the major metabolic ability of the cell (Nadanaciva *et al.*, 2012). Mitochondrial function has traditionally utilised spectrophotometric analysis to

detect biochemical defects however this tends to require a large number of cells and results obtained from skin cells (fibroblasts) often does not match that gained from muscle biopsy-derived material. The Seahorse XF Analyzer has the advantage of having significantly increased sensitivity and requires 100 times fewer cells which is valuable when assessing cells with a lower energy out-put such as skin cells (Invernizzi *et al.*, 2013).

The doses of UVA used to affect cellular respiration were similar to those which created damage within mtDNA of HDFn cells (Chapter 4), and although the decrease seen in viability of BJ fibroblasts exposed to 50 J/cm^2 UVA was not found to be statistically significant, cellular respiration was initially assessed only up to 30 J/cm^2 UVA. At this dose, drastic statistically significant decreases in both OCR and ECAR were apparent. For the 24 h assessment of the effect of UVA on cellular respiration a maximum dose of 10 J/cm^2 was used, and at this time period following irradiation, 10 J/cm^2 UVA was significant enough to ensure inhibition of cellular respiration which was determined by the undetectable levels of OCR seen. Due to this discovery the higher doses of 20 and 30 J/cm^2 were no longer considered. The main outcome from this data was that lower doses of UVA (e.g. 5 and 10 J/cm^2) primarily caused decreases in the amount of oxygen the cell consumed which seemed to be compensated for by an increase in the levels of ECAR (see section 5.3.3). This suggests that the cell has increased its rate of glycolysis to above baseline measurements to maintain the correct production of ATP (which had been reduced as shown by reduced OCR) for the cells particular energy requirements. This also suggests that lower doses of UVA cause detriment to the ETC prior to damage to the glycolysis process which can be explained by the production of ROS within a close proximity to the ETC. As the dose of UVA increases, glycolysis then becomes inhibited as well.

5.4.3 UVB Caused a Dose-Dependent Decrease in OXPHOS of HEKn

The doses of UVB used to cause an effect on cellular respiration were considerably lower than those needed to create damage within the mtDNA of both HaCaT and Primary Keratinocytes (Chapter 4). When the keratinocytes were exposed to the increasing doses of UVB early minimal decreases in oxygen consumption were apparent, although they were not found to be significant. Nevertheless 24 h following

irradiation statistically significant and dose-dependent decreases were visible. With UVB irradiation no compensatory increase with ECAR was seen, conversely, similar to OCR there was a dose-dependent decrease (see section 5.3.4). This effect on respiration can be linked with viability which was also found to be decreased (Figure **5.6**). It is difficult to make divergences either between cell or UVR type due to the fact that different cells were irradiated with a different source and additionally were cultured differently (i.e. different media and different seeding amount). However this observation supports the notion that UVA acts indirectly by production of ROS whereas UVB acts more directly within the cell. Conversely, this could be due to differences in the particular cells glycolytic capabilities, i.e. skin fibroblasts can increase glycolysis in response to mitochondria respiration dysfunction more readily than keratinocytes. This is because if a cell can improve its glycolytic capabilities, considerably, in response to mitochondrial insults (such as UVR) then they are more proficient in responding to cellular ATP demands which increases their likelihood of being able to tolerate such adversities on the mitochondria. However if the cell cannot increase glycolysis when mitochondria respiration is compromised then this means that the cell is unable to keep up with ATP requirements and are therefore more susceptible to insults in the mitochondria (Nadanaciva *et al.*, 2012). The differences seen being due to a difference between the cells is a possible observation because Djavaheri-Mergny *et al*., 2001 found that increase in exposure of UVA of up to 18 J/cm^2 caused a dose-dependent decrease in oxygen consumption in NCTC 2544 keratinocytes and MRC5 human fibroblast cells. However they found that this effect was more pronounced in the keratinocytes where oxygen consumption was 56 % of that of the control, without effecting membrane potential. These researchers also found ATP levels to decrease in the keratinocytes with these doses which would relate to an inability to increase glycolysis in a response to diminished production via the ETC (Djavaheri-Mergny *et al.*, 2001). To analyse these questions more accurately further experiments interested in differences in the UVR or cell type would assess the effect using the same UVR source upon the same cell type, under the same conditions. Had the time restraints of this study not been so severe this question would have been addressed.

5.4.4 UVA and UVB Caused Instability in a Cells Ability to Deal with Stress

During further analysis, 24 h following 10 J/cm^2 UVA saw inhibition of OXPHOS which was further supported by the statistically significant undetectable levels of OCR seen at all parameters of mitochondrial function measured. The reduction in oxygen consumption induced by 10 J/cm^2 UVA immediately can be attributed completely to a reduction in ATP turnover which is determined by no difference in the levels of proton leak seen when compared with the control. At 24 h doses of 1 and 5 J/cm^2 were shown not to induce any change in mitochondrial function. When these doses were assessed immediately however (akin with 10 J/cm^2) statistically significant and dose-dependent decreases in the maximum respiratory capacity of the cells were seen and therefore similar decreases of the respiratory reserve capacity of the cells were also seen (see section 5.3.5). This reduction in maximal respiratory capacity may lead to an energetic crisis for the cells (Invernizzi *et al.*, 2013), and this finding shows that UVA not only suppresses the basal levels of mitochondrial respiration but also the ability of the fibroblasts to up-regulate mitochondrial respiration in response to agents that uncouple the mitochondrial proton gradient from ATP production, such as FCCP. This means cells irradiated with UVA will be more susceptible in stressful situations.

When the effect UVB had on mitochondrial function in HEKn was assessed, it was clear that the non-significant decrease in basal respiration seen, when the cells were irradiated with 30 mJ/cm^2 UVB, was due to a decrease in ATP turnover, and not due to any differences in proton leak. Further to this (as seen with UVA irradiation of BJ fibroblasts) a decrease in respiratory capacity, and therefore respiratory reserve, was also apparent which again showed that 30 mJ/cm^2 UVB reduced the keratinocytes ability to up-regulate OXPHOS in response to uncoupling agents. 24 h following irradiations all doses caused a decrease in basal respiration (7.5, 15 and 30 mJ/cm^2 UVB). This was also true for all the parameters mitochondrial function measured showing that OXPHOS had been severely impaired with all the doses of UVB assessed by this time-point (see section 5.3.6). Although, as mentioned earlier, no clear comparisons can be made between the cell or UVR type, this suggests that UVA and UVB could have differential effects upon the ETC. It seems minor immediate

detriments of the ETC created by UVA could be recovered, whereas similar immediate detriments created by UVB lead to a more devastating effect for the cell. Although the different types of UVR both caused instability in cell types of which they were used to irradiate.

5.4.5 Idebenone Caused an Increase in OXPHOS due to an Increase in Proton Leak Rather that ATP Production

Idebenone encompasses a quinone structure which allows it to mediate the transfer of electron through the ETC as well be an effective antioxidant via its redox abilities (Wempe *et al.*, 2009; Montenegro *et al.*, 2012). It therefore would understandably have a substantial effect on the mitochondrial function of the cell. That was indeed the case; as addition of 25 µM idebenone caused an increase (not always statistically significant) in baseline respiration (OCR and ECAR) of both the fibroblasts and the keratinocytes with and without the exposure to UVA and UVB, respectively. This demonstrates an ability, not only to encourage mitochondrial respiration but also glycolysis. Further analysis by means of oligomycin confirmed that this increase in basal oxygen consumption was due to an increase in proton leak rather than ATP turnover. It also found that idebenone tended to increase the respiratory reserve capacity of the cells, as well as reverse the detrimental effect 5 J/cm^2 UVA and 30 J/cm^2 UVB had on maximum respiratory capacity. This shows that idebenones effect was irrespective of cell type or UVR source used (see sections 5.3.7 and 5.3.8) A large increase in proton leak could suggest severely damaged mitochondria (e.g. uncoupled). Another possibility that could explain a moderate change in proton leak is a change in the cells proton leakiness or even differences in membrane potential caused by altered substrate oxidation. This was tested by the addition of FCCP which decreased the potential and caused a change in maximum respiration rate (Brand and Nicholls, 2011).

This result however supports recent findings which have indicated that idebenone may interfere with the mitochondrial permeability transition pore (MPTP). Induction of MPTP causes an increase in the permeability of mitochondrial membranes leading to depolarisation. Therefore the membrane potential is lost and protons as well as other small molecules are uninhibited in their flow across the outer mitochondrial

membrane. This leads to a consequential decrease in ATP production because the proton gradient is lost (Giorgio *et al.*, 2012). Futhermore, Lim *et al.*,2008 found idebenone, at concentrations of 25 and 50 µM, actually reduced cellular viability in human skin fibroblasts when used as a control for treatment of Friedreich's Ataxia (a progressive disorder of the nervous system leading to disorders in movement and speech) (Lim *et al.*, 2008). However clinical evidence supports the notion that idebenone is safe and well tolerated (Giorgio *et al.*, 2012) and it has been publicised to have a beneficial effect on photo-damaged skin. The reversal effects included a 29 % reduction in fine lines/wrinkles as well as decreases in IL-1b, IL-6, and MMP-1 and an increase in collagen I leading to a stated 33 % improvement in overall global assessment of photo-damaged skin (McDaniel *et al.*, 2005a).

5.4.6 Summary

10 J/cm^2 UVA inhibited cellular respiration of BJ fibroblasts 24 h following irradiation. 5 and 10 J/cm^2 UVA primarily caused decreases in OXPHOS which seemed to be compensated for by an increase in glycolysis possibly in an aim to maintain ATP levels. 24 h following all UVB irradiations of HEKn saw decreases in both OXPHOS and glycolysis. Experimental procedures were too variable to make divergences still differences in the particular cells glycolytic capabilities was discussed, however further experiments are needed to accurately analyse this.

The reduction in oxygen consumption by UVA and UVB was attributed to a reduction in ATP production and not differences in proton leak. This means that UVA and UVB exposure renders cells more susceptible to stressful situations.

An increase in oxygen consumption seen with 25 µM idebenone was likely to be due to an increase in proton leak rather than ATP production.

Chapter 6

Results 4 – UVR-Induced nDNA Damage

Chapter 6 Results 4 – UVR-Induced nDNA Damage

6.1 Introduction

nDNA acts as a chromophore for UVR by directly absorbing photons (mainly UVC and UVB but also UVA at its shorter wavelengths (Ravanat *et al.*, 2001; Tewari *et al.*, 2012)). This leads to wide DNA damage (for more information see Chapter 1), with the most relevant for this chapter being the production of dimeric photoproducts. Such lesions will undergo repair by the nucleotide excision repair (NER) pathway; a mechanism where any damage and alterations in the structure of DNA can be recognised and are then removed as a fragment, and the gap created is filled by use of DNA polymerase (Yokoyama *et al.*, 2013). Mutations related to these lesions are commonly found within the p53 gene of UVR-induced cancer cells (Dayagrosjean *et al.*, 1995). The p53 gene responds to this UVR-induced DNA damage by activating downstream genes which induce cell cycle arrest, thus allowing time for DNA repair by NER. If the damage is too vast and cannot be repaired p53 initiates a cascade of events which ultimately lead to apoptosis (Paz *et al.*, 2008). However, if left unrepaired, these lesions can form related mutations common of skin cancer which are known as "UVB signature" mutations (C→T or CC→TT) (Tewari *et al.*, 2012).

A common method for mutation/polymorphism analysis is the scanning of DNA by denaturing high performance liquid chromatography (DHPLC), which has a reported sensitivity of 96-100 % (Huang *et al.*, 2009). With this method, areas of interest are amplified by PCR and then these products undergo heteroduplexing; this is where they are heated and then cooled to allow homoduplexes and heteroduplexes to form. This sample is then injected into the path of a flow of buffer which contains triethyammonium acetate (TEAA) and acetonitrile (ACN). TEAA in this state forms a positively charged triethylammonium ion (TEA+) which attracts the negatively charged DNA. This produces a hydrophobic entity which is attracted to a hydrophobic column within the system. As this occurs the concentration of ACN is increased which reduces the positive charge thereby releasing the DNA. The less structurally stable heteroduplexes elute off first followed by homoduplexes. They then pass through a

UVR detector which measures absorbance over time. If there is no mutation then the DNA will elute at the same time creating a single peak on the data sheet, if heteroduplexes are present then four peaks will be visible.(Liu *et al.*, 1998).

Dimeric photoproducts are formed by the chemical effect of UVR on DNA where there are two pyrimidines adjacent, see Figure 6.1. CPDs are the most abundant photoproduct and they are the formation of a four-member ring structure created by covalent bonds between the C5 and the C6 of neighbouring bases (Ravanat *et al.*, 2001; Rastogi *et al.*, 2010). The second most abundant is the 6-4 PP. With this, lesion single bonds are created between the C4 and C6 of two carbon rings. Following formation 6-4 PPs are easily converted by further UVB exposure into the related Dewar valence isomers (Ravanat *et al.*, 2001; Ichihashi *et al.*, 2003; Melnikova and Ananthaswamy, 2005). The 6–4 PPs are less prevalent than CPDs, but are more mutagenic by approximately tenfold (Yokoyama *et al.*, 2013). They are also mainly created by UVB with few reports of UVA induction (Tewari *et al.*, 2012). For the detection and quantification of CPDs and 6–4 PPs, a series of monoclonal antibodies have been created by Mori *et al*., 1991. These antibodies include the TDM-2 and the 64M-2 which were shown to be highly specific for CPDs and 6-4 PPs respectively and which have been utilised in this study (Mori *et al.*, 1991).

UVA is not as directly absorbed by DNA as UVB and indeed UVA has a lower phototoxic effect than that of UVB (Ichihashi *et al.*, 2003). However, both UVA and UVB are absorbed by other non-DNA chromophores in the skin, which react with oxygen to and lead to the generation of ROS and consequently oxidative stress. High levels of ROS have the ability to cause various forms of damage by the oxidation of DNA, proteins and lipids. One particular target is the DNA base guanine which gives rise to 8-OHdG, a miscoding lesion leading to G to T transversion (Ichihashi *et al.*, 2003; Paz *et al.*, 2008; Birch-Machin and Swalwell, 2010). Although 8-OHdG is possible by UVB exposure the production is much less than that of photoproducts (Ravanat *et al.*, 2001). Determination of 8-OHdG induction, as a marker of oxidative stress is desirable as it is the most abundant oxidative lesion which is pro-mutagenic. This means it would make a useful biomarker of carcinogenesis as well as for oxidative stress and ageing (Valavanidis *et al.*, 2009).

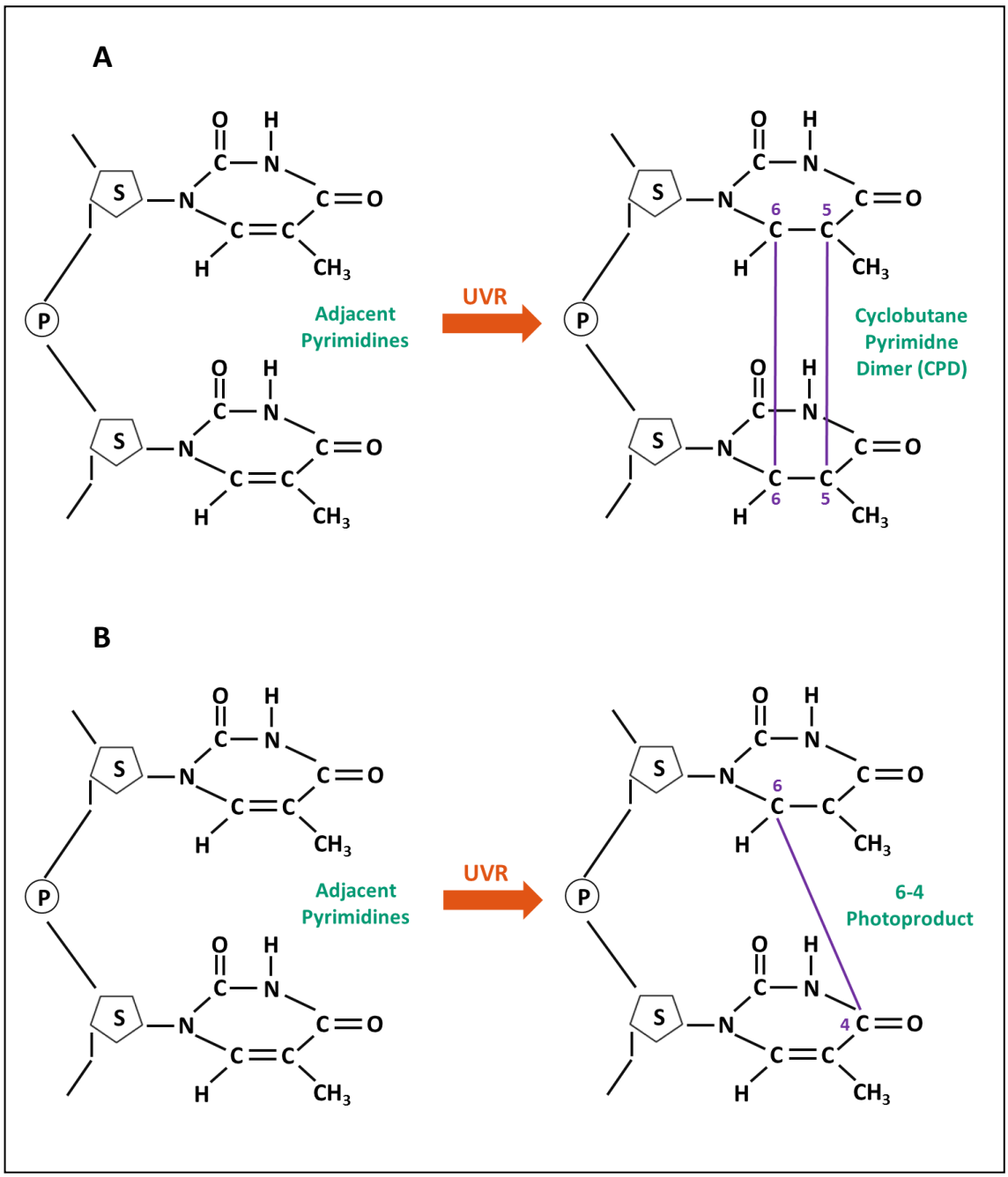

Figure 6.1: Structure of UVR-Induced Photoproducts. This figure illustrates how the two major photoproducts, cyclobutane pyrimidine dimers (CPDs; A) and pyrimidine pyrimidone photoproducts (6-4 photoproducts; B).

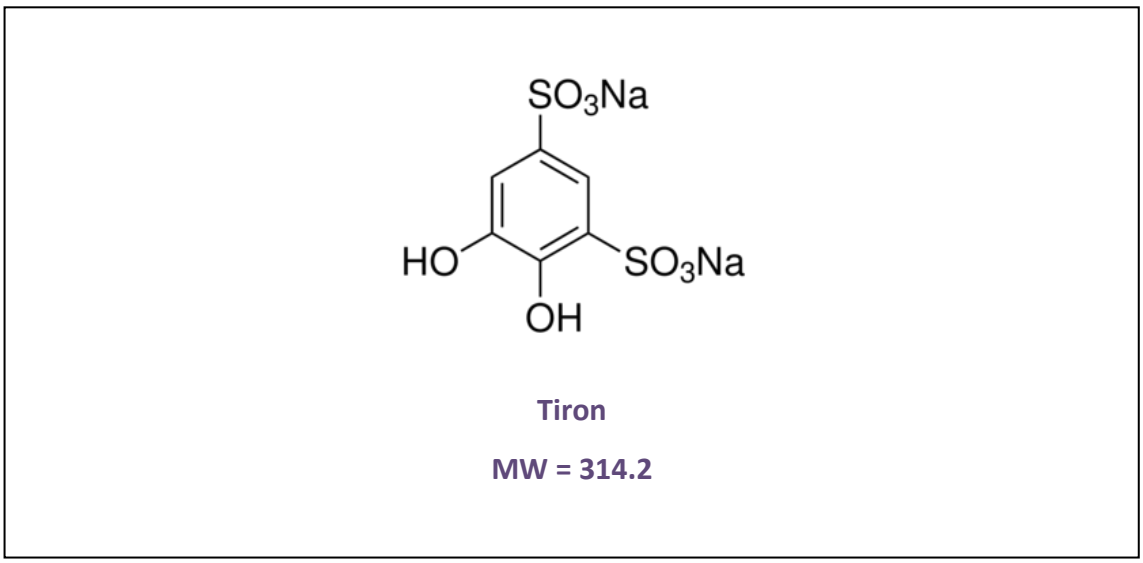

Figure 6.2: The Molecular Structure of Tiron. This figure shows the structure and molecular weight of Tiron (sodium 4,5-dihydroxy-1,3-benzenedisulfonate) (Sigma, 2010).

Tiron (sodium 4,5-dihydroxy-1,3-benzenedisulfonate) is a synthetic analogue of vitamin E (Figure 6.2) (J. Yang *et al.*, 2007). It is a metal chelator which has been found to be rather non-toxic and has consequently been explored for the treatment of various metal poisonings (Taiwo, 2008; Nirala *et al.*, 2009). Tiron has been identified as a useful antioxidant due to its redox capabilities (Krishna *et al.*, 1992).

Part of the study outlined in this chapter encompasses the use of 96-well plate, pathway focused, gene arrays which are readily available from Qiagen, UK. Each plate analyses 84 genes related to specific pathways or biological processes by SYBR green QPCR. They also utilise five housekeeping genes as well as several controls to monitor genomic DNA contamination (GDC) as well as the first strand synthesis (RTC) and QPCR efficiency (PPC). These arrays have been marketed as highly reliable, reproducible and accurate, and as a sensitive gene expression profiling technology. They provide a more cost and time effective alternative to full genome arrays. Allowing expression profiling in the everyday laboratory (SABiosciences, 2011). For reference, Figure 6.3 shows the layout of a typical plate.

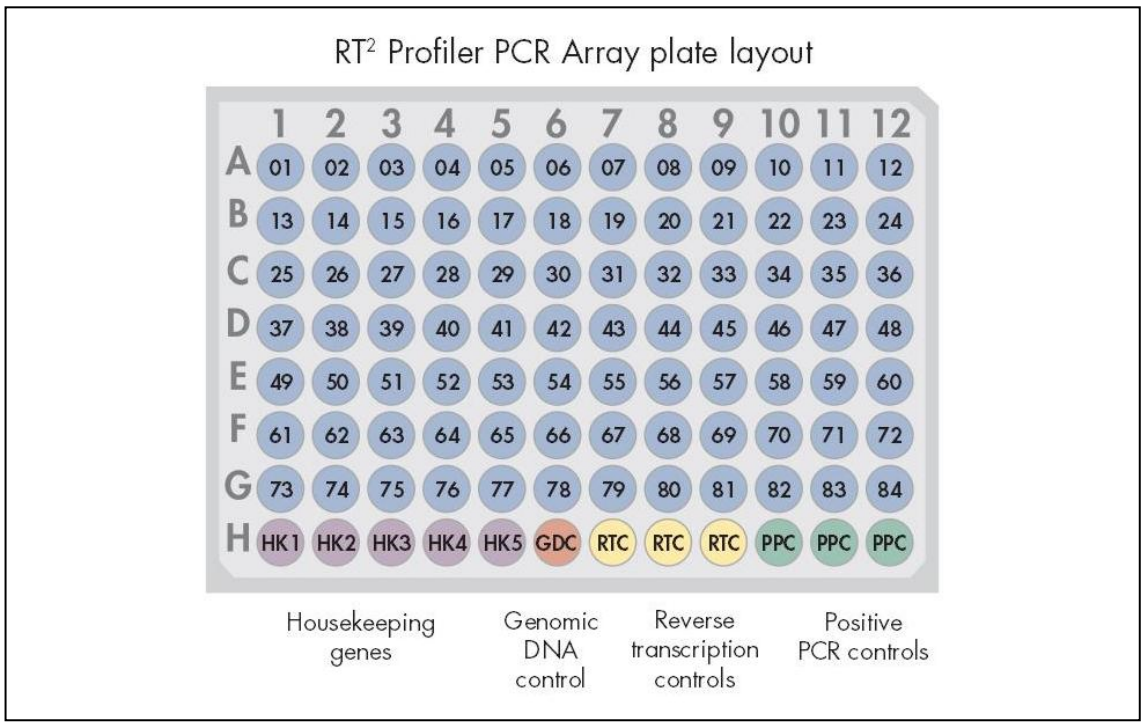

Figure 6.3: Pathway Specific Gene Array 96 well Plate Layout. Each well in an RT Profiler PCR Array measures the expression of 84 genes related to a pathway or disease state. They also utilise five housekeeping genes as well as several controls to monitor genomic DNA contamination (GDC) as well as the first strand synthesis (RTC) and real-time PCR efficiency (PPC) (SABiosciences, 2011).

6.1.1 Aims

This chapter aims to determine the various effects that the different sources of UVR on nDNA. Damaging effects will be examined by means of differential induction of mutations in the p53 gene, photoproducts and the oxidative damage marker, 8-OHdG. Whether antioxidants can protect against this nDNA damage will also be discussed.

A second aim is to determine the action spectrum of UVR-induced nDNA damage. This should provide a more relevant entity to compare the action spectrum of mtDNA damage than previously determined by Setlow et al (Setlow, 1974) as cell type will be kept consistent.

Finally downstream effects of the UVR sources examined in this study will be explored by analysing differences in gene expression. This will utilise an assay analysing nuclear genes specifically related to the mitochondria.

6.2 Methods

The methods shown here are specific for this chapter; for general methods including cell culture techniques, UVR irradiations and dose curve plots please refer to Chapter 2.

6.2.1 Amplification of Exons 5 and 6, exon 7, and exons 8 and 9 of the P53 gene and WAVE analysis

The PCR was performed in 25 µl reactions containing: 50 ng DNA, 10 µM of each primer, 10 mM dNTP, 1 x buffer, 1.25 units of HF Fast Start Taq enzyme (Roche, UK) and made up to the required volume with high grade PCR water. The primers used were dependent on the section of the gene being evaluated (see Table 6-1) and were purchased from MWG (UK). The cycling conditions were 95 °C for 6 min, 35 cycles of 30 s denaturation at 95°C, 30 s annealing at either 56 °C (exons 5 and 6), 66 °C (exon 7) or 54 °C (exons 8 and 9) and 1 min extension at 72 °C; then 72 °C for 5 min. Cycling was carried out on the GeneAmp PCR system 9700 (Applied Biosystems, UK).

Table 6-1: p53 Primers.

Target	Name	Oligonucleotide Sequence (5' → 3')
Exons 5 and 6	Forward	5'- CCG TGT TCC AGT TGC TTT AT -3'
Exons 5 and 6	Reverse	5'- TTA ACC CCT CCT CCC AGA -3'
Exon 7	Forward	5'- GCC ACA GGT CTC CCC AAG GC -3'
Exon 7	Reverse	5'- TGG GGC ACA GCA GGC CAG TG -3'
Exons 8 and 9	Forward	5'- TTC CTT ACT GCC TCT TGC TT-3'
Exons 8 and 9	Reverse	5'- AGA AAA CGG CAT TTT GAG TG -3'

Primers used to detect mutations in the p53 gene (exons 5 and 6, exon 7 and exons 8 and 9)

Heteroduplexing was performed by heating the PCR products at 95 °C for 5 min followed by cooling at a rate of 1-2 °C per min until reaching 25 °C. Samples were analysed immediately with the WAVE^{TM} System (Transgenomic, UK) by Helen Brown (Genesis Genomics, UK) according to manufactures instructions.

6.2.2 Immunofluorescence

HDFn or Primary Keratinocytes were seeded onto coverslips distributed within a 12-well plate at $6x10^4$ cells/well in phenol red free DMEM + FCS. Cells were incubated at 37 °C with 5 % CO_2 overnight. Each experiment was performed in duplicate.

6.2.2.1 Primary Antibodies

The antibodies used for the analysis of CPDs and 6-4 PPs were the mouse monoclonal antibodies TDM-2 and 64M-2 respectively (at 1:300 0.1 % BSA; a kind gift from Professor O Nikaido, Kanazawa, Japan). To determine 8-OHdG prevalence, the antibody 8-Hydroxy-2'-deoxyguanosine (8-OHdG; Immundiagnostik AG, Germany) was utilised. Referring to the manufacturer's specification (Immunodiagnostik, 2011), the 20 µg lyophilized 8-OHdG was re-suspended in 200 µL Milli-Q water. Concentrations were varied from 0.05-1 µg/ml) by serial dilution in 0.1 % BSA.

6.2.2.2 MitoTracker Deep Red

MitoTracker Deep Red (abs/em ~644/665 nm; Life technologies, UK) is a far-red fluorescent dye used for mitochondrial localisation by staining the mitochondria in live cells. This dye was administered to cells grown on coverslips post UVR treatment but prior to the fixation stage of immunofluorescence. The cells were exposed to 100 nM MitoTracker Deep Red (diluted in phenol red free DMEM – FCS from a 1 mM stock) for 20 min whilst protected from light. When using MitoTracker Deep Red the entire immunofluorescence method was performed protected from light.

6.2.2.3 Method

Following the required treatment cells were washed with PBS and were fixed in paraformaldehyde (1:10 37-41 % paraformaldehyde in PBS; Fisher Scientific, USA) for 10 minutes. Cells were then washed with PBS-T (0.05 % Tween-20 in PBS; Sigma, UK), and then permeabilised with Triton-X (0.2 % in PBS; Invitrogen-Gibco, UK) for 10 minutes. Cells were washed thrice with PBS-T and were then blocked with goat serum (1:60 in 0.1 %BSA; Sigma-Aldrich, UK) for 30 min. Following blocking cells were exposed to the required primary antibody for 60 min. After washing thrice with PBS-T, cells were protected from light before incubation with Alexa Fluoro goat anti-mouse 488 (Invitrogen-Gibco, UK) at 1:300 and DAPI (Invitrogen-Gibco, UK) at 1:100 (both

diluted in 0.1 % BSA) for 60 min. From this point cells remained protected from light during a thrice washing with PBS-T, a wash with distilled water, then with 100 % ethanol (Invitrogen-Gibco, UK), before coverslips were attached to slides using Mowiol (Merck-Millipore, UK). Cells were refrigerated overnight and then were stored away from light.

6.2.2.4 Microscopic Analysis and Quantification

The fluorescent imaging was performed using the wide-field microscope, Zeiss Axio Imager II (Carl Zeiss Microscopy, Germany) with an x 20 magnification. The exposure time for FITC (Alexa Fluoro 488 emission; green) was set to the control slide of each experiment. Images were analysed using the imaging software Volocity (PerkinElmer, USA) where the mean FITC fluorescence per DAPI (nuclear DNA stain; blue) detected nuclei of >100 cells/treatment was quantified. Post-Volocity analysis, data was normalised to the control.

6.2.3 The Protective Effect of Tiron on UVR-Induced Photoproducts

6.2.3.1 Treatment with Tiron

Cells were treated with 3 mM Tiron (As optimised by Dr Anne Oyewole; Sigma-Aldrich, UK) diluted from a 250 mM stock in phenol red free DMEM + FCS for 24 h prior to UVR exposure.

6.2.3.2 Autofluorescence of Tiron

Various concentrations of Tiron (0.5, 1 and 3 mM) were administered in quadruplicate into a clear-bottom 96-well plate as well as control wells containing only PBS. Fluorimetric analysis was performed using a Cary Eclipse spectrophotometer (Varian, UK) with settings of 488 nm excitation, 535 nm emission and slit width 10.

6.2.4 Optimisation of 8-OHdG for Immunofluorescence

6.2.4.1 Viability of HDFn Cells Exposed to Increasing Concentrations of H_2O_2

HDFn cells were seeded ($5x10^3$ cells per well) in phenol red free DMEM + FCS in to a 96-well plate and were then incubated at 37 °C with 5 % CO_2 overnight. Cells were then exposed to varying concentrations (25, 50, 100 and 200 µM) of H_2O_2

(Acros Organics, UK) diluted in phenol red free DMEM – FCS. For each concentration the exposure time was also varied (15, 30 or 60 min). Column 1 was the blank and contained no cells; column 2 was the control and received no treatment. During treatment the plate was protected from light. Following this cells were assessed for viability by addition of 20 µl MTS (CellTiter-96 Aqueous, Promega, UK) The cells were then incubated at 37 °C for 5 h. Absorbance was measured at 490 nm using the Spectromax 250 microplate reader (Molecular Devices, UK).

6.2.4.2 Treatment with H_2O_2

Prior to the immunofluorescence protocol, cells were treated with either 100 or 200 µM H_2O_2 for 30 or 60 min. Control wells were treated with phenol red free DMEM - FCS only. The plate was protected from light during treatment.

6.2.4.3 Alternative Fixation Protocol

- Fixation with acetone (-20°C; Fisher Scientific, USA) for 10 min.
- Fixation with methanol (-20°C; Fisher Scientific, USA) for 10 min.
- Fixation with combined acetone-methanol (1:1; -20°C) for 10 min.

No subsequent permeabilisation was required for any of the alternative fixation protocols.

6.2.5 Pathway Specific Array Analysis

Following treatment, cellular RNA was isolated using the RNeasy mini kit (Qiagen, UK) as per manufactures instructions including the addition of β-mercaptoethanol (β-ME; Sigma, UK) and the additional DNase digestion step using the RNase-Free DNase Set (Qiagen, UK) as per manufactures instructions. After isolation, RNA was quantified and quality (A_{260}:A_{230} > 1.7; A_{260}:A_{280} 1.8-2.0) was assessed using the Nanodrop ND-100 (Nanodrop technologies) - 1 ul of each RNA sample was pipetted onto the spectrophotometer. cDNA synthesis of 0.5 µg of the RNA sample was then performed using the RT^2 First Strand Kit (Qiagen, UK) as per manufactures instructions. The cDNA sample was then combined with 2x RT^2 SYBR Green Mastermix and RNase-free water to create the mix required for PCR. A 25 µl sample of this PCR mix was added to each well of the 96-well array. The cycling conditions were 95 °C for 10 min and then 40 cycles of 15 sec at 95 °C and 1 min at 60 °C, analysis included the melt curve

selection. Cycling was performed on the StepOnePlus (Applied Biosystems, UK). Analysis encompassed the use of the following arrays: the human oxidative stress and antioxidant defence array (PAHS-065A), the human mitochondrial energy metabolism array (PAHS-008C-2) and the oxidative stress plus PCR array (PAHS-065Y) (Qiagen, UK).

6.2.6 Statistical Analysis

Statistical evaluation was performed by a one-way ANOVA with Dunnett's correction post-hoc analysis test for comparison to the control or an unpaired t-test. P-values below 0.05 were considered significant.

6.3 Results

6.3.1 The Relationship between UVR and Mutations in exons 5-9 of the p53 Gene

Exons 5-9 of the nuclear p53 gene were analysed for any mutations which may have been induced by UVR. The specific exons of un-irradiated and TL12, TL01, Helarium, Arimed B and TL09 ± filter irradiated HDFn cell samples were amplified using the particular PCR method. The irradiations used were acute doses which produced maximum mtDNA damage shown in the previous chapter. These PCR products were then analysed using denaturing high-performance liquid chromatography by WAVE analysis. Typical WAVE analysis of the exons 5 and 6 (Figure 6.4), exon 7 (Figure 6.5) and exons 8 and 9 (Figure 6.6) are shown. For all samples analysed a single peak was observed.

6.3.2 Distribution of Photoproducts in HDFn Cellular DNA

Initial investigations found that HaCaT cells stained unevenly, particularly when exposed to MitoTracker (data not shown). These cells were therefore not included in the research into the effects of the different UVR sources on the induction of photoproducts. This first inquiry examined where the major photoproducts were distributed. Figure 6.7 shows the distribution of photoproducts within nDNA compared with mtDNA. A strong correlation was shown between the dapi staining and the antibody raised to CPDs, whereas the correlation is not as strong between MitoTracker and the same antibody.

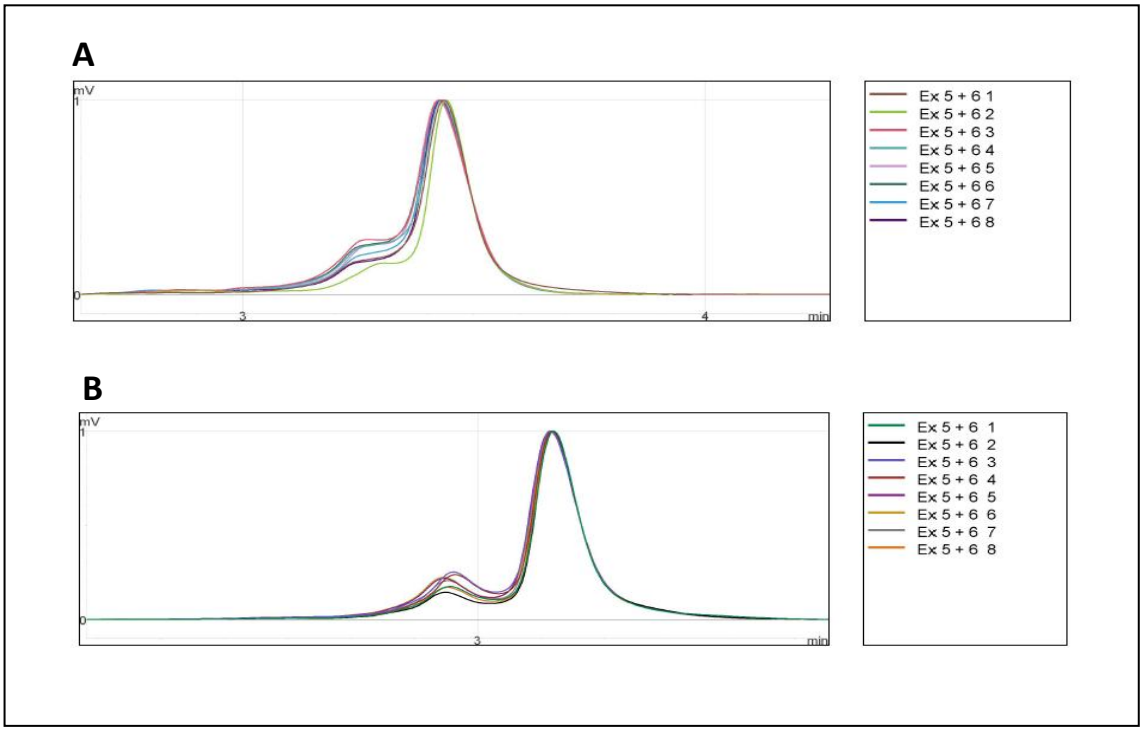

Figure 6.4: Mutations in Exons 5 and 6 of the p53 Gene Developed by Various UVR Exposure. Typical WAVE analysis of exons 5 and 6 at 60 °C (A) and 63 °C (B). The samples analysed were HDFn cells which had received either no irradiation (1 + 8), TL12 (2), TL01 (3), Helarium (4), Arimed B (5), TL09 – filter (6), TL09 + filter (7).

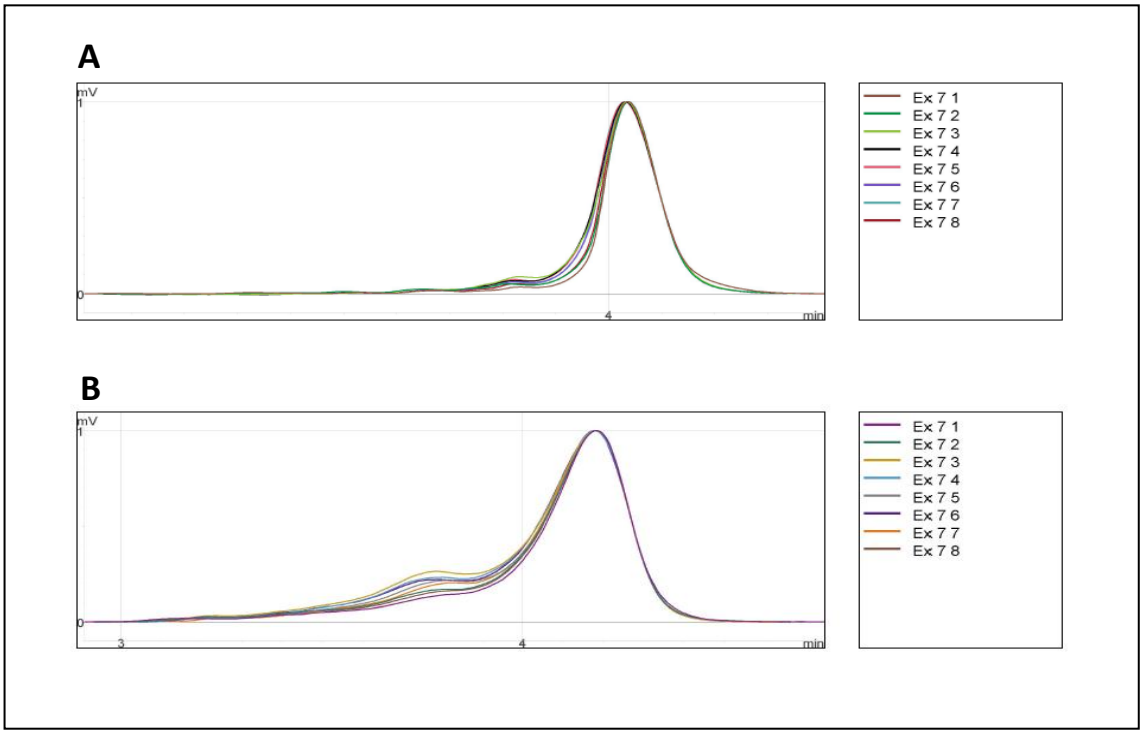

Figure 6.5: Mutations in Exon 7 of the p53 Gene Developed by Various UVR Exposures. Typical WAVE analysis of exon 7 at 61 °C (A) and 63 °C (B). The samples analysed were HDFn cells which had received either no irradiation (1 + 8), TL12 (2), TL01 (3), Helarium (4), Arimed B (5), TL09 – filter (6), TL09 + filter (7).

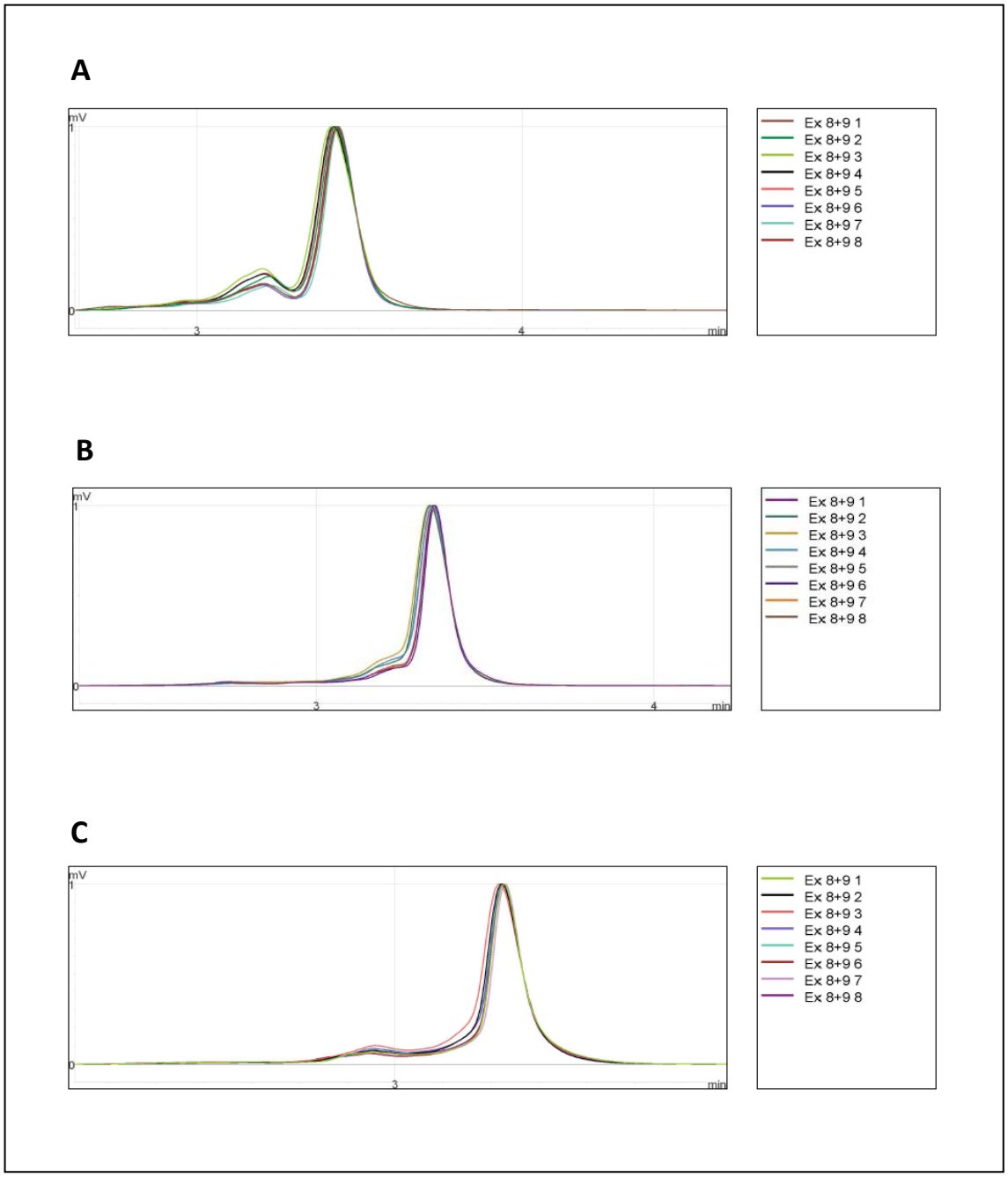

Figure 6.6: Mutations in Exons 8 and 9 of the p53 Gene Developed by Various UVR Exposures. Typical WAVE analysis of exons 8 and 9 at 57 °C (A), 60 °C (B) and 62 °C (C). The samples analysed were HDFn cells which had received either no irradiation (1 + 8), TL12 (2), TL01 (3), Helarium (4), Arimed B (5), TL09 – filter (6), TL09 + filter (7).

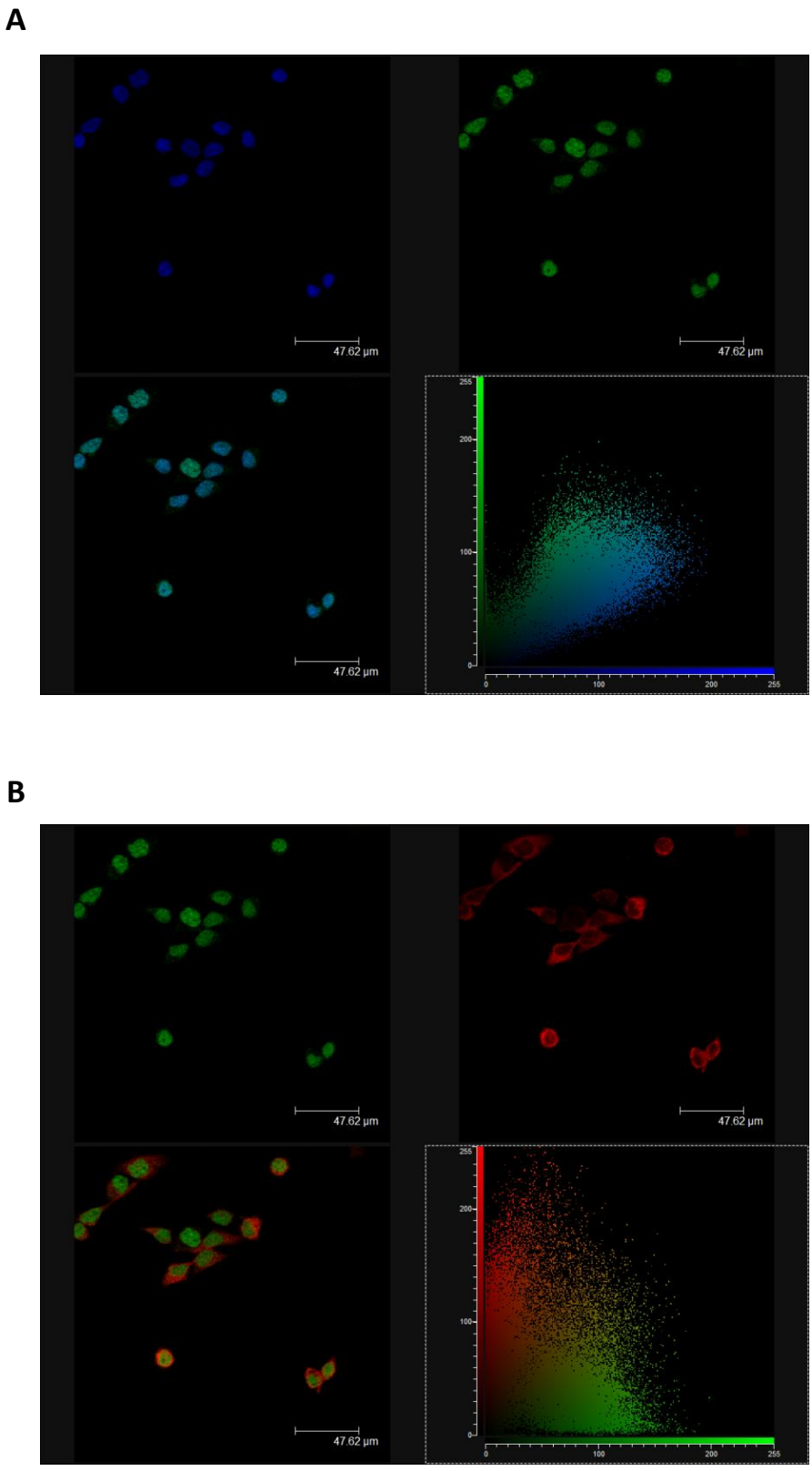

Figure 6.7:Distribution of Photoproducts in HDFn Total Cellular DNA Using Immunofluorescence. HDFn cells were exposed to 1500 mJ/cm^2 UVR emitted from the TL12 UVR source. They were then stained with Dapi (nuclear DNA stain; blue), Mitotracker deep red (mitochondria stain; red) and TDM-2 monoclonal antibody (CPD specific; green). Correlation graphs show the correlation of CPDs in nDNA (A) and mtDNA.

6.3.3 The UVR-Induction of Photoproducts in HDFn Cells

Due to the majority of photoproduct induction being in nDNA this was where they were assessed. There was a visual increase in fluorescence when both the TDM-2 and 64M-2 antibodies were utilised to detect CPDs and 6-4 PPs respectively. Figure 6.8 shows one particular example of this where there was not only an increase in fluorescence seen with UVR, but it was also dose-dependently increased. The trend for the induction of photoproducts by the majority of the various UVR sources explored was for it to be dose-dependent (Figure 6.9). CPD induction was increased 3.4 fold (TL12), 1.9 fold (TL01), 3.1 fold (Helarium), 2.0 fold (Arimed B) and 1.1 fold (Cleo + filter) at the maximum dose, all of which were statistically significant ($P<0.001$). 6-4 PPs were increased 2.6 fold (TL12), 1.5 fold (TL01), 2.0 fold (Helarium), 1.4 fold (Arimed B) and 1.2 fold (Cleo + filter) at the maximum dose, all of which were statistically significant ($P<0.001$). Exceptions to the dose-dependent rule included TL12 induction of 6-4 PPs where a larger increase of 2.7 fold was seen with the medium (1.6 J/cm^2) dose used. This was also true with TL01 induction of 6-4 PPs where no difference between the doses was seen, although all doses of TL01 caused an increase when compared with the control. Further to this, Cleo + filter induction of CPDs was inconsistent with statistically significant increases seen at the low (25 J/cm^2) and high (100 J/cm^2) doses whereas a statistically significant decrease was seen at the medium dose (50 J/cm^2).

An additional observation showed that the same doses of UVR caused more induction of CPDs compared with 6-4 PPs with the exception of the Cleo + filter UVR source, where instead the opposite was seen. The dose-dependent data was plotted into three parameter sigmoidal plots in an aim to prepare the data for action spectrum determination.

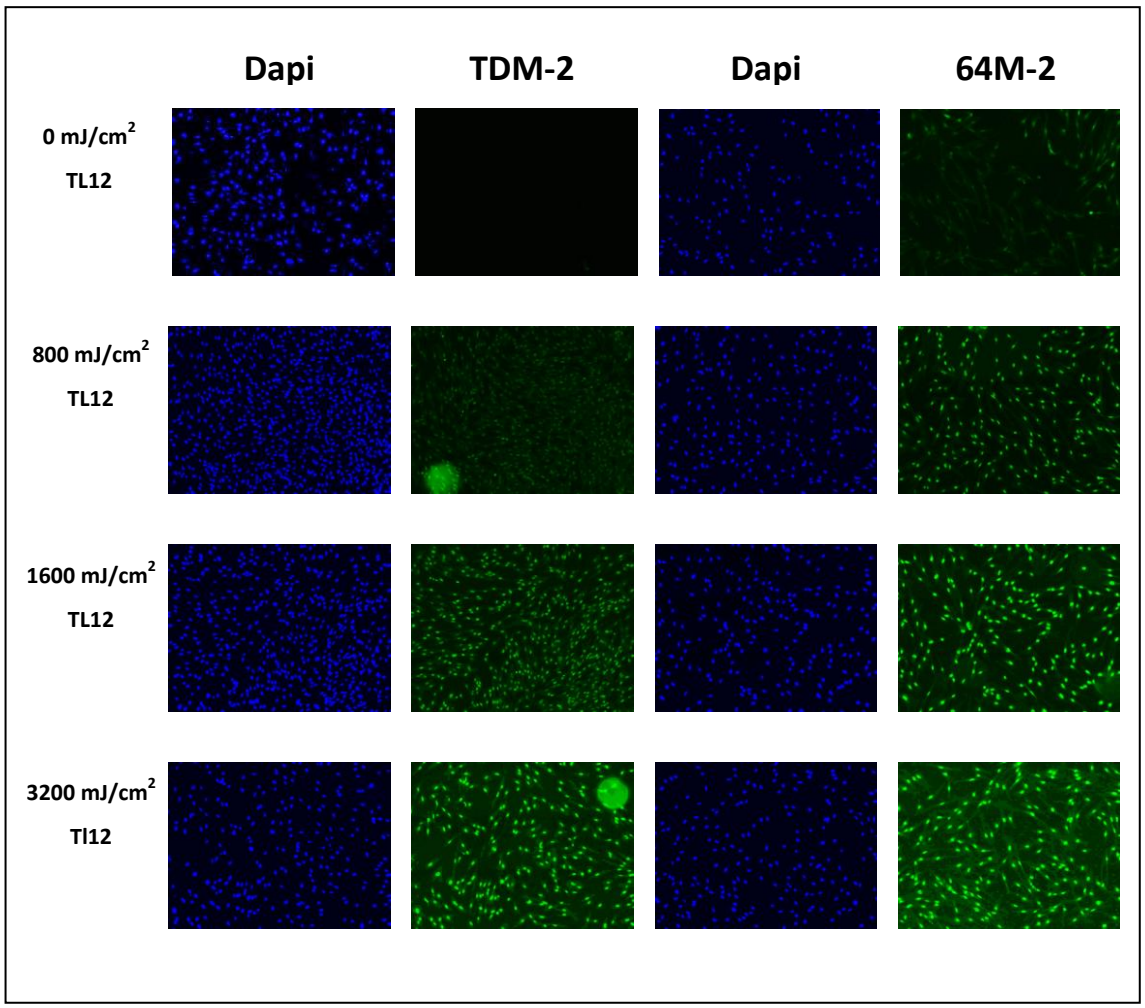

Figure 6.8: Typical Microscope Images Showing the Induction of Photoproducts in HDFn Cells Exposed to UVR. HDFn cells were exposed to 800, 1600 and 3200 mJ/cm^2 UVR emitted from the TL12 UVR source. They were then stained with Dapi (nuclear DNA stain; blue), and either TDM-2 monoclonal antibody (CPD specific; green) or TDM-2 monoclonal antibody (6-4 PPs specific; green).

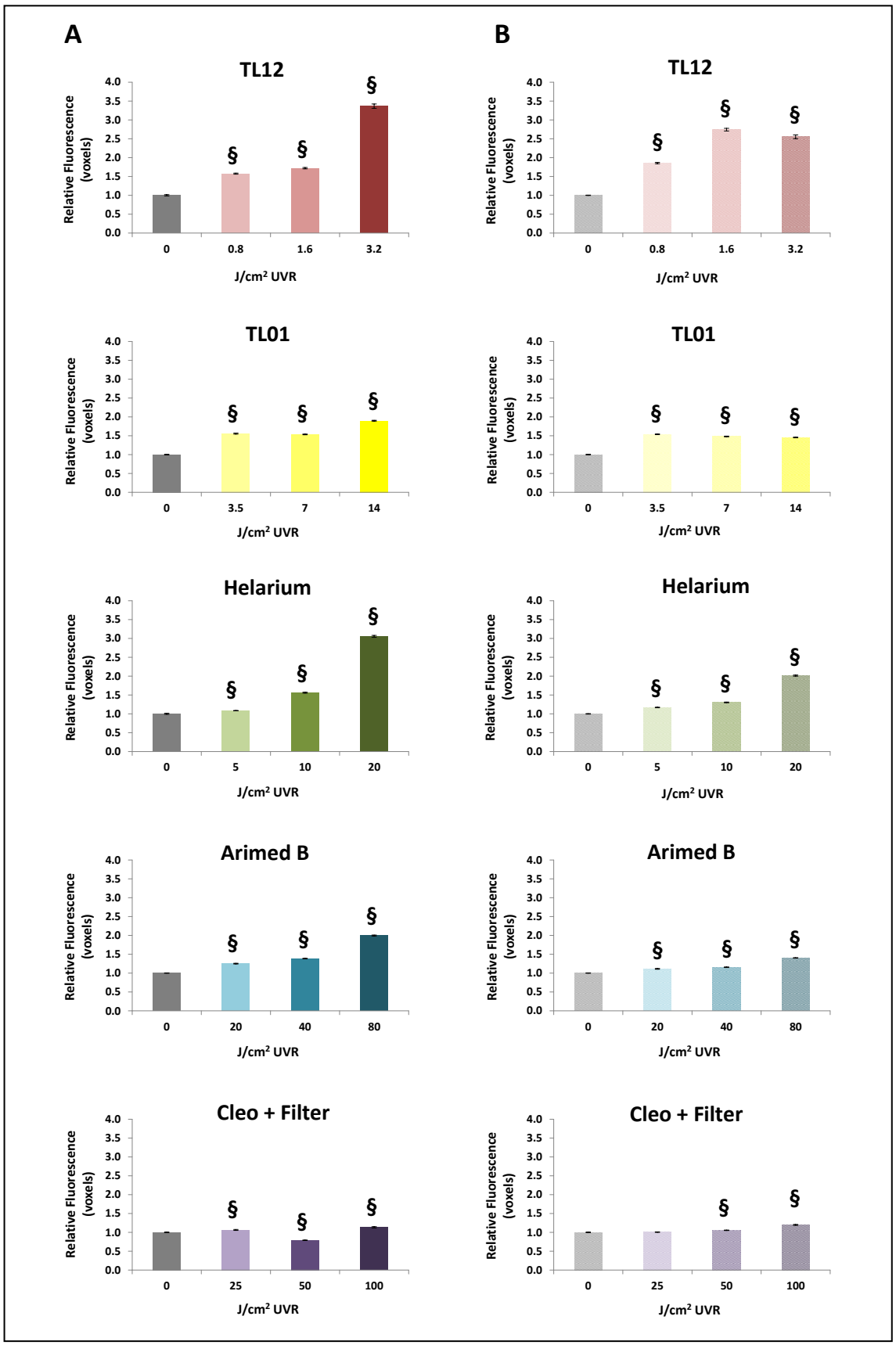

Figure 6.9: The Induction of Photoproducts in HDFn Cells by Various UVR Sources. HDFn cells were irradiated with TL12, TL01, Helarium, Arimed B and Cleo + filter. CPDs (A) and 6-4 PPs (B) were detected by immunofluorescence using the monoclonal antibodies TDM-2 and 64M-2 respectively. The mean FITC fluorescence visualised by wide-field microscopy in >100 cells was quantified using the imaging software Volocity. Fluorescence was normalised to relevant individual un-irradiated control. Data expressed as mean n=3 ± SEM; §P<0.001.

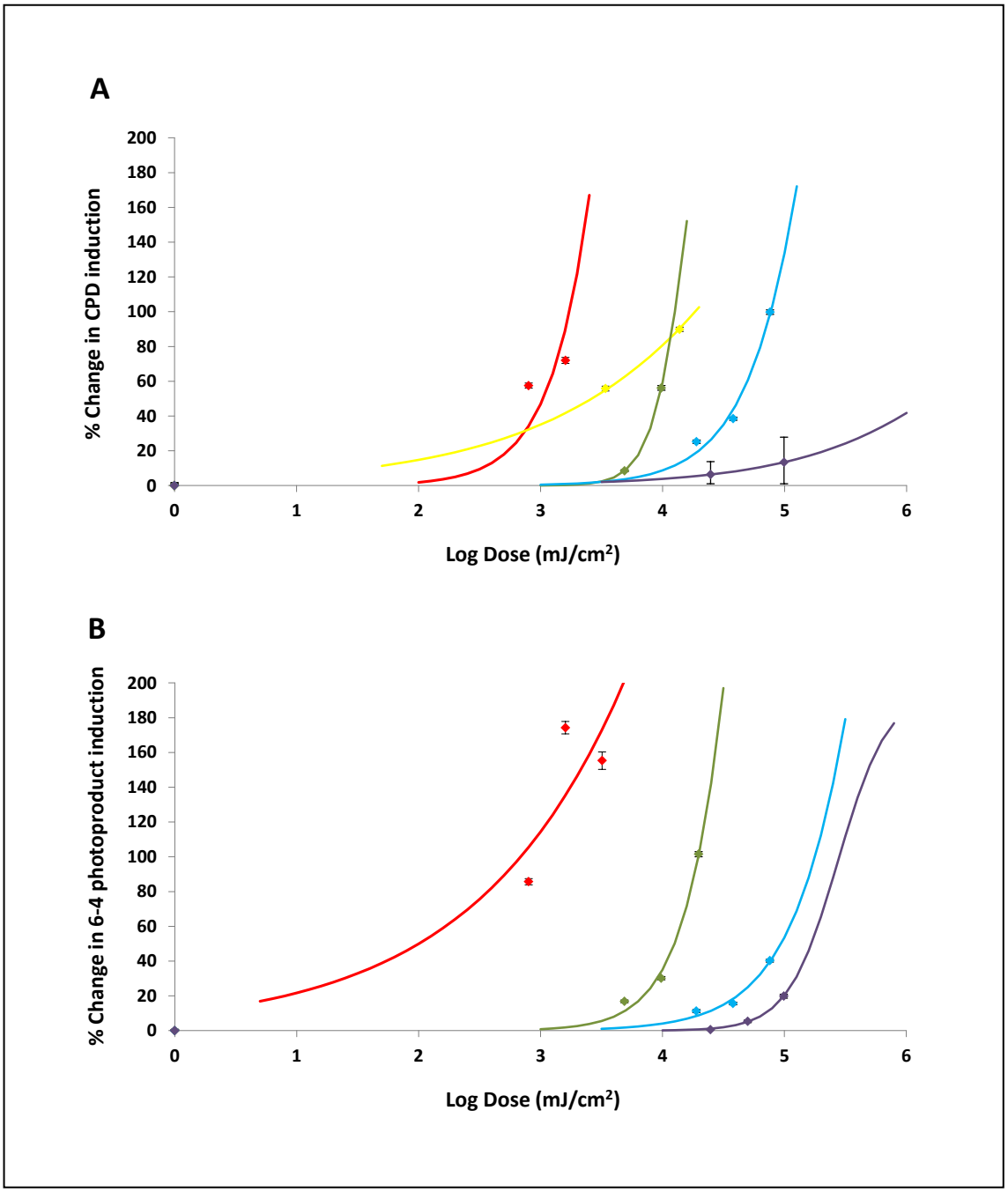

Figure 6.10: The Dose-Dependent Induction of Photoproducts in HDFn Cells by Various UVR Sources. HDFn cells were irradiated with TL12 (-), TL01 (-), Helarium (-), Arimed B (-), Cleo + filter (-). CPDs (A) and 6-4 PPs (B) were detected by immunofluorescence using the monoclonal antibodies TDM-2 and 64M-2 respectively. The mean FITC fluorescence visualised by wide-field microscopy in >100 cells was quantified using the imaging software Volocity. A percentage increase in fluorescence compared to an un-irradiated control was calculated, curves were fitted to a three parameter sigmoidal plot.

6.3.4 The UVR-Induction of Photoproducts in Primary Keratinocyte Cells

Further assessment of UVR photoproduct induction utilised Primary Keratinocyte cells. Again a visual increase in fluorescence with the TDM-2 and 64M-2 antibodies were used to detect CPDs and 6-4 PPs, respectively, is seen in Figure 6.11. This particular example shows that the increase in fluorescence seen with TL12 UVR was also dose-dependent, although a less consistent pattern in fluorescence increase was seen when compared with the HDFn cell data (Figure 6.8). The trend for the induction of photoproducts by the majority of the various UVR sources explored was less reliable in Primary Keratinocyte cells when compared with that seen of HDFn cells in section 6.3.3 . However a dependable statistically significant increase in induction was seen with all UVR sources with the exception of Cleo + filter induced 6-4 PPs. Figure 6.12 demonstrates an increase in CPD induction of 2.3 fold (TL12), 1.4 fold (TL01), 1.6 fold (Arimed B) and 1.3 fold (Cleo + filter) at the maximum dose, all of which were statistically significant ($P<0.001$). 6-4 PPs were increased 3.3 fold (TL12), 1.2 fold (TL01), and 1.2 fold (Arimed B) at the maximum dose, all of which were statistically significant ($p<0.001$). At the maximum dose Cleo + filter induced a non-statistically significant decrease in 6-4 PP induction. The inconsistent dose-dependent effect seen with this data meant that it was not used for action spectrum determination.

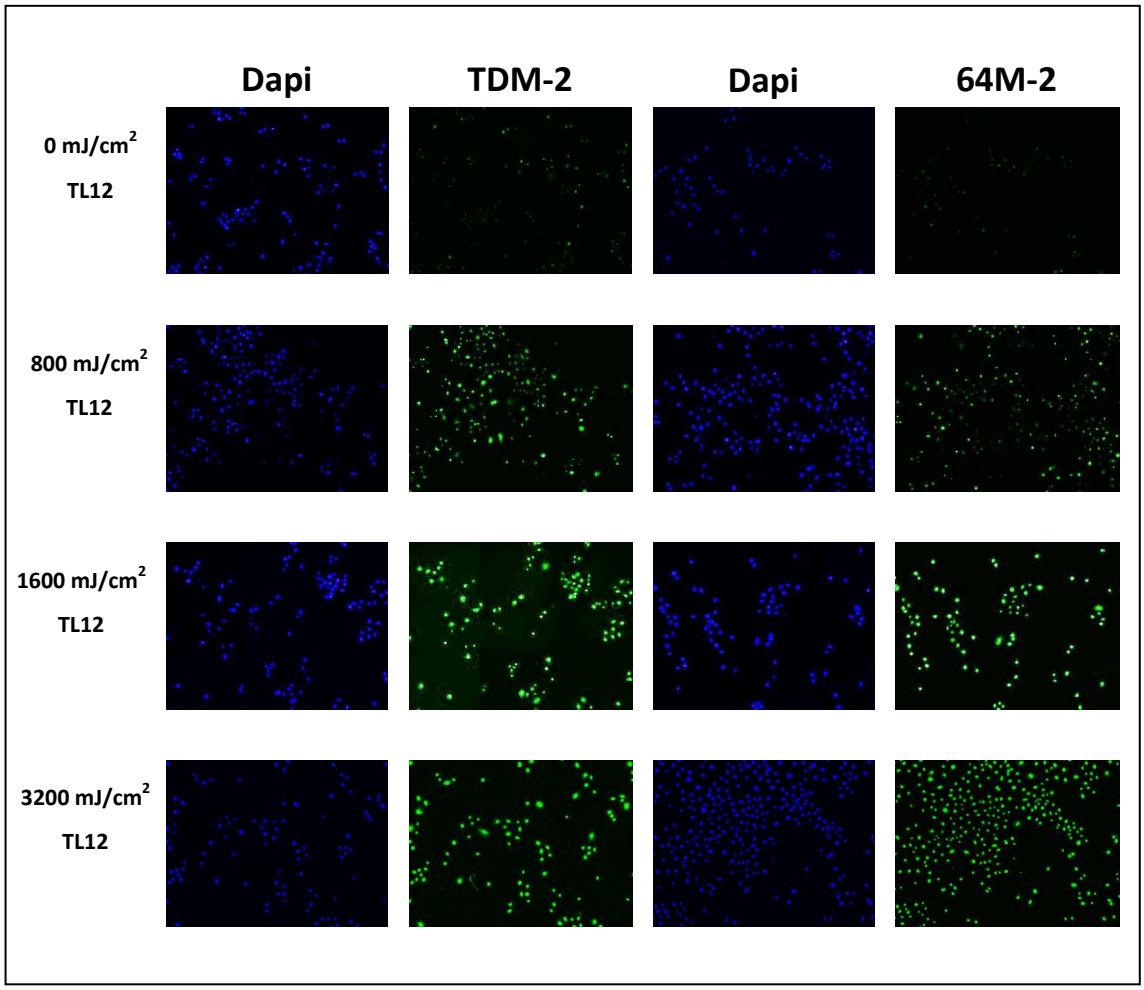

Figure 6.11: Typical Microscope Images Showing the Induction of Photoproducts in Primary Keratinocyte Cells Exposed to UVR. Primary Keratinocyte cells were exposed to 0, 800, 1600 and 3200 mJ/cm^2 UVR emitted from the TL12 UVR source. They were then stained with Dapi (nuclear DNA stain; blue), and either TDM-2 monoclonal antibody (CPD specific; green) or TDM-2 monoclonal antibody (6-4 PP specific; green).

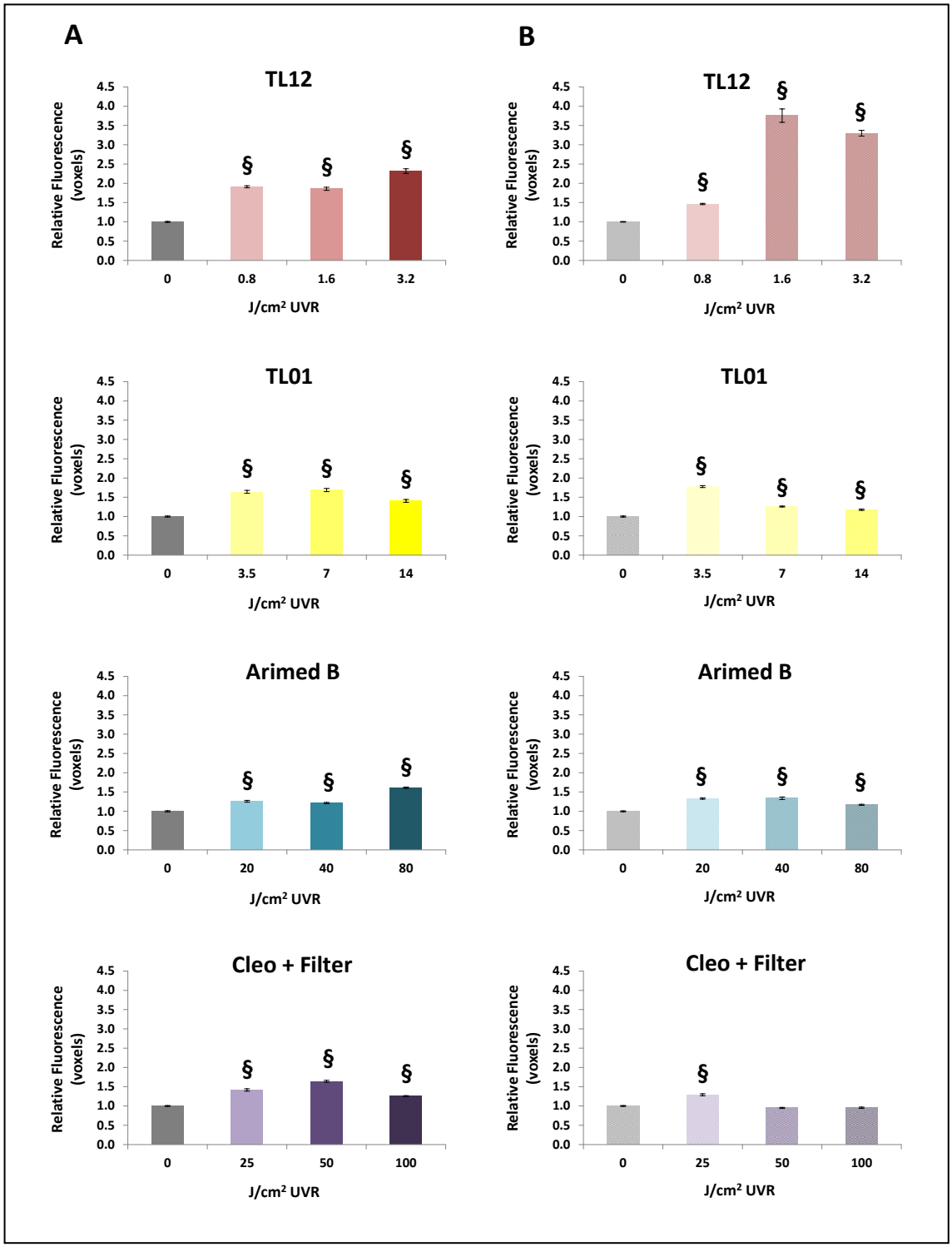

Figure 6.12: The Induction of Photoproducts in Primary Keratinocyte Cells by Various UVR Sources. Primary Keratinocytes cells were irradiated with TL12, TL01, Arimed B and Cleo + filter. CPDs (A) and 6-4 PPs (B) were detected by immunofluorescence using the monoclonal antibodies TDM-2 and 64M-2 respectively. The mean FITC fluorescence visualised by wide-field microscopy in >100 cells was quantified using the imaging software Volocity. Fluorescence was normalised to relevant un-irradiated control. Data expressed as mean n=3 ± SEM; §p<0.001.

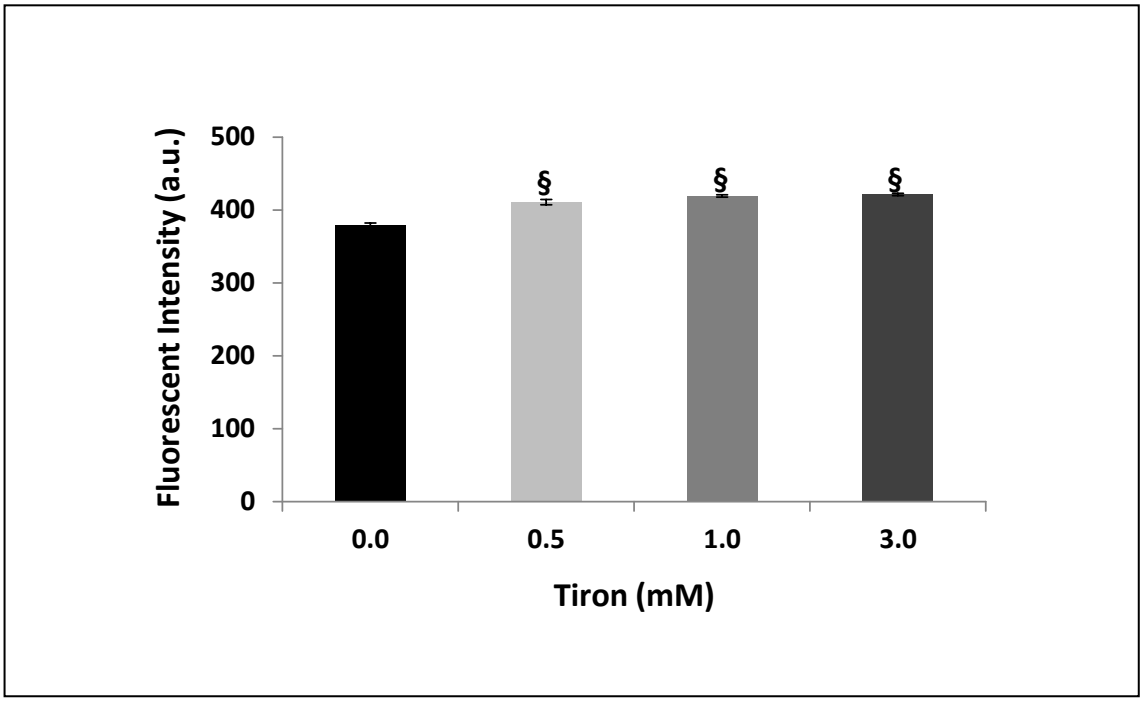

Figure 6.13: The Auto-Fluorescence of Tiron. The auto-fluorescence of varying concentrations of Tiron (0.5-3 mM) was determined by fluorimetric analysis (488 nm excitation, 535 nm emission and slit width 10). Statistical significance to the control (PBS only) was assessed using one-way ANOVA with Dunnett's post-hoc analysis (n=8 ± SEM, §P<0.001). Statistical significance between all columns was assessed using one-way ANOVA with Bonferonni's post-hoc analysis (ns P>0.05).

6.3.5 The Effect Tiron had on UVR-Induced Photoproducts

Previous work within our laboratory has shown that the synthetic antioxidant Tiron has a protective effect on UVR-induced mtDNA damage in skin cells. It was therefore the project of an MRes student (Miss Emma Russell) of whom I supervised and collaborated with to see if this protective effect was also demonstrated with nDNA.

The auto-fluorescent of Tiron was first assessed prior to its use in immunofluorescence which is a fluorescence-sensitive assay. Increasing concentrations of Tiron were tested for auto-fluorescence and the result is shown in Figure 6.13. Although not dose-dependent, a consistent statistically significant increase of approximately 10 % (P<0.001) with all concentrations when compared to the control was seen. This was a crucial observation needed to avoid the recording of incorrect increases in the fluorescence of cells exposed to Tiron. The following immunofluorescence experimental analysis therefore normalised Tiron-treated UVR-irradiated cells to a Tiron control thereby removing a non-specific increase of fluorescence caused by Tiron.

The effect that Tiron had on the induction of photoproducts by the TL12 UVR source in HDFn cells is demonstrated in Figure 6.14 (A). A dose of 1.6 J/cm^2 caused a statistically significant (P<0.001) increase in the induction of both CPDs and 6-4 PPs (data not shown). This data shows that Tiron treatment caused a small, yet still statistically significant, reduction of 13 and 3 % of the induction of CPDs and 6-4 PPs by TL12 respectively.

Due to time constraints, it was only possible to assess the protection of Tiron against Arimed B induced CPDs. As previously seen, a dose of 76 J/cm^2 Arimed B caused a statistically significant increase in the induction of CPDs (p<0.001). Figure 6.14 (B) shows that incubation with Tiron caused a reduction in Arimed-B induced CPDs by ~22 % which was statistically significant (P<0.001).

Figure 6.14 (C) shows the effect that Tiron has on the induction of photoproducts by the Cleo + filter UVR source in HDFn cells. A dose of 126 J/cm^2 was able to create a statistically significant increase in both CPDs and 6-4 PPs (P<0.001). Following incubation with Tiron this induction of photoproducts had been statistically significantly reduced by ~42% with CPDs and ~22% with 6-4 PPs (P<0.001).

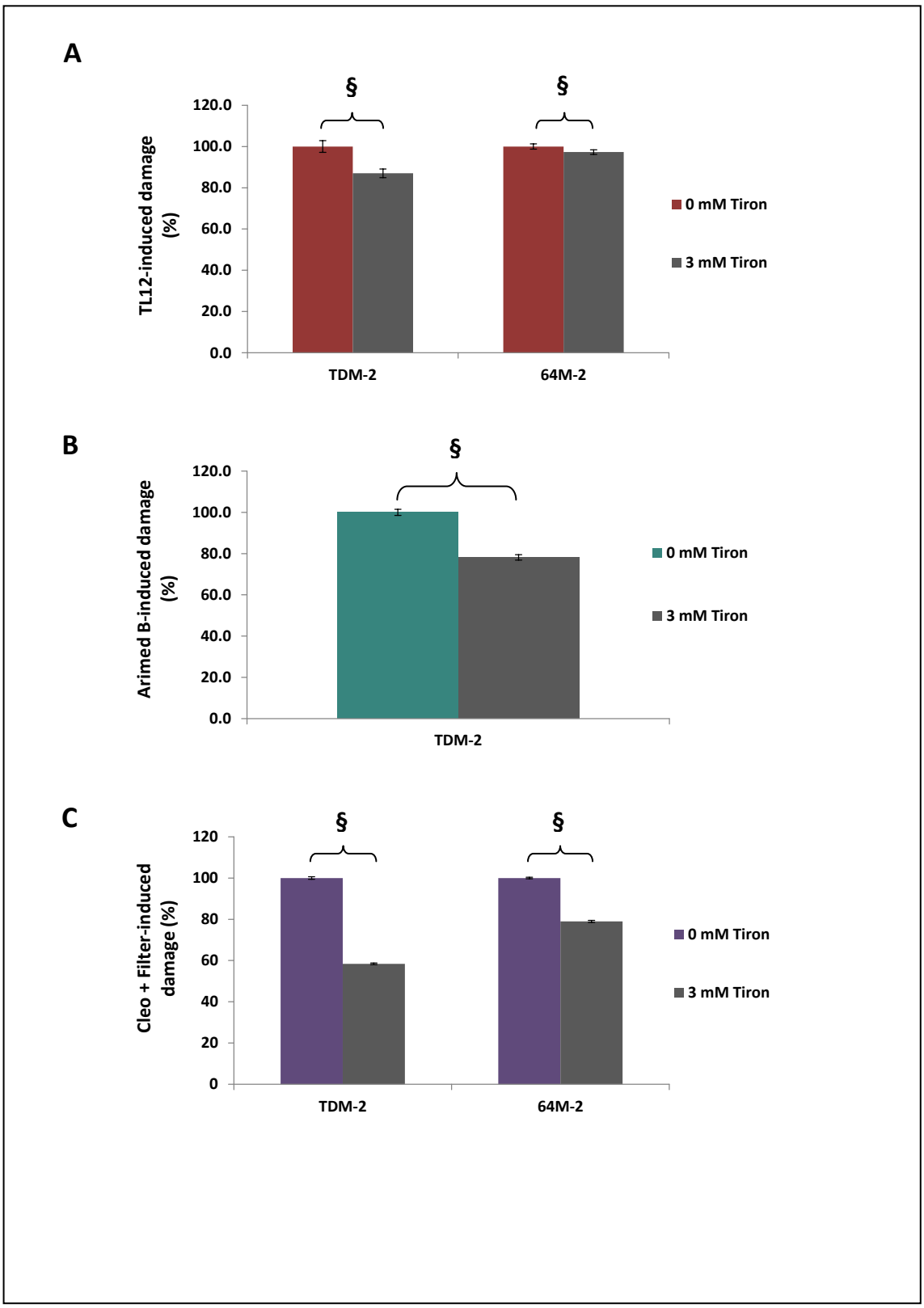

Figure 6.14: The Effect of Tiron on the Various UVR-Induced Photoproducts. HDFn cells were irradiated with ~1.6 J/cm^2 TL12 (A), ~76 J/cm^2 Arimed B (B) and ~125 J/cm^2 Cleo + filter (C) either with or without a 24 h 3 mM treatment of Tiron. CPDs and 6-4 PPs were detected by immunofluorescence using the monoclonal antibodies TDM-2 and 64M-2 respectively. The mean FITC fluorescence visualised by wide-field microscopy in >100 cells/treatment was quantified using the imaging software Volocity. Fluorescence was normalised to relevant individual control to account for Tiron's auto-fluorescence. Data expressed as mean n=3 (except (B) where n=2) ± SEM; §P<0.001.

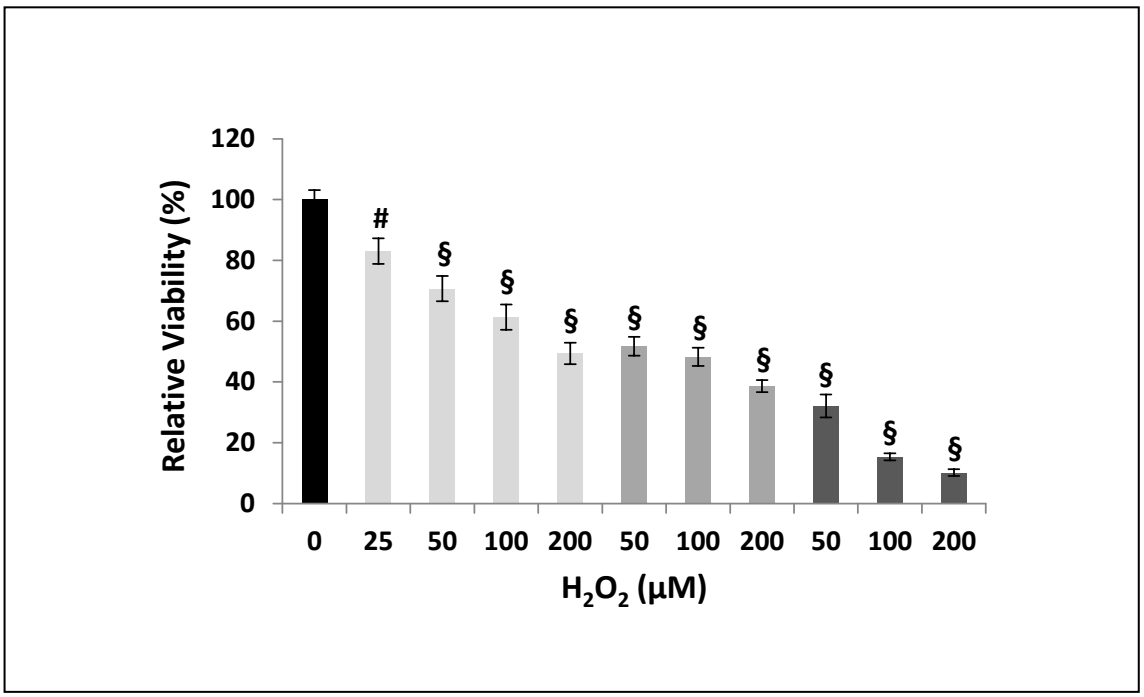

Figure 6.15: Viability of HDFn Cells Exposed to H_2O_2. HDFn cells were exposed to varying concentrations (25-200 µM) of H_2O_2 at varying time periods; 15 (▫), 30 (▪) or 60 min (▪) and cell viability was determined using the MTS Assay. Absorbance was measured at 490nm. Data represents the mean value n=3 ± SEM, #P<0.01, §P<0.001 compared to the control.

6.3.6 Optimisation of 8-OHdG Antibody for Immunofluorescence

This section of results was performed in collaboration with Miss Emma Russell (MRes student). Initial experiments for the optimisation of 8-OHdg utilised H_2O_2, in an aim to yield a high and consistent generation of oxidative stress.

A preliminary experiment investigated the viability of HDFn cells to increasing concentrations of H_2O_2 by using the MTS assay (Figure 6.15). This was to determine the maximum dose of H_2O_2 which would induce a high level of oxidative stress in HDFn cells (for detection by immunofluorescence with 8-OHdG) without causing substantial cell death. A statistically significant reduction in cell viability was observed when cells were exposed to all doses of H_2O_2 in comparison to the control. This cell death ranged from 20 to 85 % with the treatment of 25 µM H_2O_2 for 15 min and the largest dose of 200 µM H_2O_2 for 60 min respectively. The trend was for cell death to increase with an increase in dose as well as with an increase in exposure time.

For detection of oxidative stress in HDFn cells, induced by a 100 µM for 30 min H_2O_2 treatment, a concentration of 5 µg/ml (the high end of the dose range as recommended by the manufacturer (Immunodiagnostik, 2011)) and 1 µg/ml 8-OHdG

was used (Figure 6.16 [A]). The data shows statistically significant increases in fluorescence when compared to the control of ~10 % ($P<0.001$) and ~54 % ($P<0.001$) for 5 µg/ml and 1 µg/ml 8-OHdG respectively. This experiment also confirmed that cell viability was sufficient for analysis (data not shown) therefore a higher dose of 200 µM of H_2O_2 for 60 min was utilised in the subsequent experiment to increase oxidative stress in an aim to intensify the response of 8-OHdG. In this subsequent experiment (Figure 6.16[B]) a further dilution of the antibody (0.5 µg/ml) was used. The results found that fluorescence statistically significantly decreased when compared to the control by ~5 % ($P<0.001$) when using the 1 µg/ml 8-OHdG. Conversely the lower concentration of 0.5 µg/ml 8-OHdG, saw a statistically significant increase in fluorescence of ~6 % ($P<0.001$).

Due to the discrepancies of 1 µg/ml 8-OHdGs ability to detect oxidative stress seen between the first two experiments a further experiment was performed. The only variable was the dose of H_2O_2 so the third experiment utilised the initial dose of 100 µM for 30 min H_2O_2, because this treatment had previously created detectable oxidative stress (Figure 6.16[C]). This experiment also included the addition of lower concentrations of 0.1 µg/ml and 0.005 µg/ml 8-OHdG in an aim to determine a dose-dependent effect. The data showed statistically significant differences in fluorescence when compared to the control when detected by 1, 0.5, 0.1 and 0.005 µg/ml 8-OHdG of an increase of ~10 % ($P<0.001$), a decrease of ~4 % ($P<0.01$), an increase of ~10 % ($P<0.001$) and a decrease of ~15 % ($P<0.001$) respectively.

Initial experiments showed no consistent pattern or strong ability of 8-OHdG to detect oxidative stress, and therefore a further experiment, comparing alternative fixation methods, was performed (Figure 6.16[D]). The fixation methods applied were the original paraformaldehyde fixation, acetone fixation, methanol fixation and an acetone-methanol fixation. The data showed statistically significant differences in fluorescence when compared to the control of a decrease of ~7 % ($P<0.001$), an increase ~8 % ($P<0.001$) with paraformaldehyde fixation and methanol fixation respectively. With the acetone and acetone-methanol fixations and no detectable difference ($P>0.05$) from the control was evident.

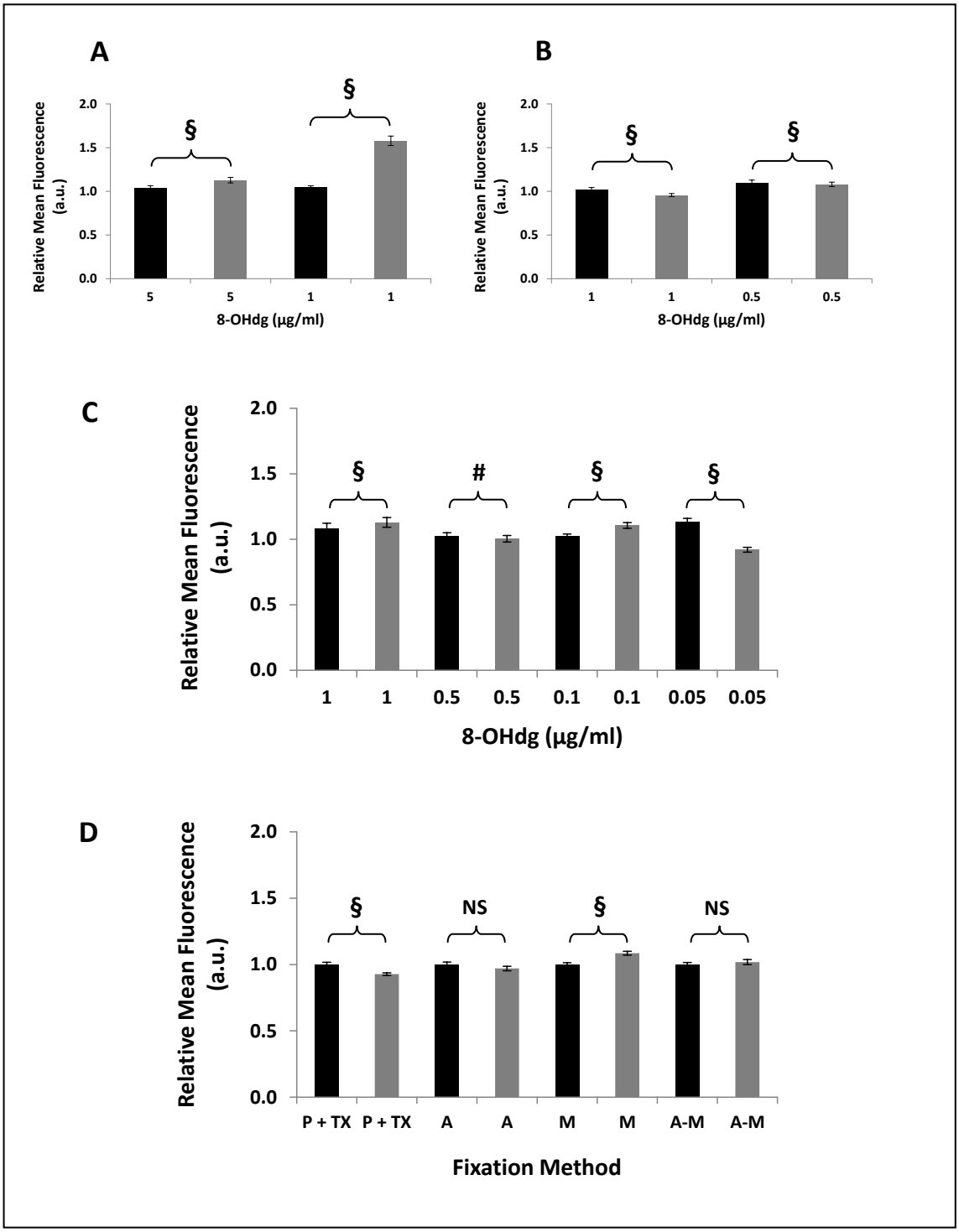

Figure 6.16: Optimisation of the 8 OHdG Antibody. HDFn cells were treated with either 100 µM H_2O_2 for 30 min (A + C) or 200 µM H_2O_2 for 60 min (B + D). Treatment with H_2O_2 is represented by (▪), treatment without H_2O_2 (control) is represented by (▪). The concentration of the 8-OHdG antibody was also varied; 5 µg/ml and 1 µg/ml (A), 1 µg/ml and 0.5 µg/ml (B), 1 µg/ml, 0.5 µg/ml, 0.1 µg/ml and 0.05 µg/ml (C) and 1 µg/ml (D). Further to this the fixation method for the immunofluorescence protocol was also varied (D) as follows; paraformaldehyde and Triton-X (P + TX), acetone (A), methanol (M) and acetone-methanol (A-M). For each experimental analysis >100 cells were assessed where mean FITC fluorescence was normalised to the relevant individual control, n=1 ± SEM, NS P>0.05, #P<0.01, §P<0.001). Data shows singular experiments due to variability; most notably of which is seen between experiments shown in A + B.

6.3.7 Determination of the Most Relevant Pathway Specific Gene Array to Encompass

Prior to pathway specific gene array analysis, two different pathway specific arrays were analysed for their usability in future experiments. These arrays included the human oxidative stress and antioxidant defence array (Figure 6.17; A) and the human mitochondrial energy metabolism array (Figure 6.17; B). Difference in gene expression between two samples is shown on the heat map as an increase in the intensity of the particular colour. With this analysis, red shows an up-regulation in expression and green shows a down-regulation, whereas grey shows that gene expression was not detected. This preliminary experiment showed many differences (more than 2-fold) in the expression of the genes utilised in the human oxidative stress and antioxidant defence array in HDFn cells exposed to TL01 (narrowband UVB) irradiation compared with TL12 (broadband UVB) irradiation. With the mitochondrial energy metabolism array there were less genes that showed a difference in expression in the cells exposed to the two different irradiation treatments. With this array there was indication that one gene was largely down-regulated with TL01 irradiation compared with TL12 irradiation however on further investigation there was an error with this particular samples PCR curve and therefore cannot be confirmed.

6.3.8 Analysis of the Difference in Expression of Genes Related to Oxidative Stress in Cells Exposed to Different UVR Sources.

Following the preliminary experiments shown in the previous section it was decided that the most relevant pathway specific array to use to further analyse the effect of the different UVR sources used in this study was the human oxidative stress and antioxidant defence array. This was because this array highlighted many more differences than the mitochondrial energy metabolism array. Due to the time between the ordering of the arrays the human oxidative stress and antioxidant defence array had been further optimised to the oxidative stress plus PCR array. These two arrays showed minor differences in the genes examined and therefore the oxidative stress plus PCR array was used for all further array experiments.

The oxidative stress plus PCR array comprised of the following genes (full details of the genes, as well as raw data can be found in Appendix III):

- Antioxidants
  - Glutathione Peroxidases (GPx) - GPX1, GPX2, GPX3, GPX4, GPX5, GSTP1, GSTZ1
  - Peroxiredoxins (TPx) - PRDX1, PRDX2, PRDX3, PRDX4, PRDX5, PRDX6 (AOP2)
  - Other Peroxidases - CAT, CYBB, CYGB, DUOX1, DUOX2, EPX, LPO, MPO, PTGS1, PTGS2 (COX2), TPO, TTN
  - Other Antioxidants - ALB, APOE, GSR, MT3, SELS, SOD1, SOD3, SRXN1, TXNRD1, TXNRD2
- Genes Involved in ROS Metabolism
  - Superoxide Dismutases (SOD) - SOD1, SOD2, SOD3
  - Other Genes Involved in Superoxide Metabolism - ALOX12, CCS, DUOX1, DUOX2, MT3, NCF1, NCF2, NOS2 (iNOS), NOX4, NOX5, UCP2
  - Other Genes Involved in ROS Metabolism - AOX1, BNIP3, EPHX2, MPV17, SFTPD
  - Oxidative Stress Responsive Genes - APOE, ATOX1, CAT, CCL5 (RANTES), CYGB, DHCR24, DUOX1, DUOX2, DUSP1 (PTPN16), EPX, FOXM1, FTH1, GCLC, GCLM, GPX1, GPX2, GPX3, GPX4, GPX5, GSR, GSS, HMOX1, HSPA1A, KRT1, LPO, MBL2, MPO, MSRA, NQO1, NUDT1, PDLIM1, PRDX2, PRDX5, PRDX6 (AOP2), PRNP, RNF7, SELS, SEPP1, SIRT2, SOD1, SOD2, SQSTM1, SRXN1, TPO, TTN, TXN, TXNRD1, TXNRD2.
- Oxygen Transporters - CYGB, MB.
- Pathway Activity Signature Genes - AKR1C2, BAG2, FHL2, GCLM, GLA, HMOX1, HSP90AA1, LHPP, NCOA7, NQO1, PTGR1, SLC7A11, SPINK1, TRAPPC6A, TXN, TXNRD1.

For reference to the analysed data, the layout of the different genes on the 96-well array is depicted in Figure 6.18 and relates to the heat maps shown in Figure 6.19 and Figure 6.20. For the array experiments HDFn cells were exposed to three different UVR sources. These were the TL12 (broadband UVB), TL01 (narrowband UVB) and the Cleo + filter (UVA). For consistency the cell were exposed to 1 SED of each of the

sources, which equated to ~0.04 J/cm^2, ~0.18 J/cm^2 and 19 J/cm^2 for the TL12, TL01 and Cleo + filter respectively. Initial analysis was the comparison of each of the different UVR sources and an un-irradiated control (Figure 6.19). Further analysis saw comparisons between the different UVR sources (Figure 6.20).

Four genes were not expressed in any of the treated or the control cells; these were Albumin (ALB), Glutathione peroxidase 5 (GPX5), Keratin 1 (KRT1) and thyroid peroxidase (TPO). Furthermore the expression of several of the genes remained unchanged across the treated and control cells. UVB treated cells (TL12 and TL01) generally caused more of a widespread down-regulation of gene expression when compared with the un-irradiated control than UVA did (Cleo + filter). Three genes were identified showing a consistent up-regulation with all UVR exposures when compared with the un-irradiated control, these were as follows: glutathione reductase (GSR), methionine sulfoxide reductase A (MSRA) and neutrophil cytosolic factor 1 (NCF1).

When the difference in expression between the UVR treatments was investigated, a more widespread down-regulation of expression was seen in the UVB (TL12 and TL01) treatments compared with the UVA (Cleo + filter) treatment. Furthermore a wider spread of up-regulation of gene expression was seen in the TL12 treated cells compared with the TL01 treated cells. The largest differences in expression between the TL12 and the TL01 treatments saw an up-regulation of dual oxidase 2 (DUOX2) and a down-regulation of nitric oxidase synthase 2, inducible (NOS2) in the TL12 treated cells compared with the TL01 treated. The major consistent difference between the UVB treatments compared with the UVA treatment saw a down-regulation of neutrophil cytosolic factor 1 (NCF1).

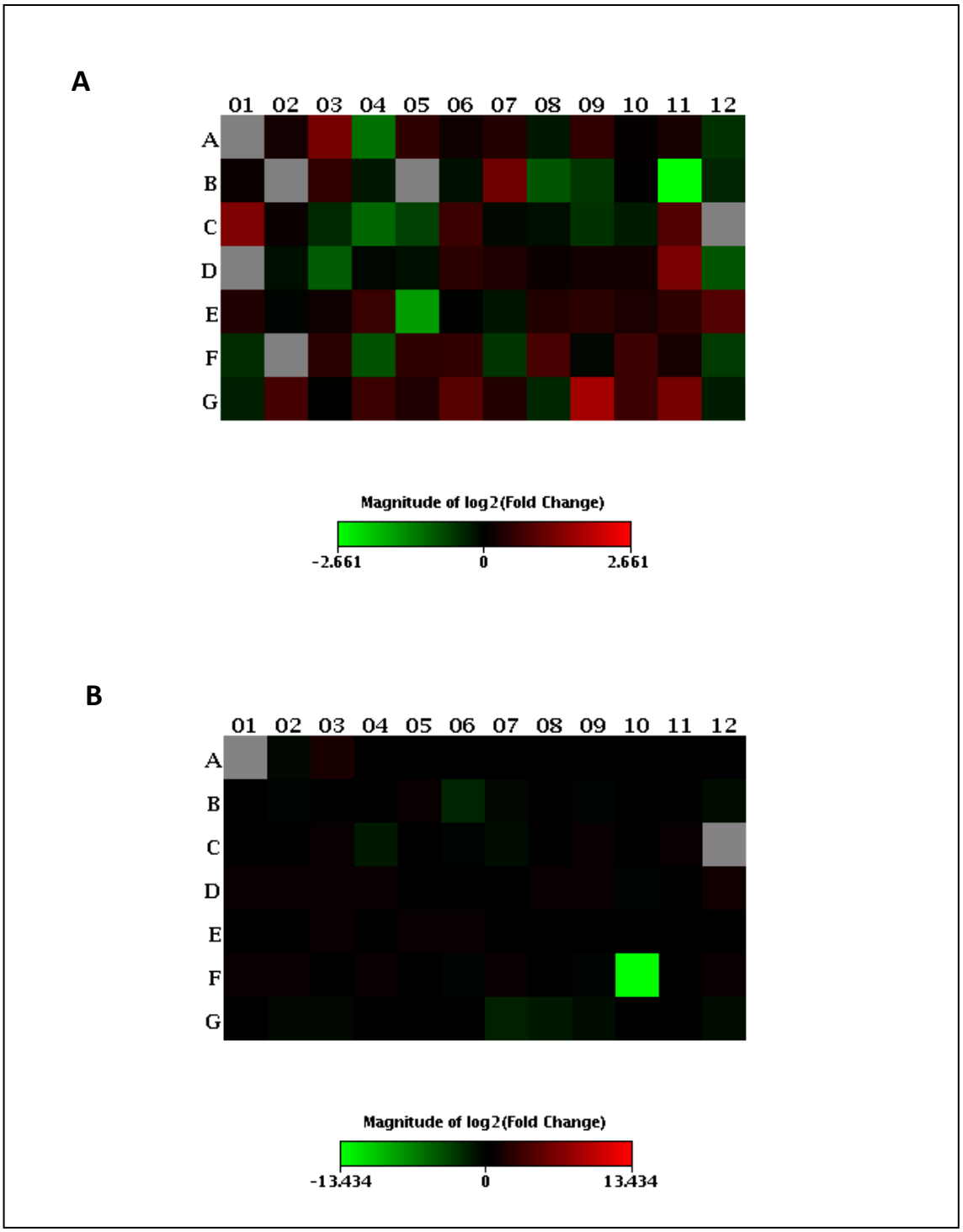

Figure 6.17: Heat Map Analysis of the Difference between TL12 and TL01 Irradiation on Genes Related to either Oxidative Stress and Antioxidant Defence or Mitochondrial Energy Metabolism. HDFn cells were irradiated with either 0.8 J/cm^2 TL12 or 3.5 J/cm^2 TL01 (the equivalent of 20 SEDs). Analysis of this difference in gene expression encompassed the use of pathway specific 96-well plate gene arrays. It utilised both (A) the human oxidative stress and antioxidant defence array (PAHS-065A) and (B) the human mitochondrial energy metabolism array (PAHS-008C-2). The data shows the fold change in expression in cells irradiated with TL01 when compared with cells irradiated with TL12. Red shows up-regulation, green shows down-regulation, grey shows that the gene expression was not detected.

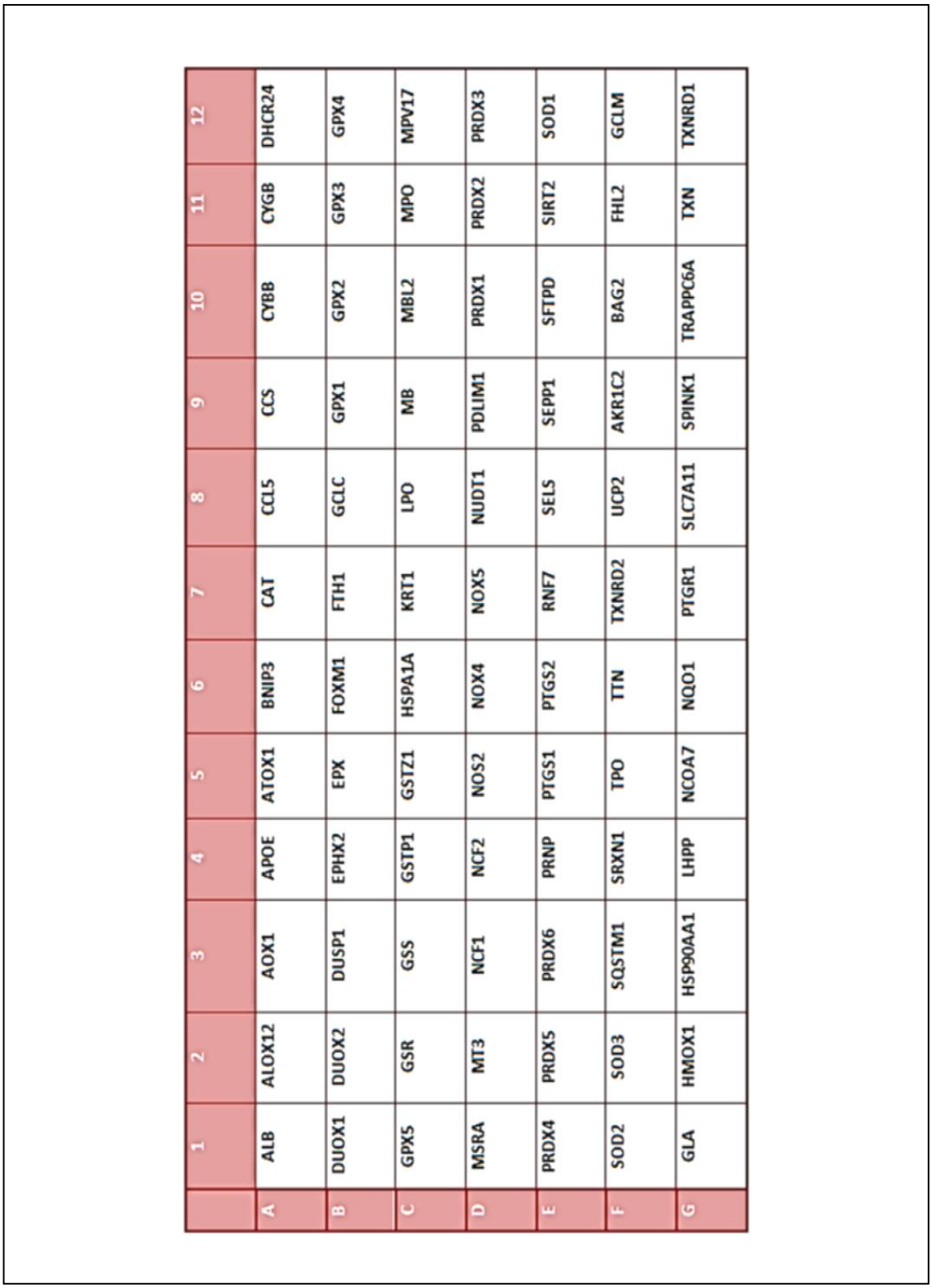

	1	2	3	4	5	6	7	8	9	10	11	12
A	ALB	ALOX12	AOX1	APOE	ATOX1	BNIP3	CAT	CCL5	CCS	CYBB	CYGB	DHCR24
B	DUOX1	DUOX2	DUSP1	EPHX2	EPX	FOXM1	FTH1	GCLC	GPX1	GPX2	GPX3	GPX4
C	GPX5	GSR	GSS	GSTP1	GSTZ1	HSPA1A	KRT1	LPO	MB	MBL2	MPO	MPV17
D	MSRA	MT3	NCF1	NCF2	NOS2	NOX4	NOX5	NUDT1	PDLIM1	PRDX1	PRDX2	PRDX3
E	PRDX4	PRDX5	PRDX6	PRNP	PTGS1	PTGS2	RNF7	SELS	SEPP1	SFTPD	SIRT2	SOD1
F	SOD2	SOD3	SQSTM1	SRXN1	TPO	TTN	TXNRD2	UCP2	AKR1C2	BAG2	FHL2	GCLM
G	GLA	HMOX1	HSP90AA1	LHPP	NCOA7	NQO1	PTGR1	SLC7A11	SPINK1	TRAPPC6A	TXN	TXNRD1

Figure 6.18: Plate Layout of Genes on the Oxidative Stress Plus 96-Well Plate Gene Array. For reference for the following heat maps this figure shows a schematic representation of the layout of the 84 genes associated with the oxidative stress plus 96-well plate gene array (PAHS-065Y).

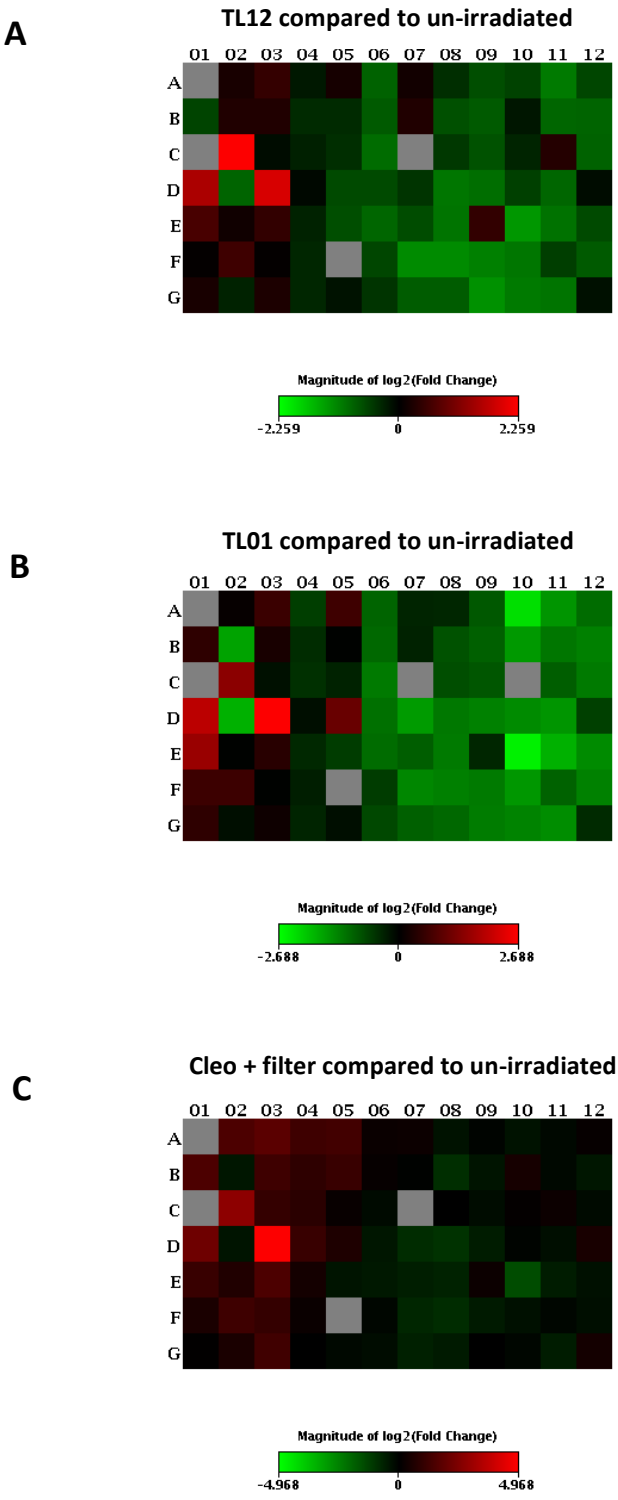

Figure 6.19: Differential Gene Expression in HDFn Cells when Exposed to Various UVR when Compared to a Control. HDFn cells were exposed to ~0.04 J/cm^2 TL12 (A), ~0.18 J/cm^2 TL01 (B) or 19 J/cm^2 Cleo + filter (C) (the equivalent of 1 SED). Analysis of gene expression encompassed the use of a pathway specific 96-well plate gene array - the oxidative stress plus array (PAHS-065Y). The data shows the fold change in expression in cells irradiated with the various UVR compared with un-irradiated control cells (n=2). Red shows up-regulation, green shows down-regulation, grey shows that the gene expression was not detected.

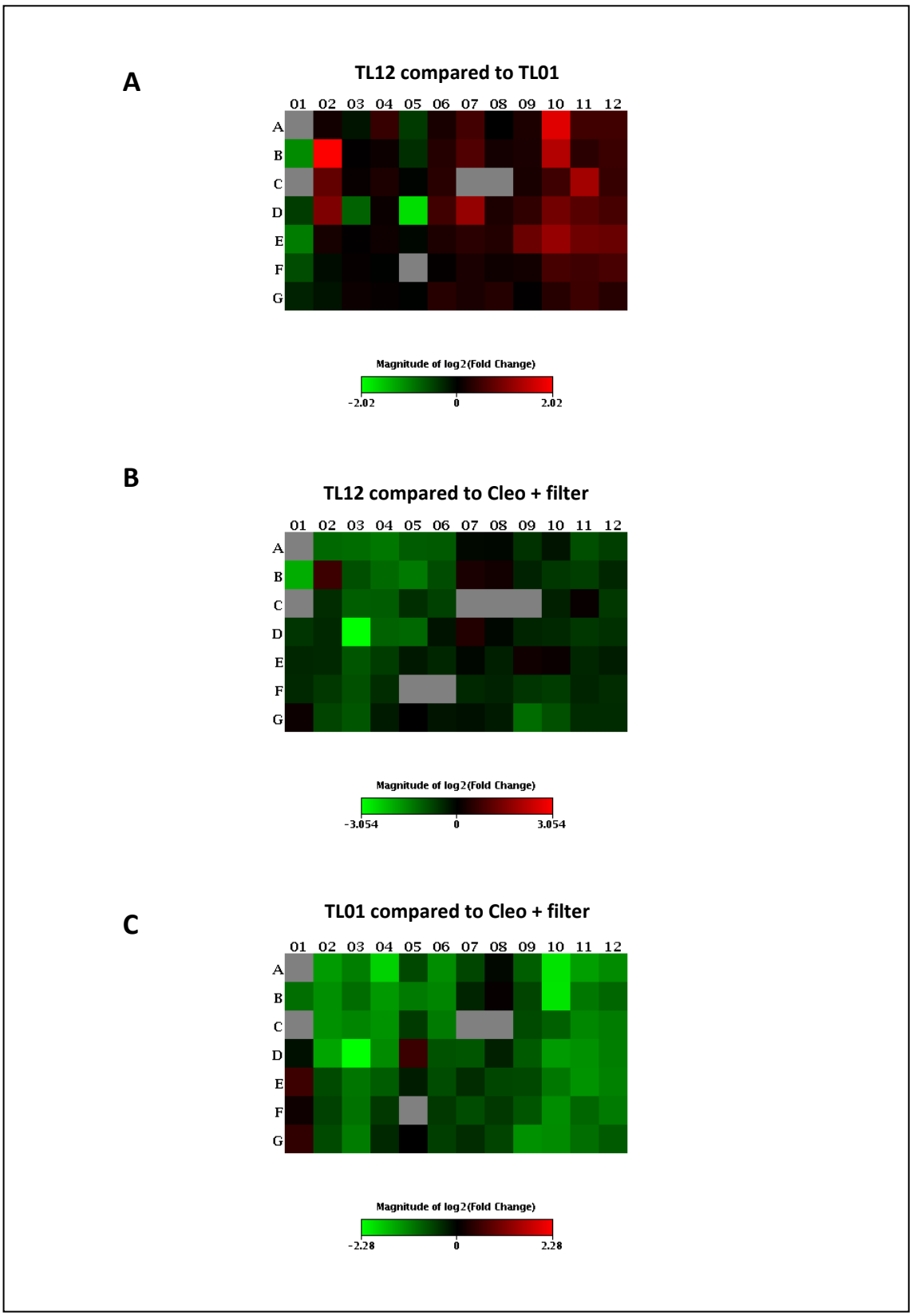

Figure 6.20: Differential Gene Expression in HDFn Cells when Exposed to Emissions from Different UVR Sources. HDFn cells were exposed to ~0.04 J/cm^2 TL12, ~0.18 J/cm^2 TL01 or 19 J/cm^2 Cleo + filter (the equivalent of 1 SED). Analysis of gene expression encompassed the use of a pathway specific 96-well plate gene array - the oxidative stress plus array (PAHS-065Y). The data shows the fold change in expression in cells irradiated with TL12 compared with TL01 (A) or Cleo + filter (B) and TL01 compared with Cleo + filter (C) (n=2). Red shows up-regulation, green shows down-regulation, grey shows that the gene expression was not detected.

6.4 Discussion

6.4.1 No Mutations found within Exons 5-9 of the p53 Gene of UVR Irradiated HDFn Cells

For this analysis only the irradiated HDFn samples were used because HaCaT cells have an altered p53 gene which may have affected the results. Mutations within the p53 gene are associated with chronic exposure to UVR and analyses have shown that tumour mutations outside exons 5 to 9 are rare (Hollstein *et al.*, 1991). This study sought to determine whether any mutations developed within this gene upon irradiation with the maximal acute doses of the various UVR sources used throughout this study.

Following DHPLC performed on the WAVE, analysis of exons 5-9 showed only single peaks. This indicates an absence of mutations in the p53 gene with these acute doses of UVR within these exons. A small second peak is visible from the traces, which was attributed to normal miss-incorporation due to the polymerase. This effect of acute UVR exposure was also noted by Huang *et al.*, 2009, who found that mutations in exons 5-9 of the p53 gene could not be induced in cells of engineered human skin, irradiated with either UVA and UVB, until they had received a minimum of four exposures (Huang *et al.*, 2009).

6.4.2 An Inconsistent Dose-Dependent Induction of Photoproducts was seen with the Various UVR Sources

Figure 6.7 demonstrated a clear correlation between the induction of CPDs (as detected by its relevant antibody) and the nucleus (as detected by the nuclear stain dapi). The correlation between CPDs and the mitochondria (as detected by MitoTracker) was much less strong, indicating a higher prevalence in the nucleus. This led to investigations of photoproduct induction solely within nDNA.

The UVR sources chosen for this investigation were not of the complete set seen in previous chapters. Due to time restraints, sources that still covered the most biologically relevant UVA/UVB spectrum were utilised. A loose dose-dependent increase in the induction of CPDs and 6-4 PPs with the various UVR sources

investigated was seen. Furthermore induction of CPDs tended to be higher than 6-4 PP induction with the exception of irradiation with the Cleo + filter UVR source (100 % UVA).

The maximum doses used were 3.2 (TL12), 14 (TL01), 20 (Helarium), 80 (Arimed B) and 100 J/cm^2 (Cleo + filter) which are the approximate equivalents of 80, 80, 40, 45 and 5 SEDs. The high initial doses were chosen in an aim to create dose curves; however with the minimal approach used it was difficult to determine whether maximum damage had been reached Figure 6.10. This meant that by fitting with a three parameter sigmoidal plot gave rise to high estimates for maximum damage which would create flaws in the determination of an action spectrum. The high SED values were not able to be maintained across the differential UVR source exposure due to unrealistic irradiation times which would have severely compromised cell viability. Nonetheless, Figure 6.10 shows that the induction of photoproducts was wavelength dependent, depicted by the shift to the right in the dose curve when the cells were irradiated with UVR sources of a higher long wavelength (UVA) content.

With the exception of the TL01 UVR source, a decrease in induction of both types of photoproducts was seen with a decrease in the in the amount of “UVB” each UVR source emitted, see Figure 6.21. An interesting observation shows that TL01 induced similar 1.9 fold and 1.5 fold increases in CPDs and 6-4 PPs respectively, when compared to the 2.0 fold and 1.4 fold increases seen with Arimed B. When comparing the spectra of these two lamps the shorter wavelengths emitted begin within approximately 10 nm of each other, perhaps indicating that it is these shorter wavelengths that are key for photoproduct induction with these two lamps.

A less dependable dose response was seen in the induction of photoproducts in Primary Keratinocytes although an increase was created by all UVR sources. This was with the exception of Cleo + filter induced 6-4 PPs where no difference was seen. Due to the inconsistencies dose curves could not be plotted and consequently no action spectrum determined. It is possible higher doses may have created a more dose-dependent effect in Primary Keratinocyte cells, however time restraints meant that this could not be investigated.

It was unsurprising that the UVB associated lamps caused a greater induction of photoproducts as this division of UVR is well known to be a major cause (Ravanat *et al.*, 2001). A recent report by Tewari *et al*., 2012 looked at the induction of both CPDs and 6-4 PPs in human skin by either UVB or UVA1 (340-400 nm). They found a higher induction of CPDs with UVB than UVA1, and that UVA1 was unable to create 6-4 PPs (Tewari *et al.*, 2012). This conflicts slightly with that found in this study, where a small increase in 6-4 PPs by Cleo + filter was seen in HDFn cells (but not Primary Keratinocytes). However this can be accounted for by the difference in UVA source as wavelengths 320-340 nm are not emitted from the UVA1 used in the Tewari study. Further to this the doses of UVR used were much lower (~31-61 J/cm^2).

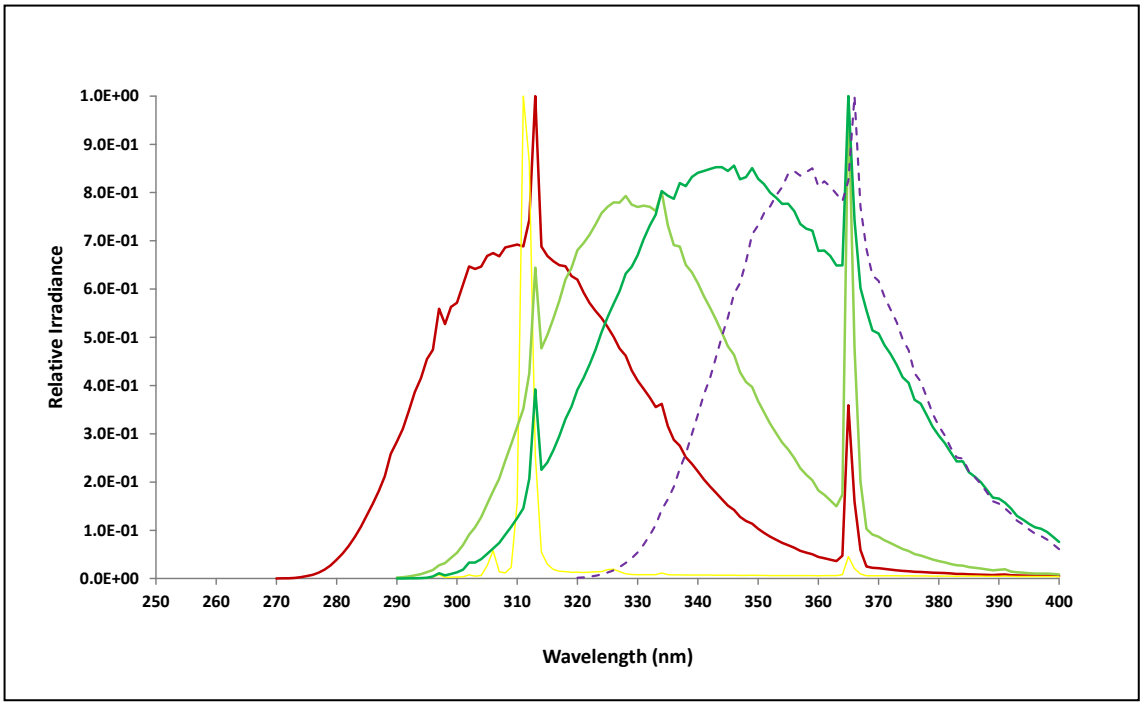

Figure 6.21: Spectral Chart Adapted from Chapter 3. This figure shows the spectral output of the different UVR lamps used in the study and is adapted from that found in chapter 3. The various lamps are as follows: TL12 (-),TL01 (-), Helarium (-), Armed B (-), Cleo + filter (--).

A desirable aim of this chapter was determine a new, more relevant, UVR-induced action spectrum of nDNA damage. The previously utilised UVR-induced action spectrum of nDNA damage by Setlow (Setlow, 1974) was not entirely relevant to the discussions of this thesis as it determined photoproduct formation in the DNA of E.*coli* cells (Setlow and Carrier, 1966). Due to the time restraints that any study has to cope with, the collection of this data was stringently cut to just four data points per UVR source. This unfortunately produced less defined dose response curves which would

create an inaccurate action spectrum. Therefore this action spectrum was not determined. However the data produced did follow the same pattern of Setlow's action spectrum where the shorter wavelengths are more proficient in creating photoproducts, meaning that they considered more detrimental in nDNA.

6.4.3 Tiron Offered Protection of UVR-Induced Photoproducts

Work within our research group by Dr Anne Oyewole has found that the antioxidant Tiron can offer 100 % protection to mtDNA damage (assessed by the 11 kb assay) in HDFn cells irradiated with UVA. It was therefore interesting to discover whether Tiron could offer similar protection to damage within nDNA.

This data shows that Tiron was able to offer protection against UVR-induced photoproducts and that this protection was found to be greater against photoproducts induced by the Cleo + filter UVR source (100 % UVA). Further to this, the protection of Tiron was higher against UVR-induced CPDs compared to 6-4 PPs.

The fact that Tiron offered more protection to UVA-induced photoproducts than UVB-induced collaborates with other laboratory findings. It also supports the notion that Tiron acts as a ROS scavenger (Taiwo, 2008), due to UVAs indirect damaging effect by ROS production compared with UVB which has a more direct DNA absorbing effect (Ichihashi *et al.*, 2003; Tewari *et al.*, 2012).

Tiron did offer a reduced amount of protection against TL12-induced photoproducts (broadband UVB) and an intermediary amount of protection against Arimed B-induced CPDs (closest to sunlight). These differences in the ability of Tiron to protect correlate well with each of the UVR sources long wavelength (UVA) content. This was again possibly due to the ROS scavenging mechanism by which Tiron acts as the protection maps well with damage via ROS production (Taiwo, 2008). There is a fine line between the UVA and UVB divisions and the boundary wavelengths will encompass properties which are not typically known as UVA or UVB and indeed the crude determination of "UVB-irradiation" also produces ROS to a lesser extent (Ichihashi *et al.*, 2003).

As previously mentioned there is no definite boundary between the divisions of UVR and consequently the shorter wavelengths of UVA may behave similarly to UVB and

act directly upon DNA. This may account for why Tiron did not offer a higher degree of protection against photoproducts induced by the Cleo + filter (100 % UVA) UVR source. Another possibility could be due to the fact that irradiation with UVA, as well as ROS production, can lead to the rise in intracellular iron, consequentially leading to a further production of ROS (Pygmalion *et al.*, 2010). The metal chelating capabilities of Tiron (Nirala *et al.*, 2009) could mean its ability to reduce ROS is due to the reduction in ROS associated with UVA-induced iron production (Pygmalion *et al.*, 2010). Another observation of this data identified that Tiron provided greater protection against CPDs compared to 6-4 PPs, with both sources of UVR-irradiation. This could correlate well with this theory because, as previously discussed, 6-4 PPs are largely UVB-induced (Tewari *et al.*, 2012).

Nonetheless, based on this study, Tiron can offer a significant amount of protection against UVR-induced nDNA damage in HDFn cells. This is predominantly seen against UVA damage, the major constituent of sunlight (94 % (Paz *et al.*, 2008)), and therefore Tiron could be potentially used as a protective agent against the damage created by sun exposure.

6.4.4 The Optimisation of the 8-OHdg Antibody was Unsuccessful

Optimisation of the 8-OHdG antibody was sought after as it would detect the 8-OHdg oxidative DNA lesion which was a desirable marker of UVR-induced oxidative damage. Initial optimisation utilised a treatment of H_2O_2 which would cause substantial oxidative stress. Unfortunately various methods identified that this particular antibody poorly detected this marker of oxidative damage in HDFn cells. Optimisation was halted as it was thought uneconomical to continue.

The variation that the antibody showed in its detection of the oxidative damage marker was wide. Increases in the concentration of the antibody caused no clear or consistent pattern in detection of fluorescence. Further to this irregularities were seen between experiments. Nonetheless the changes seen in fluorescence in comparison to the control were considered to be statistically significant ($P<0.001$) however these changes were minor in comparison to the previous data for the detection of photoproducts. Due to the variability between experiments no definite conclusions

were drawn from the highly significant fluctuations; owing perhaps to the analysis of a large group size (>100 cells).

Following MTS analysis the optimal dose of H_2O_2 determined was 100 µM for 30 min as it was decided this dose would be sufficient to induce considerable oxidative damage whilst maintaining adequate cell viability. To further support this decision Li *et al*., 2006 found a similar dose of H_2O_2 created a high increase in 8-OHdG detected by immunofluorescence in cardiomyocytes (Li *et al.*, 2006). Furthermore comparable doses of H_2O_2 are frequently used within our laboratory to elicit substantial mtDNA damage. This means that the 8-OHdG antibody lacked sensitivity for detecting oxidative damage as consistently considerable increases of oxidative damage should have been shown with this H_2O_2 treatment. An additional experiment explored the effect of alternative fixation methods within the immunofluorescence protocol. However, altering the fixation method had no effect on the sensitivity of the antibody.

Little data reports on the use of this particular antibody in immunofluorescence especially in cells, and not at all in skin cells to my knowledge. The manufacturer's identified one study (Lee *et al.*, 2008) who used the 8-OHdg antibody as a marker for oxidative damage in lung fibroblasts. However, although an increase in 8-OHdg was reported following a substantial dose of 300 µM H_2O_2 for 2 h, the actual microscope images are not so clear. I find it difficult to judge a strong increase in fluorescence between the control and the H_2O_2 treated images, further to this the background staining of the control images is quite high. This is also true for their DAPI staining showing poor images overall.

There tends to be large inconsistencies across laboratories for the detection of 8-OHdg, such as the exaggeration of background levels meaning a wide variation in results. Further to this the preferential method for the detection of 8-OHdg is by HPLC, which has shown to deliver high sensitivity (Valavanidis *et al.*, 2009). This, coupled with the lack of literature on immunofluorescence 8-OHdg detection, supports the decision to abandon further work with this antibody. This particular investigation was beyond the remit of this PhD, had this been the main focus a HPLC method would have been followed.

6.4.5 The Human Oxidative Stress and Antioxidant Defence Array was most Relevant for this Study

Free samples of the Qiagen 96-well, pathway specific, PCR arrays were obtained by our laboratory and therefore stringent preliminary experiments were planned. These experiments aimed to determine which plate from two identified possible pathways (human oxidative stress and antioxidant defence or mitochondrial energy metabolism) would give us the most usable data. Differences were made between cells irradiated with TL12 (broadband UVB) and those irradiated with TL01 (narrowband UVB). The preliminary data demonstrated more difference in the expression of genes found on the human oxidative stress and antioxidant defence plate as opposed to the mitochondrial energy metabolism plate. This determined that further experiments would encompass the use of the human oxidative stress and antioxidant defence plate (now updated to the oxidative stress plus PCR array).

6.4.6 Array Analysis

Array analysis sought to detect differences in the expression on 84 genes related to oxidative stress when cells were exposed acute UVR treatments. Due to expense and time constraints these experiments were carefully selected identifying minimal experiments that would deliver the most meaningful results. Therefore HDFn cells were chosen as the cell of choice, this minimised any donor differences that would have been present in Primary Keratinocytes. Furthermore levels of protein oxidation levels in epidermal cells are generally very low, even with UVR-exposure (Sander *et al.*, 2002). As well as this only three UVR treatments were chosen for analysis. For these experiments the HDFn cells were exposed to TL12 (broadband UVB), TL01 (narrowband UVB) and the Cleo + filter (UVA) at a constant dose of 1 SED. This equated to ~0.04 J/cm^2, ~0.18 J/cm^2 and 19 J/cm^2 respectively. Heat map analysis consisted of the comparison of each of the different UVR sources with an un-irradiated control as well as comparisons between the different UVR sources themselves.

The following genes were not found to be expressed in any of the treated or the control cells; these were ALB, GPX5, KRT1 and TPO. This was not surprising as these proteins are normally associated with blood (Sugio *et al.*, 1999), epididymal epithelium

(Williams *et al.*, 1998), the epidermis (Gene, 2013a) and the thyroid (Kimura *et al.*, 1987) rather than dermal fibroblasts. This highlights that there are still in-specificities with this type of array analysis. Furthermore, UVB treated cells (TL12 and TL01) generally caused more of a widespread down-regulation of gene expression when compared with the un-irradiated control than UVA did (Cleo + filter). An effect possibly due to the suggestion that UVB can elicit free radical production as well as induce a significant decrease in skin antioxidants (Svobodova *et al.*, 2006).

Three genes were identified as showing a consistent up-regulation with all UVR exposures when compared with the un-irradiated control, these were as follows: GSR, MSRA and NCF1.

The enzyme GSR reduces glutathione disulphide to GSH, an important cellular antioxidant, and is therefore activated in a response to oxidative stress. Mainly associated with the epidermis, up-regulation has been reported with low UVA exposure in human skin equivalents (Meloni *et al.*, 2010). However Marionnet *et al*., 2010 found no increase in keratinocytes or fibroblasts irradiated with 13 J/cm^2 of a UVR source which mimicked non-zenithal UVR, 2, 6 or 24 h following exposure (Marionnet *et al.*, 2010). A further study was also unable to induce an increase in expression following a 12 J/cm^2 UVA irradiation 0-5 days following exposure (Shindo and Hashimoto, 1997). However activity of this enzyme has been reported to have been found within both the dermis and epidermis (Shindo *et al.*, 1994) and therefore the induction by UVR is not unlikely. Differences in irradiations protocols, UVR sources and doses could be the reasoning behind the disparities between studies.

MSRA reduces the products of methionine oxidation; methionine-S-sulfoxide and methionine-R-sulfoxide. MSRA has been found to be present in keratinocytes, melanocytes and dermal fibroblasts; however information about this system during UVR exposure is minimal. An up-regulation of MSRA has been reported in HaCaT cells exposed to low doses of UVA; conversely this was not mirrored with an acute 5 mJ/cm^2 UVB irradiation when examined 24 h following irradiaiton (Ogawa *et al.*, 2006). The conflict seen when compared to the study in this thesis could be due to the difference in dose which was eight times lower (using a broadband UVR source similar to the

TL12) as well as variations in the time between irradiation an analysis. Interestingly, 24 h following a high UVA dose of 15 J/cm^2 Picot *et al*., 2007 found that the MSRA protein was reduced in keratinocytes, as well as a similar reduction in sun-exposed skin as opposed to sun-protected skin. They deduced that this was due to the direct effect of UVA on the protein itself at these high doses (Picot *et al.*, 2007).

NCF1, also known as p47 phox, is a cytosolic subunit of NADPH oxidase (Gene, 2013b). Stimulation of NADPH oxidase leads to an increase in ROS, the superoxide anion specifically (Tyrrell, 2012). No data, to my knowledge, describes the occurrence of NCF1, in particular, in the skin or the effect that UVR may have on it. However, the induction of NADPH oxidase, primarily by UVA, is a well-known source for ROS generation in the skin (Tyrrell, 2012). I suggest that this up-regulation of NCF1 expression in UVR exposed cells may be the initial steps leading to an increase in NADPH oxidase and therefore cellular oxidative stress. Support for NADPH oxidase induction in response to predominantly UVA exposure was shown by a down-regulation of the expression of NCF1 in cells exposed to the UVB treatments compared with the UVA treatment.

These findings show that an acute induction, of all the UVR sources investigated, caused an increase in the expression of genes associated proteins which cause an increase in ROS. Even at this early stage this this UVR can also trigger the expression of genes associated with oxidative stress response. With this in mind, it was also found that there was a down-regulation of the majority of expressed genes in cells exposed to the UVB (TL12 and TL01) treatments compared with the UVA (Cleo + filter) treatment. This highlights how the different wavelengths of UVR create damage differently, and supports that the damaging effects of UVA are primarily via ROS production. This is further supported by the fact that an up-regulation of gene expression was seen in the TL12 treated cells compared with the TL01 treated cells. The broadband nature of the TL12 UVR source means that a wider spread of wavelengths are emitted, although some shorter than the TL01 UVR source some are also longer – including some in the UVA range. This means that these longer wavelengths, although minimal, are sufficient to create damage via oxidative stress.

When expression in cells exposed to TL12 was compared with TL01 treatments, a major up-regulation of DUOX2, a NADPH oxidase, was seen. DUOX2 is expressed in human fibroblasts and is associated with the generation of ROS (Salmeen *et al.*, 2010). This again shows that the small numbers of UVA wavelengths emitted by the TL12 lamp are sufficient enough to cause more of an induction than the narrowband UVB source. Further comparison of these two different UVB treatments also saw a down-regulation of NOS2. NOS2 is an isoform of nitric oxide synthase a primary inducer of the RNS NO. NOS2 is usually expressed in response to inflammation and can be found in inflammatory skin diseases such as psoriasis and atopic dermatitis. Found expressed in the epidermis and the dermis normal human skin, the UVR-induction of NOS2 is largely associated with UVB irradiation. However the irradiation of inflammatory skin disorders actually causes a reduction in NOS2 expression (Cals-Grierson and Ormerod, 2004). The induction of NO is well known to be induced by both UVA and UVB (Aitken *et al.*, 2007) however my research did not uncover any direct comparisons. This observation therefore may underline differential induction of ROS/RNS with UVA or UVB induction. This would suggest that UVA predominates in ROS production and UVB in RNS.

This data recognises particular genes which are differentially expressed following an acute dose of UVR and which therefore may identify early signalling pathways involved in the response to UVR stress. Although some of these effects have previously been demonstrated the variance between different UVR sources is not extensive. This means early detection of gene expression could be related to the type of UVR damage created.

6.4.7 Summary

No mutations were found within exons 5-9 of the p53 gene of acutely UVR irradiated HDFn cells.

UVR caused a wavelength dependent increase of photoproducts in the nDNA of HDFn and Primary Keratinocyte cells. These increases were loosely dose-dependent, but not of a quality of which an action spectrum could be determined.

The antioxidant Tiron offered more protection to UVA-induced photoproducts than UVB-induced photoproducts, showing its potential as sunlight protection agent.

The 8-OXdg antibody was not sensitive enough to detect oxidative damage by immunofluorescence.

The array analysis recognised particular genes which are differentially expressed following an acute dose of UVR, and which therefore may identify early signalling pathways involved in the response to UVR stress. It also led to the consideration of potential differences in ROS and RNS induction by either UVA or UVB exposure.

Chapter 7

Discussion

Chapter 7 Discussion

7.1 Overview

UVR is well known to be harmful to the skin; various studies have implicated its contribution to induction of erythema (McKinlay and Diffey, 1987), nDNA damage (Setlow, 1974), carcinogenesis (Degruijl *et al.*, 1993) as well as photo-ageing. This thesis supports this, finding that UVR was a severely detrimental entity to human skin. Although this is not a new concept, the methods utilised and specifics investigated are.

The major result of this thesis was the determination of UVR wavelength specific damaging of mtDNA, by the modelling of an action spectrum. Due to the close proximity of mtDNA to the ETC and UVA's effect being predominantly via ROS production (Ichihashi *et al.*, 2003) it was initially hypothesised that UVA could have a greater detrimental effect on the mtDNA than nDNA. Determining the action spectrum of UVR- induced mtDNA damage in HDFn and HaCaT cells has shown that this notion could possibly be correct. However this was not confirmed in the action spectrum prediction of UVR-induced mtDNA in damage Primary Keratinocytes, potentially due to the heterogeneity of these cells.

Subsequent investigations have identified other methods for the examination of detrimental UVR-induced cellular effects. Some of these methods have proved to produce quantitative assessment of which could be utilised to evaluate the effectiveness of UVR-protecting/UVR damage modifying treatments.

7.2 Irradiation Procedures

The initial investigations aimed to optimise experimental procedures and discover any hindrances which could have affected future experiments. This was required to minimise errors and reduce time spent on unnecessary procedures.

The foremost task was to determine the spectral output of the UVR sources obtained for the potential further use in this thesis. The main requirement of these UVR sources

was for them to overlap and cover the entire UVA and UVB spectrum. This is because, to determine an action spectrum of a specific entity of radiation, all the wavelengths should be covered. The use of a monochromator for such an investigation would be less efficient. The measurement at every wavelength would prove unrealistically time consuming, and the selection of specific wavelengths would lead to an uncertainty of those not measured. Furthermore the irradiance from a monochromator is low, leading to impractically time consuming experiments with potential effects on cell viability. The use of fewer UVR sources emitting a wider span of wavelengths has been successfully validated (Flockhart *et al.*, 2008) and represents a method which measures the effect of the entire wavelength span. As well as the UVA and UVB emitting lamps a Germicidal lamp was used to add completion to the data by means of a UVC dimension. However this lamp only covered a narrowband of chiefly UVC, peaking at 252 nm. This lead to an uncertainty of the effect of the wavelengths between 255-270 nm; therefore the data from this UVR source was not included into the action spectrum analysis in Chapter 4. However, data on this UVR source was produced in Chapters 3 and 4 showing a higher amount of cell death and mtDNA damage, respectively, compared to all of the other UVR sources used. The effect of UVC is not biologically relevant as its wavelengths do not reach the earth's surface (Lloyd, 2006) and therefore the exclusion of the Germicidal lamp data from the action spectrum was no considered detrimental to the overall aim.

Evaluation of UVR distribution highlighted the importance of standard protocols for cell placement and precise UVR measurements for accurate data collection. Furthermore investigations into cellular heating without UVR exposure as well as the effect of differential irradiation media saw no difference in mtDNA damage when using the 11 kb assay. This was important as, even though no difference was seen, any effect by these variables could have led to problems in analysis and inaccuracies in later experiments.

7.3 UVR Source Specific Induced Cell Death

The viability of cells exposed to UVR is quite well reported; however the data usually involves the crude separation of just UVA and UVB and does not determine specific

UVR source effects. Although some literature describes the spectra of the sources utilised, they usually incorporate solar simulators and the use of filters. Therefore comparisons to the numerous UVR sources used in this thesis were difficult. Loose comparisons of the data obtained established similarities in the tendencies for death in cells exposed to UVR which supported the MTS assay as an adequate measure for cell viability. Furthermore, variables meant that it was necessary to determine cell death using the experimental procedures in this thesis for accurate analysis of viability following exposures from the various UVR sources.

A dose-dependent decrease in cell viability was apparent and, as a general rule, the longer the wavelengths that the UVR source emitted the higher the dose required to cause the same amount of cell death. This trend for shorter wavelengths of UVR to cause more cell death is well reported in various cell types (Andley *et al.*, 1994; Aoki *et al.*, 2004). The HaCaT cells were, for the most part, consistently more resistant to UVR than the HDFn cells; an effect between keratinocytes and dermal fibroblasts which has previously been reported (Otto *et al.*, 1999).

It was important to clarify at what doses the cells were susceptible to death for determination of the action spectrum in Chapter 4. Prior to, and a requirement of, the modelling of the action spectrum was the production of dose curves of mtDNA damage. To produce adequate dose curves of mtDNA damage, where a plateau was reached high doses of UVR were needed. With some of the UVR sources the maximum doses would have also caused substantial cell death. Therefore to ensure that effects seen were not confounded by cell death a consistent low value of the dose required to induce just a 10 % increase in damage was utilised in action spectrum analysis. This value was low so only minimal cell death would be occurring but also at a point where the dose curves were extending, producing a comparable value for the different UVR sources.

7.4 The effect of UVR exposure on mtDNA content

A constant amount of total cellular DNA was used as a non-variable in the various PCR analyses for mtDNA detention shown in Chapter 4. To avoid inaccuracies in damage detection it was critical that total cellular amount consistently related to the same

quantity of mtDNA across samples. mtDNA is well known to vary between individual subjects as well as between an individual's tissues and can also differ with the age of the sample (Venegas *et al.*, 2011). To my knowledge, no data exists however on the effect of UVR on mtDNA copy number in cultures cells. This study found that both an acute and repeated exposure of the various cell types to a selection of the UVR sources had no effect on mtDNA content. This meant that there was no need for the correction of DNA amount used in the PCR analysis.

7.5 Determining the Action Spectrum of UVR-Induced mtDNA Damage

Modelling of the action spectra employed the use of a three-exponential curve. A curve of this type matched that of the previously determined action spectrums used for comparison in this thesis (UVR-induced erythema and nDNA damage) which were fitted to a model with two inflection points which decreased exponentially.

The action spectra for UVR-induced mtDNA damage in all three cell types seemed more sensitive to the shorter wavelengths of UVR compared to the nDNA damage action spectrum (Setlow and Carrier, 1966). However not too many conclusions can be drawn from this because the action spectrum of UVR-induced nDNA damage was not performed in skin cells. Attempts were made at producing a more relevant comparison, however time and experimental limitations proved this aim unfeasible.

The action spectrum of UVR-induced mtDNA damage in HDFn and HaCaT cells differed from that in Primary Keratinocytes; the difference saw that with an increase in wavelengths from 320 nm, another increase in damage started to occur. This possibly suggests an increase in vulnerability of the mtDNA of these cells to wavelengths in the UVA range. Although further modelling including a dimension of error could clarify this finding.

A consistent increase in sensitivity of HDFn cells to all the wavelengths of UVR was seen compared to HaCaT and Primary Keratinocytes. A higher sensitivity of dermal fibroblasts to UVR has been previously reported by several research groups (Bernerd and Asselineau, 1998; Otto *et al.*, 1999; Marionnet *et al.*, 2010). It has also been shown

throughout this thesis. Differences in cell viability were noted, and the induction of photoproducts in (Chapter 6) was more apparent in HDFn cells than Primary Keratinocytes. This increased sensitivity could possibly due to an increased response to oxidative stress of keratinocytes, or possibly that keratinocytes increased resistance due to the high prevalence of keratin – a phenomenon required perhaps due to the more exposed positioning of keratinocytes in the skin. Owing to the reality that within our skin dermal fibroblasts will only receive UVR within the UVA range, and because of their suggested increased sensitivity than keratinocytes, perhaps more emphasis should be put on protecting our skin from UVA.

7.6 Creation of UVR Specific Deletions

The 4977 bp (Koch *et al.*, 2001) and the 3895 bp (Harbottle *et al.*, 2010) deletions have both been found to be more prevalent in sun exposed skin as opposed to sun protected skin and therefore represent important biomarkers for sun exposure. They have also been reportedly induced *in vitro* (Berneburg *et al.*, 1999; Krishnan *et al.*, 2004; Schroeder *et al.*, 2008). Due to the association with mtDNA replication (See Chapter 1) a repeated exposure to UVR is required to induce either of the deletions. Initial investigations determined that the TaqMan technology was the most accurate for determination of both the 4977 bp and 3895 bp mtDNA specific deletions. However these deletions were not induced *in vitro* in keratinocytes or fibroblasts following various UVR source exposures and regimes. This was contrary to previous findings and was possibly due to a difference in the methods utilised.

7.7 The Seahorse XF Analyzer is Adequate as a Method for Detecting the Effect of UVR on Cellular Respiration

Part of this thesis involved a project within P&G which developed a method to quantify UVR-induced damage, the investigations of which are described in Chapter 5. This was then used to measure the effectiveness of specific UVR damage modulators. The main focus of the project was on cellular respiration, the main source of ATP. Detrimental effects associated with cellular respiration could lead to dire consequences for the cell. Damage to mtDNA as described in Chapter 4 could also lead to defects in the assembly

of the ETC complexes which could ultimately lead to the loss of mitochondrial respiration. UVR-induced ROS can also damage the ETC leading to further ROS production (Dranka *et al.*, 2011). It is thought that OXPHOS decreases with UVR exposure (Djavaheri-Mergny *et al.*, 2001) although the relationship between OXPHOS and glycolysis in cells exposed to UVR does not seem to have been established.

Various methods for measuring cellular respiration are discussed in the introduction of Chapter 5; this project utilised the fairly modern and innovative Seahorse XF Analyzer technology. The results obtained found that the Seahorse XF Analyzer was sufficient in reliably detecting simultaneous differences in OXPHOS and glycolysis following both UVA and UVB irradiation. This technology was also sensitive in detecting changes in respiration following doses of UVR which could not inflict substantial mtDNA damage as shown in Chapter 4. Furthermore, using specific metabolic modulators allowed this technology to additionally investigate mitochondrial function; comprising of basal respiration, ATP turnover, proton leak, respiratory capacity and respiratory reserve.

Specific UVA irradiations of BJ fibroblasts primarily caused a decrease in OXPHOS which seemed to be compensated for by an increase in glycolysis possibly in an aim to maintain ATP levels. Whereas, specific UVB irradiations of HEKn, caused decreases in both OXPHOS and glycolysis. Experimental procedures were too variable to make divergences, still differences in the particular cells glycolytic capabilities is possible, however further experiments are needed to accurately analyse this. Nonetheless mitochondrial function analysis found that the reduction in OXPHOS created by both UVA and UVB was attributed to a reduction in ATP production and not differences in proton leak. This means that UVA and UVB exposure renders cells more susceptible to stressful situations.

Once this method had been optimised, the effect of specific UVR damage modulators on UVR-induced differences of cellular respiration was explored using this assay. The chosen modulator was idebenone which caused an increase in the decrease of OXPHOS following UVR exposure. This meant that this assay was sufficient for quantifying the effect of UVR protectants/UVR damage modulators. As well as this, when the mitochondrial function analysis assay was performed, mechanisms for the action of these protectants/modulators could be assumed. For example, this study

found that the increase in OXPHOS seen with idebenone was likely to be due to an increase in proton leak rather than ATP production. This means that the effect of this active may not be as useful as first thought.

7.8 Methods Efficient in Detecting Acute UVR-Induced nDNA Damage

Various methods were undertaken in an aim to detect UVR-induced nDNA damage and some were more effective at this than others. For example, no mutations within exons 5-9 of the p53 gene of acutely UVR irradiated HDFn cells were detected. Additionally the 8-OXdg antibody was not sensitive enough to detect oxidative damage by immunofluorescence. Therefore these assays would not be useful in the measuring of potential UVR protectant/UVR damage modulating actives.

One particular assay involved the induction of photoproducts by the various UVR sources. The induction of photoproducts was consistent across UVR source type and therefore a specific active was assessed for its UVR protectant potential. This active was the antioxidant Tiron and the results confirmed that this entity could offer protection against UVR-induced photoproducts. This meant that this assay was sufficient for measuring protectant effects. Furthermore, this assay showed that Tiron offered more protection to UVA-induced photoproducts than UVB-induced photoproducts; this indicates an ability of the assay to estimate an actives mechanism of action. This assay was also further utilised to determine UVR wavelength dependent effects. The reasoning for this was because the previously determined action spectrum of UVR-induced nDNA damage by Setlow, 1974(Setlow, 1974)(Setlow, 1974)(Setlow, 1974)(Setlow, 1974)(Setlow, 1974)(Setlow, 1974)(Setlow, 1974)(Setlow, 1974)(Setlow, 1974) was not entirely relevant to the discussions of this thesis as it determined photoproduct formation in the nDNA of E.*coli* cells (Setlow and Carrier, 1966). UVR did cause a wavelength dependent increase of photoproducts in the nDNA of HDFn and Primary Keratinocyte cells. These increases were loosely dose-dependent, but not of a quality of which an action spectrum could be determined. A similar trend was seen for this data and Setlow's action spectrum however, where the shortest wavelengths of UVR were the most detrimental. This meant that comparisons between Setlow's action

spectrum and the UVR-induced mtDNA action spectrum of Chapter 4 could still be examined.

One further method considered for detecting UVR-induced cellular changes encompassed the use of a pathway specific gene array. All the genes associated with the array were related to oxidative stress. Following acute UVR irradiation the array was sufficient recognising particular genes which are differentially expressed. This meant that this assay may identify early signalling pathways involved in the response to UVR stress and therefore could be useful in measuring the effectiveness of UVR protectant/UVR damage modulators.

7.9 Future Work

This thesis determined the action spectrum of UVR-induced mtDNA damage, of which identified a possible heightened response to UVA in HDFn and HaCaT cells. Further experimental procedures could involve the aim to increase the data points at these longer wavelengths. To increase certainty of this data, further work should involve the study of additional computational models which could more robustly predict the action spectrum. This would add a confidence of error to the curves that would enable us to clarify or dismiss any of the differences seen.

This thesis also established various quantitative assessments for UVR exposure. Furthermore it showed that these could be successfully utilised for the evaluation of specific UVR treatments either for protection or modulation of UVR-induced damage. It is well established that the detrimental effects of UVR on the skin are complex and wide and therefore measuring of the usefulness of potential actives requires various assays to predict the complete effectiveness. There is major scope for further associated experiments to this.

Preliminary work has investigated the effect of IRR on skin cells. Initial results show an ability of IRR to increase cellular ROS but not cause detectable mtDNA damage measured by the 11 kb assay. Further investigation of potential damaging effects of IRR would be useful to determine the need for protection from this radiation. If

detrimental effects are confirmed a quantitative assay could be designed for UVR-protection/UVR damage modulation treatments.

7.10 Concluding Remarks

The major aim of this thesis was to determine the action spectrum of UVR-induced mtDNA damage. Analysis found higher sensitivity of dermal fibroblast cells to UVR compared to keratinocytes and also indicated a possible heightened response to UVA in HDFn and HaCaT cells.

If the increase in mtDNA damage in HDFn cells with wavelengths >320 nm was found to be a valid result this could mean that there should be changes in the way we protect our skin from the sun. mtDNA damage has been found in skin cancer cells and perhaps indicates that the longer wavelengths of UVR are even more damaging than presently thought. As well as this, due to the higher sensitivity of dermal fibroblasts than keratinocytes and their predominant UVA exposure within human skin, this would emphasise the need to protect against this division of UVR. A division of which the protection from is not as well characterised as from protection of UVB. This may also provide evidence to further increase restrictions on the largely UVA emitting sun-beds.

Appendices

Appendix IUVR Source Spectral Chart (Enlarged)

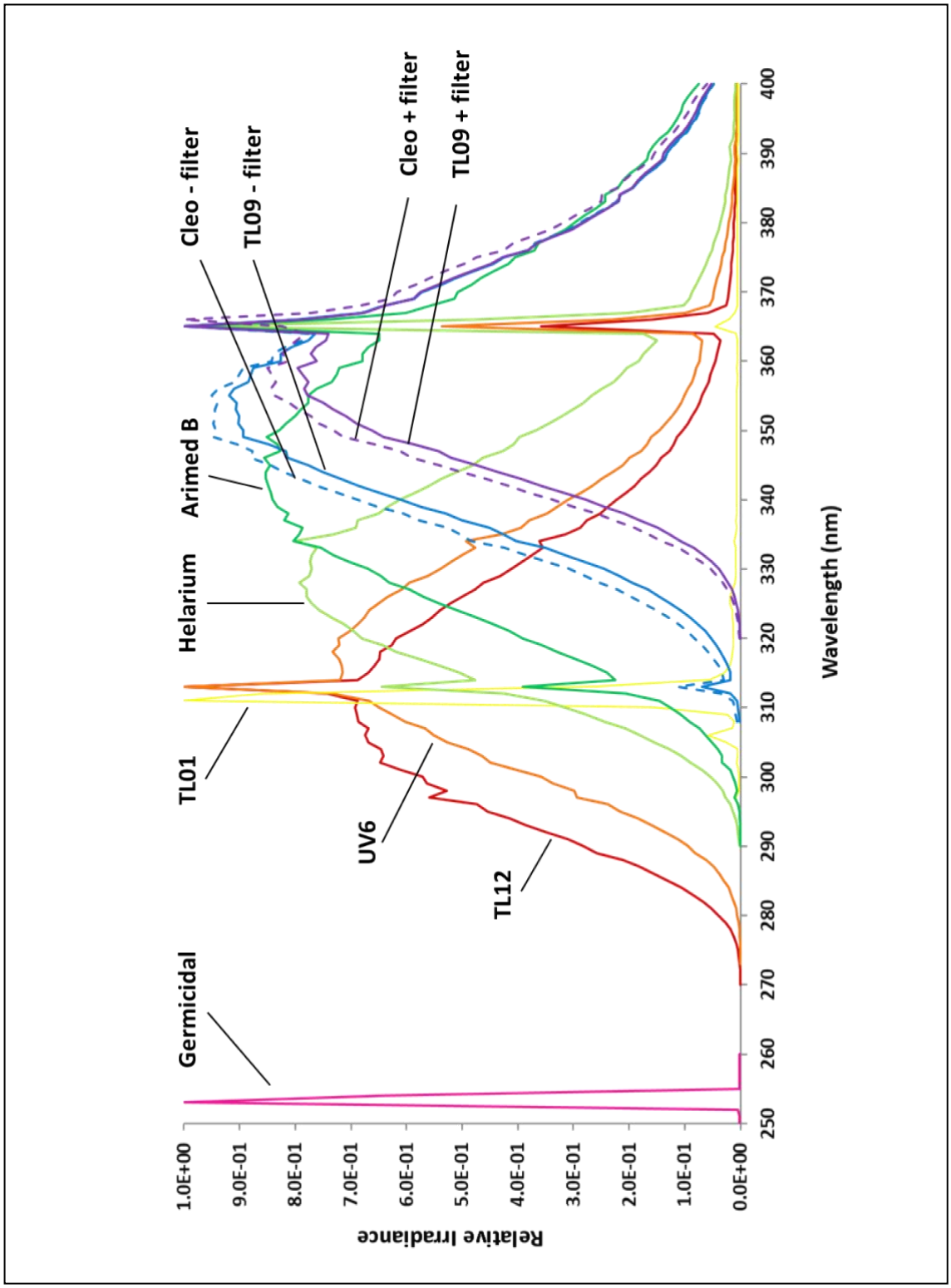

Spectral Chart An Enlarged Spectral Chart of the Various UVR Sources Used within this Thesis

Appendix II Action Spectrum Analysis

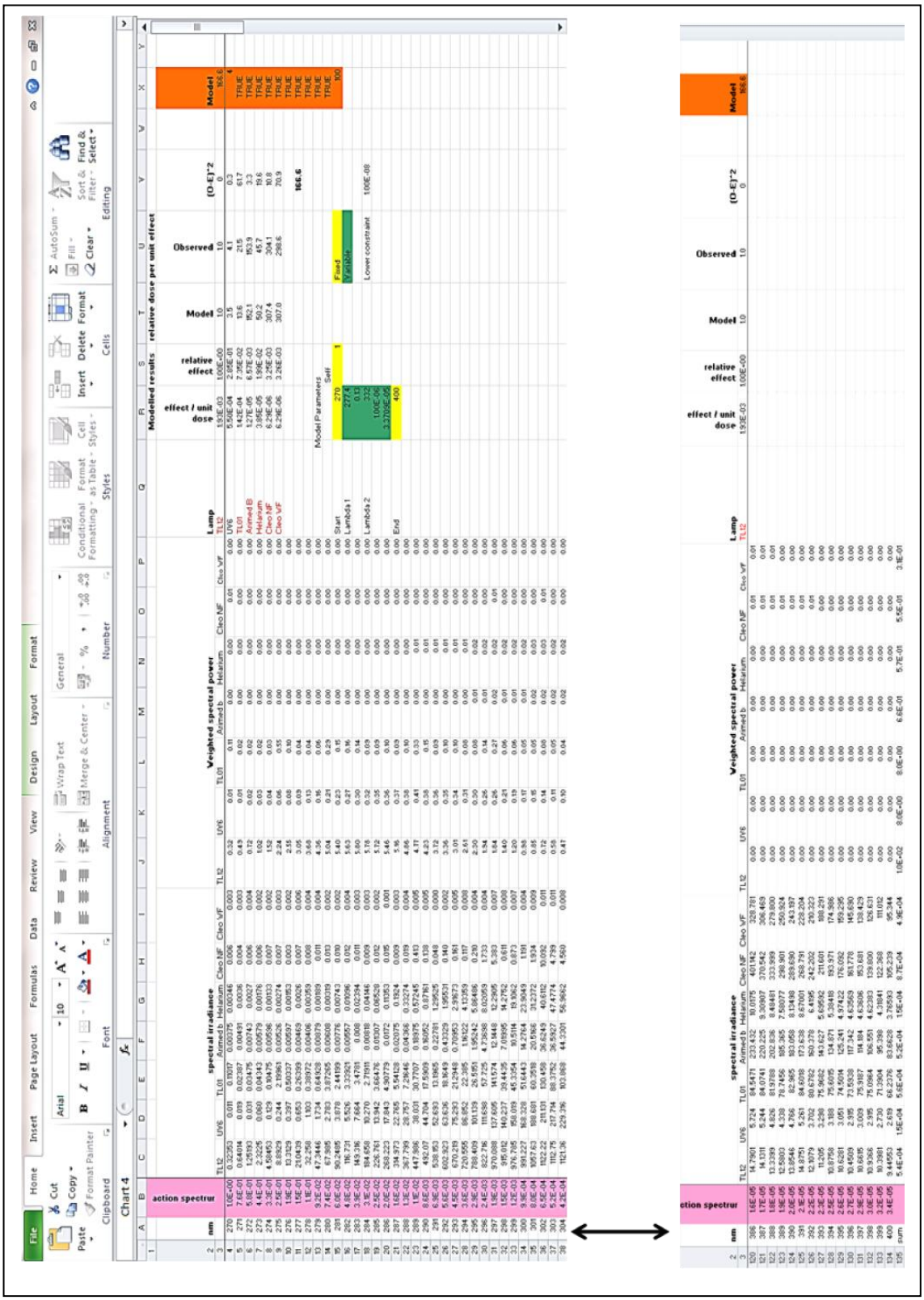

A Screenshot Illustrating the Typical Excel File Analysis for Action Spectrum Prediction. The determined action spectrum is highlighted in pink, determined by the model parameters highlighted in green. The solver function alters the model parameters to minimise the total differences seen ((O-E)^2) between the observed and modelled effects.

Action spectrum analysis for HaCaT cells.

Lamp	Modelled Results		Relative Dose Per Unit Effect		(O-E)^2
	Effect Per Unit Dose	Relative Effect	Model	Observed	
TL12	1.93E-03	1.00E+00	1.0	1.0	0
UV6	5.50E-04	2.85E-01	3.5	4.1	0.3
TL01	1.42E-04	7.35E-02	13.6	21.5	61.7
Arimed B	1.27E-05	6.57E-03	152.1	153.9	3.3
Helarium	3.85E-05	1.99E-02	50.2	45.7	19.6
Cleo NF	6.29E-06	3.25E-03	307.4	304.1	10.8
Cleo WF	6.29E-06	3.26E-03	307.0	298.6	70.9
					166.6

From the dose curves of mtDNA damage created by the TL12, UV6, TL01, Helarium, Arimed B, Cleo - filter and Cleo + filter UVR sources a consistent value was obtained. This value was the UVR dose required to create a 10 % increase in mtDNA damage from the control. From this data a dose per unit effect for each of the UVR sources was calculated (observed effect). From a predicted three-exponential model action spectrum a relative dose per unit effect for each of the UVR sources was obtained (modelled effect). The action spectrum for UVR-induced mtDNA damage was then predicted using the solver function within excel to find the minimum sum of the squared differences between the observed effect and the modelled effect.

Action spectrum analysis for Primary Keratinocyte cells.

Lamp	Modelled Results		Relative Dose Per Unit Effect		(O-E)^2
	Effect Per Unit Dose	Relative Effect	Model	Observed	
TL12	1.97E-03	1.00E+00	1.0	1.0	0
UV6	5.67E-04	2.87E-01	3.5	4.7	1.4
TL01	1.48E-04	7.52E-02	13.3	14.0	0.5
Arimed B	9.95E-06	5.04E-03	198.3	258.1	3576.3
Helarium	3.97E-05	2.01E-02	49.7	54.8	26.5
Cleo NF	2.53E-06	1.28E-03	778.3	694.7	6995.9
Cleo WF	1.13E-06	5.75E-04	1739.4	1719.5	394.4
					10994.9

From the dose curves of mtDNA damage created by the TL12, UV6, TL01, Helarium, Arimed B, Cleo - filter and Cleo + filter UVR sources a consistent value was obtained. This value was the UVR dose required to create a 10 % increase in mtDNA damage from the control. From this data a dose per unit effect for each of the UVR sources was calculated (observed effect). From a predicted three-exponential model action spectrum a relative dose per unit effect for each of the UVR sources was obtained (modelled effect). The action spectrum for UVR-induced mtDNA damage was then predicted using the solver function within excel to find the minimum sum of the squared differences between the observed effect and the modelled effect.

Action spectrum analysis for HDFn cells.

Lamp	Modelled Results		Relative Dose Per Unit Effect		(O-E)^2
	Effect Per Unit Dose	Relative Effect	Model	Observed	
TL12	3.66E-03	1.00E+00	1.0	1.0	0
UV6	1.05E-03	2.88E-01	3.5	4.8	1.8
TL01	2.68E-04	7.34E-02	13.6	23.2	91.0
Arimed B	3.78E-05	1.03E-02	96.7	81.4	232.6
Helarium	8.26E-05	2.26E-02	44.3	26.8	304.8
Cleo NF	2.79E-05	7.64E-03	130.9	162.5	998.6
Cleo WF	2.92E-05	7.97E-03	125.5	93.2	1046.6
					2675.5

From the dose curves of mtDNA damage created by the TL12, UV6, TL01, Helarium, Arimed B, Cleo - filter and Cleo + filter UVR sources a consistent value was obtained. This value was the UVR dose required to create a 10 % increase in mtDNA damage from the control. From this data a dose per unit effect for each of the UVR sources was calculated (observed effect). From a predicted three-exponential model action spectrum a relative dose per unit effect for each of the UVR sources was obtained (modelled effect). The action spectrum for UVR-induced mtDNA damage was then predicted using the solver function within excel to find the minimum sum of the squared differences between the observed effect and the modelled effect.

Appendix III 96-Well Gene Array Gene List and Raw Data

A comprehensive list of the details of the genes found on the oxidative stress plus array (PAHS-065Y)

Position	Unigene	GeneBank	Symbol	Description	Gene Name
A01	Hs.418167	NM_000477	ALB	Albumin	DKFZp779N1935, PRO0883, PRO0903, PRO1341
A02	Hs.654431	NM_000697	ALOX12	Arachidonate 12-lipoxygenase	12-LOX, 12S-LOX, LOG12
A03	Hs.406238	NM_001159	AOX1	Aldehyde oxidase 1	AO, AOH1
A04	Hs.654439	NM_000041	APOE	Apolipoprotein E	AD2, LDLCQ5, LPG, MGC1571
A05	Hs.125213	NM_004045	ATOX1	ATX1 antioxidant protein 1 homolog (yeast)	ATX1, HAH1, MGC138453, MGC138455
A06	Hs.144873	NM_004052	BNIP3	BCL2/adenovirus E1B 19kDa interacting protein 3	NIP3
A07	Hs.502302	NM_001752	CAT	Catalase	MGC138422, MGC138424
A08	Hs.514821	NM_002985	CCL5	Chemokine (C-C motif) ligand 5	D17S136E, MGC17164, RANTES, SCYA5, SISd, TCP228
A09	Hs.502917	NM_005125	CCS	Copper chaperone for superoxide dismutase	MGC138260
A10	Hs.292356	NM_000397	CYBB	Cytochrome b-245, beta polypeptide	CGD, GP91-1, GP91-PHOX, GP91PHOX, NOX2, p91-PHOX

Position	Unigene	GeneBank	Symbol	Description	Gene Name
A11	Hs.95120	NM_134268	CYGB	Cytoglobin	HGB, STAP
A12	Hs.498727	NM_014762	DHCR24	24-dehydrocholesterol reductase	DCE, KIAA0018, Nbla03646, SELADIN1, seladin-1
B01	Hs.272813	NM_175940	DUOX1	Dual oxidase 1	LNOX1, MGC138840, MGC138841, NOXEF1, THOX1
B02	Hs.71377	NM_014080	DUOX2	Dual oxidase 2	LNOX2, NOXEF2, P138-TOX, TDH6, THOX2
B03	Hs.171695	NM_004417	DUSP1	Dual specificity phosphatase 1	CL100, HVH1, MKP-1, MKP1, PTPN10
B04	Hs.212088	NM_001979	EPHX2	Epoxide hydrolase 2, cytoplasmic	CEH, SEH
B05	Hs.279259	NM_000502	EPX	Eosinophil peroxidase	EPO, EPP, EPX-PEN
B06	Hs.239	NM_021953	FOXM1	Forkhead box M1	FKHL16, FOXM1B, HFH-11, HFH11, HNF-3, INS-1, MPHOSPH2, MPP-2, MPP2, PIG29, TGT3, TRIDENT
B07	Hs.645560	NM_002032	FTH1	Ferritin, heavy polypeptide 1	FHC, FTH, FTHL6, MGC104426, PIG15, PLIF
B08	Hs.654465	NM_001498	GCLC	Glutamate-cysteine ligase, catalytic subunit	GCL, GCS, GLCL, GLCLC
B09	Hs.76686	NM_000581	GPX1	Glutathione peroxidase 1	GSHPX1, MGC14399, MGC88245

Position	Unigene	GeneBank	Symbol	Description	Gene Name
B10	Hs.2704	NM_002083	GPX2	Glutathione peroxidase 2 (gastrointestinal)	GI-GPx, GPRP, GSHPX-GI, GSHPx-2
B11	Hs.386793	NM_002084	GPX3	Glutathione peroxidase 3 (plasma)	GPx-P, GSHPx-3, GSHPx-P
B12	Hs.433951	NM_002085	GPX4	Glutathione peroxidase 4 (phospholipid hydroperoxidase)	MCSP, PHGPx, snGPx, snPHGPx
C01	Hs.248129	NM_001509	GPX5	Glutathione peroxidase 5 (epididymal androgen-related protein)	-
C02	Hs.271510	NM_000637	GSR	Glutathione reductase	MGC78522
C03	Hs.82327	NM_000178	GSS	Glutathione synthetase	GSHS, MGC14098
C04	Hs.523836	NM_000852	GSTP1	Glutathione S-transferase pi 1	DFN7, FAEES3, GST3, GSTP, PI
C05	Hs.655292	NM_001513	GSTZ1	Glutathione transferase zeta 1	GSTZ1-1, MAAI, MAI, MGC2029
C06	Hs.728810	NM_005345	HSPA1A	Heat shock 70kDa protein 1A	FLJ54303, FLJ54370, FLJ54392, FLJ54408, FLJ75127, HSP70-1, HSP70-1A, HSP70I, HSP72, HSPA1, HSPA1B

Position	Unigene	GeneBank	Symbol	Description	Gene Name
C07	Hs.80828	NM_006121	KRT1	Keratin 1	CK1, EHK, EHK1, EPPK, K1, KRT1A, NEPPK
C08	Hs.234742	NM_006151	LPO	Lactoperoxidase	MGC129990, MGC129991, SPO
C09	Hs.517586	NM_005368	MB	Myoglobin	MGC13548, PVALB
C10	Hs.499674	NM_000242	MBL2	Mannose-binding lectin (protein C) 2, soluble	COLEC1, HSMBPC, MBL, MBP, MBP-C, MBP1, MGC116832, MGC116833
C11	Hs.458272	NM_000250	MPO	Myeloperoxidase	-
C12	Hs.75659	NM_002437	MPV17	MpV17 mitochondrial inner membrane protein	MTDPS6, SYM1
D01	Hs.490981	NM_012331	MSRA	Methionine sulfoxide reductase A	PMSR
D02	Hs.73133	NM_005954	MT3	Metallothionein 3	GIF, GIFB, GRIF
D03	Hs.647047	NM_000265	NCF1	Neutrophil cytosolic factor 1	FLJ79451, NCF1A, NOXO2, SH3PXD1A, p47phox
D04	Hs.587558	NM_000433	NCF2	Neutrophil cytosolic factor 2	FLJ93058, NCF-2, NOXA2, P67-PHOX, P67PHOX
D05	Hs.709191	NM_000625	NOS2	Nitric oxide synthase 2, inducible	HEP-NOS, INOS, NOS, NOS2A
D06	Hs.371036	NM_016931	NOX4	NADPH oxidase 4	KOX, KOX-1, RENOX

Position	Unigene	GeneBank	Symbol	Description	Gene Name
D07	Hs.657932	NM_024505	NOX5	NADPH oxidase, EF-hand calcium binding domain 5	MGC149776, MGC149777
D08	Hs.534331	NM_002452	NUDT1	Nudix (nucleoside diphosphate linked moiety X)-type motif 1	MTH1
D09	Hs.368525	NM_020992	PDLIM1	PDZ and LIM domain 1	CLIM1, CLP-36, CLP36, hCLIM1
D10	Hs.180909	NM_002574	PRDX1	Peroxiredoxin 1	MSP23, NKEFA, PAG, PAGA, PAGB, PRX1, PRXI, TDPX2
D11	Hs.432121	NM_005809	PRDX2	Peroxiredoxin 2	MGC4104, NKEFB, PRP, PRX2, PRXII, TDPX1, TPX1, TSA
D12	Hs.523302	NM_006793	PRDX3	Peroxiredoxin 3	AOP-1, AOP1, MER5, MGC104387, MGC24293, PRO1748, SP-22
E01	Hs.83383	NM_006406	PRDX4	Peroxiredoxin 4	AOE37-2, PRX-4
E02	Hs.502823	NM_181652	PRDX5	Peroxiredoxin 5	ACR1, AOEB166, B166, MGC117264, MGC142283, MGC142285, PLP, PMP20, PRDX6, PRXV
E03	Hs.120	NM_004905	PRDX6	Peroxiredoxin 6	1-Cys, AOP2, KIAA0106, MGC46173, NSGPx, PRX, aiPLA2, p29

Position	Unigene	GeneBank	Symbol	Description	Gene Name
E04	Hs.472010	NM_183079	PRNP	Prion protein	ASCR, CD230, CJD, GSS, MGC26679, PRIP, PrP, PrP27-30, PrP33-35C, PrPc, prion
E05	Hs.201978	NM_000962	PTGS1	Prostaglandin-endoperoxide synthase 1 (prostaglandin G/H synthase and cyclooxygenase)	COX1, COX3, PCOX1, PGG, HS, PGHS-1, PGHS1, PHS1, PTGHS
E06	Hs.196384	NM_000963	PTGS2	Prostaglandin-endoperoxide synthase 2 (prostaglandin G/H synthase and cyclooxygenase)	COX-2, COX2, GRIPGHS, PGG, HS, PGHS-2, PHS-2, hCox-2
E07	Hs.134623	NM_014245	RNF7	Ring finger protein 7	CKBBP1, ROC2, SAG
E08	Hs.32148	NM_203472	SELS	Selenoprotein S	ADO15, MGC104346, MGC2553, SBBI8, SEPS1, VIMP
E09	Hs.275775	NM_005410	SEPP1	Selenoprotein P, plasma, 1	SELP, SeP
E10	Hs.253495	NM_003019	SFTPD	Surfactant protein D	COLEC7, PSP-D, SFTP4, SP-D
E11	Hs.466693	NM_012237	SIRT2	Sirtuin 2	FLJ35621, FLJ37491, SIR2, SIR2L, SIR2L2
E12	Hs.443914	NM_000454	SOD1	Superoxide dismutase 1, soluble	ALS, ALS1, IPOA, SOD, hSod1, homodimer

Position	Unigene	GeneBank	Symbol	Description	Gene Name
F01	Hs.487046	NM_000636	SOD2	Superoxide dismutase 2, mitochondrial	IPOB, MNSOD, MVCD6
F02	Hs.2420	NM_003102	SOD3	Superoxide dismutase 3, extracellular	EC-SOD, MGC20077
F03	Hs.437277	NM_003900	SQSTM1	Sequestosome 1	A170, OSIL, PDB3, ZIP3, p60, p62, p62B
F04	Hs.516830	NM_080725	SRXN1	Sulfiredoxin 1	C20orf139, FLJ43353, Npn3, SRX1, YKL086W, dJ850E9.2
F05	Hs.467554	NM_000547	TPO	Thyroid peroxidase	MSA, TDH2A, TPX
F06	Hs.134602	NM_003319	TTN	Titin	CMD1G, CMH9, CMPD4, DKFZp451N061, EOMFC, FLJ26020, FLJ26409, FLJ32040, FLJ34413, FLJ39564, FLJ43066, HMERF, LGMD2J, TMD
F07	Hs.443430	NM_006440	TXNRD2	Thioredoxin reductase 2	SELZ, TR, TR-BETA, TR3, TRXR2
F08	Hs.80658	NM_003355	UCP2	Uncoupling protein 2 (mitochondrial, proton carrier)	BMIQ4, SLC25A8, UCPH

Position	Unigene	GeneBank	Symbol	Description	Gene Name
F09	Hs.498513	NM_001354	AKR1C2	Aldo-keto reductase family 1, member C2 (dihydrodiol dehydrogenase 2; bile acid binding protein; 3-alpha hydroxysteroid dehydrogenase, type III)	AKR1C-pseudo, BABP, DD, DD2, DDH2, FLJ53800, HAKRD, HBAB, MCDR2
F10	Hs.729098	NM_004282	BAG2	BCL2-associated athanogene 2	BAG-2, KIAA0576, MGC149462, dJ417I1.2
F11	Hs.443687	NM_001450	FHL2	Four and a half LIM domains 2	AAG11, DRAL, FHL-2, SLIM-3, SLIM3
F12	Hs.315562	NM_002061	GCLM	Glutamate-cysteine ligase, modifier subunit	GLCLR
G01	Hs.69089	NM_000169	GLA	Galactosidase, alpha	GALA
G02	Hs.517581	NM_002133	HMOX1	Heme oxygenase (decycling) 1	HO-1, HSP32, bK286B10
G03	Hs.525600	NM_001017963	HSP90AA1	Heat shock protein 90kDa alpha (cytosolic), class A member 1	FLJ31884, HSP86, HSP89A, HSP90A, HSP90N, HSPC1, HSPCA, HSPCAL1, HSPCAL4, HSPN, Hsp89, Hsp90, LAP2
G04	Hs.527748	NM_022126	LHPP	Phospholysine phosphohistidine inorganic pyrophosphate phosphatase	FLJ44846, FLJ46044, HDHD2B, MGC117251, MGC142189, MGC142191

Position	Unigene	GeneBank	Symbol	Description	Gene Name
G05	Hs.171426	NM_181782	NCOA7	Nuclear receptor coactivator 7	ERAP140, ESNA1, FLJ45605, MGC88425, Nbla00052, Nbla10993, dJ187J11.3
G06	Hs.406515	NM_000903	NQO1	NAD(P)H dehydrogenase, quinone 1	DHQU, DIA4, DTD, NMOR1, NMORI, QR1
G07	Hs.584864	NM_012212	PTGR1	Prostaglandin reductase 1	FLJ99229, LTB4DH, MGC34943, PGR1, ZADH3
G08	Hs.390594	NM_014331	SLC7A11	Solute carrier family 7 (anionic amino acid transporter light chain, xc- system), member 11	CCBR1, xCT
G09	Hs.407856	NM_003122	SPINK1	Serine peptidase inhibitor, Kazal type 1	PCTT, PSTI, Spink3, TATI
G10	Hs.466929	NM_024108	TRAPPC6A	Trafficking protein particle complex 6A	MGC2650, TRS33
G11	Hs.435136	NM_003329	TXN	Thioredoxin	DKFZp686B1993, MGC61975, TRX, TRX1
G12	Hs.728817	NM_003330	TXNRD1	Thioredoxin reductase 1	GRIM-12, MGC9145, TR, TR1, TRXR1, TXNR
H01	Hs.520640	NM_001101	ACTB	Actin, beta	PS1TP5BP1
H02	Hs.534255	NM_004048	B2M	Beta-2-microglobulin	-

Position	Unigene	GeneBank	Symbol	Description	Gene Name
H03	Hs.592355	NM_002046	GAPDH	Glyceraldehyde-3-phosphate dehydrogenase	G3PD, GAPD, MGC88685
H04	Hs.412707	NM_000194	HPRT1	Hypoxanthine phosphoribosyltransferase 1	HGPRT, HPRT
H05	Hs.546285	NM_001002	RPLP0	Ribosomal protein, large, P0	L10E, LP0, MGC111226, MGC88175, P0, PRLP0, RPP0
H06	N/A	SA_00105	HGDC	Human Genomic DNA Contamination	HIGX1A
H07	N/A	SA_00104	RTC	Reverse Transcription Control	RTC
H08	N/A	SA_00104	RTC	Reverse Transcription Control	RTC
H09	N/A	SA_00104	RTC	Reverse Transcription Control	RTC
H10	N/A	SA_00103	PPC	Positive PCR Control	PPC
H11	N/A	SA_00103	PPC	Positive PCR Control	PPC
H12	N/A	SA_00103	PPC	Positive PCR Control	PPC

Raw data of the oxidative stress plus array analysis – values indicate a fold change.

Position	Gene Symbol	Cleo + filter VS Control	TL01 VS Control	TL12 VS Control	TL12 VS TL01	TL12 VS Cleo + filter	TL01 VS Cleo + filter
A01	ALB	1	0.57	0.72	1.26	0.72	0.57
A02	ALOX12	2.76	1.05	1.16	1.1	0.42	0.38
A03	AOX1	3.35	1.53	1.37	0.89	0.41	0.46
A04	APOE	2.34	0.64	0.86	1.35	0.37	0.27
A05	ATOX1	2.45	1.57	1.15	0.73	0.47	0.64
A06	BNIP3	1.15	0.48	0.55	1.14	0.48	0.42
A07	CAT	1.19	0.77	1.11	1.44	0.94	0.65
A08	CCL5	0.79	0.75	0.75	1	0.95	0.95
A09	CCS	0.94	0.53	0.62	1.17	0.66	0.56
A10	CYBB	0.79	0.19	0.67	3.45	0.84	0.24
A11	CYGB	0.9	0.33	0.47	1.41	0.52	0.37
A12	DHCR24	1.08	0.46	0.65	1.43	0.6	0.42
B01	DUOX1	2.78	1.41	0.66	0.47	0.24	0.51
B02	DUOX2	0.74	0.3	1.22	4.06	1.66	0.41
B03	DUSP1	2.32	1.19	1.21	1.02	0.52	0.51
B04	EPHX2	1.88	0.72	0.78	1.07	0.41	0.38
B05	EPX	2.11	0.99	0.77	0.78	0.36	0.47
B06	FOXM1	1.08	0.47	0.57	1.22	0.53	0.43
B07	FTH1	0.98	0.78	1.21	1.56	1.24	0.8
B08	GCLC	0.53	0.55	0.61	1.11	1.15	1.04
B09	GPX1	0.76	0.5	0.58	1.16	0.76	0.65

Position	Gene Symbol	Cleo + filter VS Control	TL01 VS Control	TL12 VS Control	TL12 VS TL01	TL12 VS Cleo + filter	TL01 VS Cleo + filter
B10	GPX2	1.36	0.32	0.87	2.68	0.64	0.24
B11	GPX3	0.89	0.42	0.53	1.26	0.6	0.48
B12	GPX4	0.74	0.39	0.54	1.37	0.73	0.53
C01	GPX5	1	0.57	0.72	1.26	0.72	0.57
C02	GSR	6.88	2.79	4.79	1.71	0.7	0.41
C03	GSS	2.03	0.89	0.93	1.05	0.46	0.44
C04	GSTP1	1.78	0.71	0.82	1.16	0.46	0.4
C05	GSTZ1	1.11	0.78	0.76	0.98	0.68	0.7
C06	HSPA1A	0.87	0.41	0.51	1.25	0.59	0.47
C07	KRT1	1	0.57	0.72	1.26	0.72	0.57
C08	LPO	0.99	0.57	0.71	1.26	0.72	0.57
C09	MB	0.84	0.53	0.61	1.14	0.72	0.63
C10	MBL2	1.04	0.57	0.8	1.4	0.77	0.55
C11	MPO	1.17	0.5	1.25	2.47	1.06	0.43
C12	MPV17	0.88	0.41	0.55	1.34	0.62	0.47
D01	MSRA	4.39	3.96	2.86	0.72	0.65	0.9
D02	MT3	0.76	0.27	0.54	1.99	0.71	0.36
D03	NCF1	31.29	6.44	3.77	0.58	0.12	0.21
D04	NCF2	2.14	0.9	0.96	1.06	0.45	0.42
D05	NOS2	1.49	2.14	0.63	0.3	0.42	1.44
D06	NOX4	0.74	0.44	0.63	1.43	0.86	0.6
D07	NOX5	0.55	0.32	0.73	2.28	1.34	0.58
D08	NUDT1	0.51	0.42	0.49	1.16	0.96	0.82

Position	Gene Symbol	Cleo + filter VS Control	TL01 VS Control	TL12 VS Control	TL12 VS TL01	TL12 VS Cleo + filter	TL01 VS Cleo + filter
D09	PDLIM1	0.68	0.39	0.51	1.31	0.75	0.57
D10	PRDX1	0.94	0.36	0.67	1.87	0.71	0.38
D11	PRDX2	0.83	0.33	0.53	1.6	0.64	0.4
D12	PRDX3	1.38	0.63	0.93	1.47	0.67	0.46
E01	PRDX4	2.14	3.1	1.56	0.5	0.73	1.45
E02	PRDX5	1.56	0.98	1.11	1.13	0.71	0.63
E03	PRDX6	2.77	1.34	1.35	1.01	0.49	0.48
E04	PRNP	1.32	0.75	0.81	1.08	0.61	0.57
E05	PTGS1	0.76	0.64	0.62	0.97	0.82	0.84
E06	PTGS2	0.73	0.46	0.53	1.17	0.73	0.63
E07	RNF7	0.66	0.5	0.63	1.26	0.96	0.76
E08	SELS	0.63	0.41	0.49	1.2	0.78	0.65
E09	SEPP1	1.19	0.76	1.36	1.79	1.14	0.64
E10	SFTPD	0.36	0.17	0.39	2.32	1.1	0.47
E11	SIRT2	0.68	0.27	0.5	1.83	0.73	0.4
E12	SOD1	0.8	0.36	0.63	1.76	0.79	0.45
F01	SOD2	1.42	1.54	1.02	0.66	0.72	1.09
F02	SOD3	2.31	1.56	1.46	0.94	0.63	0.67
F03	SQSTM1	1.99	0.99	1.02	1.04	0.51	0.5
F04	SRXN1	1.13	0.8	0.79	0.99	0.7	0.71
F05	TPO	1	0.57	0.72	1.26	0.72	0.57
F06	TTN	0.91	0.64	0.65	1.02	0.72	0.71
F07	TXNRD2	0.59	0.37	0.42	1.15	0.71	0.62

Position	Gene Symbol	Cleo + filter VS Control	TL01 VS Control	TL12 VS Control	TL12 VS TL01	TL12 VS Cleo + filter	TL01 VS Cleo + filter
F08	UCP2	0.56	0.39	0.42	1.08	0.76	0.71
F09	AKR1C2	0.7	0.41	0.45	1.11	0.65	0.59
F10	BAG2	0.8	0.33	0.49	1.47	0.61	0.41
F11	FHL2	0.92	0.49	0.69	1.41	0.74	0.53
F12	GCLM	0.83	0.39	0.57	1.48	0.69	0.47
G01	GLA	1.04	1.39	1.15	0.83	1.11	1.34
G02	HMOX1	1.43	0.9	0.81	0.9	0.57	0.63
G03	HSP90AA1	2.4	1.11	1.18	1.07	0.49	0.46
G04	LHPP	0.99	0.77	0.8	1.03	0.8	0.78
G05	NCOA7	0.9	0.91	0.9	0.99	1	1
G06	NQO1	0.86	0.59	0.73	1.24	0.85	0.68
G07	PTGR1	0.65	0.49	0.57	1.16	0.88	0.76
G08	SLC7A11	0.71	0.46	0.57	1.22	0.8	0.66
G09	SPINK1	1	0.4	0.41	1.02	0.41	0.4
G10	TRAPPC6A	0.91	0.38	0.47	1.24	0.52	0.42
G11	TXN	0.69	0.35	0.49	1.39	0.71	0.51
G12	TXNRD1	1.3	0.74	0.91	1.23	0.7	0.57
H01	ACTB	0.97	1.11	0	0	0	1.14
H02	B2M	1.17	1.06	0	0	0	0.91
H03	GAPDH	1.73	0.81	0	0	0	0.47
H04	HPRT1	1.17	1.17	1.08	0.92	0.92	1
H05	RPLP0	0.85	0.86	0.93	1.08	1.09	1

Appendix IV Publications Arising From this Thesis

Published

Swalwell, H., Latimer, J., Haywood, R. M. and Birch-Machin, M. A. (2012) 'Investigating the role of melanin in UVA/UVB- and hydrogen peroxide-induced cellular and mitochondrial ROS production and mitochondrial DNA damage in human melanoma cells', *Free Radic Biol Med*, 52(3), pp. 626-34.

Birch-Machin, M. A., Russell, E. V. and Latimer, J. A. (2013) 'Mitochondrial DNA damage as a biomarker for ultraviolet radiation exposure and oxidative stress', *British Journal of Dermatology*.

Abstracts

Nichols, J. A., Lloyd, J. and Birch-Machin, M. A. (2011) 'The action spectrum of UVR-induced damage within an 11 kb segment of mitochondrial DNA in human skin cells', *British Journal of Dermatology*, 164(4), pp. 924-924.

Latimer, J. A., Russell, E. V. and Birch-Machin, M. A. (2012) 'The Effects of Infrared Radiation versus Ultraviolet Radiation in Human Skin Cells ', *Journal Of Invesigative Dermatology*, 132(2), pp. S122-S122.

Russell, E. V., Latimer, J. A., Oyewole, A. and Birch-Machin, M. A. (2012) 'Investigating the Protective Potential of the Antioxidant Tiron in Human Skin Cells Exposed to Ultraviolet Radiation ', *Journal Of Invesigative Dermatology*, 132(2), pp. S121-S121.

Chapter 8

References

Chapter 8 References

4Below1 (2013) *Structure of the epidermis*. Available at: http://www.4below1.co.uk/about-skin (Accessed: 15th May).

Aitken, G. R., Henderson, J. R., Chang, S. C., McNeil, C. J. and Birch-Machin, M. A. (2007) 'Direct monitoring of UV-induced free radical generation in HaCaT keratinocytes', *Clin Exp Dermatol*, 32(6), pp. 722-7.

Alexeyev, M. F., LeDoux, S. P. and Wilson, G. L. (2004) 'Mitochondrial DNA and aging', *Clinical Science*, 107(4), pp. 355-364.

Amerio, P., Carbone, A., Auriemma, M., Varrati, S. and Tulli, A. (2009) 'UV Induced Skin Immunosuppression', *Anti-Inflammatory & Anti-Allergy Agents in Medicinal Chemistry*, 8(1), pp. 3-13.

Andley, U. P., Lewis, R. M., Reddan, J. R. and Kochevar, I. E. (1994) 'Action spectrum for cytotoxicity in the UVA- and UVB-wavelength region in cultured lens epithelial cells', *Invest Ophthalmol Vis Sci*, 35(2), pp. 367-73.

Anon (1997) *A guide to Spectroradiometry - Instruments & Applications for the Ultraviolet*. Available at: http://www.bentham.co.uk/pdf/UVGuide.pdf.

Aoki, M., Furusawa, Y., Higashi, S. and Watanabe, M. (2004) 'Action spectra of apoptosis induction and reproductive cell death in L5178Y cells in the UV-B region', *Photochem Photobiol Sci*, 3(3), pp. 268-72.

Bajdik, C. D., Gallagher, R. P., Astrakianakis, G., Hill, G. B., Fincham, S. and McLean, D. I. (1996) 'Non-solar ultraviolet radiation and the risk of basal and squamous cell skin cancer', *Br J Cancer*, 73(12), pp. 1612-4.

Balk, S. J., Fisher, D. E. and Geller, A. C. (2013) 'Teens and indoor tanning: a cancer prevention opportunity for pediatricians', *Pediatrics*, 131(4), pp. 772-85.

Barbi de Moura, M., Vincent, G., Fayewicz, S. L., Bateman, N. W., Hood, B. L., Sun, M., Suhan, J., Duensing, S., Yin, Y., Sander, C., Kirkwood, J. M., Becker, D., Conrads, T. P.,

Van Houten, B. and Moschos, S. J. (2012) 'Mitochondrial respiration--an important therapeutic target in melanoma', *PLoS One*, 7(8), p. e40690.

Beaumont, K. A., Wong, S. S., Ainger, S. A., Liu, Y. Y., Patel, M. P., Millhauser, G. L., Smith, J. J., Alewood, P. F., Leonard, J. H. and Sturm, R. A. (2011) 'Melanocortin MC(1) receptor in human genetics and model systems', *Eur J Pharmacol*, 660(1), pp. 103-10.

Berneburg, M., Grether-Beck, S., Kurten, V., Ruzicka, T., Briviba, K., Sies, H. and Krutmann, J. (1999) 'Singlet oxygen mediates the UVA-induced generation of the photoaging-associated mitochondrial common deletion', *Journal of Biological Chemistry*, 274(22), pp. 15345-15349.

Berneburg, M., Plettenberg, H., Medve-Konig, K., Pfahlberg, A., Gers-Barlag, H., Gefeller, O. and Krutmann, J. (2004) 'Induction of the photoaging-associated mitochondrial common deletion in vivo in normal human skin', *Journal of Investigative Dermatology*, 122(5), pp. 1277-1283.

Bernerd, F. and Asselineau, D. (1998) 'UVA exposure of human skin reconstructed in vitro induces apoptosis of dermal fibroblasts: subsequent connective tissue repair and implications in photoaging', *Cell Death Differ*, 5(9), pp. 792-802.

Birch-Machin, M. A. (2000) 'Mitochondria and skin disease', *Clinical and Experimental Dermatology*, 25(2), pp. 141-146.

Birch-Machin, M. A. (2006) 'The role of mitochondria in ageing and carcinogenesis', *Clinical and Experimental Dermatology*, 31(4), pp. 548-552.

Birch-Machin, M. A. and Swalwell, H. (2010) 'How mitochondria record the effects of UV exposure and oxidative stress using human skin as a model tissue', *Mutagenesis*, pp. 1-7.

Birch-Machin, M. A., Tindall, M., Turner, R., Haldane, F. and Rees, J. L. (1998) 'Mitochondrial DNA deletions in human skin reflect photo rather than chronologic aging', *Journal of Investigative Dermatology*, 110(2), pp. 149-152.

Birch-Machin, M. A. and Wilkinson, S. C. (2008) 'Skin Photobiology', in Chilcott, R. P. and Price, S. (eds.) *Principles and Practice of Skin Toxicology*. Chichester: John Wiley and Sons, Ltd., pp. 51-65.

Birket, M. J. and Birch-Machin, M. A. (2007) 'Ultraviolet radiation exposure accelerates the accumulation of the aging-dependent T414G mitochondrial DNA mutation in human skin', *Aging Cell*, 6(4), pp. 557-564.

Birket, M. J., Passos, J. F., von Zglinicki, T. and Birch-Machin, M. A. (2009) 'The relationship between the aging- and photo-dependent T414G mitochondrial DNA mutation with cellular senescence and reactive oxygen species production in cultured skin fibroblasts', *J Invest Dermatol*, 129(6), pp. 1361-6.

Boukamp, P., Petrussevska, R. T., Breitkreutz, D., Hornung, J., Markham, A. and Fusenig, N. E. (1988) 'Normal keratinization in a spontaneously immortalized aneuploid human keratinocyte cell line', *J Cell Biol*, 106(3), pp. 761-71.

Boulton, S., Anderson, A., Swalwell, H., Henderson, J. R., Manning, P. and Birch-Machin, M. A. (2011) 'Implications of using the fluorescent probes, dihydrorhodamine 123 and 2',7'-dichlorodihydrofluorescein diacetate, for the detection of UVA-induced reactive oxygen species', *Free Radic Res*, 45(2), pp. 139-46.

Brand, M. D. and Nicholls, D. G. (2011) 'Assessing mitochondrial dysfunction in cells', *Biochem J*, 435(2), pp. 297-312.

Butler, R. N., Fossel, M., Harman, S. M., Heward, C. B., Olshansky, S. J., Perls, T. T., Rothman, D. J., Rothman, S. M., Warner, H. R., West, M. D. and Wright, W. E. (2002) 'Is there an antiaging medicine?', *J Gerontol A Biol Sci Med Sci*, 57(9), pp. B333-8.

Cals-Grierson, M. M. and Ormerod, A. D. (2004) 'Nitric oxide function in the skin', *Nitric Oxide*, 10(4), pp. 179-93.

Cancer Research, U. (2011) *Skin cancer incident statistics*. Available at: http://www.cancerresearchuk.org/cancer-info/cancerstats/types/skin/incidence/uk-skin-cancer-incidence-statistics#nmsc (Accessed: 10th May 2013).

Carbone, C., Pignatello, R., Musumeci, T. and Puglisi, G. (2012) 'Chemical and technological delivery systems for idebenone: a review of literature production', *Expert Opin Drug Deliv*, 9(11), pp. 1377-92.

Chinnery, P. F. and Schon, E. A. (2003) 'Mitochondria', *Journal of Neurology Neurosurgery and Psychiatry*, 74(9), pp. 1188-1199.

Chinnery, P. F. and Turnbull, D. M. (2000) 'Mitochondrial DNA mutations in the pathogenesis of human disease', *Molecular Medicine Today*, 6(11), pp. 425-432.

Chomyn, A. and Attardi, G. (2003) 'MtDNA mutations in aging and apoptosis', *Biochem Biophys Res Commun*, 304(3), pp. 519-29.

Cortopassi, G. A., Shibata, D., Soong, N. W. and Arnheim, N. (1992) 'A pattern of accumulation of a somatic deletion of mitochondrial DNA in aging human tissues', *Proc Natl Acad Sci U S A*, 89(16), pp. 7370-4.

Dayagrosjean, L., Dumaz, N. and Sarasin, A. (1995) 'The Specificity of P53 Mutation Spectra in Sunlight-Induced Human Cancers', *Journal of Photochemistry and Photobiology B-Biology*, 28(2), pp. 115-124.

de Gruijl, F. R. and Van der Leun, J. C. (1994) 'Estimate of the wavelength dependency of ultraviolet carcinogenesis in humans and its relevance to the risk assessment of a stratospheric ozone depletion', *Health Phys*, 67(4), pp. 319-25.

Degruijl, F. R., Sterenborg, H., Forbes, P. D., Davies, R. E., Cole, C., Kelfkens, G., Vanweelden, H., Slaper, H. and Vanderleun, J. C. (1993) 'Wavelength Dependence of Skin-Cancer Induction by Ultraviolet-Irradiation of Albino Hairless Mice', *Cancer Research*, 53(1), pp. 53-60.

Del Bino, S., Sok, J. and Bernerd, F. (2013) 'Assessment of ultraviolet-radiation-induced DNA damage within melanocytes in skin of different constitutive pigmentation', *Br J Dermatol*, 168(5), pp. 1120-3.

Diffey, B. (2004) 'Climate change, ozone depletion and the impact on ultraviolet exposure of human skin', *Phys Med Biol*, 49(1), pp. R1-11.

Diffey, B. L. (2002) 'Sources and measurement of ultraviolet radiation', *Methods*, 28(1), pp. 4-13.

Djavaheri-Mergny, M., Marsac, C., Maziere, C., Santus, R., Michel, L., Dubertret, L. and Maziere, J. C. (2001) 'UV-A irradiation induces a decrease in the mitochondrial respiratory activity of human NCTC 2544 keratinocytes', *Free Radic Res*, 34(6), pp. 583-94.

Dranka, B. P., Benavides, G. A., Diers, A. R., Giordano, S., Zelickson, B. R., Reily, C., Zou, L., Chatham, J. C., Hill, B. G., Zhang, J., Landar, A. and Darley-Usmar, V. M. (2011) 'Assessing bioenergetic function in response to oxidative stress by metabolic profiling', *Free Radic Biol Med*, 51(9), pp. 1621-35.

Eshaghian, A., Vleugels, R. A., Canter, J. A., McDonald, M. A., Stasko, T. and Sligh, J. E. (2006) 'Mitochondrial DNA deletions serve as biomarkers of aging in the skin, but are typically absent in nonmelanoma skin cancers', *J Invest Dermatol*, 126(2), pp. 336-44.

Fawcett, A. (1994) *Textbook of Histology*.

Fisher, G. J., Datta, S. C., Talwar, H. S., Wang, Z. Q., Varani, J., Kang, S. and Voorhees, J. J. (1996) 'Molecular basis of sun-induced premature skin ageing and retinoid antagonism', *Nature*, 379(6563), pp. 335-339.

Flockhart, R. J., Diffey, B. L., Farr, P. M., Lloyd, J. and Reynolds, N. J. (2008) 'NFAT regulates induction of COX-2 and apoptosis of keratinocytes in response to ultraviolet radiation exposure', *Faseb Journal*, 22(12), pp. 4218-4227.

Forslind, B. and Lindberg, M. (2004) 'Structure and function of the skin barrier: an introduction', in Forslind, B., Lindberg, M. and Norlen, L. (eds.) *Skin, Hair and Nails*. New York: Marcel Dekker Inc, pp. 11-25.

Frisch, S. M. and Francis, H. (1994) 'Disruption of epithelial cell-matrix interactions induces apoptosis', *J Cell Biol*, 124(4), pp. 619-26.

Frisch, S. M. and Screaton, R. A. (2001) 'Anoikis mechanisms', *Curr Opin Cell Biol*, 13(5), pp. 555-62.

Gawkrodger, D. J. (1997) *Dermatology*. 2nd edn. Churchill Livingstone.

Gebbers, N., Hirt-Burri, N., Scaletta, C., Hoffmann, G. and Applegate, L. A. (2007) 'Water-filtered infrared-A radiation (wIRA) is not implicated in cellular degeneration of human skin', *Ger Med Sci*, 5, p. Doc08.

Gene, E. (2013a) *KRT1 keratin 1 [Homo sapiens (human)]* Available at: http://www.ncbi.nlm.nih.gov/gene?Db=gene&Cmd=ShowDetailView&TermToSearch=3848 (Accessed: 4th June).

Gene, E. (2013b) *NCF1 neutrophil cytosolic factor 1 [Homo sapiens (human)]* Available at: http://www.ncbi.nlm.nih.gov/gene?Db=gene&Cmd=ShowDetailView&TermToSearch=653361 (Accessed: 5th June).

Geromel, V., Darin, N., Chretien, D., Benit, P., DeLonlay, P., Rotig, A., Munnich, A. and Rustin, P. (2002) 'Coenzyme Q(10) and idebenone in the therapy of respiratory chain diseases: rationale and comparative benefits', *Mol Genet Metab*, 77(1-2), pp. 21-30.

Gibbs, N. K. and Norval, M. (2011) 'Urocanic acid in the skin: a mixed blessing?', *J Invest Dermatol*, 131(1), pp. 14-7.

Gibbs, N. K. and Norval, M. (2013) 'Photoimmunosuppression: a brief overview', *Photodermatol Photoimmunol Photomed*, 29(2), pp. 57-64.

Gilchrest, B. A., Eller, M. S. and Yaar, M. (2009) 'Telomere-mediated effects on melanogenesis and skin aging', *J Investig Dermatol Symp Proc*, 14(1), pp. 25-31.

Giorgio, V., Petronilli, V., Ghelli, A., Carelli, V., Rugolo, M., Lenaz, G. and Bernardi, P. (2012) 'The effects of idebenone on mitochondrial bioenergetics', *Biochim Biophys Acta*, 1817(2), pp. 363-9.

Green, A., Autier, P., Boniol, M., Boyle, P., Dore, J. F., Gandini, S., Newton-Bishop, J., Secretan, B., Walter, S. J., Weinstock, M. A. and Westerdahl, J. (2007) 'The association of use of sunbeds with cutaneous malignant melanoma and other skin cancers: A systematic review', *Int J Cancer*, 120(5), pp. 1116-22.

Green, C., Diffey, B. L. and Hawk, J. L. (1992) 'Ultraviolet radiation in the treatment of skin disease', *Phys Med Biol*, 37(1), pp. 1-20.

Haake, A., Scott, G. A. and Holbrook, K. A. (2001) 'Strucure and function of the skin: overview of the epidermis and dermis', in Freinkel, R. K. and Woodley, D. T. (eds.) *Biology of the skin*. London: The Parthenon Publishing Group, pp. 19-47.

Haefeli, R. H., Erb, M., Gemperli, A. C., Robay, D., Courdier Fruh, I., Anklin, C., Dallmann, R. and Gueven, N. (2011) 'NQO1-dependent redox cycling of idebenone: effects on cellular redox potential and energy levels', *PLoS One*, 6(3), p. e17963.

Häggström, M. (2010) *Layers of the epidermis*. Available at: http://en.wikipedia.org/wiki/File:Epidermal_layers.png.

Harbottle, A. and Birch-Machin, M. A. (2006) 'Real-time PCR analysis of a 3895 bp mitochondrial DNA deletion in nonmelanoma skin cancer and its use as a quantitative marker for sunlight exposure in human skin', *Br J Cancer*, 94(12), pp. 1887-93.

Harbottle, A., Maki, J., Reguly, B., Wittock, R., Robinson, K., Parr, R. and Birch-Machin, M. A. (2010) 'Real-time polymerase chain reaction analysis of a 3895-bp mitochondrial DNA deletion in epithelial swabs and its use as a quantitative marker for sunlight exposure in human skin', *Br J Dermatol*, 163(6), pp. 1291-5.

Harrington, C. R., Beswick, T. C., Leitenberger, J., Minhajuddin, A., Jacobe, H. T. and Adinoff, B. (2011) 'Addictive-like behaviours to ultraviolet light among frequent indoor tanners', *Clin Exp Dermatol*, 36(1), pp. 33-8.

Helleday, T., Lo, J., van Gent, D. C. and Engelward, B. P. (2007) 'DNA double-strand break repair: from mechanistic understanding to cancer treatment', *DNA Repair (Amst)*, 6(7), pp. 923-35.

Hoenigsmann, H. (2013) 'History of phototherapy in dermatology', *Photochemical and Photobiological Sciences* 12(1), pp. 16-21.

Hoerter, J. D., Ward, C. S., Bale, K. D., Gizachew, A. N., Graham, R., Reynolds, J., Ward, M. E., Choi, C., Kagabo, J. L., Sauer, M., Kuipers, T., Hotchkiss, T., Banner, N., Chellson,

R. A., Ohaeri, T., Gant, L. and Vanderhill, L. (2008) 'Effect of UVA fluence rate on indicators of oxidative stress in human dermal fibroblasts', *Int J Biol Sci*, 4(2), pp. 63-70.

Hollstein, M., Sidransky, D., Vogelstein, B. and Harris, C. C. (1991) 'P53 Mutations in Human Cancers', *Science*, 253(5015), pp. 49-53.

Holman, C. D., Armstrong, B. K. and Heenan, P. J. (1984) 'Cutaneous malignant melanoma in women: exogenous sex hormones and reproductive factors', *Br J Cancer*, 50(5), pp. 673-80.

Honigsmann, H. (2013) 'History of phototherapy in dermatology', *Photochem Photobiol Sci*, 12(1), pp. 16-21.

Horan, M. P., Pichaud, N. and Ballard, J. W. (2012) 'Review: quantifying mitochondrial dysfunction in complex diseases of aging', *J Gerontol A Biol Sci Med Sci*, 67(10), pp. 1022-35.

Huang, X. X., Bernerd, F. and Halliday, G. M. (2009) 'Ultraviolet A within sunlight induces mutations in the epidermal basal layer of engineered human skin', *Am J Pathol*, 174(4), pp. 1534-43.

Ichihashi, M., Ueda, M., Budiyanto, A., Bito, T., Oka, M., Fukunaga, M., Tsuru, K. and Horikawa, T. (2003) 'UV-induced skin damage', *Toxicology*, 189(1-2), pp. 21-39.

Immunodiagnostik (2011) *Data Sheet: 8-OHdG (8-Hydroxy-2´-deoxyguanosine)* Available at: http://www.immundiagnostik.com/fileadmin/pdf/AA1005.pdf (Accessed: 16th April 2013).

Invernizzi, F., Zeviani, M., Tiranti, V. and Jensen, P. (2013) *Measuring mitochondrial defects in human skin fibroblasts*. Available at: http://www.seahorsebio.com/resources/tech-writing/techbrief-fibroblasts.pdf.

Invitrogen (2013) *Important Parameters of Quantitative PCR (qPCR) Analysis*. Available at: http://tools.invitrogen.com/content/sfs/appendix/PCR_RTPCR/Important%20Parameters%20of%20qPCR.pdf (Accessed: 01/05/13).

Jantzen, K., Roursgaard, M., Desler, C., Loft, S., Rasmussen, L. J. and Moller, P. (2012) 'Oxidative damage to DNA by diesel exhaust particle exposure in co-cultures of human lung epithelial cells and macrophages', *Mutagenesis*, 27(6), pp. 693-701.

Jarrett, S. G., Rohrer, B., Perron, N. R., Beeson, C. and Boulton, M. E. (2013) 'Assessment of mitochondrial damage in retinal cells and tissues using quantitative polymerase chain reaction for mitochondrial DNA damage and extracellular flux assay for mitochondrial respiration activity', *Methods Mol Biol*, 935, pp. 227-43.

Jung, T., Hohn, A., Lau, A. M., Piazena, H. and Grune, T. (2012) 'An experimental setup for the measurement of nonthermal effects during water-filtered infrared A-irradiation of mammalian cell cultures', *Photochem Photobiol*, 88(2), pp. 371-80.

Karagas, M. R., Stannard, V. A., Mott, L. A., Slattery, M. J., Spencer, S. K. and Weinstock, M. A. (2002) 'Use of tanning devices and risk of basal cell and squamous cell skin cancers', *J Natl Cancer Inst*, 94(3), pp. 224-6.

Kimura, S., Kotani, T., McBride, O. W., Umeki, K., Hirai, K., Nakayama, T. and Ohtaki, S. (1987) 'Human thyroid peroxidase: complete cDNA and protein sequence, chromosome mapping, and identification of two alternately spliced mRNAs', *Proc Natl Acad Sci U S A*, 84(16), pp. 5555-9.

Kleinle, S., Wiesmann, U., Superti-Furga, A., Krahenbuhl, S., Boltshauser, E., Reichen, J. and Liechti-Gallati, S. (1997) 'Detection and characterization of mitochondrial DNA rearrangements in Pearson and Kearns-Sayre syndromes by long PCR', *Hum Genet*, 100(5-6), pp. 643-50.

Kligman, L. H. (1982) 'Intensification of ultraviolet-induced dermal damage by infrared radiation', *Arch Dermatol Res*, 272(3-4), pp. 229-38.

Koch, H., Wittern, K. P. and Bergemann, J. (2001) 'In human keratinocytes the Common Deletion reflects donor variabilities rather than chronologic aging and can be induced by ultraviolet A irradiation', *Journal of Investigative Dermatology*, 117(4), pp. 892-897.

Kohl, E., Steinbauer, J., Landthaler, M. and Szeimies, R. M. (2011) 'Skin ageing', *J Eur Acad Dermatol Venereol*, 25(8), pp. 873-84.

Krishna, C. M., Liebmann, J. E., Kaufman, D., DeGraff, W., Hahn, S. M., McMurry, T., Mitchell, J. B. and Russo, A. (1992) 'The catecholic metal sequestering agent 1,2-dihydroxybenzene-3,5-disulfonate confers protection against oxidative cell damage', *Arch Biochem Biophys*, 294(1), pp. 98-106.

Krishnan, K. J., Harbottle, A. and Birch-Machin, M. A. (2004) 'The use of a 3895 bp mitochondrial DNA deletion as a marker for sunlight exposure in human skin', *Journal of Investigative Dermatology*, 123(6), pp. 1020-1024.

Krishnan, K. J., Reeve, A. K., Samuels, D. C., Chinnery, P. F., Blackwood, J. K., Taylor, R. W., Wanrooij, S., Spelbrink, J. N., Lightowlers, R. N. and Turnbull, D. M. (2008) 'What causes mitochondrial DNA deletions in human cells?', *Nat Genet*, 40(3), pp. 275-9.

Laihia, J. K., Taimen, P., Kujari, H. and Leino, L. (2012) 'Topical cis-urocanic acid attenuates oedema and erythema in acute and subacute skin inflammation in the mouse', *Br J Dermatol*, 167(3), pp. 506-13.

Larsson, N. G. (2010) 'Somatic mitochondrial DNA mutations in mammalian aging', *Annu Rev Biochem*, 79, pp. 683-706.

Lautenschlager, S., Wulf, H. C. and Pittelkow, M. R. (2007) 'Photoprotection', *Lancet*, 370(9586), pp. 528-37.

Lee, Y. A., Cho, E. J. and Yokozawa, T. (2008) 'Protective effect of persimmon (Diospyros kaki) peel proanthocyanidin against oxidative damage under H2O2-induced cellular senescence', *Biol Pharm Bull*, 31(6), pp. 1265-9.

Li, Y., Takemura, G., Okada, H., Miyata, S., Maruyama, R., Li, L., Higuchi, M., Minatoguchi, S., Fujiwara, T. and Fujiwara, H. (2006) 'Reduction of inflammatory cytokine expression and oxidative damage by erythropoietin in chronic heart failure', *Cardiovasc Res*, 71(4), pp. 684-94.

Lim, C. K., Kalinowski, D. S. and Richardson, D. R. (2008) 'Protection against hydrogen peroxide-mediated cytotoxicity in Friedreich's ataxia fibroblasts using novel iron chelators of the 2-pyridylcarboxaldehyde isonicotinoyl hydrazone class', *Mol Pharmacol*, 74(1), pp. 225-35.

Lindelof, B., Sigurgeirsson, B., Gabel, H. and Stern, R. S. (2000) 'Incidence of skin cancer in 5356 patients following organ transplantation', *Br J Dermatol*, 143(3), pp. 513-9.

Liu, W., Smith, D. I., Rechtzigel, K. J., Thibodeau, S. N. and James, C. D. (1998) 'Denaturing high performance liquid chromatography (DHPLC) used in the detection of germline and somatic mutations', *Nucleic Acids Res*, 26(6), pp. 1396-400.

Lloyd, J. J. (2006) 'Ultraviolet Radiation in Medicine', in Webster, J. G. (ed.) *Encyclopedia of Medical Devises and Instrumentation*. 2nd edn. Chichester: John Wiley and Sons Inc., pp. 473-490.

Madan, V., Lear, J. T. and Szeimies, R. M. (2010) 'Non-melanoma skin cancer', *Lancet*, 375(9715), pp. 673-85.

Maddodi, N., Jayanthy, A. and Setaluri, V. (2012) 'Shining light on skin pigmentation: the darker and the brighter side of effects of UV radiation', *Photochem Photobiol*, 88(5), pp. 1075-82.

Mahmoud, B. H., Hexsel, C. L., Hamzavi, I. H. and Lim, H. W. (2008) 'Effects of visible light on the skin', *Photochem Photobiol*, 84(2), pp. 450-62.

Marionnet, C., Pierrard, C., Lejeune, F., Sok, J., Thomas, M. and Bernerd, F. (2010) 'Different oxidative stress response in keratinocytes and fibroblasts of reconstructed skin exposed to non extreme daily-ultraviolet radiation', *PLoS One*, 5(8), p. e12059.

Markova, A. and Weinstock, M. A. (2013) 'Risk of skin cancer associated with the use of UV nail lamp', *J Invest Dermatol*, 133(4), pp. 1097-9.

Marks, R. (1995) 'Summer in Australia. Skin cancer and the great SPF debate', *Arch Dermatol*, 131(4), pp. 462-4.

Matsumura, Y. and Ananthaswamy, H. N. (2004) 'Toxic effects of ultraviolet radiation on the skin', *Toxicol Appl Pharmacol*, 195(3), pp. 298-308.

McDaniel, D. H., Neudecker, B. A., DiNardo, J. C., Lewis, J. A., 2nd and Maibach, H. I. (2005a) 'Clinical efficacy assessment in photodamaged skin of 0.5% and 1.0% idebenone', *J Cosmet Dermatol*, 4(3), pp. 167-73.

McDaniel, D. H., Neudecker, B. A., DiNardo, J. C., Lewis, J. A., 2nd and Maibach, H. I. (2005b) 'Idebenone: a new antioxidant - Part I. Relative assessment of oxidative stress protection capacity compared to commonly known antioxidants', *J Cosmet Dermatol*, 4(1), pp. 10-7.

McKinlay, A. F. and Diffey, B. L. (1987) 'A reference action spectrum for ultraviolet induced erythema in human skin', *CIE J.*, 6, pp. 17-22.

Melnikova, V. O. and Ananthaswamy, H. N. (2005) 'Cellular and molecular events leading to the development of skin cancer', *Mutation Research-Fundamental and Molecular Mechanisms of Mutagenesis*, 571(1-2), pp. 91-106.

Meloni, M., Farina, A. and de Servi, B. (2010) 'Molecular modifications of dermal and epidermal biomarkers following UVA exposures on reconstructed full-thickness human skin', *Photochem Photobiol Sci*, 9(4), pp. 439-47.

Menton, D. N. (2009) *Skin - Our Living Armour*. Available at: http://www.answersingenesis.org/articles/am/v4/n4/skin (Accessed: 15th May).

Merwald, H., Klosner, G., Kokesch, C., Der-Petrossian, M., Honigsmann, H. and Trautinger, F. (2005) 'UVA-induced oxidative damage and cytotoxicity depend on the mode of exposure', *J Photochem Photobiol B*, 79(3), pp. 197-207.

Michikawa, Y., Mazzucchelli, F., Bresolin, N., Scarlato, G. and Attardi, G. (1999) 'Aging-dependent large accumulation of point mutations in the human mtDNA control region for replication', *Science*, 286(5440), pp. 774-9.

Montenegro, L., Sinico, C., Castangia, I., Carbone, C. and Puglisi, G. (2012) 'Idebenone-loaded solid lipid nanoparticles for drug delivery to the skin: in vitro evaluation', *Int J Pharm*, 434(1-2), pp. 169-74.

Moraes, C. T., Ricci, E., Petruzzella, V., Shanske, S., Dimauro, S., Schon, E. A. and Bonilla, E. (1992) 'Molecular Analysis of the Muscle Pathology Associated with Mitochondrial-DNA Deletions', *Nature Genetics*, 1(5), pp. 359-367.

Mori, T., Nakane, M., Hattori, T., Matsunaga, T., Ihara, M. and Nikaido, O. (1991) 'Simultaneous establishment of monoclonal antibodies specific for either cyclobutane

pyrimidine dimer or (6-4)photoproduct from the same mouse immunized with ultraviolet-irradiated DNA', *Photochem Photobiol*, 54(2), pp. 225-32.

Murphy, M. P. (2004) 'Investigating mitochondrial radical production using targeted probes', *Biochem Soc Trans*, 32(Pt 6), pp. 1011-4.

Nadanaciva, S., Rana, P., Beeson, G. C., Chen, D., Ferrick, D. A., Beeson, C. C. and Will, Y. (2012) 'Assessment of drug-induced mitochondrial dysfunction via altered cellular respiration and acidification measured in a 96-well platform', *J Bioenerg Biomembr*, 44(4), pp. 421-37.

Ness, A. R., Frankel, S. J., Gunnell, D. J. and Smith, G. D. (1999) 'Are we really dying for a tan?', *BMJ*, 319(7202), pp. 114-6.

Neuner, P., Pourmojib, M., Klosner, G., Trautinger, F. and Knobler, R. (1996) 'Increased release of the tumour necrosis factor receptor p75 by immortalized human keratinocytes results from an activated shedding mechanism and is not related to augmented steady-state levels of p75 mRNA', *Arch Dermatol Res*, 288(11), pp. 691-6.

Nirala, S. K., Bhadauria, M., Upadhyay, A. K., Mathur, R. and Mathur, A. (2009) 'Reversal of effects of intra peritoneally administered beryllium nitrate by tiron and CaNa3DTPA alone or in combination with alpha-tocopherol', *Indian J Exp Biol*, 47(12), pp. 955-63.

Ogawa, F., Sander, C. S., Hansel, A., Oehrl, W., Kasperczyk, H., Elsner, P., Shimizu, K., Heinemann, S. H. and Thiele, J. J. (2006) 'The repair enzyme peptide methionine-S-sulfoxide reductase is expressed in human epidermis and upregulated by UVA radiation', *J Invest Dermatol*, 126(5), pp. 1128-34.

Otto, A. I., Riou, L., Marionnet, C., Mori, T., Sarasin, A. and Magnaldo, T. (1999) 'Differential behaviors toward ultraviolet A and B radiation of fibroblasts and keratinocytes from normal and DNA-repair-deficient patients', *Cancer Res*, 59(6), pp. 1212-8.

Parrish, J. A. and Jaenicke, K. F. (1981) 'Action Spectrum for Phototherapy of Psoriasis', *Journal of Investigative Dermatology*, 76(5), pp. 359-362.

Passos, J. F., Saretzki, G., Ahmed, S., Nelson, G., Richter, T., Peters, H., Wappler, I., Birket, M. J., Harold, G., Schaeuble, K., Birch-Machin, M. A., Kirkwood, T. B. and von Zglinicki, T. (2007) 'Mitochondrial dysfunction accounts for the stochastic heterogeneity in telomere-dependent senescence', *PLoS Biol*, 5(5), p. e110.

Paz, M. L., Maglio, D. H. G., Weill, F. S., Bustamante, J. and Leoni, J. (2008) 'Mitochondrial dysfunction and cellular stress progression after ultraviolet B irradiation in human keratinocytes', *Photodermatology Photoimmunology & Photomedicine*, 24(3), pp. 115-122.

Petersen, B., Thieden, E., Philipsen, P. A., Heydenreich, J., Wulf, H. C. and Young, A. R. (2013) 'Determinants of personal ultraviolet-radiation exposure doses on a sun holiday', *Br J Dermatol*, 168(5), pp. 1073-9.

Petersen, M. J., Hansen, C. and Craig, S. (1992) 'Ultraviolet A irradiation stimulates collagenase production in cultured human fibroblasts', *J Invest Dermatol*, 99(4), pp. 440-4.

Piazena, H. and Kelleher, D. (2008) 'Comments on "Cellular response to infrared radiation involves retrograde mitochondrial signaling"', *Free Radic Biol Med*, 44(10), pp. 1869; author reply 1870-1.

Piazena, H. and Kelleher, D. K. (2010) 'Effects of infrared-A irradiation on skin: discrepancies in published data highlight the need for an exact consideration of physical and photobiological laws and appropriate experimental settings', *Photochem Photobiol*, 86(3), pp. 687-705.

Picot, C. R., Moreau, M., Juan, M., Noblesse, E., Nizard, C., Petropoulos, I. and Friguet, B. (2007) 'Impairment of methionine sulfoxide reductase during UV irradiation and photoaging', *Exp Gerontol*, 42(9), pp. 859-63.

Poderoso, J. J., Carreras, M. C., Lisdero, C., Riobo, N., Schopfer, F. and Boveris, A. (1996) 'Nitric oxide inhibits electron transfer and increases superoxide radical production in rat heart mitochondria and submitochondrial particles', *Archives of Biochemistry and Biophysics*, 328(1), pp. 85-92.

Polefka, T. G., Meyer, T. A., Agin, P. P. and Bianchini, R. J. (2012) 'Effects of solar radiation on the skin', *J Cosmet Dermatol*, 11(2), pp. 134-43.

Polyak, K., Li, Y., Zhu, H., Lengauer, C., Willson, J. K., Markowitz, S. D., Trush, M. A., Kinzler, K. W. and Vogelstein, B. (1998) 'Somatic mutations of the mitochondrial genome in human colorectal tumours', *Nat Genet*, 20(3), pp. 291-3.

Proksch, E., Brandner, J. M. and Jensen, J. M. (2008) 'The skin: an indispensable barrier', *Exp Dermatol*, 17(12), pp. 1063-72.

Pygmalion, M. J., Ruiz, L., Popovic, E., Gizard, J., Portes, P., Marat, X., Lucet-Levannier, K., Muller, B. and Galey, J. B. (2010) 'Skin cell protection against UVA by Sideroxyl, a new antioxidant complementary to sunscreens', *Free Radic Biol Med*, 49(11), pp. 1629-37.

Qian, W. and Van Houten, B. (2010) 'Alterations in bioenergetics due to changes in mitochondrial DNA copy number', *Methods*, 51(4), pp. 452-7.

Rastogi, R. P., Richa, Kumar, A., Tyagi, M. B. and Sinha, R. P. (2010) 'Molecular mechanisms of ultraviolet radiation-induced DNA damage and repair', *J Nucleic Acids*, 2010, p. 592980.

Ravanat, J. L., Douki, T. and Cadet, J. (2001) 'Direct and indirect effects of UV radiation on DNA and its components', *J Photochem Photobiol B*, 63(1-3), pp. 88-102.

Reinau, D., Weiss, M., Meier, C. R., Diepgen, T. L. and Surber, C. (2013) 'Outdoor workers' sun-related knowledge, attitudes and protective behaviours: a systematic review of cross-sectional and interventional studies', *Br J Dermatol*, 168(5), pp. 928-940.

Rizwan, M., Rodriguez-Blanco, I., Harbottle, A., Birch-Machin, M. A., Watson, R. E. and Rhodes, L. E. (2011) 'Tomato paste rich in lycopene protects against cutaneous photodamage in humans in vivo: a randomized controlled trial', *Br J Dermatol*, 164(1), pp. 154-62.

Roelandts, R. (2013) 'Determinants of personal ultraviolet radiation exposure doses on a sun holiday', *Br J Dermatol*, 168(5), p. 927.

SABiosciences (2011) *RT^2 Profiler PCR Arrays: Pathway Analysis*. Available at: http://www.sabiosciences.com/pathwaymagazine/pcrhandbook-qiagen/pdfs/pcrarrayguide-qiagen.pdf.

Sahin, E. and DePinho, R. A. (2010) 'Linking functional decline of telomeres, mitochondria and stem cells during ageing', *Nature*, 464(7288), pp. 520-528.

Salmeen, A., Park, B. O. and Meyer, T. (2010) 'The NADPH oxidases NOX4 and DUOX2 regulate cell cycle entry via a p53-dependent pathway', *Oncogene*, 29(31), pp. 4473-84.

Sander, C. S., Chang, H., Salzmann, S., Muller, C. S., Ekanayake-Mudiyanselage, S., Elsner, P. and Thiele, J. J. (2002) 'Photoaging is associated with protein oxidation in human skin in vivo', *J Invest Dermatol*, 118(4), pp. 618-25.

Santos, J. H., Meyer, J. N., Mandavilli, B. S. and Van Houten, B. (2006) 'Quantitative PCR-based measurement of nuclear and mitochondrial DNA damage and repair in mammalian cells', *Methods Mol Biol*, 314, pp. 183-99.

Scheffler, I. E. (2008) *Mitochondria*. 2nd edn. Chichester: John Wiley & Sons, Inc.

Schneider, W. E. and Young, R. (1998) *A guide to photometry and visible spectroradiometry*. Available at: http://biology.duke.edu/johnsenlab/pdfs/tech/spectmethods.pdf.

Schon, E. A., Rizzuto, R., Moraes, C. T., Nakase, H., Zeviani, M. and DiMauro, S. (1989) 'A direct repeat is a hotspot for large-scale deletion of human mitochondrial DNA', *Science*, 244(4902), pp. 346-9.

Schroeder, P., Gremmel, T., Berneburg, M. and Krutmann, J. (2008) 'Partial depletion of mitochondrial DNA from human skin fibroblasts induces a gene expression profile reminiscent of photoaged skin', *Journal of Investigative Dermatology*, 128(9), pp. 2297-2303.

Schroeder, P., Pohl, C., Calles, C., Marks, C., Wild, S. and Krutmann, J. (2007) 'Cellular response to infrared radiation involves retrograde mitochondrial signaling', *Free Radic Biol Med*, 43(1), pp. 128-35.

Schwarz, A., Maeda, A., Kernebeck, K., van Steeg, H., Beissert, S. and Schwarz, T. (2005) 'Prevention of UV radiation-induced immunosuppression by IL-12 is dependent on DNA repair', *J Exp Med*, 201(2), pp. 173-9.

Schwarz, T. (2005) 'Mechanisms of UV-induced immunosuppression', *Keio J Med*, 54(4), pp. 165-71.

Serpone, N., Dondi, D. and Albini, A. (2007) 'Inorganic and organic UV filters: Their role and efficacy in sunscreens and suncare product', *INORGANICA CHIMICA ACTA* 360(3), pp. 794-802.

Setlow, R. B. (1974) 'Wavelengths in Sunlight Effective in Producing Skin Cancer - Theoretical Analysis', *Proceedings of the National Academy of Sciences of the United States of America*, 71(9), pp. 3363-3366.

Setlow, R. B. and Carrier, W. L. (1966) 'Pyrimidine dimers in ultraviolet-irradiated DNA's', *J Mol Biol*, 17(1), pp. 237-54.

Shadel, G. S. and Clayton, D. A. (1997) 'Mitochondrial DNA maintenance in vertebrates', *Annual Review of Biochemistry*, 66, pp. 409-435.

Sherratt, M. J., Bayley, C. P., Reilly, S. M., Gibbs, N. K., Griffiths, C. E. and Watson, R. E. (2010) 'Low-dose ultraviolet radiation selectively degrades chromophore-rich extracellular matrix components', *J Pathol*, 222(1), pp. 32-40.

Shindo, Y. and Hashimoto, T. (1997) 'Time course of changes in antioxidant enzymes in human skin fibroblasts after UVA irradiation', *J Dermatol Sci*, 14(3), pp. 225-32.

Shindo, Y., Witt, E., Han, D., Epstein, W. and Packer, L. (1994) 'Enzymic and non-enzymic antioxidants in epidermis and dermis of human skin', *J Invest Dermatol*, 102(1), pp. 122-4.

Shoffner, J. M., Lott, M. T., Voljavec, A. S., Soueidan, S. A., Costigan, D. A. and Wallace, D. C. (1989) 'Spontaneous Kearns-Sayre/chronic external ophthalmoplegia plus syndrome associated with a mitochondrial DNA deletion: a slip-replication model and metabolic therapy', *Proc Natl Acad Sci U S A*, 86(20), pp. 7952-6.

Shokolenko, I., Venediktova, N., Bochkareva, A., Wilson, G. L. and Alexeyev, M. F. (2009) 'Oxidative stress induces degradation of mitochondrial DNA', *Nucleic Acids Research*, 37(8), pp. 2539-2548.

Sigma (2010) *Tiron; MSDS*. Available at: http://www.sigmaaldrich.com/catalog/product/sigma/d7389?lang=en&region=GB.

Skulachev, M. V., Antonenko, Y. N., Anisimov, V. N., Chernyak, B. V., Cherepanov, D. A., Chistyakov, V. A., Egorov, M. V., Kolosova, N. G., Korshunova, G. A., Lyamzaev, K. G., Plotnikov, E. Y., Roginsky, V. A., Savchenko, A. Y., Severina, II, Severin, F. F., Shkurat, T. P., Tashlitsky, V. N., Shidlovsky, K. M., Vyssokikh, M. Y., Zamyatnin, A. A., Jr., Zorov, D. B. and Skulachev, V. P. (2011) 'Mitochondrial-targeted plastoquinone derivatives. Effect on senescence and acute age-related pathologies', *Curr Drug Targets*, 12(6), pp. 800-26.

Sligh, J. E., Eshaghian, A., Musiek, A. C., Vleugels, R., Stokes, S. and Slater, A. (2002) 'Mitochondrial DNA in aging skin and in nonmelanoma skin cancer', *Journal of Investigative Dermatology*, 119(1), p. 101.

Sreevidya, C. S., Fukunaga, A., Khaskhely, N. M., Masaki, T., Ono, R., Nishigori, C. and Ullrich, S. E. (2010) 'Agents that Reverse UV-Induced Immune Suppression and Photocarcinogenesis Affect DNA Repair', *Journal of Investigative Dermatology*, 130(5), pp. 1428-1437.

Sugio, S., Kashima, A., Mochizuki, S., Noda, M. and Kobayashi, K. (1999) 'Crystal structure of human serum albumin at 2.5 A resolution', *Protein Eng*, 12(6), pp. 439-46.

Svobodova, A., Walterova, D. and Vostalova, J. (2006) 'Ultraviolet light induced alteration to the skin', *Biomed Pap Med Fac Univ Palacky Olomouc Czech Repub*, 150(1), pp. 25-38.

Swalwell, H., Latimer, J., Haywood, R. M. and Birch-Machin, M. A. (2012) 'Investigating the role of melanin in UVA/UVB- and hydrogen peroxide-induced cellular and mitochondrial ROS production and mitochondrial DNA damage in human melanoma cells', *Free Radic Biol Med*, 52(3), pp. 626-34.

Syed, D. N., Afaq, F. and Mukhtar, H. (2012) 'Differential activation of signaling pathways by UVA and UVB radiation in normal human epidermal keratinocytes', *Photochem Photobiol*, 88(5), pp. 1184-90.

Taiwo, F. A. (2008) 'Mechanism of tiron as scavenger of superoxide ions and free electrons', *Spectroscopy*, 22(6), pp. 491-498.

Tewari, A., Sarkany, R. P. and Young, A. R. (2012) 'UVA1 induces cyclobutane pyrimidine dimers but not 6-4 photoproducts in human skin in vivo', *J Invest Dermatol*, 132(2), pp. 394-400.

Tonska, K., Piekutowska-Abramczuk, D., Kaliszewska, M., Kowalski, P., Tanska, A., Bartnik, E., Pronicka, E. and Krajewska-Walasek, M. (2012) 'Molecular investigations of mitochondrial deletions: evaluating the usefulness of different genetic tests', *Gene*, 506(1), pp. 161-5.

Tosato, M., Zamboni, V., Ferrini, A. and Cesari, M. (2007) 'The aging process and potential interventions to extend life expectancy', *Clin Interv Aging*, 2(3), pp. 401-12.

Tournas, J. A., Lin, F. H., Burch, J. A., Selim, M. A., Monteiro-Riviere, N. A., Zielinski, J. E. and Pinnell, S. R. (2006) 'Ubiquinone, idebenone, and kinetin provide ineffective photoprotection to skin when compared to a topical antioxidant combination of vitamins C and E with ferulic acid', *J Invest Dermatol*, 126(5), pp. 1185-7.

Tullo, C. (2010) *Sunbeds (Regulation) Act 2010*. Available at: http://www.legislation.gov.uk/ukpga/2010/20/pdfs/ukpga_20100020_en.pdf (Accessed: 03/06/13).

Tyrrell, R. M. (2012) 'Modulation of gene expression by the oxidative stress generated in human skin cells by UVA radiation and the restoration of redox homeostasis', *Photochem Photobiol Sci*, 11(1), pp. 135-47.

Utiger, R. D. (1998) 'The need for more vitamin D', *N Engl J Med*, 338(12), pp. 828-9.

Valavanidis, A., Vlachogianni, T. and Fiotakis, C. (2009) '8-hydroxy-2' -deoxyguanosine (8-OHdG): A critical biomarker of oxidative stress and carcinogenesis', *J Environ Sci Health C Environ Carcinog Ecotoxicol Rev*, 27(2), pp. 120-39.

Varani, J. (1998) 'Preservation of human skin structure and function in organ culture', *Histol Histopathol*, 13(3), pp. 775-83.

Venegas, V., Wang, J., Dimmock, D. and Wong, L. J. (2011) 'Real-time quantitative PCR analysis of mitochondrial DNA content', *Curr Protoc Hum Genet*, Chapter 19, p. Unit 19 7.

Videira, I. F., Moura, D. F. and Magina, S. (2013) 'Mechanisms regulating melanogenesis*', *An Bras Dermatol*, 88(1), pp. 76-83.

Wallace, D. C. (1992) 'Mitochondrial Genetics - a Paradigm for Aging and Degenerative Diseases', *Science*, 256(5057), pp. 628-632.

Wang, X. and Moraes, C. T. (2011) 'Increases in mitochondrial biogenesis impair carcinogenesis at multiple levels', *Mol Oncol*, 5(5), pp. 399-409.

Weatherhead, S. C., Farr, P. M. and Reynolds, N. J. (2013) 'Spectral effects of UV on psoriasis', *Photochem Photobiol Sci*, 12(1), pp. 47-53.

Wempe, M. F., Lightner, J. W., Zoeller, E. L. and Rice, P. J. (2009) 'Investigating idebenone and idebenone linoleate metabolism: in vitro pig ear and mouse melanocyte studies', *J Cosmet Dermatol*, 8(1), pp. 63-73.

Williams, K., Frayne, J. and Hall, L. (1998) 'Expression of extracellular glutathione peroxidase type 5 (GPX5) in the rat male reproductive tract', *Mol Hum Reprod*, 4(9), pp. 841-8.

Wojtczak, L. and Zablocki, K. (2008) 'Basic Mitochondrial Physiology in Cell Viability and Death', in Dykens, J. A. and Will, Y. (eds.) *Drug-induced Mitochondrial Dysfunction*. Chichester: John Wiley & Sons, Inc., pp. 3-37.

Yang, J., Su, Y. and Richmond, A. (2007) 'Antioxidants tiron and N-acetyl-L-cysteine differentially mediate apoptosis in melanoma cells via a reactive oxygen species-independent NF-kappaB pathway', *Free Radic Biol Med*, 42(9), pp. 1369-80.

Yang, J. H., Lee, H. C., Chung, J. G. and Wei, Y. H. (2004) 'Mitochondrial DNA mutations in light-associated skin tumors', *Anticancer Res*, 24(3a), pp. 1753-8.

Yang, J. H., Lee, H. C., Lin, K. J. and Wei, Y. H. (1994) 'A specific 4977-bp deletion of mitochondrial DNA in human ageing skin', *Arch Dermatol Res*, 286(7), pp. 386-90.

Yokoyama, H., Mizutani, R. and Satow, Y. (2013) 'Structure of a double-stranded DNA (6-4) photoproduct in complex with the 64M-5 antibody Fab', *Acta Crystallogr D Biol Crystallogr*, 69(Pt 4), pp. 504-12.

Young, A. R., Chadwick, C. A., Harrison, G. I., Nikaido, O., Ramsden, J. and Potten, C. S. (1998) 'The similarity of action spectra for thymine dimers in human epidermis and erythema suggests that DNA is the chromophore for erythema', *J Invest Dermatol*, 111(6), pp. 982-8.

Zs -Nagy, I. (1990) 'Chemistry, toxicology, pharmacology and pharmacokinetics of idebenone: a review', *Arch Gerontol Geriatr*, 11(3), pp. 177-86.